STUDIES OF ALTERNATIVE ANODES AND ETHANOL FUEL FOR SOFCS

Gaël Pierre Germain Corre

A Thesis Submitted for the Degree of PhD
at the
University of St. Andrews

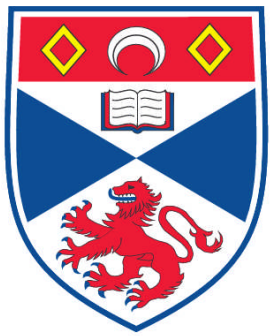

2009

STUDIES OF ALTERNATIVE ANODES

AND

ETHANOL FUEL

FOR SOFCS

A thesis presented for the degree of Doctor of Philosophy

by

Gaël Pierre Germain Corre

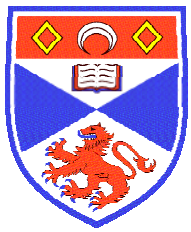

University
of
St Andrews

Supervised by Prof. J.T.S. Irvine

Submitted April 2009

I, Gael Pierre Germain Corre, hereby certify that this thesis, which is approximately 44000 words in length, has been written by me, that it is the record of work carried out by me and that it has not been submitted in any previous application for a higher degree.

I was admitted as a research student in October 2005 and as a candidate for the degree of Doctor of Philosophy in September 2006; the higher study for which this is a record was carried out in the University of St Andrews between 2005 and 2009.

date …… signature of candidate ……

I hereby certify that the candidate has fulfilled the conditions of the Resolution and Regulations appropriate for the degree of Doctor of Philosophy in the University of St Andrews and that the candidate is qualified to submit this thesis in application for that degree.

date …… signature of supervisor ……

In submitting this thesis to the University of St Andrews we understand that we are giving permission for it to be made available for use in accordance with the regulations of the University Library for the time being in force, subject to any copyright vested in the work not being affected thereby. We also understand that the title and the abstract will be published, and that a copy of the work may be made and supplied to any bona fide library or research worker, that my thesis will be electronically accessible for personal or research use unless exempt by award of an embargo as requested below, and that the library has the right to migrate my thesis into new electronic forms as required to ensure continued access to the thesis. We have obtained any third-party copyright permissions that may be required in order to allow such access and migration, or have requested the appropriate embargo below.

The following is an agreed request by candidate and supervisor regarding the electronic publication of this thesis:

Access to Printed copy and electronic publication of thesis through the University of St Andrews.

date …… signature of candidate …… signature of supervisor ……

PREFACE

The research presented in this thesis is divided into two distinctive parts. The research addressing SOFC anodes development, part II, chapters 3 to 9, has been realized within the framework of a collaboration between the University of St-Andrews and the University of Pennsylvania. The work presented in those chapters has been jointly carried out by myself, Gael Pierre Germain Corre, and Dr Gun Tae Kim. Experimental has been carried out at both Universities. The research addressing direct ethanol SOFCs, part III, chapters 10 to 12, has been realized by myself, at the University of St Andrews.

ACKNOWLEDGEMENTS

First I would like to deeply thank Professor John Irvine for giving me the opportunity to work on this project. Prof. John Irvine gave me the chance to take a new start in my scientific career and to work on renewable energies, which I have always wanted to. I was coming from a different field when I first started on this project and I had to learn a lot, but Prof. John Irvine has always been patient with me and has always given me the time I required to adjust my knowledge. I enjoyed a great support, the opportunity to travel and collaborate with another research team, and a great flexibility.

I am really grateful to both Professor Raymond Gorte and Professor John Vohs for warmly welcoming me in their laboratory at the University of Pennsylvania in Philadelphia. The research work we have carried out during my two stays in Philadelphia has been really productive and enjoyable. I have always enjoyed the interesting scientific discussions we had about the research.

This collaboration would not have been so productive without the help and dedication of Dr. Gun Tae Kim. We had a great time working together, and I really do hope we can collaborate again in the future.

I would like to thank some members of our research group who have been particularly helpful throughout my PhD. I would like to warmly thank Sneh Jain for all the times she has helped me both in the lab and outside when I needed to. I am really thankful to Mark Cassidy who has supported me in many ways. Mark has helped me with SEM studies and always provided me with useful advices, productive scientific discussions and of course some of his time when I needed help. Finally, I am grateful to all group members and university workers who had some input in my research work.

Summary

This thesis explores the development of efficient engineered composite alternative anodes and the use of ethanol as a fuel for Solid Oxide Fuel Cells. SOFCs can in theory operate with fuels other than hydrogen. However, this requires the design of efficient alternative anode material that do not catalyze carbon formation and that are tolerant to redox cycles. An innovative concept has been developed that relies on the impregnation of perovskites into porous YSZ structures to form the anode functional layer. Catalysts are added to provide sufficient catalytic activity. Cells with anodes containing LSCM and Ce/Pd have displayed excellent performance. At 800°C, and with a 65 µm thick electrolyte, the power outputs were above 1W/cm^2 in humidified hydrogen and 0.7 W/cm^2 in humidified methane. These electrodes have shown the ability to reduce CO2 electrochemically with an efficiency that is similar to that which can be achieved for H_2O electrolysis and the anodes could operate on pure CO_2. The importance of incorporating an efficient catalyst was demonstrated. The use of 0.5 wt% of Pd is sufficient to dramatically improve the performance in such electrodes. The microstructure of impregnated LSCM-YSZ composites plays an important role in the high performance obtained. A layer of LSCM nanoparticles covering the YSZ is formed upon reduction, offering a great surface area for electrochemical reactions. The fabrication method presented in this thesis is a powerful tool for designing microstructures in situ.

Among the various fuels under consideration for SOFCs, ethanol offers outstanding advantages. Half cell measurements have been performed to characterize the performance of different types of anodes when operated on ethanol/steam mixtures. Steady performance was achieved on LSCM-CGO anodes. Carbon deposits from gas phase reactions have been evidenced and were found to be responsible for the performance enhancement when the cell is operated in diluted ethanol as compared to hydrogen. At high steam content, polarization resistances of LSCM-CGO-YSZ anodes in ethanol/ steam mixtures were shown to be below 0.3 Ω.cm^2 at 950°C.

Contents

INTRODUCTION

Modern life is mainly based on the supply of electricity and transport of goods and people, two sectors that are deeply related to mass consumption of energy. Our important energy demand is mainly fulfilled by the combustion of fossil fuels as can be seen on Figure 1. Oil, coal and natural gas accounted for 85% of the world energy usage in 2006.

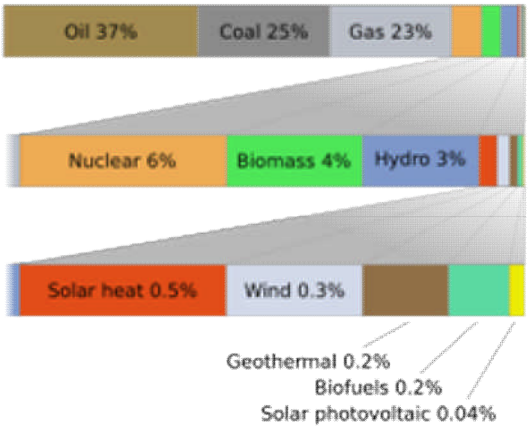

Figure 1: Current global world energy usage[1]

The world energy demand is constantly increasing. An important contribution to those ever growing energy needs is the rapid development of third world economies such as China and India. The best example is certainly China, whose energy consumption is displayed on Figure 2, along with projected data. The impressive growth in the energy needs of those countries will very likely be mainly matched by the use of fossil fuels.

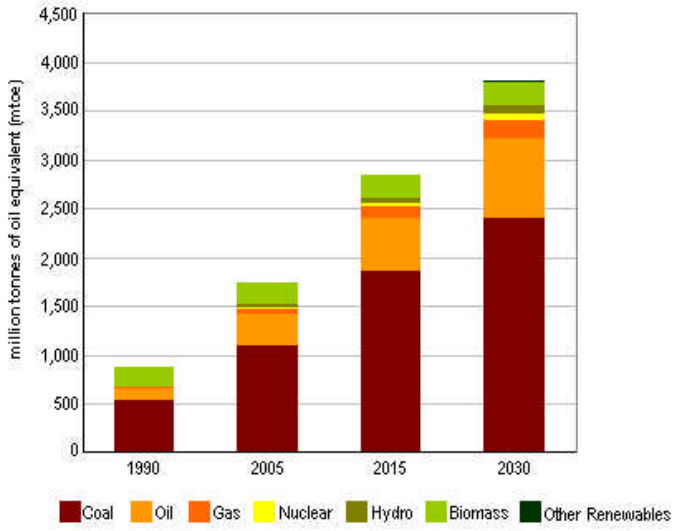

Figure 2: China's projected energy consumption[2]

For several decades, limitations of our fossil based economy have become

increasingly apparent and problematic. A global fossil fuel based economy is indeed unsustainable in many aspects.
Fossil fuel reserves are limited and therefore are bound to become increasingly scarce with the rise of the global energy demand. Reserves cannot last forever meaning that energy sources will have to be diversified. Expected consequences of an increased demand facing a limited availability have already been spectacular on the price of oil. The barrel of oil reached the worrying threshold of 150$ in 2008. Although the oil price has dropped during the 2008/2009 credit crunch, a serious warning has been given to governments.
An important characteristic of the fossil based economy is that many countries need to import most of the fuel required for their energy needs and hence must rely on other countries. As an example, most of the natural gas consumed in Europe is provided by Russia. Energy independence can be an economic advantage and is a form of freedom sought by many governments. It was a major factor in the USA's recent decision to invest massively on locally produced biofuels to replace oil importations.
In terms of pollution, the combustion of fossil fuels induces substantial emissions of greenhouse gases such as CO_2, and pollutants such as SOx and NOx. Atmospheric pollution and global warming are becoming major concerns that need to be addressed.
Finally, most of processes used in converting fossil fuels to energy suffer from low energy efficiency. Those processes require the intermediate use of heat energy and are therefore limited by the Carnot efficiency.

The energy challenges that our world is facing are therefore multiple. A transition to a sustainable economy will be required. In a sustainable economy, energy sources should be renewable and their conversion to energy should be as pollution free as achievable. Greenhouse gases emissions should be reduced to acceptable levels. Energy sources have to be better used, meaning that energy conversion processes featuring high efficiencies need to be developed and widely used. The transition to a sustainable economy requires to considerably modifying the energy consumption habits in the developed countries, while ensuring that the development of emerging economies is performed in a sustainable way.

With respect to the depicted global context and changes required, fuel cells could play a major role in the near future in helping to make a better use of our energy sources. The key feature of a fuel cell is the energy efficiency. Since chemical energy is directly converted to electricity, fuel cells are not limited by the Carnot efficiency and thus offer considerable higher energy efficiencies than conventional energy conversion processes. Fuels cells have a huge potential for power generation in stationary, portable and transport applications. Different types of fuel cells exist, that work at different temperature. The preferred fuel for fuel cells is hydrogen. High temperature cells such as Solid Oxide Fuel Cells (SOFC) can theoretically operate with any fuel capable of oxidation. (Chapter 1).

Fuel-cell technology has hence been much heralded in recent years as a keystone of the future energy economy. In association with the hydrogen economy, it has been strongly promoted by the governments of most of the world's leading industrialized nations. There is now a phenomenal commercial interest in fuel-cell technology with new start-up companies being established and major players in the energy market turning their attention to it. The degree and extent of market penetration and establishment really only depend on the ability to reduce the cost of these devices

while ensuring their long-term stability. In the long term, fuel cells will be an essential component of any hydrogen or similar clean-energy economy not only because they can very efficiently convert fuels to electricity but because they may also work well as electrolysers for storing excess energy as hydrogen or convert CO_2 (chapter 6). In the short-term, they promise greatly enhanced conversion efficiencies of more conventional fuels, and so will deliver large reductions in carbon dioxide emissions[3].

The hydrogen economy might become a reality in the future but many technological hurdles related to its storage, production and transport need to be lifted before the widespread use of hydrogen as en energy carrier could be considered (chapter 10). Among the potential fuels that could play a role in the future economy, second generation cellulosic bioethanol is of particular interest. Sources that can be used in the production process are multiple and renewable. Cellulosic ethanol can be produced from feedstocks that are today considered as waste, which is still a largely untapped source of energy in the present economy (chapter 10).

The focus of this thesis is to investigate the use of bioethanol as a fuel for SOFCs. As outlined above, fuel cells will surely play a major role in the development of a sustainable economy due to their high efficiency, while second generation cellulosic ethanol is a very attractive energy source. Therefore, combining those two promising elements of the future economy can provide a suitable answer to the problems we need to address today.

In a SOFC, the fuel is oxidized on the anode. Standard anodes materials used in SOFC are Ni-YSZ cermets (chapter 3). Those anodes work well with hydrogen but suffer from severe limitations when hydrocarbon fuels are used. An intensive research topic within the SOFC community is hence to develop efficient alternative anodes that can operate on hydrocarbons (chapter 3). Part of this thesis has been dedicated to the development of such anodes by using an innovative concept that combines the materials expertise developed at The University of St Andrews with the anode fabrication method developed at The Universitry of Pennsylavannia (Part II, chapters 2 to 8).

Using ethanol at the high temperatures at which a SOFC operates involves multiple and complex processes. Before the electrochemical oxidation occurs, both homogeneous and heterogeneous chemistry play an important role in converting the ethanol and forming carbon deposits (Chapter 10). The other part of this thesis has been dedicated to the study of the operation of anodes, involving different type of materials, on ethanol/steam mixtures (PART III, chapter 9 to 12).

---

[1]BP statistical review of world energy June 2006, British petroleum, 2006
[2] World energy outlook 2007, International Energy agency
[3]A. Atkinson, S. Barnett, R.J. Gorte, J.T.S. Irvine, A.J. McEvoy, M. Mogensen, S.C. Singhal and J.M.Vohs., *Nature materials*, 3 (2004) 17-27

PART I

FUEL CELLS AND GENERAL EXPERIMENTAL TECHNIQUES

FUEL CELL TECHNOLOGY

1.1. Principle

A fuel cell is an energy conversion device that produces electricity, and heat, by electrochemical combination of a fuel with an oxidant, which can be viewed as a battery with external fuel supply. A fuel cell consists of four components: two electrodes, the *anode* and the *cathode*, separated by an *electrolyte*, and connected by an external circuit or *interconnect*, as shown on Figure 3. Fuel is fed to the anode where it is oxidized, releasing electrons to the external circuit. Oxidant is fed to the cathode where it is reduced using the electrons delivered by the external circuit. The electrons flow through the interconnect, from the anode to the cathode, produces direct-current electricity.

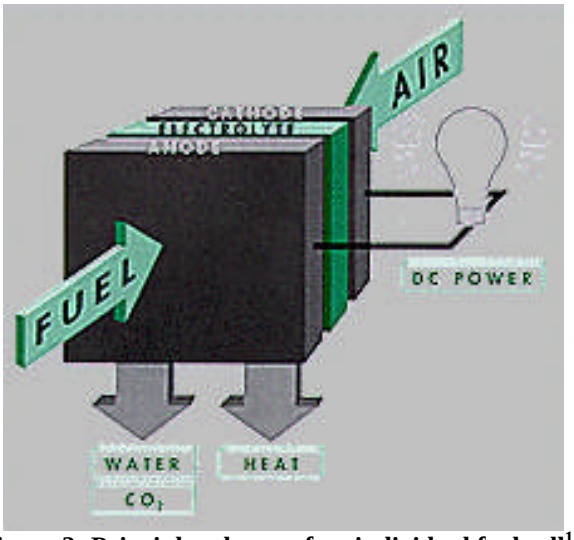

Figure 3: Principle scheme of an individual fuel cell[1].

In theory, any gases capable of electrochemical oxidation and reduction can be used as fuel and oxidant in a fuel cell. Oxygen is the most common oxidant for fuel cells since it is readily and economically available from air. Hydrogen, which offers high electrochemical reactivity, is the most common fuel. However, fuel cells can be developed to work with alternative fuels to hydrogen.

1.1.1. Features

The key feature of a fuel cell is its high energy conversion efficiency. Because fuel cells convert the chemical energy of the fuel directly to electrical energy without the

intermediate of thermal energy (unlike indirect conversion in conventional systems), their conversion efficiency is not subject to the Carnot limitation. Further energy gains can be achieved when the produced heat is used in combined heat and power, or gas turbine applications. The improved efficiency as compared to conventional energy conversion devices is the main reason fuel cells are receiving considerable attention. Besides their high energy conversion efficiency, fuel cells offer several additional advantages over conventional methods of power generation. They offer a much lower production of pollutants. A fuel cell fuelled with H_2 and air only produces water. Other significant advantages offered are modular construction and size flexibility, which makes them well suited for decentralized applications, high efficiency at part load, fuel flexibility and remote/unattended operation. Moreover, their vibration free operation eliminates noise usually associated with conventional power generation systems. More details concerning general features of fuel cells can be found in the literature[1,2].

1.1.2. History

The fuel cell concept, ascribed to Sir Humprey Davy, dates from the beginning of the 19th century. The first hydrogen-oxygen cell was successfully operated by Sir William Grove in 1839[3], generally referred to as the start of fuel cell history. While investigating the electrolysis of water, Grove observed that when the current was switched off, a small current flowed through the circuit in the opposite direction, as a result of a reaction between the electrolysis products, hydrogen and oxygen, catalysed by the platinum electrodes. Grove recognized the possibility of combining several of these in series to form a gaseous voltaic battery[4], and also made the crucially important observation that there must be a 'notable surface of action' between the gas, the electrolyte and the electrode phases in a cell. Maximizing the area of contact between those three phases remains at the forefront of fuel cell research and development. Some 50 years after Grove's 'gas battery', Mond and Langer introduced the term fuel cell[5] to describe their device which had a porous platinum black electrode structure, and used a diaphragm made of a porous non-conducting substance to hold the electrolyte.

Despite the fact that the fuel cell was discovered over 160 years ago, and the high efficiencies and environmental advantages offered, only now are fuel cells approaching commercial reality.

1.1.3. Different types of fuel cells

There is a whole range of fuel cells in different stages of development. Although all types of fuel cells have the same basic operating principle, they have different characteristics that stem from the nature of electrolyte involved. The 5 main types are summarized in Table 1. The nature of the electrolyte dictates the nature of ions transferred and the direction of this transport, which in turn determines on which side of the electrolyte water is produced. Moreover, each electrolyte requires to be operated in a specific temperature range, which is a major difference in characteristics between different types of fuel cells. Molten Carbonate Fuel Cells (MCFC) and Solid Oxide Fuel Cell (SOFC) have elevated operating temperature, compared to much

lower operating temperature for Alkaline (AFC), Polymer electrolyte Membrane (PEMFC) and Phosphoric Acid (PAFC) fuel cells. The operating temperature dictates in turn the physicochemical and thermo mechanical properties of materials to be used as cell component as well as the type of fuel the cell can be operated on. Moreover, this difference in operating temperatures has a number of implications for the applications for which particular fuel cell types are most suited.

Type	Temp. (°C)	Fuel	Electrolyte	Charge carrier
Polymer Electrolyte Membrane(PEM)	70-110	H_2, methanol	Suffocated polymers	$(H_2O)_nH^+$
Alkali Fuel Cell (AFC)	100-250	H_2	Aqueous KOH	OH^-
Phosphoric Acid Fuel Cell (PAFC)	150-250	H_2	H_3PO_4	H^+
Molten Carbonate Fuel Cell (MCFC)	500-700	H_2, hydrocarbons, CO	$(Na,K)_2CO_3$	CO_3^{2-}
Solid Oxide Fuel Cell (SOFC)	600-1000	H_2, CO, hydrocarbons, alcohols	$(Zr,Y)O_{2-\delta}$	O^{2-}

Table 1: Different types of fuel cells and characteristics[1]

Large differences exist in application, design, size, cost and operating range for the different type of fuel cells. Of the available fuel-cell technologies, PEFC and SOFC are thought to have the most potential to achieve cost and efficiency targets for widespread use in power generation, and have been the most investigated types.

In general, high temperature fuel cells exhibit higher efficiency and are less sensible to fuel composition. PEMFC systems require a pure H_2 fuel stream because the precious metal anode catalysts are poisoned by even low levels of CO or other compounds such as those containing sulfur. Current PEFC systems operate below 100°C, but there is a great deal of research to find polymer electrolytes that can operate at higher temperatures since increasing the operating temperature relaxes the fuel-purity requirements relative to catalyst poisoning. In contrast, due to their high operating temperature, CO is rather a fuel than a poison for SOFC. Hence, high temperature fuel cells can be operated on fuels other than H_2.

1.1.4. Applications

The potential applications of fuel cells in society are ever increasing, driven by the various benefits that the implementation of fuel cells would bring over current technologies, such as environmental and efficiency considerations. Application range all the way from very small scale ones requiring only a few watts to larger-scale distributed power generation of hundreds of MW.

The small scale power supply is a well suited market for fuel cells. Indeed, fuel cells offer significantly higher power densities than batteries, as well as being smaller and lighter and having much longer lifetimes. Hence, an increasing number of applications are emerging where only a few watts are required, such as palm-top and lap-top computers, mobile phones and other portable electronic devices.

Their potentially high reliability and low maintenance coupled to their quiet operation and modular nature makes fuel cells particularly suited to localised 'off grid' power generation, either for high quality uninterrupted power supplies, or remote applications. High temperature fuel cells (MCFC and SOFC) are suitable for continuous power production, where the cell temperature can be maintained. If the released heat is used to drive a gas turbine to produce extra energy, the system efficiency can be increased to levels as high as 80%, significantly higher than any conventional electricity generation process. Moreover, the produced heat makes SOFC particularly suitable to combined heat and power (CHP) applications ranging from less than 1 kW to several MW, which covers individual households, larger residential units and business and industrial premises, providing all the power and hot water from a single system.

The combination of their high efficiency and significantly reduced emissions of pollutants mean that fuel cell powered vehicles are a very attractive proposition, especially in heavily populated urban areas. The efficiency is to be compared with about 20% for a combustion engine. Low temperature fuel cells, in particular PEMFC, are the most suited to transport applications, because of the need for short warm-up and cool down time and because there are no problem with temperature cycling. The concept of a fuel cell powered vehicle running on hydrogen, the so-called 'zero emission vehicle', is a very attractive one and is currently an area of intense activity for almost all the major motor manufacturers. As an example, fuel cell powered buses running on compressed hydrogen are successfully operated in several cities around the world.

1.2. SOFC

1.2.1. General considerations

A SOFC is defined by its solid ceramic electrolyte, which is a non porous metal oxide. Such electrolytes are oxygen-ion (O^{2-}) conductors, impervious to gas flow and have negligible electronic conductivity. **S**olid oxide electrolytes require a high

operating temperature to display suitable conductivities, typically in the range 700-1000°C, which has a number of consequences on SOFCs operation[6].

SOFC involve multiple complex physico-chemical processes. The principle of an SOFC, involving hydrogen as a fuel is illustrated in Figure 4.

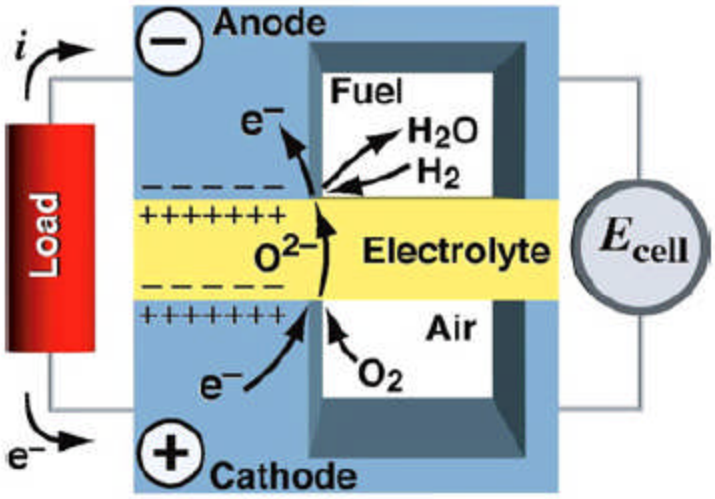

Figure 4: Principle of a Solid Oxide Fuel Cell involving H_2 as a fuel[7].

Oxygen is electrochemically reduced at the cathode-electrolyte-gas interface. Electrons are delivered to the cathode through the interconnect where they react with oxygen molecules in the gas phase to deliver oxygen ions to the electrolyte via a charge transfer reaction:

$$\frac{1}{2}O_2(g) + 2e^-(c) \Leftrightarrow O^{2-}(e) \quad \textbf{(Equation 1)}$$

In this equation, the three phases are denoted as (g) for the gas, (c) for the cathode and (e) for the electrolyte. Oxygen ions migrate through the electrolyte via a vacancy hoping mechanism towards the anode-electrolyte-fuel interface where they participate in the fuel oxidation, written as follows for hydrogen:

$$H_2(g) + O^{2-}(e) \Leftrightarrow H_2O(g) + 2e^-(a) \quad \textbf{(Equation 2)}$$

where (a) denotes the anode. The hydrogen in the gas phase reacts with the oxygen ions provided by the electrolyte to deliver electrons to the anode.As long as a load is connected between the anode and the cathode, the electrons from the anode will flow through the load back to the cathode, and electrical current will flow through the circuit.

The overall electrochemical cell reaction in a SOFC, based on oxygen and hydrogen, is written as follow:

$$O_2 + H_2 \Leftrightarrow H_2O \quad \textbf{(Equation 3)}$$

Another accurate way to represent the overall reaction occurring in the cell, regardless of the fuel involved, is to describe the oxygen transfer:

$$O_2(c) \Leftrightarrow O_2(a) \quad \textbf{(Equation 4)}$$

An SOFC can therefore be considered as an oxygen pump. The amount of oxygen transported to the anode will depend on the type of fuel used and the reactions occurring at the anode.

1.2.1.1. **History**

The solid oxide fuel cell was first conceived following the discovery of solid oxide electrolytes in 1899 by Nernst[8]. Nernst discovered that the very high electrical resistance of pure solid oxides could be greatly reduced by addition of certain other oxides. The most promising of these mixtures consisted mainly of zirconia (ZrO_2) with small amounts of added yttria (Y_2O_3). This is still the most widely used electrolyte material in the SOFC.

The first working SOFC was demonstrated by Baur and Preis in 1937, using stabilized zirconia as electrolyte and coke and magnetite respectively as a fuel and oxidant[9]. The current produced by their cell was too low for any practical purposes, but the possibility of operated SOFCs had been demonstrated. Unfortunately the high operating temperature and the reducing nature of the fuel gas led to serious materials problems and despite very significant efforts by Baur and other researchers the search for suitable materials was unsuccessful.
This effectively hindered the development of the solid oxide fuel cells until the 1960s, when a first period of intensive activity in SOFC development began. Intensive research programs that were driven by new energy needs mainly for military, space and transport applications, addressed mainly the electrolyte conductivity improvement and the first steps in SOFC technology. A second period of intense activity began in the mid 80's and is still goes on today, where research focused on electrodes and technology.
Those research efforts have led the SOFC commercialization close to reality. Different companies have developed different concepts, and several demonstration units have been operated for significant amounts of times.

1.2.1.2. **Characteristics**

Advantages of the high operating temperature include the possibility of running directly on practical hydrocarbon fuels without the need for a complex and expensive external fuel reformer and purification systems. Internal reforming can be performed at high temperatures and SOFCs are not poisoned by CO, which can be oxidized at

the anode and act as a fuel. When practical fuel are used, the environmental impact is better than for combustion technologies, in the sense than less CO_2 and NO_x are produced per unit of power generated. Looking at the overall system efficiency, the high quality exhaust heat released during operation can be used as a valuable energy source, either to drive a gas turbine when pressurized or for CHP applications.
Originally, SOFCs have been developed for operation primarily in the temperature range of 900-1000°C, which is beneficial for the fuel reforming, electrochemistry kinetics and the added value of the exhaust heat. However, some important drawbacks stem from such elevated temperatures. The materials that can be used are limited with respect to their chemical stability in oxidizing and/or reducing environment and their chemical and thermo mechanical compatibility with adjacent components. Hence there are considerable investigations in lowering the operating temperature by 200ºC or more which allows the use of a broader set of materials, is less demanding on the seals and the balance-of-plant components, simplifies thermal management, aids in faster start-up and cool down, and results in less degradation of cell and stack component[2]. Because of these advantages, activity in the development of SOFCs capable of operating in the temperature range of 600-800°C has increased dramatically in the last few years. However, at lower temperatures, electrolyte conductivity and electrode kinetics decrease significantly.

In terms of applications, the length of time that is generally required to heat up and cool down the system restricts the use of SOFCs in applications that require rapid temperature fluctuations. This is a consequence of the need to use a relatively weak, brittle component as the substrate material and because of problems associated with thermal expansion mismatches. This restriction applies particularly for transport applications, where a rapid transport start-up is essential.

Reducing the cost of SOFCs is a crucial issue for their commercialization. Currently, the high cost-to-performance ratio limits SOFC introduction on the energy market. In this respect, lower operation temperature also makes possible the use of inexpensive metallic interconnections in place of lanthanum chromite-based ceramic interconnections.

1.2.1.3. **Design**

The solid state character of all SOFC components means that, in principle, there is no restriction on the cell configuration. Instead, it is possible to shape the cell according to criteria such as overcoming design or applications issues. As with other cell types, it is necessary to stack SOFCs to increase the voltage and the power produced. A stack can in principle comprise any number of cells depending on the desired power, and a fuel cell plant can be designed in modules of stacks in series- and parallel connections. To construct an electric generator, individual cells are connected in both electrical parallel and series to form a semi-rigid bundle that becomes the basic building block of a generator.

The most two common designs of SOFCs, the tubular and the planar, are represented in Figure 5. In the tubular cells, the cell components are deposited in the form of thin layers on a cathode tube. In the planar design, the cell components are configured as thin, flat plates. The interconnection which is ribbed on both sides, forms gas flow

channels and serves as a current conductor.

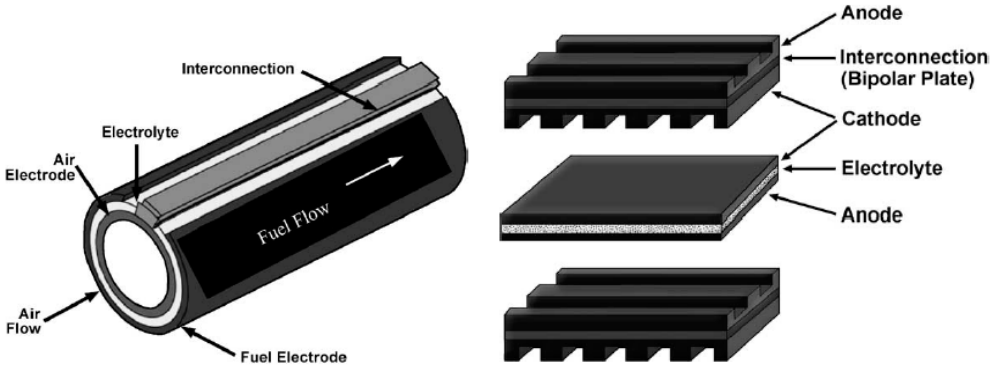

Figure 5: The two most common SOFC designs: tubular (left) and planar (right) [1].

Alternative designs have been proposed, such as the planar segmented design developed at Rolls Royce, or the SOFC roll developed at the University of St Andrews. The later is an innovative design that takes advantage of both planar and tubular designs.

1.2.2. Materials for SOFC

1.2.2.1. Electrolytes

The SOFC electrolyte materials were recently reviewed by Goodenough[10] and Skinner and Kilner[11], and are detailed in reviews addressing SOFCs[12,13]. Much of the research carried out on SOFCs in the 1960s focused on optimising the ionic conductivity of the solid electrolyte. Research on electrolyte materials is still active today, in an effort to lower operating temperatures.

The most commonly used electrolyte in SOFCs is Yttria-stabilized Zirconia (YSZ). This material possesses an adequate level of oxygen-ion conductivity and exhibits desirable stability in both oxidising and reducing atmospheres. Stabilized zirconia is usually non reactive towards other components used in the SOFC and has negligible electronic conductivity. It is also abundant, relatively low in cost and is mechanically strong whilst being easy to fabricate. The properties of stabilised zirconia have been extensively studied and several reviews dedicated to this material have been published[141516]. The most commonly used stabilizing oxides or dopants are CaO, MgO, Y_2O_3, Sc_2O_3 and certain rare-earth oxides. These oxides exhibit relatively high solubility in ZrO_2 which is stable over wide ranges of composition and temperature.
ZrO_2, in its pure from, does not serve as a good electrolyte because its ionic

conductivity is too low. The addition of certain aliovalent oxides stabilizes the cubic fluorite structure of ZrO_2 from room temperature to its melting point and, at the same time, creates a large concentration of oxygen vacancies by charge compensation according to the following equation (written for Y_2O_3 stabilization using Kroger-Vink notation):

$$Y_2O_3 \rightarrow 2Y'_{Zr} + V_O^{\cdot\cdot} + 3O_O^x \quad \textbf{(Equation 5)}$$

The high oxygen vacancy concentration gives rise to high oxygen ion mobility and leads to an extended oxygen partial pressure range of ionic conduction, making stabilized zirconia suitable for use as an electrolyte in SOFCs (the oxygen partial pressure range covers the conditions, 1 to 10^{-18} atm) to which a SOFC electrolyte is exposed in the fuel cell during operation. Oxygen-ion conduction takes place in stabilized ZrO_2 by movement of oxygen ions via vacancy. It is generally found that that the ionic conductivity is a maximum near the minimum level of dopant oxide required to fully stabilise the cubic phase. At higher dopant levels the ionic conductivity decreases. Typically, the level of Y_2O_3 present in YSZ is around 8 mol%.

The operating temperature is principally governed by the nature of the electrolyte, i.e. its ionic conductivity, and the thickness of the electrolyte layer. Indeed, the oxygen ionic conductivity for electrolyte materials σ is usually expressed as:

$$\sigma = \sigma_0 T^{-1} \exp(-E_{el} / RT) \quad \textbf{(Equation 6)}$$

For YSZ, $\sigma_0 \approx 3.6 \times 10^5$ S K/cm and $E_{el} \approx 8 \times 10^4$ J/mol [17].

Therefore, increasing the operating temperature or making thinner electrolyte layers can reduce the resistivity to oxygen ions transfer. Conventional zirconia based SOFCs generally require an operating temperature above 850 °C. This high operating temperature places severe demands on the material used as interconnects and for manfolding and sealing, and necessitate the use of expensive ceramic materials and specialist metal alloys. There is therefore considerable interest in lowering the operating temperature of SOFCs to below 700°C to enable the use of cheaper materials, such as stainless steel, and reduce fabrication costs, whilst maintaining high power outputs. Reducing the electrolyte thickness will obviously allow a reduction of the operating temperature but this approach is of course limited. The alternative route consists in developing new electrolyte materials showing higher conductivity than doped zirconia.

The search for, and study of, alternative solid electrolyte materials has been an active research area for many years. Figure 6 summarizes conductivity plots of different electrolyte materials that have been developed[13]. Among those various materials, two promising alternative electrolytes to YSZ are gadolinia-doped ceria[18,19] and lanthanum gallate based structures[20]. Both these electrolytes offer the possibility of lower temperatures operation for SOFCs between 500 and 700 °C. Scandia-doped zirconia has also received particular attention, since it has similar properties than YSZ but exhibits higher ionic conductivities, though it is also more expensive.

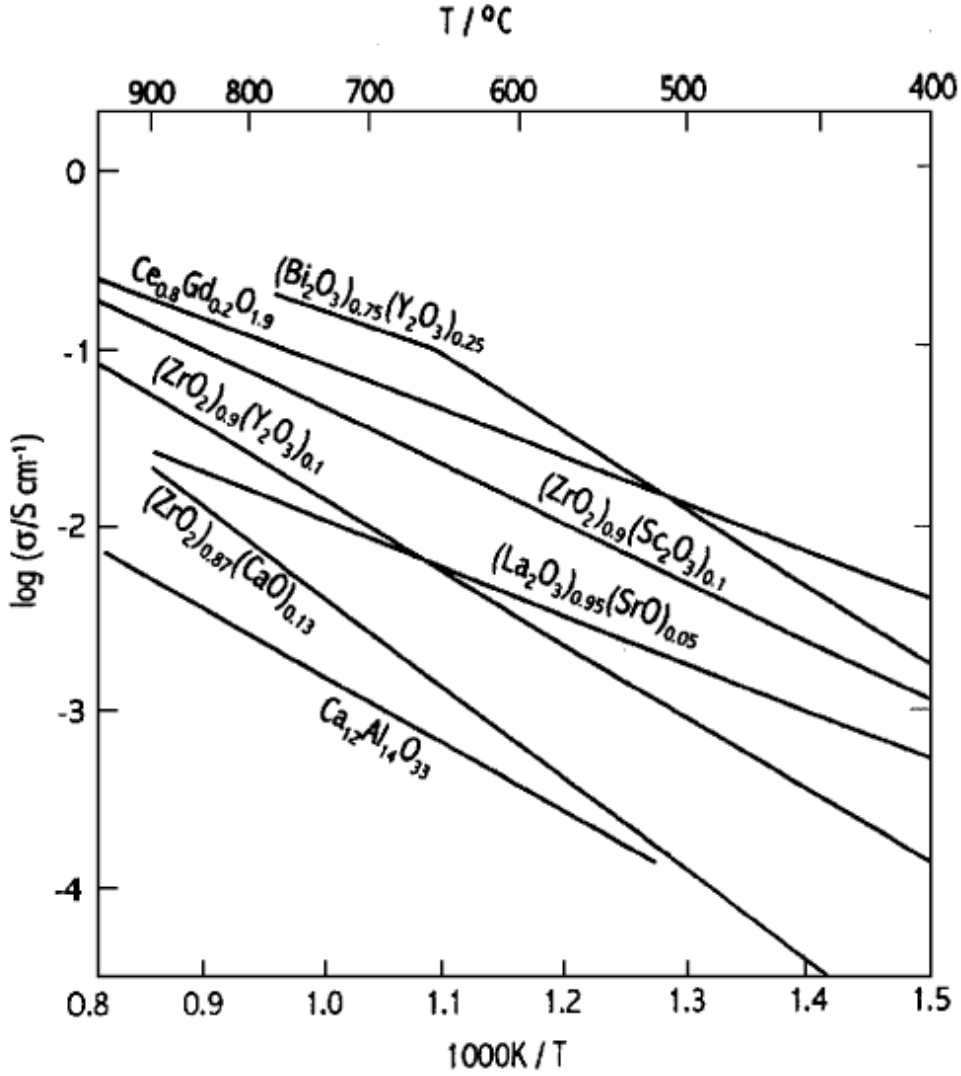

Figure 6: Specific conductivities of selected solid oxide electrolytes[13].

Gadolinia-doped ceria (CGO) offers an ionic conductivity substantially higher than YSZ. However, at elevated temperatures in a reducing atmosphere, such as that present at the anode, ceria undergoes partial reduction to Ce^{3+}, which introduces electronic conductivity that significantly lowers the efficiency of the SOFC, and also an undesirable structural change. Considerable effort has been devoted to minimizing the electronic conductivity of doped ceria under reducing conditions. One solution is to use an additional ultra-thin interfacial electrolyte layer which prevents electronic transport, and can suppress the reduction of ceria under reducing conditions.

Increased conductivity can be obtained from Lanthanum gallate, $LaGaO_3$ by substituting both the trivalent lanthanum and gallium with divalent cations, generally strontium and magnesium [18]. A favoured composition in terms of ionic conductivity is $La_{0.9}Sr_{0.1}Ga_{0.8}Mg_{0.2}O_{2.85}$. The ionic conductivity of LSGM, although significantly higher than YSZ, is slightly less than that of CGO at 500°C. However, the potential range of operating temperatures of LSGM is greater than CGO because it does not suffer from the problems exhibited by CGO at higher temperatures associated with electrolyte conduction. Thus, there is interest in the possibility of using LSGM at

temperatures around 600-700 °C, which are currently too low to obtain adequate power densities with zirconia based SOFCs. However, there are problems associated with the stability of certain compositions of LSGM. It has also proved difficult to prepare pure single phase electrolytes of LSGM, additional phases raising doubts over the long term durability of SOFCs with LSGM electrolytes, and much further research into this material is still required.

1.2.2.2. **Electrodes**

1.2.2.2.1 Requirements

Electrodes for SOFC must fulfil some important requirements to ensure high and durable power output. Electrodes serve to provide sites for electrochemical oxidation of the fuel (anode) and reduction of the oxidant (cathode). Since electrochemical reactions in a SOFC involve gaseous reactants, electrons and oxygen ions (Equations 1 and 2), reactions will occur only on sites possessing conductivities for those three phases. Those active sites, located at electrode-electrolyte-gas three-phase interface as depicted on Figure 7, are commonly referred to as the Triple Phase Boundary (TPB). Practical systems must be designed with an extended active surface area. To extend the TPB area, electrodes are fabricated as mixed ionic and electronic conductors (MIEC) porous ceramics or ceramic-metallic composites. The electrode microstructure provides interpenetrating, continuous three-dimensional electron, ion, and gas transport networks. The pore, metal, and ceramic phase typically occupy one third of the volume. An ideal microstructure would offer the highest triple phase boundary (TPB) length for electrochemical reactions, an optimized contact between the electrolyte and the anode, and be dimensionally stable during operation.

Chemical and thermal compatibility between electrode materials and the adjacent components is essential. No solid state reaction should occur between electrode materials and the interconnect or electrolyte, while thermal expansion coefficient of those materials should be close enough to allow stable long term operation. Electrodes must show high electrocatalytic activity toward oxidation/reduction of fuel/oxidant gases. High wettability with respect to the electrolyte surface is highly advantageous for competitive electrodes. Besides, ease of fabrication and low cost are of tremendous importance for a wide range of commercial applications. The ability to maintain the microstructure dimensionally stable over time is equally important. The high operating temperature can cause the microstructure to evolve with time with potential loss of connectivity in the conductive phases.

Other desirable properties include the tolerance to sulphur. This tolerance is required for the use of practical fuels such as natural gas that contain sulphur impurities. The ability to oxidize and reduce the anode regularly without modifying the electrode microstructure is highly desirable for practical systems.

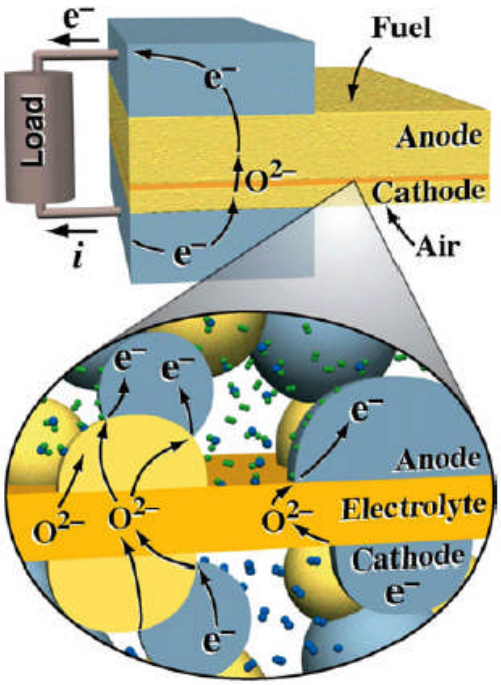

Figure 7: Illustration of fuel-cell chemical and transport processes in the three-phase regions[7].

1.2.2.2.2 Cathode Materials

Due to the high temperature of YSZ based SOFC, materials that can be used as cathode are limited to noble metals and electronic conducting oxides. Nobel metals such as platinum or palladium are unsuitable for practical applications due to prohibitive costs[12]. Several doped oxides and mixed oxides have been investigated[21,22]. The disadvantages of most of these materials are thermal expansion mismatch, incompatibility with the electrolyte, and lack of conductivity.

Doping $LaMnO_3$ with various lower-valence cations such as strontium, calcium, barium, nickel, or magnesium has been studied. Strontium-doped $LaMnO_3$ is currently the preferred cathode material in SOFC because of its high electronic conductivity in oxidizing atmospheres.

1.2.2.3. **Interconnects**

The interconnect in a solid oxide fuel cell stack is a very important component, which has two functions: firstly to provide the electrical contact between adjacent cells, and secondly to distribute the fuel to the anode and the air to the cathode [13]. This requires that the interconnect has a high electronic conductivity in both oxidizing and reducing atmospheres at high temperatures, must not react with any of the anode, cathode or electrolyte at the high operating temperatures, and it must be impermeable. These requirements severely restrict the choice of materials for the interconnect, especially at the higher operating temperatures of most zirconia-based SOFCs.

The vast majority of zirconia-based SOFCs use lanthanum chromite, $LaCrO_3$, as the interconnect. $LaCrO_3$ has a perovskite structure and is a p-type conductor, and satisfies all the above mentioned criteria. The electrical conductivity of LaCrO3 can be enhanced by substituting the La3+ with a divalent cation, such as strontium, calcium or magnesium. The main drawback associated with lanthanum chromite interconnect is their manufacturing costs.

For SOFC operating in the intermediate temperature range, 500-750 °C, it becomes feasible to use certain ferritic stainless-steel composites which fulfil the necessary criteria for the SOFC interconnect. The use of a metallic interconnect offers very substantial costs benefits compared to $LaCrO_3$ but their use is presently precluded in SOFCs operating at higher temperatures.

1.3. Thermodynamics of fuel cells

A comprehensive study of the fuel cell thermodynamics has been performed by Kee et al.[7]. The thermodynamic limit on fuel cell performance can be understood by considering the energy and entr

opy accounting associated with a generic steady flow process.

The rate at which work is done by a system, $\dot{W}$, can be obtained by combining the first and second law of thermodynamics, and equals:

$$\dot{W} = -\dot{m}(\Delta h - T_0 \Delta s) - T_0 \dot{P}_s \quad \textbf{(Equation 7)}$$

where $\Delta h = h_{out} - h_{in}$ and $\Delta S = S_{out} - S_{in}$ are respectively the net enthalpy and entropy differences associated with the flow streams entering and leaving the system. Entropy is produce within the system due to internal irreversible processes at a rate $\dot{P}_s$. Since $\dot{P}_s$ is required to be positive by the second law of thermodynamics, the greatest power is produced by a reversible process and equals:

$$\dot{W}_{rev} = -\dot{m}(\Delta h - T_0 \Delta s) \quad \textbf{(Equation 8)}$$

While this general expression applies to any steady-flow process, a relevant case for fuel cells is one in which the temperature remains fixed at T_0 and the pressure is constant, but the composition changes due to internal chemical reactions. In this case, the greatest work production rate achievable is:

$$\dot{W}_{rev} = -\sum_k \Delta\left(\dot{N}_k \, \mu_k \right) \quad \textbf{(Equation 9)}$$

where μ_k and N_k are respectively the species chemical potentials and molar flow rate, and the sum runs over all species. If depletion effects are small enough, so that $\mu_{k,in} = \mu_{k,out}$ and if $\dot{N}_k = \upsilon_k \dot{N}$ where μ_k is the stoichiometric coefficient of species k and N is a rate of progress variable for a global oxidation reaction, equation 3 reduces to:

$$\dot{W}_{rev} = -\dot{N} \sum_k \upsilon_k \mu_k \quad \textbf{(Equation 10)}$$

If the fluid stream is an ideal gas mixture, the reversible work production rate can be written as:

$$\dot{W}_{rev} = -\dot{N}\left[-\Delta G^0 - RT \ln \prod_k P_k^{\nu_k} \right] \quad \textbf{(Equation 11)}$$

where ΔG^0 represents the free-energy change between reactants and products in the global reaction, and p_k is the partial pressure. This expression also holds in the case where one or more reactants are supplied in separate streams. All that is required is to evaluate the partial pressures of each species in the stream in which it is present.

Since the cell potential can be expressed as $E_{cell} = \dot{W} / I$, equation 4 can be used to determine the reversible cell potential. The electric current generated in a fuel cell as a direct consequence of the reactions that result in oxidation of the fuel, is given by:

$$I = nF \dot{N} \quad \textbf{(Equation 12)}$$

where F is the faraday's constant and n the number of exchanged electrons.
Hence, the potential developed by a reversible cell is:

$$E_{rev} = -\frac{\Delta G^0}{nF} - \frac{RT}{nF} \ln \prod_k P_k^{\upsilon_k} \quad \textbf{(Equation 13)}$$

When using equation 4 accounting for the oxygen transfer, the reversible potential simplifies to:

$$E_{rev} = -\frac{RT}{4F} \ln \frac{P_{O_2(a)}}{P_{O_2(c)}} \quad \textbf{(Equation 14)}$$

This reversible potential is known as the Nernst potential and defines the fuel cell ideal difference of potential. This ideal potential depends on the electrochemical reactions that occur with different fuels and oxygen. The Nernst equation provides a relationship between the ideal standard potential E° for the cell reaction and the ideal

equilibrium potential (E) at other temperatures and partial pressures of reactants and products.

1.4. Fuel cell efficiency

Different efficiencies must be combined to produce the overall efficiency of a fuel cell. The overall efficiency is defined by the product of the electrochemical efficiency ε_E, and the heating efficiency ε_H. The electrochemical efficiency is in turn, the product of the thermodynamic efficiency ε_T, the voltage efficiency ε_V and the current or Faradic efficiency ε_J [1,7,23]:

$$\varepsilon_{FC} = \varepsilon_E \varepsilon_H = \varepsilon_T \varepsilon_V \varepsilon_J \varepsilon_H \quad \textbf{(Equation 15)}$$

1.4.1. Heating efficiency

The heating efficiency applies to cases where the fuel contains more species than the electrochemically active ones, such as gases, impurities and other combustibles. The heating value efficiency, ε_H, is defined as:

$$\varepsilon_H = \frac{\Delta H^\circ}{\Delta H_{com}} \quad \textbf{(Equation 16)}$$

where ΔH° represents the amount of enthalpy in the electrochemically active species and ΔH_{com} represents the amount of enthalpy included in all combustible species in the fuel gases fed to the fuel cell. A pure fuel will obviously give a heating efficiency of 100%.

1.4.2. Thermodynamic efficiency

The thermodynamic efficiency of a process measures how efficiently chemical energy extracted from the fuel stream is converted to useful power, rather than heat:

$$\varepsilon_t = \frac{\dot{W}}{\dot{W} + \dot{Q}} \quad \textbf{or,} \quad \varepsilon_t = \frac{\dot{W}}{\dot{m}\left|\Delta h\right|} \quad \textbf{(Equation 17)}$$

where Q is the heat rate production of the cell. Using the maximum work production rate achievable, which is the one of a reversible process (Eq. 8), one can write the maximum theoretical efficiency of a system as:

$$\varepsilon_t = \frac{\Delta(h - T_0 S)}{\Delta h}$$ **(Equation 18)**

The thermodynamic efficiency is an extremely important feature when analyzing a fuel cell. This efficiency justifies the need for fuel cell development. Indeed, since the chemical energy is transferred directly to electricity, the free enthalpy change of the cell reaction may be totally converted to electrical energy. In a conventional heat engine, where only the temperature is changes, ε_{rev} is limited to the familiar Carnot efficiency:

$$\varepsilon_{t,carnot} = 1 - \frac{T_0}{T}$$ **(Equation 19)**

For a constant-temperature fuel cell, the intrinsic maximum thermodynamic efficiency is given by:

$$\varepsilon_{rev} = \frac{\Delta G}{\Delta H} = 1 - \frac{T\Delta S}{\Delta H} = \frac{\Delta G^0}{\Delta H^0} + \frac{RT}{\Delta H^0} \ln \prod_k p_k^{\upsilon_k}$$ **(Equation 20)**

1.4.3. Current efficiency

The current efficiency can be commonly expressed as the fuel utilization efficiency. The efficiency of a SOFC drops if all the reactants are not converted to reaction products. For a 100% conversion of a fuel, the amount of current density, i_F, produced is given by the Faraday's law:

$$i_F = zF\left(\frac{df}{dt}\right)$$ **(Eq. 1)**

where (df/dt) is the molar flow rate of the fuel. For the amount of fuel actually consumed, the current density produced is given by:

$$i = zF\left(\frac{df}{dt}\right)_{consumed}$$ **(Equation 21)**

The current efficiency, ε_J, is the ratio of the actual current produced to the current available for complete electrochemical conversion of the fuel:

$$\varepsilon_J = \frac{i}{i_F}$$ **(Equation 22)**

This efficiency can be expressed as well in terms of fuel consumption:

$$\varepsilon_J = \frac{h_{in} - h_{out}}{h_{in} - h_{ox}} \quad \textbf{(Equation 23)}$$

where h_{ox} corresponds to the enthalpy change when all the useful fuel has been consumed.

1.4.4. Voltage efficiency

When an electrical current is drawn from a fuel cell, part of the chemical potential available must be used to overcome the irreversible internal losses. Hence, the actual cell potential is decreased from its equilibrium potential meaning that in an operating SOFC, the cell voltage is always less than the reversible voltage. The voltage efficiency, ε_V, is defined as the ratio of the operating cell voltage under load, E, to the reversible cell voltage, ε_R, and is given as:

$$\varepsilon_V = \frac{E}{E_r} \quad \textbf{(Equation 24)}$$

A voltmeter connecting the anode and cathode can measure the cell electrical potential E, which depends on the current flow. Indeed, many irreversibilities in a fuel cell scale with current density. If no current flows, the cell voltage is the open circuit potential or open circuit voltage (OCV). In most cases, the OCV will equal the potential developed by a reversible cell. The difference between the operating cell voltage and the expected reversible voltage is termed polarization or overpotential and is represented as η. This cell overpotential comprises the total ohmic losses for the cell, and the polarization losses associated with the electrodes. The useful voltage under load conditions can therefore be expressed as:

$$V = E^\circ - IR - \eta_{an} - \eta_{cath} \quad \textbf{(Equation 25)}$$

In this equation, I is the current passing through the cell. The electrical resistance R encompasses the ohmic resistance of all components. The polarization resistances, η_{an} and η_{cath} respectively for the anode and the cathode account for non ohmic losses in each electrode. The polarization loss of each electrodes are composed of: (i) activation overpotential due to energy barriers to charge transfer reactions, (ii) concentration overpotential associated with gas-phase species diffusion resistance through the electrodes, (iii) contact resistance which is caused by poor adherence between electrode and the electrolyte[7,24]. Although polarizations cannot be eliminated, accurate material choice and electrode designs can contribute to their minimization. Figure 8 shows a typical voltage-current polarization curve for a SOFC. The voltage loss increases with the current density. Activation overpotentials contribute the most at low current, while at high currents, concentration polarizations become important. Ohmic losses dominate the losses in the intermediate currents zone.

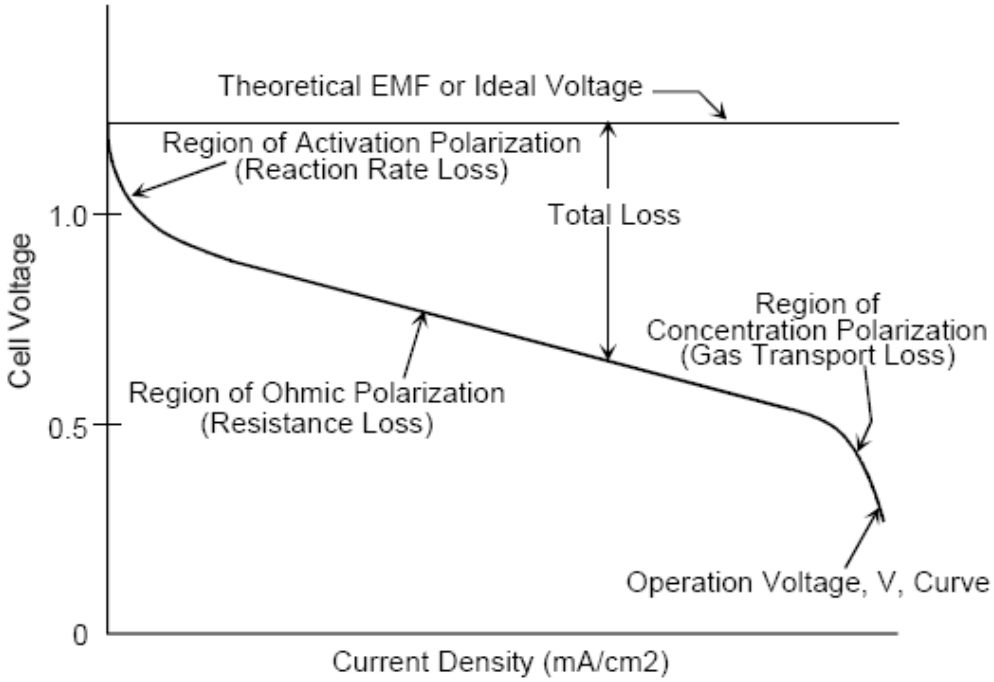

Figure 8: Ideal and actual fuel cell voltage/current characteristics[1].

The concave portion at low current density is corresponds to activation-related losses. When the current density increases, the losses are dominated by the ohmic polarization. When the current density approaches its highest values, losses are dominated by concentration polarizations that cause the concave drop in the cell voltage. Each one of those different types of losses is described hereafter.

1.4.4.1. **Internal resistance**

The size of the voltage drop due to ohmic losses is simply proportional to the current:

$$V=IR$$

The internal resistance R encompasses the contribution from the electrodes, electrolyte, interconnect and bipolar plates:

$$R=R_{Electronic} + R_{ionic} + R_{contact}$$

In most fuel cells, the electrolyte contribution to this resistance is the most important, due to the ionic nature of its conductivity. The interconnect and bipolar plates contribution can be important as well. To minimize the ohmic losses, the increasingly preferred practice is to fabricate dense, gas-tight electrolyte membrane as thin as possible.

1.4.4.2. **Charge transfer or activation polarization**

The activation polarisation is related to the charge transfer processes occurring during the electrochemical reactions on electrode surfaces. The losses are caused by the slowness of the reactions taking place on the surface of the electrodes. Electrochemical reactions involve an energy barrier that must be overcome by the reacting species. A proportion of the voltage generated is hence lost in driving the electron transfer. This energy barrier, called the activation energy, results in activation or charge transfer polarization, η_A. Activation polarization is related to current density, *i*, by the Butler-Volmer equation:

$$i = i_0 \exp\left[\frac{\beta_a \eta_A F}{RT}\right] - i_0 \exp\left[-\frac{\beta_C \eta_A F}{RT}\right] \quad \textbf{(Equation 26)}$$

where β is the symmetry coefficient and i_0 the exchange current density. The symmetry coefficient is considered as a fraction of the change in polarization which leads to a change in the reaction rate constant. The exchange current density is related to the balanced forward and reverse electrode reaction rates at equilibrium. A high exchange current density means a high electrochemical reaction rate and, in that case, a good fuel cell performance is expected.

The exchange current density can be determined experimentally by extrapolating plots of log i versus η to η=0. For large values of η (either negative or positive) one of the bracketed terms in equation x becomes negligible. After rearranging one obtains,

$$\eta_A = a \pm b \log i \quad \textbf{(Equation 27)}$$

which is usually referred to as the Tafel equation. Parameters *a* and *b* are constants which are related to the applied electrochemical material, type of electrode reaction and temperature.

The constant a (in the form v=a ln(i/io) is higher for an electrochemical reaction which is slow. The constant i_o is higher if the reaction is faster. The current density i_o can be considered as the current density at which the overvoltage begins to move from zero. The smaller is i_o, the greater is the voltage drop.

The exchange current density is a crucial factor in reducing the activation overvoltage. The cell performance can be improved through an increase of the exchange current density. This can be done in the following ways[1]:

- raising cell temperature
- using more effective catalysts
- increasing the roughness of the electrodes
- increasing reactant concentration, e.g. pure O_2 instead of air
- increasing the pressure

In low and medium temperature fuel cells activation overvoltage is the most important irreversibility and cause of voltage drop, and occurs mainly at the cathode. Activation overvoltage can be important at the anode when other fuels than hydrogen are involved.

1.4.4.3. **Diffusion or concentration polarization**

Concentration polarisation, η_D, is related to the transport of gaseous species through the porous electrodes and, thus, its magnitude is dictated by the microstructure of the electrode, specifically, the volume percent porosity, the pore size, and the tortuosity factor. It becomes imminent when the electrode reaction is hindered by mass transport effects, i.e., when the supply of reactant and/or the removal of reaction products by diffusion to or from the electrode is slower than that corresponding to the charging/ discharging current i. When the electrode process is governed completely by diffusion, the limiting current, i_L, is reached. In such a case, the demand for reactants exceeds the capacity of the porous anode to supply them by gas diffusion mechanisms. High tortuosity (bulk diffusion resistance) is often assumed to explain this behavior.

The voltage drop due to the mass transport limitations can be expressed as:

$$\Delta V = \frac{RT}{2F} \ln\left(1 - \frac{i}{i_l}\right) \quad \textbf{(Equation 28)}$$

where i_L is postulated to be the limiting current density at which the fuel is used up at a rate equal to its maximum supply speed. The current density cannot rise above this value because the fuel gas cannot be supplied at a greater rate.

[1] Fuel Cell Handbook, 7th edition, US Department of Energy (2004)
[2] S.C. Singhal, *Solid State Ionics*, 152-153 (2002) 405-410
[3] W.R. Grove, *Philos. Mag.* , 14, (1839) 127-30
[4] W.R. Grove, *phi. Mag.*, ser3., 21 (1843) 417
[5] L. Mond, C. Langer, *Proc. R. Soc. London.*, 46 (1889) 296
[6] N.Q. Minh, *J. Am. Ceram. Soc*., 76 (1993) 563-588
[7] R.J. Kee, H. Zhu, D.G. Goodwin, *Proceeding of the combustion institute*, 30 (2005) 2379-2404
[8] W. Nernst, *Z.Electrochem.*, 6, (1899), 41
[9] E. Baur and H.Z. Preis, Über Brennstoff-ketten mit FestLeitern, *Z. Electrochem.*, 43, (1937)727-32
[10] J.B. Goodenough, *Annual review of materials research*, 33 (2003) 91-128
[11] S.J. Skinner, J.A. Kilner, *mater. Today*, 6 (2003) 30-37
[12] N.Q. Minh, *J. Am. Ceram. Soc.*, 76 (1993) 563-588
[13] M. Ormerod, *Chem. Soc. Rev.*, 32 (2003) 17-28
[14] R.Stevens, *Magnesium Elektron*, London, U.K., (1986)
[15] .H. Etsell, S.N. Flengas, *Chem. Rev.*, 70 (1970)
[16] E.C. Subbarao, H.S. Maiti, *Solid State Ionics*, 11 (1984) 317-338
[17] K. Sasaki, J. Maier, *Solid State Ionics*, 134 (2000) 303-321
[18] M. Mogensen, N.M. Sammes, G.A. Tompsett, *Solid State Ionics*, 129 (2000) 63
[19] B.C.H. Steele, *Solid State Ionics*, 129 (2000) 95
[20] B.C.H. Steele, A.Heinzel, *Nature*, 414 (2001) 345
[21] N.Q. Minh, *J. Am. Ceram. Soc.*, 76 (1993) 563-588
[22] M. Ormerod, *Chem. Soc. Rev.*, 32 (2003) 17-28
[23] B. de Boer, PhD thesis, University of Twente.
[24] Fuel Cells Systems Explained; J. Larminie, A. Dicks; John Wiley & sons LTD.

GENERAL EXPERIMENTAL TECHNIQUES

This thesis is focused on the electrochemical performance of anodes for SOFCs. The research work carried out was divided into two distinctive parts: (i) a study of impregnated functional layers using thin electrolytes and (ii) a study of ethanol/steam mixtures performance on various types of anodes using thick electrolytes. The two sets of work used different types of sample, involving different preparation methods and testing systems. Experiments have been carried out both at The University of St-Andrews and The University of Pennsylvania. However, the focus being similar for the two sets of work, the same general experimental techniques were employed.

In this chapter, the main techniques employed throughout this work are presented. Two subsequent chapters are dedicated to the description of samples preparation and testing techniques relevant to each part of the work.

Electrochemical measurements

Two types of electrochemical measurements are commonly used to characterize the performance of fuel cell samples: polarization measurements, using a DC current, and impedance measurements, using an AC current.

Polarization measurements
Polarization measurements consist in applying a potential to the cell and read the current produced by the cell. When no current is drawn from the cell, the potential that can be read by connecting a voltmeter between the anode and the cathode is the Open Circuit Voltage (OCV). The OCV usually equals the theoretical potential provided by the Nernst equation. When a current is drawn from the cell, the potential is reduced due to the irreversibilities occurring in the cell. Sweeping the potential allows to plot current-voltage curves (referred to as IV curves in this thesis). A typical IV curve is represented on Figure 9. For each point of the IV curve, the product of the voltage by the current density will equal the power density, while the difference between the OCV and the voltage will equal the overpotentials. IV curves are plotted as a function of the current density (A/cm^2), meaning that the current is average by the cell active area.

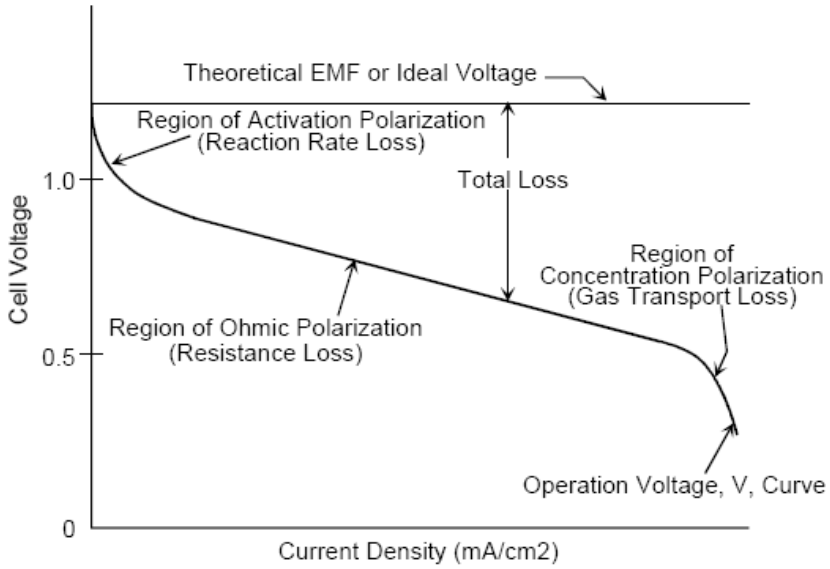

Figure 9: Typical IV curve for a fuel cell[1].

Impedance measurements

Impedance spectroscopy is a powerful tool in the analysis of solid-state systems. Like resistance, impedance is a measure of the ability of a circuit to resist to the flow of electrical current. Electrochemical impedance is usually measured by using an AC excitation voltage at different frequencies. The perturbation signal is applied to the electrochemical cell under consideration and the current response is measured.
The perturbation signal, expressed as a function of time (t) has the general form:

$$E(t) = E_0 \cos(\omega t)$$

The excitation signal used is small in amplitude, which allows the cell's response to be pseudo-linear. In linear or pseudo-linear systems, the current response to a sinusoidal perturbation will be a sinusoid featuring the same frequency but a different amplitude and a phase shift. The impedance is therefore expressed in terms of a magnitude, Z_0, and a phase shift, φ and is given by:

$$Z(\omega) = \frac{V(\varpi)}{I(\omega)} = \frac{V_0 e^{j\omega t}}{I_0 e^{j(\omega t - \varphi)}} = \frac{V_0}{I_0}(\cos\varphi - \sin\varphi)$$

The information on the impedance is obtained by reading the amplitude and the phase shift of the response current at a given frequency. A large frequency range is swept during a measurement, starting at high frequencies. Indeed, the different processes occurring in the system and contributing to the cell impedance feature different relaxation times. Hence, each of them will respond to the perturbation at a certain frequency.
The expression for Z(w) is composed of a real and an imaginary part. If the real part is plotted on the Z axis and the imaginary part on the Y axis of a chart, a "Nyquist plot" is obtained. On such plot, shown on Figure 10, the Y-axis is negative and each point is the impedance at one frequency.

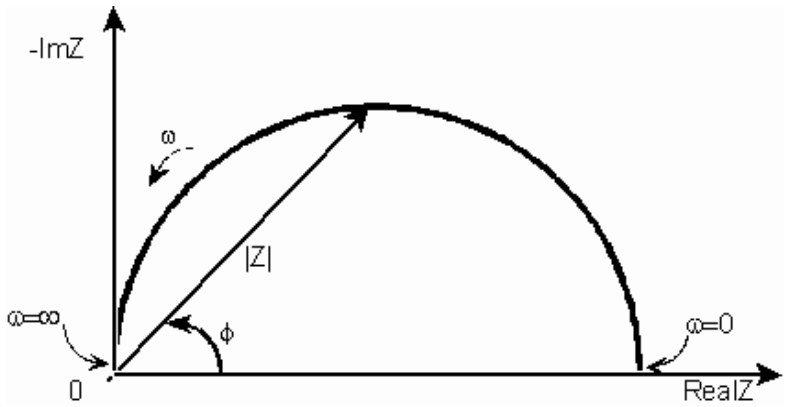

Figure 10: example of a Nyquist plot.

Such a measurement provides valuable information on the cell performance. The intercept of the impedance curve with the real axis at low frequencies provides the total cell resistance. Additionally, impedance measurements provide information on the ohmic and non ohmic contributions to the total cell resistance. The total ohmic resistance, which encompasses all conduction resistances, is given by the intercept of the curve with the real axis at high frequency. The balance to the total resistance corresponds to the total of the non ohmic losses in the cell. An impedance curve will typically show more than one arc, typically between 2 and 4.

Another common representation method is the "Bode plot". The impedance is plotted with log frequency on the x-axis and both the absolute value of the impedance and phase shift on the y-axis, as shown on Figure 11.

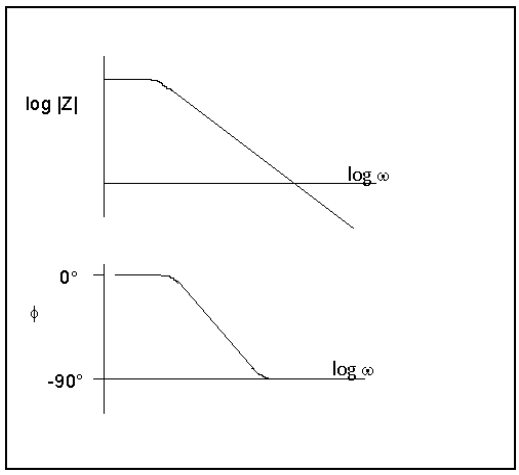

Figure 11: Bode representation of an impedance measurement.

Microscopy

The microstructure is a crucial factor in the understanding of SOFC electrode performance. Anode microstructures have been analyzed using Scanning Electron Microscopy (SEM). The scanning electron microscope is a type of electron microscope that scans the sample surface with a high-energy beam of electron. The interaction between the electrons and the atoms produces a signal that provides information about the sample's surface topography. A JEOL 5600, which employed a

secondary electron detector, was used to perform SEM studies of the fabricated SOFC anodes. An EDX system attached to the SEM was used to perform elemental analysis of electrodes.

[1] Fuel Cell Handbook, 7th edition, US Department of Energy (2004)

PART II

SOFC ANODE DEVELOPEMENT

REVIEW OF ANODE MATERIALS FOR SOLID OXIDE FUEL CELLS

This chapter reviews the different materials that have been investigated and used as SOFC anodes. The development and optimization of anode materials has been for many years, and remains today, an active and highly important concern within the SOFC research and development community. Those efforts have been reviewed in many articles published over the past few years[12345], showing the intensity of the research dedicated to anodes since Minh's review of the SOFC technology in the mid 90's[6].

The standard anode material used in SOFC is the Ni/YSZ cermet. Those cermets have been extensively studied and their performance optimized. Despite being used in most SOFC applications, they suffer from a few significant limitations. A severe limitation is their inability to operate on hydrocarbons, with the possible exception of methane diluted in large amount of steam. The ability to utilize directly practical fuels would greatly accelerate SOFCs commercialization. Hence, alternative anode materials are being developed to overcome Ni/YSZ cermets limitations and enable the direct use of hydrocarbons.

Anode materials are required to fulfill a number of requirements that have been specified in the introduction. As the main one, any anode has to be electronically conductive, and therefore contain a significant amount of an electronic conductive phase. This requirement precludes the use of precious metals for obvious economic reasons. Moreover, the high temperatures needed in an SOFC preclude the use of low-melting metals [2].

In the earliest SOFC developments, investigations have focused on single phase materials such as graphite, iron oxide, platinum group and transition metals[7,8]. Unfortunately, all-metal anodes have not found acceptance due to specific problems encountered for each of metal, which have been summarized in a recent review [2]. *Graphite is corroded electrochemically and platinum spalls off in service, presumably due to water-vapour evolution at the metal oxide interface. As for the transition metals, iron is no longer protected by the reducing activity of the fuel gas once the partial pressures of oxidation products in the anode compartment of an operating cell exceed a critical value, and it then corrodes with formation of a red iron oxide. Cobalt is somewhat more stable, but also more costly. Nickel has a significant thermal expansion mismatch to stabilized zirconia, and at high temperatures the metal aggregates by grain growth, finally obstructing the porosity of the anode and eliminating the three-phase boundaries required for cell operation.*

3.1. Ni-YSZ cermets

Nickel-zirconia cermets have been introduced by Spacil as a response to the failure of

all-metal anodes[9]. Ni constitutes the best transition metal option but all-nickel anodes suffer from two major drawbacks. First, Ni has a significant thermal expansion mismatch to stabilized zirconia, which can result in large stresses at the anode-electrolyte bound, causing cracking or delaminating during fabrication and operation[10]. Second, at high temperatures, the metal aggregates by grain growth finally obstructing the porosity of the anode and eliminating the three-phase boundaries required for cell operation. To address those two problems, Spacil associated, in the anode, nickel with the stabilised zirconia ceramic material of the electrolyte. YSZ acts as an inhibitor for the coarsening of Ni powders during both consolidation and operation, and therefore retains the dispersion of metal particles and the porosity of anode during long-term operation. Furthermore, the introduction of YSZ in the anode provides an anode thermal expansion coefficient acceptably close to those of other cell components. Indeed, the thermal expansion coefficient of nickel/YSZ cermet increases linearly with the nickel content[3].

Besides its structural functionality, YSZ offers a significant part of ionic contribution to the overall conductivity, thus effectively broadening the TPB length. Nickel serves as an excellent reforming catalyst and electrocatalyst for electrochemical oxidation of hydrogen. It also provides predominant electronic conductivity for the anode. Those cermets are chemically stable in reducing atmospheres at high temperatures. Ni and YSZ are essentially immiscible in each other and non-reactive over a wide range of temperature. More importantly, the intrinsic charge transfer resistance that is associated with the electrocatalytic activity at Ni/YSZ boundary is low[3].

Ni-YSZ cermets are currently the most common anode material for SOFC applications. A considerable amount of work has been dedicated to Ni-YSZ cermets optimization since the patent of Spacil, as detailed in many reviews addressing anode materials[1,2,3,4,5]. The optimization of Ni/YSZ cermets is achieved through the optimization of their microstructure. Indeed, the overpotential of Ni/YSZ cermets, as for any anode materials, is strongly related to the microstructural parameters. In the development of SOFCs, optimization of the microstructures to achieve low overpotential has been the subject of intense studies. An optimized microstructure of cermet electrode should show the highest TPB length so as to maximize the conversion from ionic current to electronic current. Besides, an optimized microstructure should have long range connectivity of respective ionic and electronic conductor chains stretching across the electrode and linking the current collector to electrolyte. There is also important consideration for efficient gas diffusion from the bulk into the reaction sites. This requires a properly designed electrode in terms of pore size and its distribution, porosity and the diffusion path. An example of optimized microstructure for Ni/YSZ cermets is shown on Figure 12 . Achieving anodes showing low overpotentials requires all processing variables to be optimized and meticulously controlled along with raw materials characteristics. Those variables include particles size, particle size ratio, Ni particles dispersion, Ni/YSZ volume ratio, use of pore formers, sintering temperature and sintering time as the main ones.

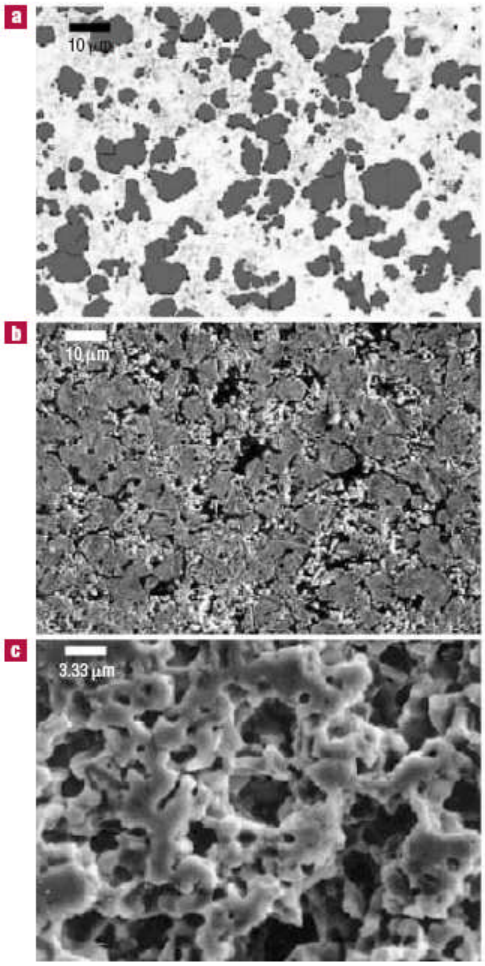

Figure 12: Image of a Ni/YSZ cermet by optical and scanning electron microscopy with elemental mapping. (A) Reverse-contrast optical micrograph, nickel distribution (dark); (b) Scanning electron microscope (SEM) of overall cermet morphology; (c) SEM after etching showing zirconia structural skeleton[11].

3.1.1. Fabrication

The non-reactivity and immiscibility of Ni and YSZ enable the preparation of cermets via conventional sintering. Nickel Oxide (NiO) and YSZ powders are homogenized by mechanical milling and mixing. The NiO/YSZ ink is then applied onto the electrolyte and sintered to form a porous cermet electrode. A general route for the preparation of Ni/YSZ cermets is shown on Figure 13.

The NiO is then reduced in situ to nickel metal when exposed to the fuel in the fuel cell. The reduced anode is more porous as a result of oxygen loss due to conversion of nickel oxide to nickel metal. During the reduction, the conductivity of the anode generally reaches a maximum very quickly then falls off slowly until a steady state is obtained[12]. The maximum occurs when enough NiO is reduced to form a conducting nickel-metal matrix; the fall-off corresponds to loss of nickel particle contact as the particles shrink due to further NiO reduction.

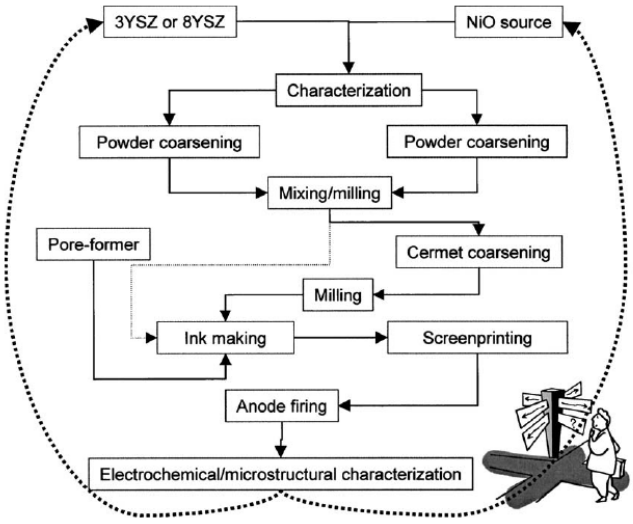

Figure 13: A general route for the preparation of Ni/YSZ cermet anodes based on conventional ceramics methods[4].

Limitations of the fabrication processes based on the conventional ceramic powder mixing process comes from the difficulties in achieving optimum phase distribution between Ni and YSZ particles. Several techniques have been developed to achieve better distribution between Ni and YSZ for the preparation of cermet anodes. The most notable one was based on electrochemical vapor deposition (EVD) developed by Westinghouse[13]. The anode is fabricated by slurry coating of nickel and YSZ incorporated into the Ni skeleton structure by EVD method. The morphology of YSZ intergrowth restricts grain growth and sintering of Ni particles and provides an effective pathway for oxygen ions from YSZ electrolyte to Ni phase. Other deposition techniques reported include sputtering[14], chemical vapor deposition (CVD)[15], a combined EVD/CVD process[15], polarized electrochemical vapor deposition (PEVD) [1617].

3.1.2. Starting powder

The impact of the starting powder on cermets performances has been reviewed by Jiang et al. [4]. The characteristics of the NiO and YSZ powders have significant effect on the fabrication process and the electrochemical performance of the Ni/YSZ cermet anodes. The properties such as the average particle size, the particle size distribution and shrinkage behavior (e.g. shrinkage and shrinkage rate) of NiO and YSZ powders are actually very different from suppliers. Figure 14 shows an example of particle size distribution of various commercial NiO powders, ranging from very fine and broad distribution to coarse and symmetric distribution[18].

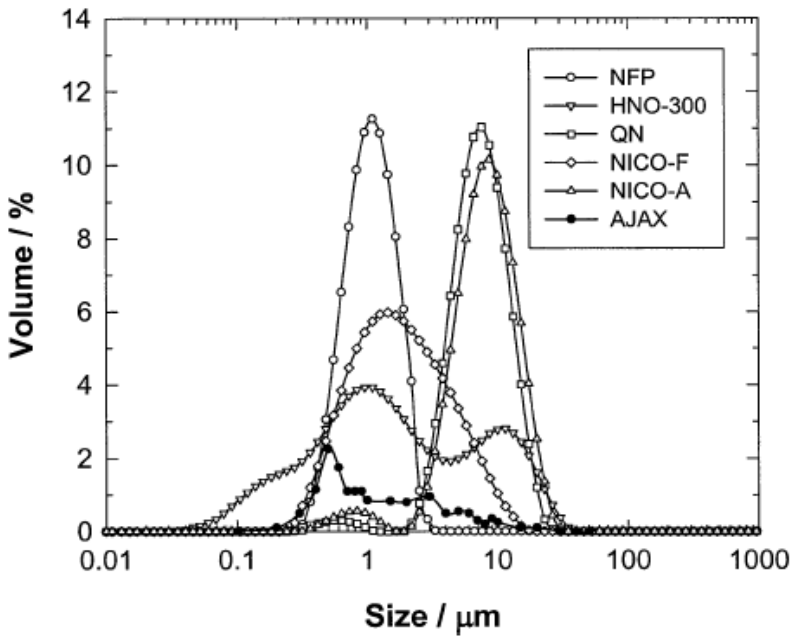

Figure 14: Particle size distribution of as-received commercial NiO powders. The particle size distribution was measured by laser scattering method [18].

Difference in the powder characteristics has a significant effect on the sintering behavior. Tietz et al. [19] evaluated eight different commercial NiO powders. The average grain size varied greatly from 0.5 to 14.7 μm with BET surface area from 0.2 to 47 m^2/g. Consequently, the sintering behavior differed significantly. The shrinkage of NiO powder ranged from 12 to 27 %. In general, high surface area corresponds to a high shrinkage and low starting sintering temperature. Similarly, the characteristics of the powder also vary considerably for commercial YSZ powders.

In the conventional powder mixing process, electrode performance is found to be affected by the initial particle size of YSZ and NiO powders. Hitika [20] showed that the electrochemical performance of Ni/8YSZ cermet anodes is related to the particle size ratio of the starting oxide powders. The minimum anode overpotential losses were obtained at initial 8YSZ/NiO particle size ratio of ~0.01. Murakami et al. [21] showed that YSZ particle size not only affects the electrode performance but also the stability and the volume concentration for the cermet. The larger the YSZ size is, the higher the YSZ content in the cermet will be required to achieve the best performance. The best performance was observed on the Ni/YSZ cermet anodes prepared from starting YSZ and NiO powders with particle size of 0.5 and 2.5 μm respectively, which corresponds to a particle size ratio of ~0.2. The results of those two studies are quite different but indicate that small YSZ/NiO ratios are preferred.

This impact of the starting powders characteristics on performance also means that comparison of results from different studies has to be proceeded carefully.

3.1.3. Sintering temperature

Sintering of the Ni/YSZ cermet coating at high temperature is essential to achieve high electrode performance and low electrode ohmic resistance. The formation of Ni-to-Ni electronic contact and YSZ- to-YSZ ionic contact networks are closely related

to the sintering temperatures of the anode. Jiang[22] has studied the effect of the sintering temperature. It appears that the lowest electrode ohmic and polarization resistance were observed for cermet anodes sintered at the highest temperatures, as seen from Figure 15. However, it was concluded from this study that 1400 °C was the optimum sintering temperatures for those conditions. This corresponds to the formation of good YSZ-to-YSZ network for the anodes sintered at high temperature. Figure 16 shows the SEM pictures of Ni/YSZ cermet electrodes sintered at different temperatures after fuel cell testing[23].

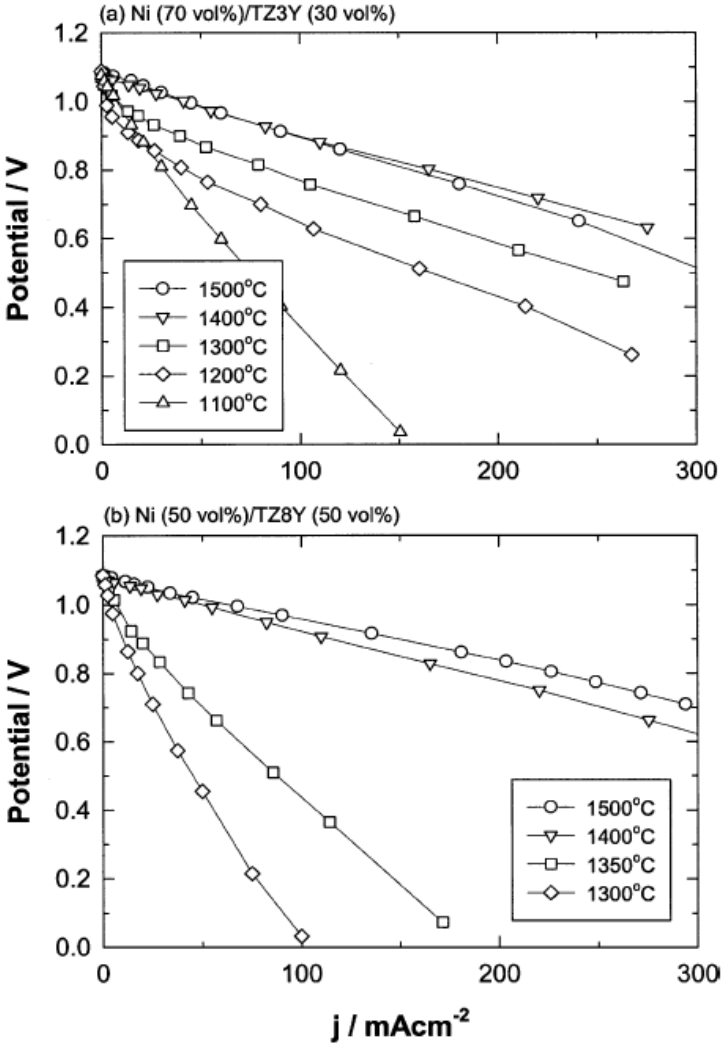

Figure 15: Polarization curves of Ni (50vol%)/8YSZ (50 vol%) cermet anodes sintered at different temperatures. Performances were measured at 1000 °C in 97%H_2/3%H_2O[22].

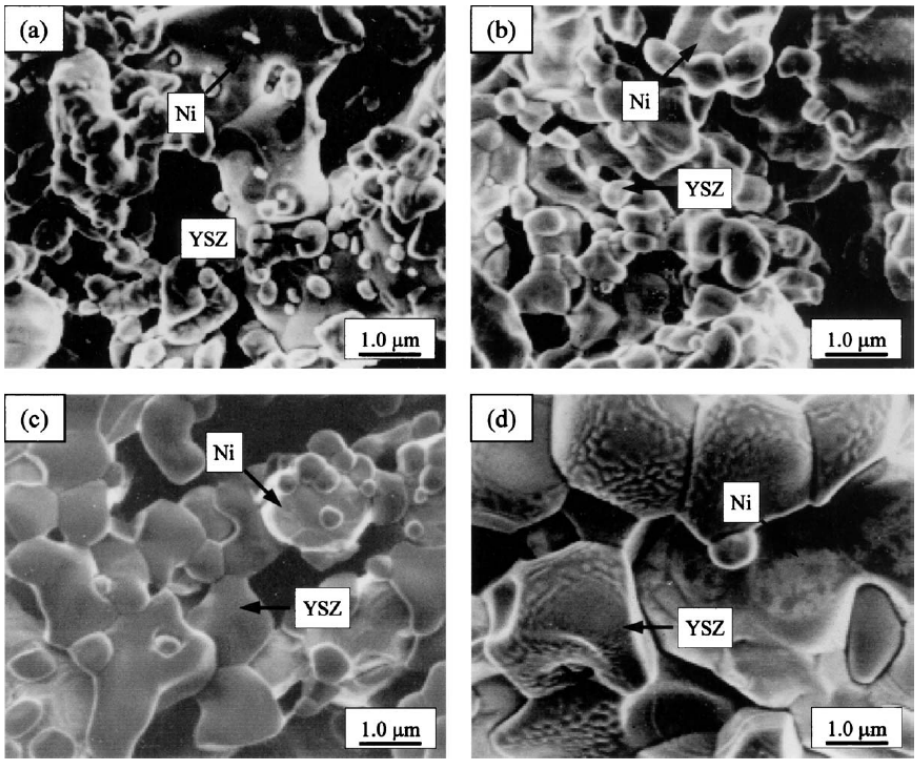

Figure 16: SEM pictures of Ni (50vol. %)/8YSZ(50 vol. %) cermet anodes sintered at (a) 1300 ºC, (b) 1350 ºC, (c) 1400ºC, (d) 1500ºC, after fuel cell testing[23].

These SEM pictures clearly show that applying higher sintering temperatures will generate bigger grains.

Another point worth noting is that high sintering temperature is essential to create a good bonding between the YSZ phase in the cermet and the YSZ electrolyte

.

Fuiki et al [24], studying anodes prepared by spray pyrolysis, noticed the same type of behavior, i.e. a decrease of electrode ohmic resistance and anode overpotential with increasing sintering temperature. The best performance was observed for anodes sintered at 1350 °C. A similar effect has been observed by Primdahl et al.[25]. Kawada et al.[26] have noted 1800 K as the optimum sintering temperature, with a precalcination step at 1700°K.

The sintering process will affect the porosity of the cermet. Studying the sintering conditions that give the desired porosity for the cermet, Lee et al.[27] obtained the best porosities with two different sintering conditions: (1400 degrees, 3 hours and 1500 degrees, 30 mins). However, it was stated in this work that 1400 °C was the best option due to concerns over the compositional variation due to evaporation of NiO at 1500 °C.

Those studies show clearly that a high sintering temperature is required for good cermet performances. The optimum sintering temperature appears to be either 1350 or 1400 °C, depending very likely on the powders used and pre-treatments. The sintering temperature should not be below 1600 K, which is the temperature at which YSZ particles begin to sinter. Good performances have been achieved using 1500°C or higher but the risk for NiO evaporation has been mentioned as a drawback. Along

with the sintering temperature, the sintering time appears to be an important parameter.

3.1.4. Electrical conductivity

The electrical conductivity of nickel/YSZ cermet is strongly dependent on its nickel content and a minimum metal proportion in the cermet is required for continuity of electronic conduction, whereas zirconia particles may be non continuous. Dees et al. [28] studied the relationship between the electrical conductivity and the volume fraction of Ni in the Ni/YSZ cermet measured at 1000°C. The conductivity of the cermet as a function of nickel content shows the S-shaped curved dictated by percolation theory, as depicted in Figure 17. The percolation threshold for the conductivity, which corresponds to the rapid rise in the electrical conductivity, is about 30 vol. % nickel. Figure 17 clearly shows that the percolation threshold depends on the sintering temperature. Increasing the sintering temperature results in lower percolation threshold, which might be due to the decreased porosity as well as narrowed pore size distribution.

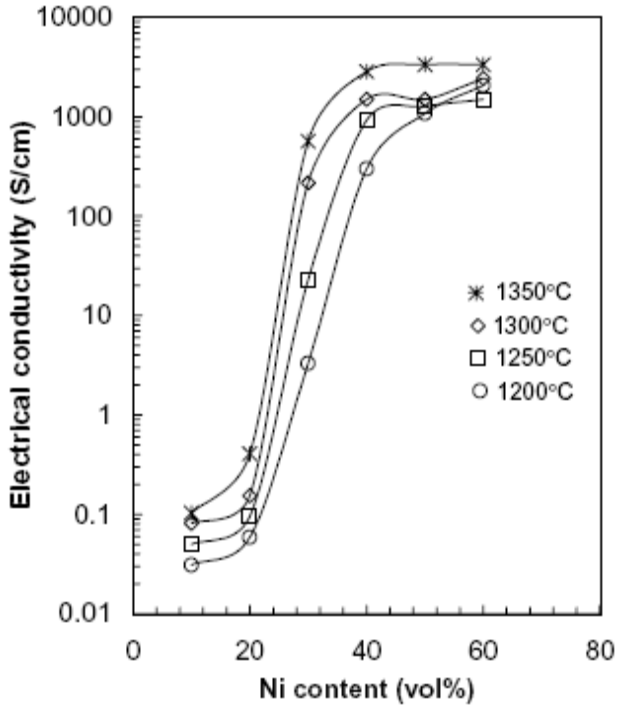

Figure 17: Conductivity of nickel/ZrO_2 cermet as a function of nickel content (T=1000°C) [28].

The percolation behavior is explained by the presence of two conduction mechanisms through the cermet, namely an electronic path through the nickel phase and a ionic path through the YSZ phase. Below about 30 vol% nickel, the conductivity of the cermet is similar to that of YSZ, indicating an ionic conduction path through the YSZ phase. Higher than about 30 %, the conductivity is about 3 orders of magnitude higher, corresponding to a change in mechanism to electronic conduction through the nickel phase. The percolation threshold is revealed to be influenced by many variables such as the porosity, pore size, size distribution, particle size ratio and size

of raw powders as well as contiguity. The electrical behavior of Ni/YSZ cermet is therefore strong function of these factors [2930] .It was noted that larger Ni particles give rise to larger threshold [31].

The conductivity is dependent on its microstructure (support surface area). At the same nickel volume percent, a support with lower surface area has a better nickel coverage, resulting in improved nickel particle to particle contact, thus higher conductivity for the cermet [4].

The electrical conductivity of Ni/YSZ anodes is also dependent on the particle size and particle size distribution, as for the conductivity threshold. Tietz et al.[32] studied the electrical conductivity of the Ni/YSZ cermet anodes prepared from different commercial NiO powders. The electrical conductivity measured at 800 °C varies between 300 S cm^{-1} to 4000 $S.cm^{-1}$ with the highest conductivity obtained on NiO powder with small grain size. Tintinelli et al. [33] have shown that the electrical conductivity increases with the YSZ/NiO ratio. Additionally, a broader size spectrum of YSZ powders shows improved packing efficiency, and hence enhanced electrical conductivity. However, coarse YSZ particles seem not to be recommended. Indeed, they are more likely to show large shrinkage, which can potentially cause macro cracks and rapid degradation of the cell [34]. From an electrocatalyst point of view, another likely consequence of using coarse YSZ powder is the decline in TPB area, thus driving up the activation polarization. The conductivity of the cermet is also dependent on its microstructure (support surface area). At the same nickel volume percent, a support with lower surface area has a better nickel coverage, resulting in improved nickel particle to particle contact, thus higher conductivity for the cermet [4].

As a compromise, in order to achieve a high conductivity and hence an excellent cell performance along with a low overall cell shrinkage, a novel conceptual microstructure that is composed of coarse YSZ, fine YSZ and NiO has been proposed[35]. Even with a fixed overall YSZ concentration (60% vol.), the electrical conductivity is found to be profoundly altered as a function of coarse YSZ content as illustrated in Figure 18.

The incorporation of fine YSZ particles seems to lead to the development of a more stable anode without sacrificing the electrical conductivity. More electrochemically active sites are introduced, contributing to a considerably suppressed polarization resistance[36].

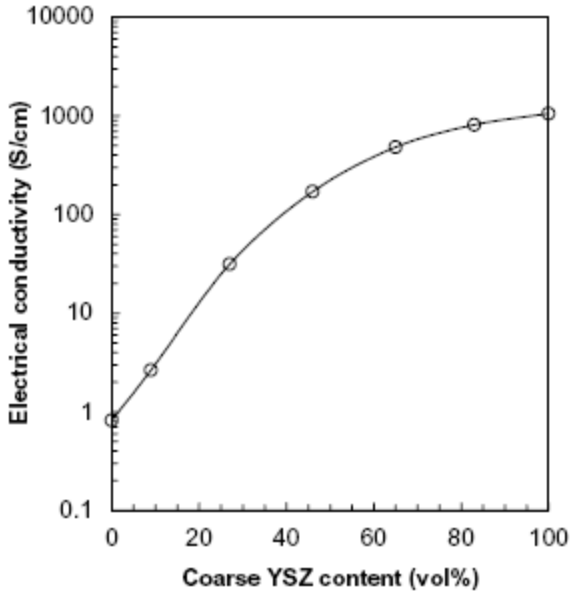

Figure 18: Electrical conductivity measured at 1000°C of Ni/YSZ cermet containing both coarse and fine YSZ particles as a function of coarse YSZ content of total YSZ[35].

The major advantage of this new anode over conventional one is long-term stability during SOFC operation as shown in Figure 19:

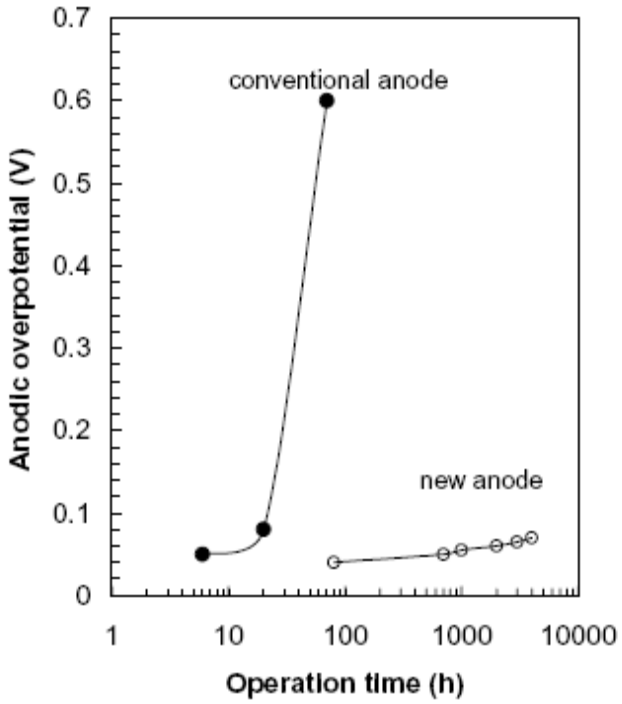

Figure 19: Comparison of polarization resistances at 0.2 A.cm-2 for the conventional and new anodes; the conventional anodes is a cermet of Ni with one type of YSZ ceramic, whilst the new anode consists of Ni, fine and coarse YSZ powders[36].

3.1.5. Degradation

In the development of SOFC anodes, the structural integrity and long term performance stability of Ni/YSZ cermet are critical issues. In long term operation, degradation of the cermet structure induces an increase of overpotentials which in turn decreases the performance of the fuel cell system. As far as the Ni/YSZ cermet anodes are concerned, the most predominant microstructure change is the agglomeration and coarsening of Ni phase. Jiang et al.[4] advanced the poor wettability between the metallic Ni and YSZ oxide phase to explain the agglomeration. The agglomeration of the Ni phase in the cermet leads to the reduction of the TPB length and therefore increases in the polarization resistance. The loss of Ni through volatile nickel hydroxide species can also contribute to the cell performance degradation.

A study carried out by Simwonis et al.[37] illustrates the changes that can occur in Ni/YSZ cermet. Structural changes were studied on 40/60 vol% Ni/YSZ cermet anodes substrates exposed to humidified Ar/4%H_2/3%H_2O atmosphere at 1000 °C up to 4000 h. The distribution of Ni, YSZ and pores of polished cross-sections of the substrate were evaluated by quantitative image analysis. After annealing for 4000h, the average particle size increased from 2 to 2.57 μm and the number of Ni grain counts decreased from 3421 to 2151. As a result, the electrical conductivity of the anode substrates decreased by 33% due to decreased electronic Ni-to-Ni contacts. There was no change in YSZ particle size distribution as expected.

Iwata [38] studied the microstructural change of Ni/YSZ cermet electrodes operating at 0.3 A.cm-2 and 1000°C. Ni particle size increased from 0.1-1 to 1-10 μm after 1015 h of operation and the specific area of the cermets was decreased by half. The performance degradation rate was 14mV over 1000 h. The main reason advanced by this degradation was the decrease of the contact area at the electrode/electrolyte interface.

High current density and high fuel utilization can cause the agglomeration of originally fine dispersed Ni in the Ni/YSZ cermet anodes, as shown by Muller [39].

As outlined by Jiang et al. [4], the structural stability of Ni/YSZ cermet anodes is critically dependent on the Ni content and Ni and YSZ phase distribution in the cermet. The uniform distribution and homogenization of NiO and YSZ phase in the preparation of NiO/YSZ cermets through ball milling and deagglomeration are effective in improving the stability of the anodes.

3.1.6. Porosity

It is estimated[34] that more than 30% by volume, of continuous porosity is required to facilitate the transport of reactant and product gases. The porosity in a Ni/YSZ cermet is created by the reduction in-situ of NiO particles and can be further increased by the

addition of pore formers. Figure 20 shows the changes in the cermet morphology induced by the reduction of NiO particles to Ni.

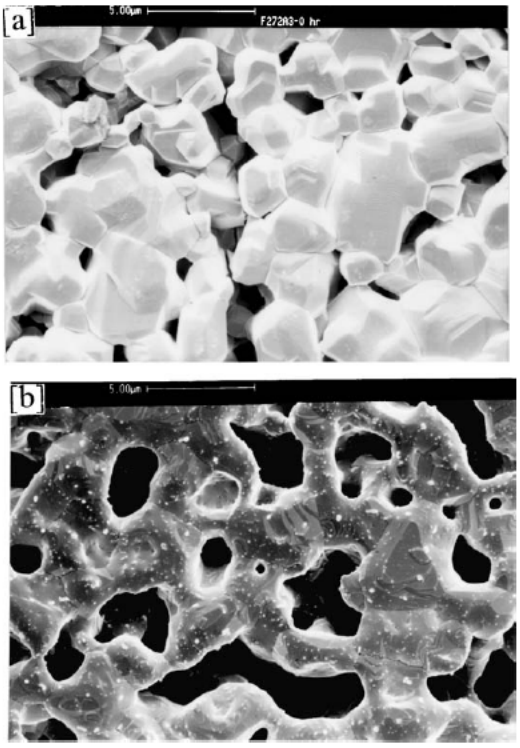

Figure 20: Change of the morphology of Ni anode before and after exposure in humidified 10% H_2/90% N_2 for 1h at 1000°C [4].

The porosity is affected by volume fraction of Ni in the cermet as there is a volume reduction of 25% when NiO is reduced to Ni metal under fuel environment. In general, the porosity increases with the increase in the Ni volume fraction and for Ni/YSZ, a typical porosity of 35% was found for Ni(40%vol)/YSZ(60%vol) and 42% when Ni content increased to 70% [40]. On the other hand, the porosity has a strong effect on the electrical conductivity through its impact on the Ni-to-Ni connectivity.

The porosity and pore morphology can also be controlled and increased by adding pore formers such as carbon fiber, graphite, polystyrene or PMMA. Addition of pore formers with geometric anisotropy such as graphite and carbon fiber can result in the formation of anisotropic porous structure on the Ni/YSZ cermets. The effect of potential anisotropy has been measured[41] . The electrical conductivity of Ni/YSZ with anisotropic porous structure was found in the range of 150 to 600 $S.cm^{-1}$ as compared to 1600 $S.cm^{-1}$ for the cermet with isotropic structure measured at 800°C. This shows that porous structure also has significant effect on the electrical conductivity of the Ni/YSZ cermet anodes in addition to the porosity.

3.1.7. Relation between microstructure and overpotential

The overpotential is found to be enormously dependent upon the content of Ni powder, the characteristics of starting raw material as well as the processing approach.

Besides electrical conductivity, activation and concentration polarizations can be optimized through a controlled microstructure. Optimising the distribution of Ni particles in the anode layer would increase the amount of electrode reaction site, i.e. the length of TPB in addition to the formation of the current path. A network of micropores in the anode is required to provide a diffusion path for gaseous reactants and products. These functions depend strongly on the morphological features of the anode.

The effect of Ni content on anodic overpotential is well documented [42,43,44]. It is revealed, in two of those studies [42,43] that as long as the Ni concentration falls into the range 40-45%, in this particular experimental condition, a minimum overpotential is achieved over entire current density range studied. This presumably corresponds to the enlargement of three-phase boundaries were anode reaction takes place. The same trend as been outlined by Koide et al.[45]. This study shows that the polarization resistance reaches a minimum value at approximately 40 vol% Ni, whereas the internal resistance decreases monotonically with the increase in Ni content, as shown on Figure 21.

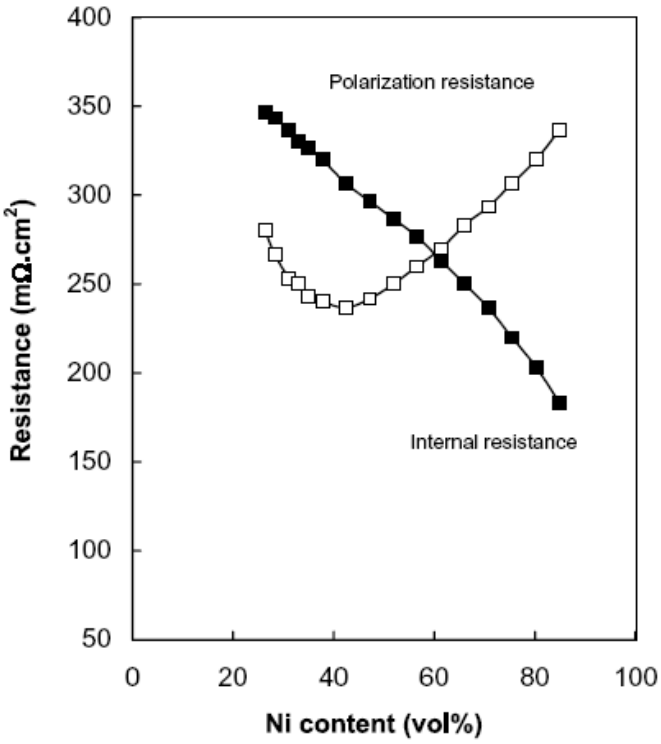

Figure 21: Effect of Ni content on the polarization and internal resistances of Ni-YSZ anodes, 200 mL.mn^{-1} of hydrogen as anode gas, 1000 ml min^{-1} of oxygen as cathode gas[46].

Besides, the overpotential is influenced as well by extrinsic factors such as fuel composition and gas flow rate. The study carried out by Koide et al. [41] points out that internal electrical resistance of Ni/YSZ anode itself is negligibly small owing to its fairly high electrical conductivity with predominant electronic contribution, and electrical losses in of such anode in a single cell stem primarily from contact resistance and polarization resistance.

In the same study, a linear relation between the IR resistance and the reciprocal contact area. This figure suggests that contact resistance between the electrolyte and Ni/cermet dominates IR resistance.

From their results, Koide et al. have proposed a double layer which consists of an interfacial layer and a bulk layer. A bulk layer of 40:60 was used to minimize the polarization resistance and interfacial layer showing high Ni content, 61:39, was applied to reduce the IR resistance. The result is interesting since the bi-layer cell shows the polarization resistance of the bulk layer and the IR resistance of the interfacial layer which was the desired performance. Moreover, a long-life test of a cell, with the double layer anode over 8000 h was carried out with a fuel utilization of 80%. There was very little changes in the cell voltage, which indicates a stable performance with the double layer.

Comparison of studies of anodes fabricated using two different processing methods clearly illustrates that undesirable microstructure such as anisotropic particle packing, insufficient porosity, poor connectivity of conducting or pore phases contributes to drastically reduced cell performance. This indicates that the electrochemical reaction process dominating the overpotential is related to the reaction involving H_2O.

3.1.8. Multilayer cermet anodes

Multilayer anodes seem to be an interesting way to increase anode performances. Some attempts can be found in the literature where multilayer anodes have been proposed to minimize both the concentration and activation polarization[43] and to improve the long term stability[40]. It should be remembered here that in cermet anodes, the TPB extends to about 10-20 μm from the electrolyte.

A two layered-anode structure for the anode supported solid oxide fuel cell has been proposed by Virkar et al.[43]. By controlling the slurry formulations, the microstructure of the interlayer is made finer than that of outer support layer in terms of volume percent porosity, pore size and its distribution. The coarse outer layer facilitates rapid transport of fuel gases into and removal of reactant gases out of anode so that the concentration polarization can be retarded. The fine interlayer is intended to maximize the Ni/YSZ/gas triple boundary area so that the number of electrochemical reaction sites can be multiplied and activation polarization can be lowered.

The development of a multilayer Ni-YSZ cermet anode has also been studied by Muller et al.[47]. Single layer nickel/YSZ cermet anodes may show high degradation during long-term operation that can be ascribed to the agglomeration of Nickel particles. This leads to a loss of electrochemical active area and therefore an increase of the polarisation resistance. To circumvent this problem, a multi layer anode could be used, which should have a gradient in particle size and Ni content and therefore a gradient of porosity, electrical conductivity, and coefficient of thermal expansion. The first layer close to the electrolyte (the electrochemical active part) should consist of small particles of both Ni and YSZ in order to have a long TPB and therefore a small polarization resistance. The CTE should be as close as possible to that of the electrolyte to prevent delamination of the anode. The top layer should have a high

amount of larger Ni particles in order to have a good electrical contact with the interconnect and high porosity to enable fast transport of fuel and exhaust gas. This layer acts as current collector and gas distributor. This way, the anode can fulfill the local different requirements and the gradient is realized by three homogeneous functional layers. Figure 22 shows a schematic representation of such a layer.

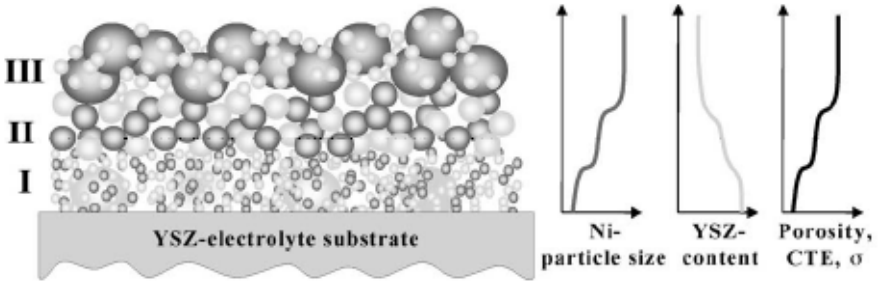

Figure 22: illustration of a multilayer anode with gradients in composition and microstructure. As a consequence of the diverse functional layers the physical properties (CTE, porosity, etc.) of the anode also vary[47].

As an example, a new configuration of anode has been put forward that comprises a double cermet layer with varying Ni contents. An interfacial layer rich in Ni (Ni:YSZ ratio 61:39) is employed in intimate contact with the electrolyte, on top of which a bulk layer (Ni:YSZ ratio 40:60) is coated. It has been tested that an anode like this exhibits the optimum performance, since there is little degradation in regards to voltage output after 8000h operation[39].

3.1.9. Limitations of Ni/YSZ cermets

Although being the current standard material for SOFCs anodes, Ni/YSZ cermets present significant limitations, especially when it comes to the use of fuels other than hydrogen.

The first drawback presented earlier comes from the coarsening at operating temperatures which hinders optimal performance to be kept during long runs. More importantly, when hydrocarbon fuels are involved, Ni/YSZ anodes suffer from coking. Direct oxidation of dry hydrocarbons and CO result in rapid anode failure due to carbon deposition. Although nickel is an excellent hydrogen oxidation and methane-steam-reforming catalyst, it also catalyses the formation of carbon filaments from hydrocarbon under reducing conditions. The mechanism involves carbon chemisorption on the nickel surface, carbon dissolution into the bulk nickel, and precipitation of graphitic carbon from some facet of the nickel particle after it becomes supersaturated in carbon[48]. Formation of carbon deposits is responsible for excessively high activation polarization, which leads to rapid deterioration of the cell performance. Besides carbon poisoning, another prominent drawback is the poor sulfur resistance of those cermets [49,50,51].

Another limitation of Ni/YSZ cermets is the TPB length, which is limited to a 10-20 μm thick layer. Any anode suppressing this limitation, by offering an extended TPB length compared to the one featured by Ni/YSZ would offer an interesting alternative to standard cermets. In this respect, any anode materials that would feature both

electronic and ionic conduction, alongside a good electrocatalytic activity would be a significant improvement.

3.2. Alternative anode materials

The important limitations from which Ni/YSZ cermet anodes suffer have led to a great deal of research efforts to find alternative anodes. The possibility to use practical fuels in SOFCs, without the need of a pre reforming step, could greatly accelerate their commercialization. Besides, the ability to operate reduction and oxidation cycling of the anode would be a definite advantage for the development of practical systems. Therefore, most research aimed at overcoming the limitations of nickel-based anodes has focused on the development of alternative anode materials that are catalytically active for the oxidation of methane and higher hydrocarbons, and inactive for cracking reactions that lead to carbon deposition. Other targeted properties are structural stability over time, insensitivity for redox and thermal cycles and high electronic conductivity. The modification of Ni/YSZ cermets, either by doping or addition of an extra phase, has been attempted but most of the research dedicated to alternative anodes has focused on the development of nickel-free anodes.

The inactivity towards cracking reactions is difficult to obtain and this requirement rules out most transition metals with the possible exception of Cu, Ag and Au[2]. Although these metals make good current collectors, they are not highly active oxidation catalysts. As many metal oxides are not active for hydrocarbons cracking and are less likely to suffer from sulfur poisoning than Ni/YSZ anodes, most of the work in this area has focused on the development of electronic or mixed electronic-ionic conducting (MEIC) single oxides. The mixed conductivity is an attractive feature that can potentially extend the TPB area to the whole anode surface area, as compared to Ni/YSZ cermets where the TPB area is limited. This however requires the oxide to have sufficient conductivities (both ionic and electronic) and to display a high enough electrocatalytic activity. Finding a single material that gathers all required properties has proven to be a difficult task. Therefore, alternative designs are often made of porous composites.

An important drawback of MIEC can be their low electronic conductivities which hinders efficient current collection. The target for electronic conductivity for anode materials is often set to be 100 S/cm, but the actual requirement depends on the cell design, and particularly the length of the current path to the current collection location. Thus, the requirement can be relaxed down to about 1 S/cm for well distributed current collection[2].

A number of MIEC materials have been investigated as potential anode material. Most research has been done on Ceria, both undoped and doped, transitional metal perovskites, such as doped $LaCrO_3$ or $SrTiO_3$, and fluorite related-structures, such as Ti doped YSZ. The chemical stability under reducing conditions is essential, meaning that oxides containing large amounts of Co and Ni are probably not viable. Hence, the emphasis is on Fe, Mn, Cr and Ti as transition metal ions that can give electronic conductivity.

3.2.1. Modified Ni/YSZ anodes

The first approach that has been investigated in the search for alternative anodes is the modification of conventional Ni/YSZ cermets anodes. Incorporation of various dopants into the cermets can improve their reforming activity, resistance to coke formation and tolerance to sulfur [4].

Takeguchi and coworkers[52,53,54] have performed a series of studies on the modification of Ni/YSZ cermets, looking at the carbon deposition during steam reforming of methane. Ni/YSZ cermet anodes were modified with alkaline earth addition of MgO, CaO, SrO and CeO_2. The study concluded the carbon deposition was suppressed by the addition of CaO, SrO and CeO2 while MgO addition promoted the carbon deposition rate and decreased the steam reforming activity of the anodes. On the other hand, it was demonstrated that high content (~2 wt. %) of SrO and CeO_2 in the Ni/YSZ cermets also significantly reduced the steam reforming activity. Further studies concluded that Ru and Pt addition to Ni-YSZ cermet could also promote steam reforming of CH_4 and suppress the deposit formation. Addition of small quantities of molybdenum (~1%) was reported to significantly reduce the carbon deposited on Ni/YSZ cermets during methane reforming[55].

Sato et al.[56] have studied Ni-Co/YSZ cermet anodes for the oxidation of H_2 and CH_4. The optimal composition reported was $Ni_{0.5}Co_{0.5}$/YSZ, and Co incorporation led to an increase in fuel cell performance with CH_4 but had little effect on operation with H_2. However, polarization resistances reported on H_2 were lower than those reported by Ringuede et al[57], in their study of Ni-Cu/YSZ and Ni-Fe/YSZ cermets for H_2 oxidation reaction in wet H_2. Carbon deposition and CH_4 oxidation on Ni-Cu/YSZ alloys have been studied as well by Kim et al. [58]. Carbon was found to deposit on such Ni-Cu alloys, although a reduction of deposits was observed as the Cu content increased. However, a similar anode, in which YSZ was replaced by GDC[59], has been reported to show no carbon deposition after operating in dry CH_4 for 40H at 800ºC.

3.2.2. Cermet anodes

3.2.2.1. Cu/Ceria based anodes

Gorte and coworkers [60,61,62,63,64,65,66,67,68] have successfully synthesized and demonstrated Cu-based SOFC cermet anodes for direct electrochemical utilization of a large variety of hydrocarbon fuels with little carbon deposition. Cu has been proposed to replace Ni as an electronic conductor in the anode due to its poor catalytic activity for C-C and C-H bond activation, which therefore inhibits carbon formation but means copper does not serve as a catalyst. Hence, Cu-YSZ anodes produced poor performances[60], and ceria was added to catalyze the reaction of hydrocarbon fuels, which considerably increased the cell performances. Ceria is indeed known as one of the best oxidation catalysts (excluding metal catalysts) and introduces both ionic and

electronic conductivity[60]. The effect of lanthanide additives on the Cu-YSZ anodes was also studied but the performance was below Cu/Ceria anodes[61].

An important limitation when using copper is the relatively low melting temperature of its oxides: 1235°C for Cu_2O and 1326°C for CuO. CuO_x/YSZ mixtures cannot be calcined to temperatures high enough to properly sinter the YSZ meaning that high temperatures traditional methods used for Ni/YSZ cermets cannot be applied. Another problem is the migration of Cu ions into the YSZ following high temperature calcinations. To overcome those limitations, a novel fabrication method has been developed in which the porous YSZ part of the cermet is prepared first, and the Cu is added in a separate step that does not require high temperature processing. This procedure allows very high temperature to be used for the densification of the YSZ, while allowing complete flexibility for the conditions used to prepare the Cu and Ceria. The addition of Cu and Ce is performed through the impregnation of the dense porous YSZ matrix with aqueous solutions using nitrate precursors [60,63].

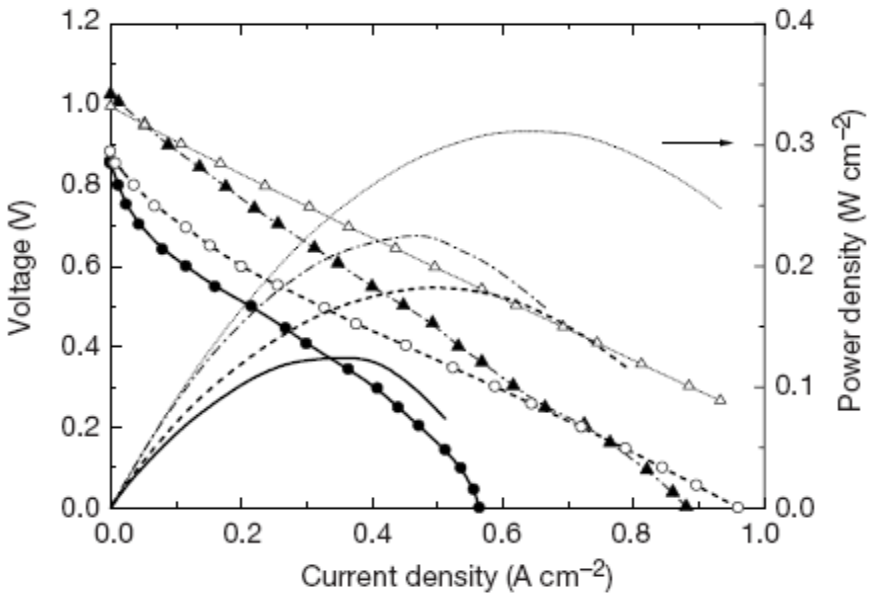

Figure 23: Power densities and current density-voltage relationships for an SOFC using the Cu-ceria composite anode. The cell had a 60µm electrolyte, and data are shown for the following fuels: filled circles, n-butane at 973 K; open circles, n-butane at 1073K, filled triangles, n-butane at 973 K; open triangles, n-butane at 1073K [67].

Cu-CeO_2/YSZ anodes exhibited similar performances when operating on H_2 or CO fuels, while Ni/YSZ exhibit substantially lower performance when operated on CO compared with H_2[66].

Particular attention has been given to n-butane[68]. Figure 23 provides typical power densities obtained for hydrogen and n-butane at 700ºC. A cell was operated at a maximum power density of 0.12 W cm^{-2} in dry butane at 700°C for a period of 48 hours with no observable change in performance. The power output was also stable at 800°C but gas phase reaction formed tar on the walls of the alumina tube at higher

temperature. Visual inspection of a cell after two days in n-butane at 800°C showed that the anode itself remained free of the tar deposits that covered the alumina walls. Final oxidation products were water and CO_2, evidencing that complete oxidation of n-butane did occur.

Direct utilization of various hydrocarbons has been reported on Cu-ceria-YSZ composite anodes. Stable power generation of ~0.1W/cm^2, for at least 12 hours, from the direct utilization, without reforming of toluene, n-decane and synthetic diesel fuel at 700ºC has been demonstrated, as displayed on Figure 24. Only little carbon deposition, in the form of tars, was observed for hydrocarbons diluted in 50%N_2[64].

Cu/Ceria anodes have been shown to be tolerant to sulfur. At 800ºC, H_2S up to level of 450 ppm had no effect on the anode performance[62].

Despite displaying stable operation on a variety of hydrocarbons and delivering satisfying performance, Cu based anodes suffer from a few limitations. Cu easily sinters at temperatures above 700ºC, inducing a decrease in the performance and shows a poor tolerance for redox cycles.

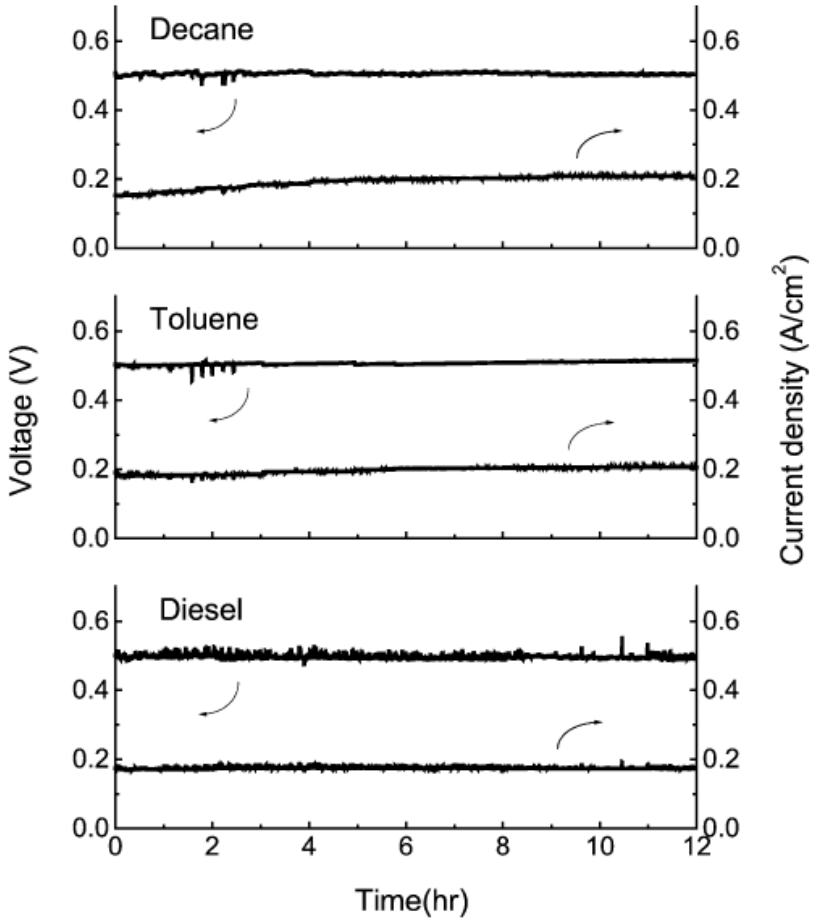

Figure 24: Plots of cell potential and current density as a function of time for n-decane, toluene, and the diesel fuel. Each of the fuels was fed to the cell with N_2 at a concentration of 40 wt. % hydrocarbon[64].

3.2.3. MIEC anodes

3.2.3.1. Doped ceria

Both doped and undoped ceria display mixed ionic and electronic conductivity. Doped ceria has been extensively investigated as alternative electrolyte to replace YSZ. Indeed, ceria doped with trivalent rare earth oxides (e.g. Gd_2O_3, Sm_2O_3, and Y_2O_3) features a ionic conductivity about ten times higher than that of YSZ [69,70]. The electronic conductivity, introduced by the reduction of Ce^{4+} to Ce^{3+} under fuel rich conditions, is a problem for electrolyte applications but has been explored for anode applications. A comprehensive and thorough evaluation on the mixed conductivity and its underlying physical mechanisms has recently been provided by Steele [70]. Furthermore, ceria based anodes are widely recognized to be efficient in limiting carbon deposition. Those materials can take advantage of the bulk ceria capability to store and transport oxygen to enhance hydrocarbon oxidation and it has been shown that CeO_2 anodes can electrochemically oxidize dry methane.

A prominent drawback that arises from the transition of Ce^{4+} to $C^{e3}+$ is the large lattice expansion that can lead to the degradation of the mechanical integrity, with the anode spilling off the electrolyte. Doping with lower valent cations such as Gd^{3+}, Sm^{3+} or Y^{3+} can significantly decrease the dimensional contraction. A reasonable compromise between the stability and the conductivity has been shown to be a 40% substitution of Ce^{4+} by a rare-earth oxide such Gd^{3+} ($Ce_{0.6}Gd_{0.4}O_{1.8}$).

3.2.3.1.1 GDC based anode

Marina et al. [71] have worked on GDC anodes ($Ce_{0.6}Gd_{0.4}O_{1.8}$) with steam diluted CH_4 as a fuel. No carbon deposition was observed after 1000h of operation at 1000°C, with H_2O/C ratios as low as 0.3. Besides, those anodes sustained several rapid thermal cycles and a full redox cycle without degradation However, studies have outlined that GDC is not such a good electro catalyst for direct electrochemical CH_4 oxidation and also shows low activity for CH_4 reforming [71,72] and it was suggested to add a catalyst (Ni, Ru, Rh) to break down the C-H bond more easily. Adding a small amount of catalyst has been found to be very efficient in improving the performance of GDC anodes by Primdhal and Mogensen, as shown on Figure 25[73].

.

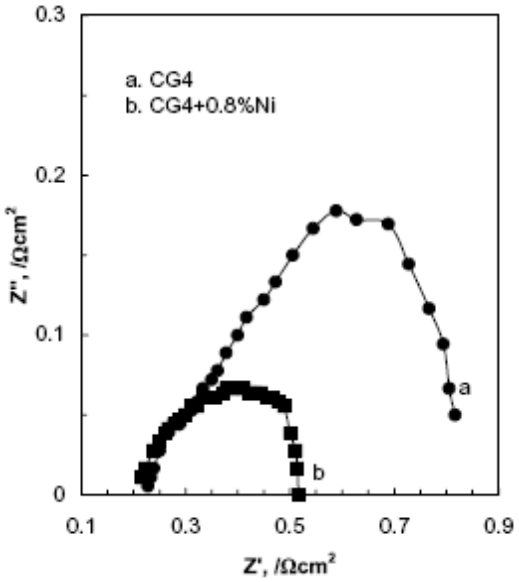

Figure 25: The AC impedance spectra of CG4 electrode fed with humidified H_2 showing dramatic suppression of the semi circle at low frequency as a result of minor Ni addition[73].

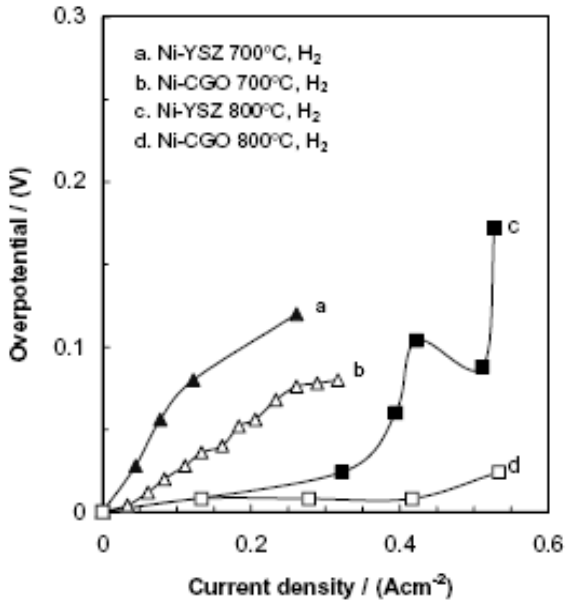

Figure 26: Comparison of anodic overpotential of two different cermet anodes operating on dry hydrogen at two temperatures, indicating that Ni/GDC yields lower overpotentials than Ni/YSZ anode[74].

Joerger and Gauckler [74] studied Ni/GDC cermets for H_2 and CH_4 oxidation reaction. A large improvement in the electrocatalytic activity was found compared to that of Ni/YSZ cermet anodes, for both H_2 and CH_4. Activation energies for the H_2 and CH_4 oxidation reactions were lower on Ni/GDC anodes than those on Ni/YSZ anodes, exhibiting the catalytic activity and electrocatalytic activities of ceria for the reforming and oxidation of hydrocarbons and hydrogen. At 800°C and 0.5 $A.cm^{-2}$, the overpotential of the anode was found to be about 20 mV for H_2 oxidation reaction, as

compared to about 80mV for conventional Ni-YSZ, as can be seen in Figure 26. When using methane, an anodic overpotential of 75 mV was reported at 800°C and 0.25 A.cm^{-2}. However, carbon deposition has been reported on Ni/GDC anodes containing 70 wt% of Ni after operating on wet methane at 850 °C for about 80h [75], showing the amount of catalyst has to be kept reasonably low.

Some works are available addressing the use of additives on Ni/GDC anodes. Using 5 wt% of Ru to Ni/GDC anodes, the electrode polarization resistance to CH_4 fuel was reported to be 0.13 Ω.cm^2 and a power density of 0.75 W cm^{-2} was found in dry CH_4 at 600 °C [76]. Sin et al.[77] have reported an anode of composition $Ni_{0.52}Cu_{0.48}$/GDC that showed no carbon deposition after operation on dry methane for 40 hours at 800 °C, while Ni-Cu/YSZ anode seems to show carbon deposition on methane . Hibino et al. [78] showed that adding precious-metal reforming catalysts (Pt, Pd, Rh, Ru) to Ni/GDC anodes can improve the cell performance for direct conversion on hydrocarbons.

Drawbacks of GDC anodes seem arise from the chemical compatibility between GDC and YSZ, which is an important factor for long term stability. GDC and YSZ react and diffuse into each other during sintering process at 1200°C forming a Gd rich phase with ionic conductivity two orders of magnitude lower than that of YSZ at 800°C [79]. Further studies seem to show that the solid state reaction can be suppressed. One way suggested is to use an interlayer of $Ce_{0.43}Zr_{0.43}Gd_{0.10}Y_{0.04}O_2$. Another way is to rely on the Ni ability to inhibit the reactivity between YSZ and ceria, and a composition Ni/GDC 40/60 vol.% has been recommended to inhibit solid state reactions[80].

3.2.3.1.2 SDC based anodes

Studies of Sm-doped CeO_2[8182] have shown that the ionic conductivity of those materials could be as high as 0.1 S/cm at 800ºC, which is about 4 times higher than that of YSZ. The electronic conductivity reported at anodic PO_2 was about 4 S/cm, rendering those materials attractive for anode applications.

Eguchi et al.[83] have reported significant improvement in the polarization resistance of Ni based cermets by replacing YSZ with ceria based oxides (CeO_2, SDC) and praseodymium oxide (PrO_x). The improved performance was attributed to an extended reaction area due to the ionic conduction of the oxides and compared as follows: Ni-YSZ<Ni-CeO_2<Ni-SDC<Ni-PrO_x.

Other studies[84,85] have confirmed the lower overpotential on Ni/SDC anodes as compared to Ni/YSZ for H_2 oxidation. Best performance was found on Ni/SDC made of 50 vol% nickel. Hibino et al.[78] have carried out some studies on Ni/SDC anodes, and the addition of Pd to the material. A cell with a Ni/SDC anode showing a power density of 0.192 W.cm-2 was reported in wet CH_4 [86]. The same cell, involving an anode made with the addition of 7 wt% PdO showed a maximum power density of 0.644 W.cm^{-2} at 550°C.

Adding metal catalyst enhances as well the performance of SDC anodes. Uchida et al.[87,88,89] have performed a series of studies on the electrocatalytic activity SDC and

Y-doped CeO_2 (YDC) for H_2 oxidation, with and without the addition of a catalyst. It was shown that the incorporation fine Ru particles reduced the activation polarization resistance, which doubled the cell current output at 800ºC. These studies revealed that a few percent of ultra-fine nanometer-sized Ni particles (as compared to the micrometer size in cermets) dispersed on SDC anodes produced better performance than that of Ni/SDC cermet anodes. This was explained by the significant increase in the number of reaction sites. Using 8 vol% of nano sized Ni particles increased the current density by a factor 4 at 800ºC as compared to pure SDC[90] .

Using Ni/La_2O_3 doped ceria, Huang et al.[91] have reported power densities of 0.9W/cm^2 at 800ºC on a 600µm thick LSGM electrolyte.

Perry Murray et al.[92] have reported the direct electrochemical oxidation of methane, generating power densities up to 0.37W.cm^{-2} at 650°C, applying $(Y_2O_3)_{0.15}(CeO_2)_{0.85}$ (YDC) porous film applied between the electrolyte and the Ni-YSZ anode and operating at low temperatures. Figure 27 displays the improvement in the anode polarization resistance obtained from the YDC layer introduction.

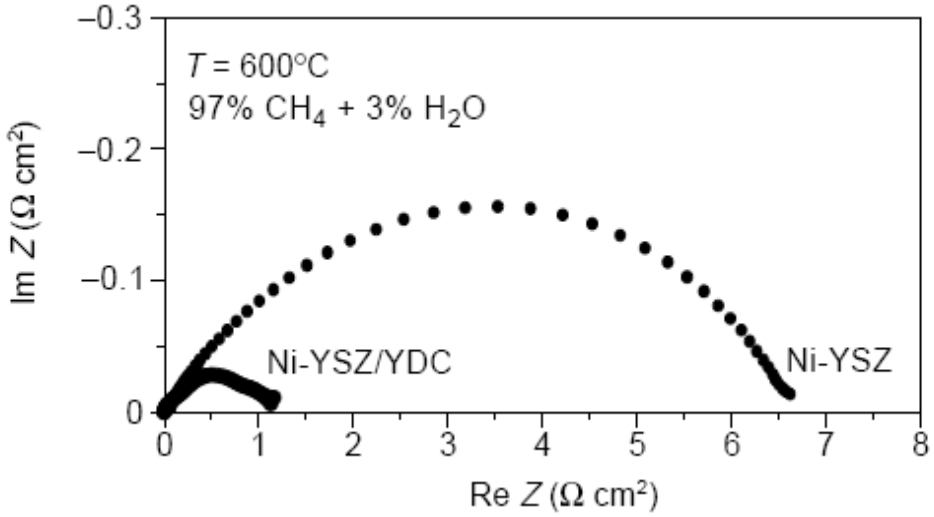

Figure 27: Impedance spectroscopy results for Ni-YSZ and Ni-YSZ/YDC anodes in 97%CH_4 + 3% H_2O at 600 ºC[92].

Results obtained on dry and wet (3% H_2O) methane were nearly identical. The cell performance was stable in the preliminary 100-h life tests, except for wet methane at low voltages where the anode Ni gradually oxidized. Power densities are about ~20 % lower than those obtained with humidified hydrogen. Examination of anodes after ~100h of operation showed no evidence of carbon deposition.

3.2.3.2. **Titanate based oxides**

Titanate-based oxides, such as $SrTiO_3$, are relatively stable in fuel reducing environment and possess high n-type conductivities at low partial pressure of oxygen, making them attractive as potential anode materials. Most studies available in the literature have investigated the conductivity of titanate based oxides[2,4,93], while some

fuel cell tests have produced promising performances. Cr/Ti have been studied by Pudmich et al.[94]. Despite some compositions show high conductivities, reported electrochemical performances were poor.

Canales-Vazquez et al.[95] have investigated $La_2Sr_4Ti_6O_{19-\delta}$ as potential anode. Those materials show a high total conductivity under reducing conditions. The polarization resistance varied from 2.97 $\Omega.cm^2$ at 900°C in wet H_2 to 8.93 Ω cm^2 at 900°C in wet CH_4. The maximum current density was 76 $mW.cm^{-2}$ both measured in wet H_2 at 900°C.

Fu et al. [96] have developed an alternative anode concept based on Y-substituted $SrTiO_3$ (SYT), YSZ and a small amount of Ni catalyst (5 wt. %). The ceramic framework SYT/YSZ did show good dimensional stability upon redox cycling and had an electrical conductivity of ~10 S/cm under anodic conditions. This anode produced a polarization resistance of 0.21 $\Omega.cm^2$ at 850ºC in wet Ar/5%H_2.

Ovalle et al. [97] have investigated Mn substituted perovskite titanates with formula $La_4Sr_8T_{12-x}Mn_xO_{38-\delta}$ as anodes for direct use of methane. This study indicated that Mn substitution does not have a large impact on the bulk conductivity but enhances electrochemical performances, especially at high temperatures. Low polarization resistances were reported for hydrogen and methane, 0.3 and 0.7 $\Omega.cm^2$ respectively at 950ºC. Studying similar oxides, Fu et al.[98]have reported a polarization resistance of 0.32 Ω.cm2 for a $La_{0.4}Sr_{0.6}Ti_{0.4}Mn_{0.6}O_{3-\delta}$/YSZ anode at 850ºC in H_2. Those oxides were shown to be thermally and chemically compatible with YSZ.

Ruiz-Morales et al. [99,100] have studied Lanthanum doped strontium titanate in which Ti was substituted with Ga and Mn to induce redox activity and allow more flexible coordination. $La_4Sr_8Ti_{11}Mn_{0.5}Ga_{0.5}O_{38-d}$ (LSTMG) has demonstrated excellent fuel cell performance in wet H_2 at 950ºC, and was shown to be very active for methane oxidation at high temperatures, with OCVs in excess of 1.2V. Optimized electrode polarization resistances were only 0.12 and 0.36 $\Omega.cm^2$ in humidified H_2 and CH_4 respectively.

Nb-doped strontium titanate, displaying high electronic and redox stability, has recently been developed in Risoe laboratory[101]. The infiltration of nano-sized GDC particles has been proposed to overcome the low electrocatalytic activity, and polarization resistance of 0.12 and 0.44 $\Omega.cm^2$ at 850ºC and 650ºC respectively have been reported[102].

3.2.3.3. **Lanthanum chromite oxides and related perovskites**

Significant research has been dedicated to the study of lanthanum chromites (LaCrO3) based materials. Lanthanum chromites have been originally investigated as interconnect material in SOFC because of their stability towards reduction and their relatively high electrical conductivity and stability in both reducing and oxidizing atmospheres at SOFC operating temperatures [103,104,105,106]. Numerous studies have demonstrated that both A- and B-site doping of lanthanum chromites could significantly affect both their conductivities and catalytic properties.

Many groups have emphasized the catalytic behavior of lanthanum chromite materials towards methane reforming. These studies indicated the importance of adding B-site transition metals on the catalytic activity of lanthanum chromites (e.g. V, Ni, Fe, Co, Mn and Ru). While the catalytic behavior of some of these compositions was promising, finding a single oxide material to fulfill all of the requirements of a high performance anode is exceedingly difficult, as highlighted by Tao and Irvine[107].

The thermodynamic stability and catalytic activity of $(LaA)(CrB)O_3$ systems (A=Ca, Sr and B=Mg, Mn, Fe, Co, Ni) have been investigated by Sfeir et al.[108,109,110]. The decomposition of transitional metal substituted LaCrO3 seems to be hindered kinetically, since those materials did not decompose easily under reducing conditions. Thermodynamically, Sr and Mn substitution would maintain the stability of the perovskite while other substitutes would destabilize the system. Ca and Sr substitution at the A-site improves the catalytic activity and for the B-site substitution, Co and Mg showed an inhibiting effect while Mn, Fe and Ni improved the activity. In this studies, $(LaSr)(CrNi)O_3$ with 10%Ni has been suggested as the most suitable composition for methane oxidation reactions, considering the catalytic activity and cracking resistance[111]. However, other authors have reported Ni exsolution in 10% Ni doped lanthanum chromites in fuel environments[112], suggesting that the surface segregation of Ni might be responsible for the high catalytic activity, which raises questions about the long term stability when fueled with hydrocarbon.

Tao and Irvine [113] have studied $La_{0.75}Sr_{0.25}Cr_{0.5}Fe_{0.5}$. Although this composition was shown to be stable under reducing atmosphere, its electrochemical performance in wet methane was reported to be very poor.

Further studies by the same authors, addressing Mn B-site substitution, $La_{0.75}Sr_{0.25}Cr_{0.5}Mn_{0.5}O_3$[114] led to really promising results. The approach of creating perovskites with dual B-site occupancy has very successfully combined the good oxidation catalysis properties of lanthanum manganite with the stability and conductivity of the chromite, without compromising any of these good properties by dilution. Compatibility with YSZ was reported to at least 1300ºC. The electronic conductivity at 900°C was about 38 S/cm in air and 1.5 S/cm in 5% H_2 (P_{O2}~10^{-21} atm) and good anode performance was achieved. The polarization resistance at 900ºC was 0.9 $\Omega.cm^2$ in wet 5%H_2/Ar and 0.47 Ω cm^2 in wet H_2. Two ways for improving the electrode performance have been suggested. One way was to introduce a thin layer of CGO coated between YSZ and LSCM anode, which reduced the polarization resistance to 0.6 $\Omega.cm^2$ in wet 5%H_2/Ar and 0.25 $\Omega.cm^2$ in wet H_2. Another way was to add a small amount of YSZ to the microstructure, which reduced the electrode polarization resistance to 0.2 $\Omega.cm^2$ in wet 97%H_2/3%H_2O. Moreover, very good performances were achieved for methane without using excess steam. Indeed, using ambient humidification (i.e. 3% H_2O), the same performance was achieved with methane at 950°C as for hydrogen at 850°C. Further studies from the same group have proved LSCM to be a full oxidation catalyst, since CO_2 production dominates CO production even in CH_4-rich CH_4/O_2 mixtures. X-ray adsorption spectroscopy confirmed that Mn was the redox active species demonstrating that the Cr only stabilizes the structure under fuel atmosphere[115].

Since the development of LSCM anodes by Tao and Irvine, this material has received

considerable attention, particularly for the direct use of methane.

The addition of YSZ was confirmed to greatly improve the adhesion and reduce the electrode polarization resistance. In their study of $(La_{0.75}\ Sr_{0.25})(Cr_{0.5}Mn_{0.5})O_3$/YSZ composites for direct use of methane, Jiang et al [116] reported an optimal composition with LSCM contents of 50-60 wt.%. It was concluded that the electrocatalytic activity of the LSCM/YSZ composite anodes for the methane oxidation is likely limited by the oxygen vacancy diffusion in the substituted lanthanum chromite-based materials. The addition of GDC to form GDC/LSCM composites has been studied by other authors as well. Using a YSZ/CGO based composite instead of YSZ, Ruiz-Morales et al.[117] have decreased by a factor 2 the polarization resistance at 950ºC. Chen et al. [118] have reported anodic overpotentials of 0.073 and 0.248V in wet H_2 and CH_4 at 850ºC respectively for LSCM/GDC composite electrodes. Further studies of LSCM/GDC composites have demonstrated their stability in 0.5%H_2S/99.5% CH_4 atmospheres under anodic polarization, demonstrating their sulfur tolerance[119].

McIntosh and coworkers have investigated the direct use of hydrocarbons on LSCM anodes. When the current density is increased, a significant decrease in anode polarization resistance was observed for H_2, CH_4 and C_4H_{10}[120]. The increased oxygen flux to the anode is believed to increase oxygen stoichiometry in the oxygen lattice, hence increasing the electrocatalytic oxidation activity. At high current density, the reaction mechanism is dominated by total oxidation of hydrocarbon fuels on the LSCM surface to form CO_2 and H_2O. The effect of the Cr/Mn ratios on the B-site of $La_{0.75}Sr_{0.25}Cr_xMn_{1-x}O_{3-\delta}$ was investigated as well[121]. The reaction rate and range of oxygen stoichiometry favouring total oxidation increased with increasing Mn content, but was accompanied by a decrease in the oxide stability. However, the authors indicated that the measurements suggest that more active catalysts are required for SOFC applications.

The addition of small amount of catalyst to improve the performance of LSCM anodes has been addressed in several studies. The impregnation of Pd nano particles in small amounts onto LSCM anodes was found to significantly reduce the anodic overpotential for the direct use of methane[122]. A factor 3 decrease in the anode polarization resistance has been reported Ye et al.[123], while Jiang et al[124] observed an increase in the power density of two and eight time in CH_4 and ethanol respectively. The use of Ni has been proposed as well. Liu et al.[125] indicated that the addition of 5% NiO in $La_{0.8}Sr_{0.2}Cr_{0.8}Mn_{0.2}O_3$/GDC anodes increased the power density by a factor 3.

A different approach to enhance the performance has been examined by Lay et al[126], where LSCM was substituted on the A-site by 10 at% of cerium. Interesting performance was achieved using $La_{0.65}Ce_{0.1}Sr_{0.25}Cr_{0.5}Mn_{0.5}O_{3-\delta}$ as anode, with polarization resistances of 0.2 and 1.6 $\Omega.cm^2$ at 900ºC in wet (3%H_2O) H_2 and CH_4 respectively. The Ce substitution is found to enhance the performance without additional microstructural modification and to increase the OCV in moist methane.

3.3. Conclusions

As demonstrates the numerous studies reviewed in this chapter, the activity of the research for the development of alternative development is rather intense. Although catalytic anodes that allow for the operation of SOFCs directly on hydrocarbons have been developed and different routes have been investigated, the performance of these anodes (for example, maximum current density) is still not at the level obtained in state-of-the-art SOFCs with Ni/YSZ anodes operating on hydrogen. Thus there is still much room for improvement in the catalytic properties of SOFC anodes designed to use hydrocarbons directly[2]. However, important advances have been achieved over the recent years culminating in the development of alternative anode design being claimed to display performance comparable to Ni-YSZ standards.

This review illustrates the difficulty of identifying a single material that would cover all the requirements for high performance anodes. Although some single materials can display acceptable polarization resistances for practical applications, this occurs mainly at high temperatures, e.g. above 900ºC. Hence, if temperatures have to be kept in the range 700-800 ºC, the most attractive design for alternative anodes is likely to be a composite one, in which an oxide that does not catalyze carbon formation provides a redox and thermally stable conductive framework, and small amounts of catalyst enhance the electrochemical performance. The amount of catalyst can be kept low enough to avoid carbon deposition. For oxides that offer limited ionic conductivity, it is critical that any added catalyst lies at the TPB to ensure efficient performance improvements.

As outlined by Atkinson et al.[2],understanding the mechanisms of the surface reactions that occur on the anode near the three-phase-boundary is likely to be the key to further advances in this area. Unfortunately, fundamental insight into these reaction mechanisms is rather limited. For systems that directly use hydrocarbon fuels, the mechanism of the surface oxidation reactions is undoubtedly highly complex, and involves multiple elementary steps and reaction intermediates. At the very least it would be useful to identify the rate limiting step or steps in the reaction mechanism. Even for Ni/YSZ cermet anodes, the mechanism for hydrogen oxidation reactions is not completely understood[2]. Many in situ spectroscopic probes such as Raman and infrared spectroscopy are routinely used in catalysis research to characterize surface intermediates and reaction mechanisms. It is very difficult, however, to apply those techniques to an operating SOFC anode. Nonetheless, some in roads are being made in this area. For example, the application of infrared emission spectroscopy to characterize working SOFC anodes is being pioneered[127]. Development of models of anodes that allow other spectroscopic probes, such as photoelectron spectroscopy and detailed kinetic measurements, to be made are also needed in order to advance research in this area.

3.4. Proposed Work

The aim of this part of the research is to develop a concept of high-performance

ceramic anodes capable of direct use of hydrocarbons, that are redox stable and can deliver satisfying performance without requiring too high temperatures. To reach this target, an innovative strategy is used that releases the stringent requirements on materials. This collaborative work between the University of St Andrews and the University of Pennsylvania takes advantage of the complementary in research groups' expertise. The research at the University of Pennsylvania has focused on heterogeneous catalysis and novel approach for electrode fabrication while at the University of St-Andrews, important advances have been made on conductive ceramic oxides.

In an attempt to address the issues related to the development of alternative anodes that have been described above, an innovative strategy is here being introduced. The concept involves the separation of the anode into two distinct layers that have different functionalities. As previous works have suggested , only a thin layer adjacent to the electrolyte is believed to be electro-catalytically active, and has been estimated to be in the range of 10 to 20 μm. The remaining part of the anode hence does not require any electrocatalytic properties and acts mainly as a porous electronic conductor. Based on this important evidence, anodes can be designed as two layers having different property needs, since no electrocatalytic activity is required outside of the active layer. Different materials can thus be used for each layer consequently placing less stringent requirements on the materials properties. In the proposed design, the anode functional layer, adjacent to the electrolyte, performs the electrochemistry, and can potentially be designed to be as thin as 10-20 μm. Due to this small thickness, the conductivity of the functional layer can be minimal, considerably broadening the range of materials that can be used. As an example, a 10 μm thick functional layer having a conductivity as low as 0.1 S/cm would only contribute for 0.01 $\Omega.cm^2$ of the ohmic losses. High electrocatalytic properties are of course necessary for the functional layer. The conduction layer that links the functional layer to the interconnect is expected to have a high conductivity but does not need to show any catalytic activity. The work presented in this study focuses on the anode functional layer.

The fabrication method for the functional layer is the impregnation approach that has been developed at the University of Pennsylvania. Using this method, the functional is prepared layer from a YSZ porous structure that has been co-sintered with the electrolyte. The active anode components are then added by infiltration methods. Using this approach offers many advantages[128,129]. First, the interface between the dense YSZ electrolyte and the YSZ used in the functional layer to form the composite has been sintered at high temperature, typically 1500ºC. This results into an optimum bondage between those two phases, which practically become a single phase, hence optimizing the ionic conduction path contribution to the TPB area. Moreover, the functional layer active components are sintered after the dense YSZ has been formed, allowing the use of lower temperatures which limits the risks of solid state reactions during the fabrication and broadens the range of materials that can be used as active components. Finally, since the functional layer prepared this way is a composite of YSZ and active components, high ionic conductivity in the active components is not necessary.

The possibility of achieving outstanding performances using a thin ceramic functional layer has been demonstrated at the University of Pennsylvania[130]. The functional layer

in this study was a 12 μm thick layer with 40 wt% CeO_2 and 1% Pd. Ag paste was used as a current collection layer, while the electrolyte was 75 μm thick YSZ. The cell was supported by a 300 μm cathode that was a composite of YSZ and LSF. Such cells produced power densities of 249 mW/cm^2 at 650ºC and 865 mW/cm^2 at 800ºC, even using a relatively thick YSZ electrolyte. While those cells have been tested using Ag paste in the current collection layer, it was shown that replacing Ag paste with an electronically conductive ceramic had only little effect of the performance. In this work, a 100μm current collection layer of porous $La_{0.3}Sr_{0.7}TiO_3$ (LST). Because the conductivity of this layer was only 0.2 S/cm at 700ºC, the small ohmic contribution from this layer slightly decreased the cell performance compared to the Ag paste conduction layer, as indicated by the comparison of impedance data for both cells. Polarization resistances were identical, indicating that the two layers behave independently.Although thin functional layers prepared by infiltration have shown really good initial performance for nickel free anodes, materials that have been used to provide the electronic conductivity, namely copper or ceria, suffer from intolerance to redox cycles and thermal instability.

In a different approach, research carried out at the University of St-Andrews has investigated the development of conductive oxides. Some of those oxides previously described, such as LSCM and LSTM have shown high conductivity under reducing conditions and promising performances when used as SOFCs anodes. Such oxides have been shown to be tolerant towards redox cycles and are thermally stable. Those intrinsic properties could provide an answer to the issues related to performance stability for functional layers previously developed at Upenn using copper and ceria. However, the main drawback of conductive oxide is their need for high temperatures to be activated. At temperatures below 900ºC, polarization resistances can be too high to compete with Ni-YSZ standards.

Taking into account those considerations, a suitable approach seem to use conductive oxides developed at St Andrews in functional layers to provide the electronic conductivity. Proceeding this way, a better thermal stability can be expected along with tolerance towards redox cycles. As was concluded from the above review on anode development, the poor polarization resistance issues at low temperatures can be addressed by the infiltration of small amount of catalysts such as ceria and palladium. This can be expected to decrease the non ohmic losses associated with conductive oxides at lower temperatures.

The study reported hereafter investigates this new concept of anodes in an attempt to produce efficient redox stable alternative anode that can operate on strategic fuels. The first series of experiments involved the use of LSCM in the functional layer to provide the electronic conductivity. Ce/Pd catalyst was first added to the functional layer. After having been tested as SOFC anodes, these LSCM based electrodes have been employed for the electrolysis of CO_2. Following those initial results, both the catalyst effect and the microstructure were further investigated to better understand the performance of these anodes. Different catalysts have been used. The microstructural study has been extended to the $La_{0.33}Sr_{0.67}Ti_xMn_{1-x}O_{3+/-\delta}$ (LSTM) perovskite family to help to understand the phenomena occurring in such YSZ-oxide composites, paying particular attention to the role of Mn content in controlling the interface.

[1] M. Ormerod, *Chem. Soc. Rev.*, 32 (2003) 17-28
[2] A. Atkinson, S. Barnett, R.J. Gorte, J.T.S. Irvine, A.J. McEvoy, M. Mogensen, S.C. Singhal and J.Vohs., *Nature materials*, 3 (2004) 17-27
[3] W.Z. Zhu, S.C. Deevi, *Materials Science and engineering*, A362 (2003) 228-239
[4] S.P. Jiang, S.H. Chan, *Journal of materials science*, 39 (2004) 4405-4439
[5] J.W. Fergus, *Solid State Ionics*, 177 (2006) 1529-1541
[6] N.Q. Minh, *J. Am. Ceram. Soc.*, 76 (1993) 563-588
[7] E. Baur, H. Preis, Uber die Eisenoxyd-Kathode in der Kohle-Luft-Kette. *Z. Elektrochem.* 43**,** 727 (1937).
[8] H. Möbius, On the history of solid electrolyte fuel cells, *J. Solid State Electrochem.*, 1**,** 2 (1997).
[9]S. Spacil, Electrical device including nickel-containing stabilized zirconia electrode. US Patent 3,558,360 (1970).
[10] M.L. Toebes, J.H. Bitter, A.J. van Dillen, K.P. de Jong, *catalysis today*, 76 (2002)
[11] H. Lee, H. Moon, H-W.Lee, J.Kim, J-D. Kim, K-H Yoon, *Solid state ionics*, 148 1-2 (2002)
[12] W. Dees, T.D. Claar, T.E. Easler, D.C. Fee, F.C. Mazrek, *J. Electrochemical Soc.*, 134 (1987) 2141-2146
[13] B. Pal, S.C. Singhal, *J. Electrochem. Soc.*, **137** (1990) 2937.
[14] L. S . Wang, S.A. Barnett, *Solid State Ionics*, **61** (1993) 273
[15] Z. Ogumi, T. Ioroi, Y. Uchimoto, Z. Takehara, T. Ogawa, K. Toyama, *J. Amer. Ceram. Soc.*, **78** (1995) 593.
[16] E.Z. Tang, T.H. Etsell, D.G. Ivey, *ibid.*, **83** (2000) 1626.
[17] J. L. Young, T.H. Etsell, *Solid State Ionics*, **135** (2000) 457.
[18] D. Simwonis, F. Tietz, D. Stover, *Solid State Ionics*, **132** (2000) 241.
[19] F. Tietz, F.J. Dias, D. Simwonis and D. Stover, *J. Euro. Ceram. Soc.*, **20** (2000) 1023.
[20] Hikita, in "Science and Technology of Zirconia V," edited by S. P. S. Badwal, M. J. Bannister and R. H. J. Hannink (Technomic Publishing Co., Lancaster, PA, 1993) p. 674.
[21] S . Murakami, Y. Akiyama, N. Ishida, T. Yasuo, T. Saito and N. Furukawa, in "SOFC-II," edited by F. Grosz, P. Zegers, S. C. Singhal and O. Yamamoto (Commission of The European Communities, Luxembourg, 1991) p. 561.
[22] S.P. Jiang, *ibid.* **150** (2003) E548.
[23] S.P. Jiang, S.H. Chan, *Journal of materials science*, 39 (2004) 4405-4439
[24] T. Fukui, S. Ohara, M. Naito, K. Nogi, *J. Power Sources*, **110** (2002) 91.
[25] S . Primdahl, B. F . Sorensen, M. Mogensen, *J. Amer. Ceram. Soc.* **83** (2000) 489.
[26] T. Kawada, N. Sakai , H. Yokokawa , M.Dokiya, M. Mori, T. Iwata, S*olid State Ionics*, 40-41 (1990)
[27] J-H. Lee, H. Moon, H-W.Lee, J.Kim, J-D. Kim, K-H Yoon, *Solid State Ionics*, 148 (2002) 15-26
[28] D.W. Dees, T.D. Claar, T.E. Easler, D.C. Fee, F.C. Mazrek, *J. Electrochemical Soc.*, 134 (1987) 2141-2146
[29] H. Itoh, T. Yamamoto, M. Mori, T. Horita, N. Sakai, H. Yokokawa, M. Dokiya, *J. Electrochem. Soc.*, 144 (1997) 641
[30] Iwata, *J. Electrochem. Soc.*, 143 (1996) 1521
[31] W. Huebner, H.U. Anderson, D.M. Reed, S.R. Sehlin, X. Deng, in: M. Dokiya, O. Yamamoto, H. Tagawa, S.C. Singhal (Eds.), Proceedings of the Fourth International Symposium on Solid Oxide Fuel Cells (SOFC-IV), Yokohama, Japan, 6–9 June 1995, p. 159.
[32] F. Tietz, F.J. Dias, D. Simwonis and D. Stover, *J. Euro. Ceram. Soc.*, **20** (2000) 1023.
[33] A. Tintinelli, C. Rizzo, G. Giunta, A. Selvaggi, in "1st European SOFC Forum," edited by U. Bossel (European Fuel Cells Forum, Lucerne, Switzerland, 1994) p. 455
[34] M. Susuki, H. Sasaki, S. Otoshi, A. Kajimura, M. Ippommatsu, *Solid State Ionics*, 62 (1993) 125.
[35] H. Itoh, T. Yamamoto, M. Mori, N. Mori, T. Watanabe, in: B. Thorstensen (Ed.), Proceedings of the Second European Solid Oxide Fuel Cell Forum, vol. 1, Oslo, Norway, 6–10 May 1996, p. 453.
[36] H. Itoh, Y. Hiei, T. Yamamoto, M. Mori, T. Watanabe, in: H. Yokokawa, S.C. Singhal (Eds.), Proceedings of the Seventh International Symposium on Solid Oxide Fuel Cells (SOFC VII), Tsukuba, Ibaraki, Japan, 3–8 June 2001, p. 750.
[37] D. Simwonis, F. Tietz, D. Stover, *Solid State Ionics*, 132 (2000) 241.
[38] T. Iwata, *J. Electrochem. Soc.*, 143 (1996) 1521.
[39] A. Muller, in "3rd European SOFC Forum," edited by P. Stevens (European Fuel Cell Group, Lucerne, Switzerland, 1998) p. 353.
[40] A.C. Muller, D. Herbstritt, E. Ivers-Tiffee, *Solid State Ionics*, 152-153 (2002) 537-542
[41] H. Koide, Y. Someya, T. Yoshida, T. Maruyama, *Solid State Ionics*, 132 (2000) 253.
[42] .H. Lee, J.W. Heo, D.S. Lee, J. Kim, G.H. Kim, H.W. Lee, H.S. Song, J.H. Moon, *ibid.*, 158 (2003)

225
[43] A.V. Virkar, J. Chen, C.W. Tanner, J.W. Kim, Solid State Ionics, 152-153 (2000) 189
[44] A.C. Muller, D. Herbstritt, E. Ivers-Tiffee, *Solid State Ionics*, 152-153 (2002) 537-542
[45] H. Koide, Y. Someya, T. Yoshida, T. Maruyama, *Solid State Ionics*, 132 (2000) 253.
[46] A.C. Muller, D. Herbstritt, E. Ivers-Tiffee, *Solid State Ionics*, 152-153 (2002) 537-542
[47] A. Muller, in "3rd European SOFC Forum," edited by P. Stevens (European Fuel Cell Group, Lucerne, Switzerland, 1998) p. 353.
[48] M.L. Toebes, J.H. Bitter, A. Jos van Dillen, K.P. de Jong, *Catalysis today*, 76 (2002) 33-42
[49] T. Kobayashi, J. Otomo, C. Wen, H. Takahashi, *Journal of power sources*, 124 (2003) 34-39
[50] W.J.Zhou, W.Z. Li, S.Q. Song, Z.H. Zhou, L.H. Jiang, G.Q. Sun, Q. Xin, K. Poulianitis, S. Kontou, P. Tsiakaras, *Journal of power sources*, 131 (2004) 217-223
[51] R.J. Gorte, J.M. Vohs, S. McIntosh, *Solid State Ionics*, 175 (2004) 1-6
[52] . Takeguchi, Y. Kani, T. Yano, R. Kikuchi, K. Eguchi, K. Tsujimoto, Y. Uchida, A. Ueno, K. Omoshiki, M. Aizawa, *ibid.*, **112** (2002) 588.
[53] T. Takeguchi, T. Yano, Y. Kani, R. Kikuchi, K. Eguchi, in "SOFC-VIII," edited by S. C. Singhal and M. Dokiya (Electrochem. Soc., Pennington, NJ, 2003) Vol.
[54] T. Takeguchi, R. Kikuchi, T. Yano, K. Eguchi, K. Murata, *Catalysis Today*, 84 (2003) 217.
[55] C.M. Finnerty, N.J Coe, R.H. Cunningham, R.M. Ormerod, *Catalysis Today*, 46 (1998) 137-145
[56] K. Sato, Y. Ohmine, K. Ogasa, S. Tsuji, in "SOFC-VIII," edited by S. C. Singhal and M. Dokiya (Electrochem. Soc., Pennington, NJ, 2003) Vol. 2003–07, p. 695.
[57] A. Ringuede, D.P. Fagg, J.R. Frade, *J. Euro. Ceram. Soc.*, 24 (2004) 1355.
[58] H. Kim, C. Lu, W.L. Worrell, J.M. Vohs, R.J. Gorte, *J. Electrochem. Soc.*, 149 (2002) A247.
[59] A. Sin, A. Tavares, Y. Doubitsky, A. Zaopo, A.S. Arico, L.R. Gullo, D. La Rosa, S . Siracunaso and V. Antonucci, in "SOFC-VIII," edited by S. C. Singhal and M. Dokiya (Electrochem. Soc., Pennington, NJ, 2003) Vol. 2003–07, p. 745.
[60] R.J. Gorte, J.M. Vohs, S. McInstosh, *SSI*, 175 (2004) 1-6
[61] S. McIntosh, J.M.Vohs, R.J. Gorte, *Electrochemica acta*, 47 (2002) 3815-3821
[62] H.He, R.J. Gorte, J.M. Vohs, *ESSL*, 8 (6) (2005) A279-A280
[63] H.Kim, S.Park, J.M.Vohs, R.J. Gorte, *Journal of the Electrochemical Society*, 148 (7) (2001) A693-A695
[64] R.J. Gorte, J.M. Vohs, *Journal of catalysis*, 216 (2003) 477-486
[65] S. McIntosh, J.M. Vohs, R.J. Gorte, *Journal of the Electrochemical society*, 150 (10) (2003) A1305-A1312
[66] O. Costa-nunes, R.J. Gorte, J.M. Vohs, *Journal of power sources*, 141 (2005) 24-249
[67] R.J. Gorte, S.Park, J.M.Vohs, C.wang, *Advanced materials*, 12 (19) (2000)
[68] O.Costa-Nunes, J.M.Vohs, R.J.Gorte, *Journal of the electrochemical society*, 150 (7) (2003) A858-A863
[69] M. Mogensen, N.M. Sammes, G.A. Tompsett, *Solid State Ion.*, 129 (2000) 63–94.
[70] B.C.H. Steele, *Solid State Ion.*, 129 (2000) 95–110.
[71] O.A. Marina, C. Bagger, S. Primdahl, M. Mogensen, *Solid State Ion.*, 123 (1999) 199–208.
[72] O.A. Marina, M. Mogensen, *Appl. Catal.*, A 189 (1999) 117–126.
[73] S. Primdahl, M. Mogensen, *Solid State Ionics*, 152–153 (2002) 597.
[74] M.B. Joerger, L.J. Gauckler, in "SOFC-VII," edited by H. Yokokawa and S. C. Singhal (Electrochem. Soc., Pennington, NJ, 2001) Vol. 2001–16, p. 662.
[75] B.Madsen, S.Barnett, *SSI*, 176 (2005) 2545-2553
[76] E. P . Murray, S.J. Harris, H.Jen, *J. Electrochem. Soc.* **149** (2002) A1127.
[77] - A. Sin, A. Tavares, Y. Doubitsky, A. Zaopo, A.S. Arico, L.R. Gullo, D. la Rosa, S . Siracusano, V. Antonucci, in "SOFC-VIII," edited by S. C. Singhal and M. Dokiya (Electrochem. Soc., Pennington, NJ, 2003) Vol. 2003–07, p. 745.
[78] T. Hibino, A. Hashimoto, K. Asano, M. Yano, M. Suzuki, M. Sano, *Electrochem. Solid-State Lett.*, 5 (2002) A242–A244
[79] A. Tsoga, A. Naoumidis, A.Gupta, D. Stover, *Mater. Sci. Forum* **308–311** (1999) 234.
[80] A. Tsoga, A. Gupta, A. Naoumidis, P. Nikolopoulos, *Acta Mater.* **48** (2000) 4709.
[81] K. EGUCHI, *J. Alloys Comp.* **250** (1997) 486.
[82] G. B. BALAZS and R. S . GLASS, *Solid State Ionics* **76,**(1995) 155.
[83] K. Eguchi, T. Setoguchi, K. Okamoto and H. Arai, in Proc. of the International Fuel Cell Conf. (Makihari, Japan, 1992) p. 373.
[84] C.J . Wen, T. Masuyama, T. Yoshikawa, J. Otomo, H. Takahashi, K. Eguchi, K. Yamada, in "SOFC-VII," edited by H. Yokokawa and S. C. Singhal (Electrochem. Soc., Pennington, NJ, 2001) Vol. 2001–

16, p. 671.
[85] T. Inagaki, H. Yoshida, K. Miura, S. Ohara, R. Maric, X. Zhang, K. Mukai, T. Fukui, in "SOFC-VII," edited by H. Yokokawa and S. C. Singhal (Electrochem. Soc., Pennington, NJ, 2001) Vol. 2001–16, p. 963.
[86] X. Zhang, S. Ohara, R. MAaric, T. Fukui, H. Yoshida, M. Nishimura, T. Inagaki, K. Miura, *J. Power Sources* **83** (1999) 170.
[87] M. Watanabe, H. Uchida, M. Shibata, N. Mochizuki, K. Amikura, *Electrochem. Solid-State lett.*, 141 (1994) 342–345.
[88] H. Uchida, T. Osuga, M. Watanabe, *J. Electrochem. Soc.*, 146 (1999) 1677–1682.
[89] H. Uchida, S. Suzuki, M. Watanabe, *Electrochem. Solid-State Lett.*, 6 (2003) A174–A177.
[90] H. Uuchida, S. Suzuki, M. Watanabe, in "SOFCVIII," edited by S. C. Singhal and M. Dokiya (Electrochem. Soc., Pennington, NJ, 2003) Vol. 2003–07, p. 728.
[91] K. Huang, J.H. Wan, J.B. Goodenough, *J.*Electrochem. Soc. **148** (2001) A788.
[92] E. Perry Murray, T. Tsai, and S. A. Barnett, *Nature*, 400, (1999) 649
[93] J.W. Fergus, Solid State Ionics, 177 (2006) 1529-1541
[94] G. Pudmich, B.A. Boukamp, M. Gonzalez-Cuenca, W. Juengen, W.Zipprich, F.Tietz, Solid State Ionics, 135 (2000) 433-438
[95] J. Canales-Vasquez, S.W. Tao, J.T.S. Irvine, *Solid State Ionics*, 159 (2003) 159-165
[96] Q.Fu, F.Tietz, D.Sebold, S.Tao, J.T.S. Irvine, Journal of power sources, 171 (2007) 663-669
[97] A.Ovalle, J.C. Ruiz Morales, J. Canales-Vasquez, D. Marrero-Lopez, J.T.S. Irvine, Solid state Ionics, 177 (2006) 1997-2003
[98] Q.X. Fu, F.Tietz, D.Stover, Journal of the electrochemical society, 153 (4) D74-D83 (2006)
[99] J. C. Ruiz-Morales, J. Canales-Vazquez, C. Savaniu, D. Marrero- Lopez, W. Z. Zhou and J. T. S. Irvine, *Nature*, 2006, 439, 568–571.
[100] J. C. Ruiz-Morales, J. Canales-Vazquez, C. Savaniu, D. Marrero- Lopez,P.Nunez, W. Z. Zhou and J. T. S. Irvine, Phys. Chem. Chem. Phys., 9 (2007) 1821-1830
[101] P. Blennow, K. K. Hansen, L. R. Wallenberg, and M. Mogensen, *Solid State Ionics*, (submitted for publication) (2007).
[102] P.Blennow, K.H. Hansen, L. R. Wallenberg, M. Mogensen, *ECS transactions*, 13 (26) (2008) 181-194
[103] H. Yokokawa, N. Sakai, T. Kawada and M. Dokiya, *Solid State Ionics* **52** (1992) 43.
[104] N. Sakai, K. Yamaji, T. Horita, H. Yokokawa, T. Kawada and M. Dokiya, *J. Electrochem. Soc.* **147** (2000) 3178.
[105] . M. Mori and Y. Hier, *J. Amer. Ceram. Soc.* **84** (2001) 2573.
[106] . S . Tanasescu, D. Berger, D. Neiner and N. D.Totir, *Solid State Ionics* **157** (2003) 365.
[107] S. Tao, J.T.S. Irvine, *Chem. Rec.*, 4 (2004) 83
[108] J . Sfeir, J. van Herle, A.J. Mcevoy, *J. Euro. Ceram. Soc.*, **19** (1999) 897.
[109] J. Sfeir, P.A. Buffat, P. Mockli, N. Xanthopoulos, R. Vasquez, H.J. Mathieu, J. van Herle, K.R. Thampi, *J. Catal.*, **202** (2001) 229.
[110] J . Sfeir, *J. Power Sources*, **118** (2003) 276.
[111] J . Sfeir, J. Van Herle and R. Vasquez, in "5th European SOFC Forum," edited by J. Huijsmans (European SOFC Forum, Switzerland, 2002) p. 570.
[112] A. L. Sauvet and J.T.S. Irvine, in "5th European SOFC Forum," edited by J. Huijsmans (European SOFC Forum, Switzerland, 2002) p. 490.
[113] S . Tao, J.T.S. Irvine, in "SOFC-VIII," edited by S.C. Singhal and M. Dokiya (Electrochem. Soc., Pennington, NJ, 2003) Vol. 2003–07, p. 793.
[114] S.Tao, J.T.S. Irvine, *Journal of the electroch. Soc.*, 151(2) (2004) A252-A259
[115] S.Tao, J.T.S. Irvine, S.M. Plint, J. Phys. Chem: B, 110 (2006) 21771-21776
[116] S.P. Jiang, X.J. Chen, S.H. Chan, J.T. Kwok, K.A Khor, *Solid State Ionics*, 177 (2006) 149-157
[117] J.C. Ruiz-Morales, J.Canales-Vasquez, B. Ballesteros-Perez, J. Pena-Martinez, D. Marrero-Lopez, J.T.S. Irvine, P. Nunez, *Journal of the European ceramic society*, 27 13-15 (2007) 4223-4227
[118] X.J. Chen, Q.L. Liu, K.A. Khor, S.H. Chan, *Journal of power sources*, 165 1 (2007) 34-40
[119] X.J. Chen, Q.L. Liu, S.H. Chan, N.P. Brandon, K.A. Khor, *Journal of the electrochemical Society*, 154 11 (2007) B1206-B1210
[120] M.K. Bruce, M. van den Bosche, S.McIntosh, *Journal of the elctrochemical society*, 155 (11) B1202-B1209 (2008)
[121] M. Van den Bossche, S. McIntosh, *Journal of catalysis*, 255 -2 (2008) 313-323
[122] X.C. Lu, J.H. Zhu, *Solid State Ionics*, 178 25-26 (2007) 1467-1475
[123] Y.Ye, T.He, Y.Li, E.H. Tang, T.L. Reitz, S.P.Jiang, *Journal of the electrochemical society*, 155 (8)

B811-818 (2008)
[124] S.P. Jiang, Y.M. He, T.M. He, S.B. Ho, Journal of power sources, 185 1 (2008) 179-182
[125] J. Liu, B.D. Madsen, J. Ji, S.A. Barnett, *Electrochem. Solid-State Lett.*, 5 (6) (2002) A122.
[126] E. Lay, G. Gauthier, S. Rosini, C. Savaniu, J.T.S. Irvine, *16th International conference on solid state ionics, Shangai*, China, 2008
[127] X.Y. Lu, P.W. Faguy, M.I. Liu, *J. Electrochem. Soc*,. **149,** A1293–A1298 (2002).
[128] R.J. Gorte, S.Park, J.M. Vohs and C.H. Wang, *Adv. Mater.*, 12, 1465-1469 (2000)
[129] S. Park, R. J. Gorte, and J. M. Vohs, *Journal of the Electrochemical Society*, 148 (2001) A443-A447
[130] M.D. Gross, J.M. Vohs, R.J. Gorte, *ESSL*, 10 (4) (2007) B65-B69

Experimental Methods

All fuel cells samples used in the study of oxides impregnated functional layers have been prepared following the standard procedure used at the University of Pennsylvania. Such button cells are planar and feature a 300 μm thick cathode, supporting a relatively thin 65 μm electrolyte. The functional layers were about 60μm for all the cells. The active area of the cells, equal to the anode area, was 0.35 cm^2, but the area of the electrolyte and cathode were approximately 1 cm^2.

The first step in preparing fuels cells is to make a YSZ wafer consisting of two porous layers (electrodes) separated by a dense layer (electrolyte). This porous-dense-porous YSZ structure is obtained by laminating three green tapes, with the ones to be porous containing pore formers. The green tapes were prepared by mixing YSZ powder (Tosoh Corp., 8 mol % Y_2O_3-doped ZrO_2, 0.2 μm) with distilled water, a dispersant (1.27 g, Duramax 3005, Rohm & Haas), and binders (10.2 g HA12 and 14.4 g B1000, Rohm & Haas). Porosity was created by adding graphite to the slurry used for the anode, while graphite and polystyrene were used for the cathode. Polystyrene is used to introduce bigger pores in the cathode. Pore formers were added in amounts to obtain a 65% porous structure. The laminated green tapes are then fired at 1500ºC for several hours to produce the porous-dense-porous YSZ structure. After the three-layer YSZ wafer has been synthesized, 45 wt% of conductive oxide was added to the porous anode layer using aqueous nitrate solutions. For LSCM, the impregnating solution was prepared by adding $La(NO_3)_3.6H_2O$ (Alfa Aesar, ACS 99.9%), $Sr(NO_3)_2$ (Alfa Aesar, ACS 99.0%), $Cr(NO_3)_3{\cdot}9H_2O$ (Alfa Aesar, ACS 98.5%), and $Mn(NO_3)_2{\cdot}4H_2O$ (Alfa Aesar, ACS 99.98%) to distilled water in the correct molar ratios, then mixing this with citric acid (99.5%, Aldrich) to produce a solution with a citric acid/metal-ion ratio of 2:1. For LSTM, the impregnating solution was prepared by using the same precursors for La, Sr and Mn, but using $(CH_3CH(O-)CO_2{\cdot}NH_4)_2{\cdot}Ti(OH)_2$ (Dihydroxy-bis-ammonium, lactate, titanium (IV), Alfa Aesar) as a Ti precursor. No citric acid was added for LSTM solutions.

Infiltrating porous layers with such solutions is a multi step process. When the porous layer has been infiltrated, the ceramic wafer is heated in air to 450ºC to decompose the nitrate ions and the citric acid. This procedure has to be repeated until the desired weight loading of oxide is achieved. Finally, when the required loading has been reached, the wafer is heated in air at high temperature to form the perovskite phase. XRD was used to verify that the correct phase had been formed within the scaffold.

After forming the oxide phase in the anode layer, the $La_{0.8}Sr_{0.2}FeO_3$(LSF)–YSZ cathodes were synthesized by impregnating the 300 μm thick layer with an aqueous solution containing $La(NO_3){\cdot}6H_2O$, $Sr(NO_3)_2$, and $Fe(NO_3)_3{\cdot}9H_2O$, to a loading of 40 wt % LSF, followed by calcination to 850ºC. For the present studies, it is only important that the impedance of LSF–YSZ cathodes prepared in this way is between 0.1 and 0.15 Ù.cm2 at 700º C and is independent of current density[1].

Ag Paste (SPI supplies, Lot #1120912) was used as a conductive layer for both the anode and the cathode. To determine the effect of the current-collector catalytic properties, one study used Pt ink (Engelhard, A3788A) as the anode current collector.

Fuel cell tests were performed by attaching the samples to an alumina tube with a ceramic adhesive (Aremco, Ceramabond 552). Electrical connections were achieved using Ag wire at both the anode and cathode. The fuel to the anode was either humidified (3% H_2O) H_2 or CH_4, while the cathode was exposed to air. Impedance

spectra were measured at open circuit in the galvanostatic mode with a frequency range of 0.1 Hz to 100 kHz and a 5 mV ac perturbation using a Gamry Instruments potentiostat.

For each oxide used in anodes, electronic conductivities of impregnated YSZ structures have been measured as a function of temperature in air and in humidified H_2 using standard four-probe measurements. Oxide-YSZ composites were prepared by impregnating porous YSZ bars that were made with the same YSZ slurries used for the anode green tapes. The electronic conductivities of impregnated YSZ composites were measured. Slabs were about 1 x 1 x 10 mm in size.

The 45-wt% LSCM-YSZ composite samples used for conductivity measurements have been used to measure their redox properties using coulometric titration. This device used was a sealed YSZ tube with Ag-paste electrodes on both sides. After placing the sample in the tube, the $P(O_2)$ was determined from the open-circuit potential. Oxygen could be added or removed from the tube by passing a current through the same electrodes used in measuring the potential. In this study, the oxidation isotherms were obtained following sample reduction in a flowing mixture of 90% N_2 and 10% H_2 for 1.5 h at 1023 K. The sample was then allowed to come to equilibrium using the criterion that the potential of the oxygen sensor change by less than 1 mV/h. Additional oxygen was added to the sample by passing charge through the same electrodes used for oxygen sensing.

[1] W. S. Wang, M. D. Gross, J. M. Vohs, R. J. Gorte, *J. Electrochem. Soc.*, 154 (2007) B439.

Initial performances

5.1. Introduction

The most promising oxide developed at the University of St Andrews, LSCM, has been first used to impregnate functional layers. The composition used was $La_{0.75}Sr_{0.25}Cr_{0.5}Mn_{0.5}O_3$ and the phase was sintered at 1200ºC for 4 hours. The target loading of LSCM was 45 wt.%. To provide sufficient electrocatalytic activity, 5 wt% CeO_2 and 0.5 wt.% Pd were added after the LSCM phase had been formed.

One concern when infiltrating conductive oxides into porous YSZ structures stems from the composite conductivity. Indeed, the electronic conductivity of porous composites is typically 100-1000 times less than the one of the electronic conductor in the composite. As an example, the conductivity of a typical Ni-YSZ cermet is about 1000 S/cm [1] [2], three order of magnitudes lower than pure Ni conductivity, and the conductivity of a LSM-YSZ is typically near 1 S/cm [3], 100 times lower than bulk LSM conductivity. Therefore, conductivity tests were first carried out on impregnated LSCM-YSZ composites to ensure sufficient electronic conductivity was provided.

5.2. Results

Figure 28 reports the XRD diffraction pattern of the LSCM infiltrated structure, showing that the correct phase has been formed in situ. Figure 29 shows a SEM micrograph of a typical fuel cell. The top part of the SEM picture is the anode. Note that bigger pores can be seen in the cathode due to the use of polystyrene as a pore former.

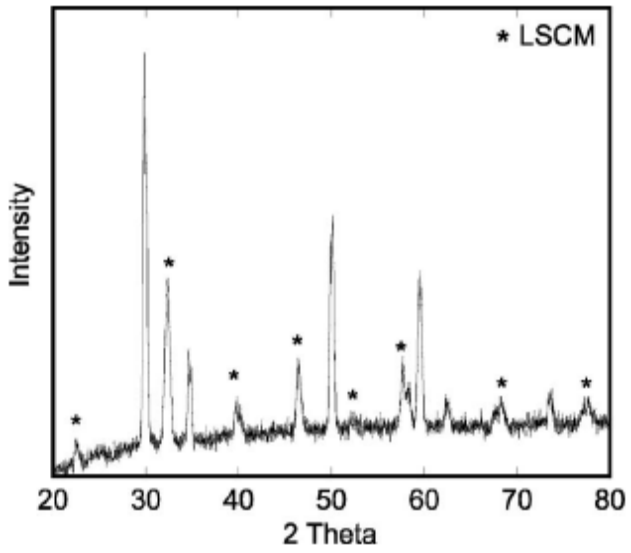

Figure 28: An XRD of an LSCM-YSZ composite with 45 wt % LSCM formed by infiltration into porous YSZ.

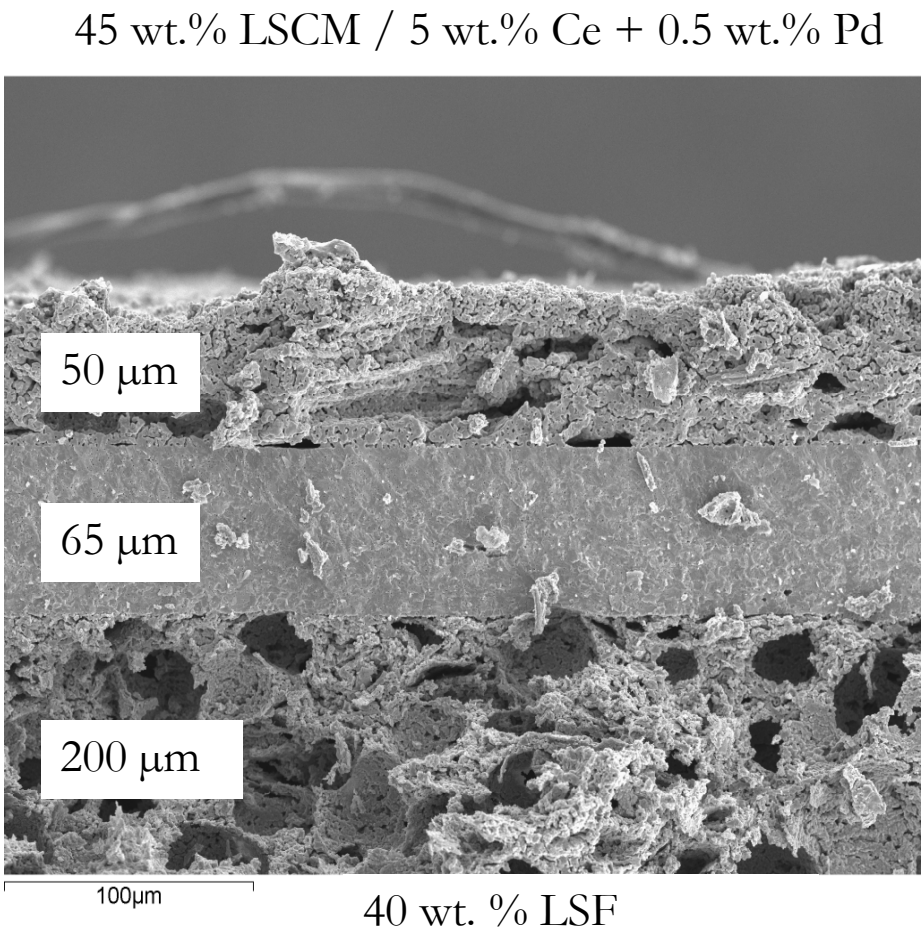

Figure 29: SEM image of a button cell used in this study showing from top to bottom: the LSCM impregnated functional layer, the dense YSZ electrolyte, the LSF impregnated cathode.

Conductivity of LSCM impregnated YSZ structures were first measured to ensure that such a composite complies with conductivity requirement for a functional layer. Figure 30 reports the conductivities obtained from of 45 wt.% impregnated YSZ structures as a function of temperature in both humidified (3% H_2O) H_2 and air.

The conductivities of those composites are weakly temperature dependent, with values of approximately 1 S/cm in air and 0.1 S/cm in wet H_2 at 800ºC. The lower conductivity in a reducing environment is an intrinsic property of p-type conductors such as LSCM[4]. A conductivity of 0.1 S/cm meets the requirements for the functional layer of an electrode that have been specified above. Based on those measurements, a 60 μm layer relying on LSCM for the electronic conductivity would show ohmic losses of 0.06 $\Omega.cm^2$, which can be considered as a fairly low ohmic loss for an alternative electrode. While the conductivities of those composites are significantly lower than that of the bulk LSCM, they are relatively high for a composite that is only 28 vol.% LSCM. Bulk LSCM conductivity has been reported to be 30 S/cm in air and 1-2 S/cm in H_2 at 900°C.

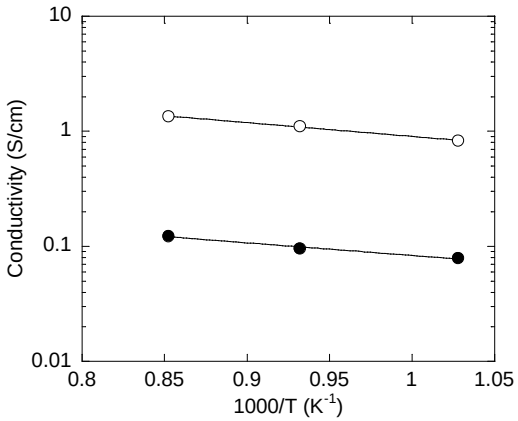

Figure 30: The electrical conductivities for the 45 wt. % LSCM-YSZ composite in air (open circles) and humidified H_2 (filled circles) as a function of temperature.

The initial voltage-current density polarization and impedance data for those cells are reported in Figure 31 and Figure 32 for different temperatures in humidified H_2. The OCV was close to the theoretical Nernst potential, 1.1V. The maximum power densities obtained were 520 mW/cm^2 at 700ºC, 1.1 W/cm^2 at 800ºC and 1.4 W/cm^2 at 900ºC. A few comments can be made about those power densities. First, they are higher than any other power density obtained on the same type of cells using other materials as electronic conductors. Moreover, such power densities compare well with fuel cells using standard Ni/YSZ anodes and are excellent for alternative anode materials, even in the range 700-800ºC.

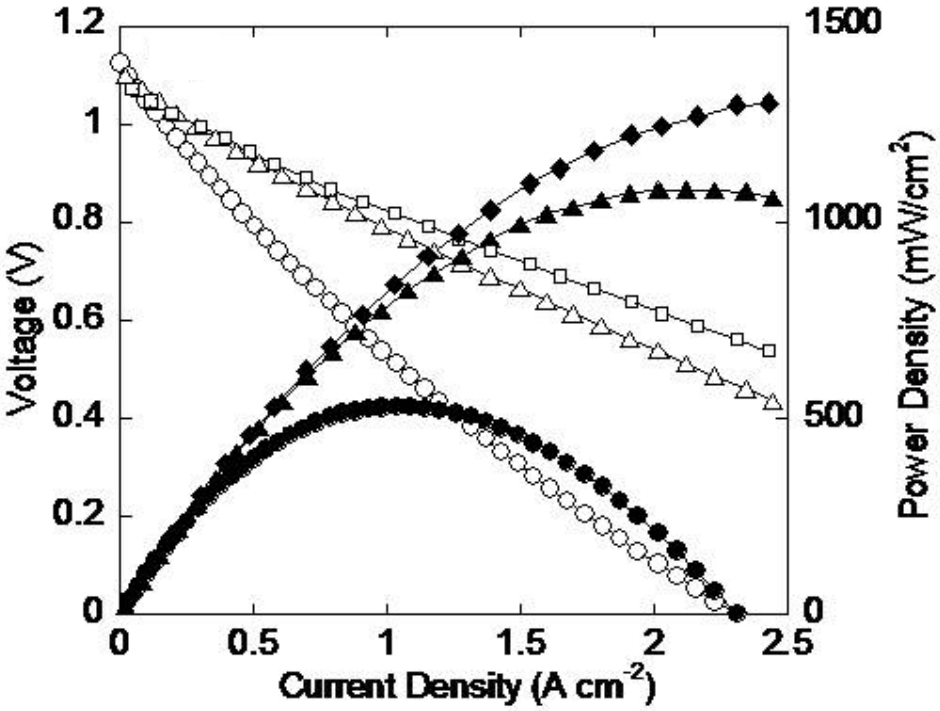

Figure 31: V-I polarization curve for the cell with the anode containing 0.5 wt. % Pd and 5 wt. % CeO_2, measured in humidified H_2 (3% H_2O) at (○) 700°C, (Δ) 800°C and (□) 900°C.

Concerning the evolution of power densities with temperatures, performances increase substantially from 700ºC to 800ºC, but such a difference does not occur from 800 to 900ºC. Impedances recorded were 0.57 $\Omega.cm^2$ at 700ºC, 0.3 $\Omega.cm^2$ at 800ºC and 0.25 $\Omega.cm^2$ at 900ºC. Impedances clearly show the substantial improvement from 700ºC to 800ºC, while they are somewhat similar at 800 and 900ºC. The arc at low frequency, which can be attributed to concentration polarization, is temperature independent, indication small fuel conversions[5].

It is important to note here that while a 65µm electrolyte is quite thin, its resistance will still account for most of the losses in the cell. The high performances of those anodes can be understood by singling out the different contributions to the impedance. At 700ºC, the expected resistance for the electrolyte is 0.35 $\Omega.cm^2$ and a LSF impregnated YSZ cathode has been shown to offer a resistance in the range 0.1-0.15 $\Omega.cm^2$ at 700ºC. Based on those values, the contribution of the anode would be only in the range 0.07- 0.12 $\Omega.cm^2$ at 700ºC, which can be claimed as a definite satisfying value for an alternative anode at such a low temperature.

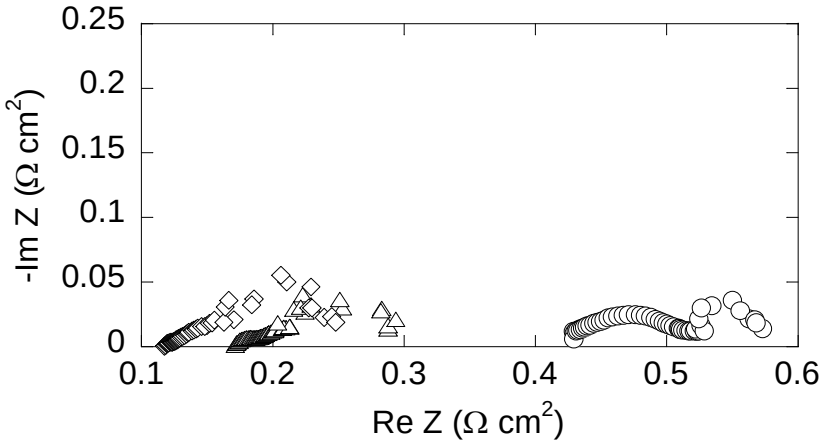

Figure 32: Impedance spectra for V-I polarization curve for the cell with the anode containing 0.5 wt. % Pd and 5 wt. % ceria, measured in humidified H_2 (3% H_2O) at at (○) 700°C, (Δ) 800°C and (□) 900°C.

Those cells have been tested in humidified (3% H_2O) CH_4. Figure 33 and Figure 34 respectively report the IV curves and impedances as a function of temperature. OCVs in wet CH_4 were higher than with wet H_2, around 1.15 V. The curvature in the IV curve observed near OCV, which cannot be seen with hydrogen, indicates that methane activation by polarization is required. This can be seen as well by comparing the impedance spectra obtained on H_2 (Figure 32) and CH_4 (Figure 34). At 800ºC, while the ohmic resistances are similar for both fuels, the non-ohmic resistance is higher for methane, indicating higher losses in the electro-oxidation processes. Those losses in turn induce a drop in the maximum power densities compared to H_2 oxidation, and were 400 mW/cm^2 at 700ºC and 710 mW/cm^2 at 800ºC. Those values are remarkably high and compare well to previously reported works in the absence of high steam content. To our knowledge, those performances are the highest that have been reported in the literature for direct methane oxidation, noting that a 65 µm electrolyte would be considered as relatively thick by many authors. Previous published studies have reported maximum power densities of 550 W cm−2 for

Pd/CeO2 impregnated YSZ[6] and 400 W.cm^{-2} for Sr_2MgMoO_6[7] , while various studies on $(Gd,Ce)O_{2-x}$ impregnated LSCM have achieved 158 mW.cm^{-2} power output and 0.44 Ω.cm^2 polarization resistance at 800ºC in humidified methane[89] .

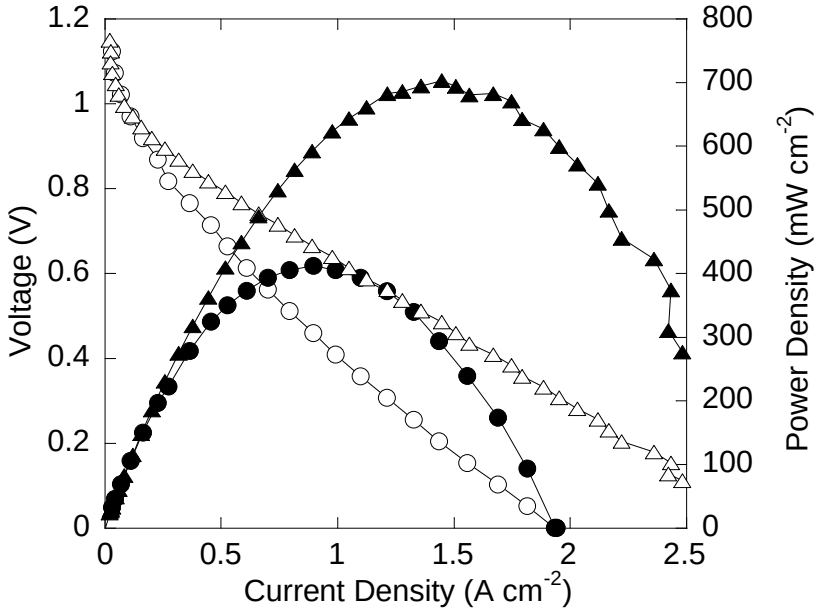

Figure 33: V-I polarization curve for the cell with the anode containing 0.5 wt. % Pd and 5 wt. % CeO_2, measured in humidified H_2 (3% H_2O) at (○) 700°C and (Δ) 800°C.

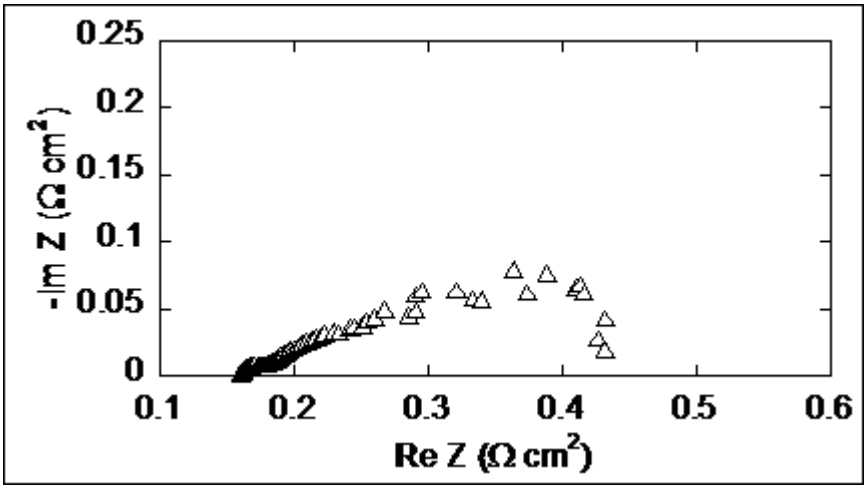

Figure 34: Impedance spectra for V-I polarization curve for the cell with the anode containing 0.5 wt. % Pd and 5 wt. % CeO_2, measured in humidified CH_4 (3% H_2O) at 800°C.

5.3. Conclusion

Outstanding performance for alternative anodes was achieved on hydrogen, with power densities above 1 W/cm^2 at 800°C. It is important to note that the electrolyte accounts for most of the losses in our samples. The functional anode resistance is

close to 0.1 $\Omega.cm^2$ at 700°C, which is a remarkably low resistance for such a low temperature. The direct oxidation of wet methane without carbon deposition has been demonstrated. The power densities obtained on methane are the highest that have been reported in the literature so far.

[1] W. Z. Zhu, S. C. Deevi, *Matls. Sci.*, & Eng., A362, 228 (2003).
[2] J.-H. Lee, J.-W. Heo, D.-S. Lee, J. Kim, G.-H. Kim, H.-W. Lee, H.S. Song, J.-H. Moon, *SSI*, 158, 225 (2003)
[3] H. He, Y. Huang, J. Regal, M. Boaro, J. M. Vohs, and R. J. Gorte, *Journal of the American Ceramic Society*, 87 (2004) 331-336.
[4] S. Tao, J.T.S. Irvine, *Journal of the electroch. Soc.*, 151(2) (2004) A252-A259
[5] B. Barfold, A. Hagen, S. Ramousse, P.V. Hendriksen, M. Mogensen, *Fuel Cells*, 6 (2) (2006) 141-145
[6] M. D. Gross, J. M. Vohs, and R. J. Gorte, *Electrochem. Solid-State Lett.*, 10, B65(2007).
[7] Y. H. Huang, R. I. Dass, Z. L. Xing, and J. B. Goodenough, *Science*, 312, 254 (2006).
[8] X. J. Chen, Q. L. Liu, S. H. Chan, N. P. Brandon, K. A. Khor, *Electrochem. Commun.*, 9, 767 (2007)
[9] S. P. Jiang, X. J. Chen, S. H. Chan, and J. T. Kwok, *J. Electrochem. Soc.*, 153, A850 (2006)

CO_2 Electrolysis

In this chapter, we describe the performance characteristics for CO_2 electrolysis of an SOE with a fuel-electrode based on LSCM impregnated functional layer. Samples used to investigate the feasibility of CO_2 electrolysis were identical to the fuel cells presented in the previous chapter, though a different catalyst has been used. 0.5-wt% Pd and 5 wt. % of the mixed oxide, $Ce_{0.48}Zr_{0.48}Y_{0.04}O_2$ (CZY), were added as catalysts to the LSCM-containing layer using the standard procedure described in the experimental part. Pd supported on ceria-zirconia is known to be highly active for oxidation catalysis[1] and Y doping of the ceria-zirconia maintains the mixed oxide as a single-phase material following high-temperature treatments[2].

6.1. CO_2 Electrolysis

The ability to reduce CO_2 efficiently is a topic receiving a growing attention nowadays. It could play a role in reducing greenhouse gas emissions and moving us towards a more sustainable economy [3]. CO produced by CO_2 reduction can be used in chemical production or reacted with H_2 to produce liquid fuel via the fischer-tropsch reaction [4]. Indeed, in the search of sustainable energy carriers to replace petroleum, synthetic fuels are likely to play an important part, if we acquire the ability to produce them efficiently from renewable sources. At first, synfuels might likely utilize CO_2 from industrial sources, where the CO_2 is concentrated in process outflows. In the long term, it may be possible to capture CO2 directly from the air, forming a closed-loop hydrocarbon cycle. Those two possible cycles are illustrated on Figure 35. To fully make sense, the CO_2, as much as H_2O for H_2 production, must undergo dissociation without the use of fossil energies.

When the economy is based on renewable energy sources, such as wind and solar, the major source of H_2 for chemical production and energy storage will be from the electrolysis of water.

In the search for efficient processes to reduce CO_2, Solid Oxide Electrolysers (SOE) appear to promising candidates. Solid Oxide Electrolysers (SOEs) are essentially SOFCs operated in reverse, meaning that a current is applied to the cell instead of being drawn from the cell. In an SOE, the cathode (the fuel-side electrode) reaction for water electrolysis is the electrochemical dissociation of steam to produce H_2 and O^{2-} anions (Eq. 29), while recombination of the oxygen ions to O_2, (Eq 30.), occurs at the anode (the air-side electrode):

$$H_2O + 2e^- \rightarrow O^{2-} + H_2 \quad \textbf{(Equation 29)}$$

$$O^{2-} \rightarrow 2e^- + \tfrac{1}{2}O_2 \quad \textbf{(Equation 30)}$$

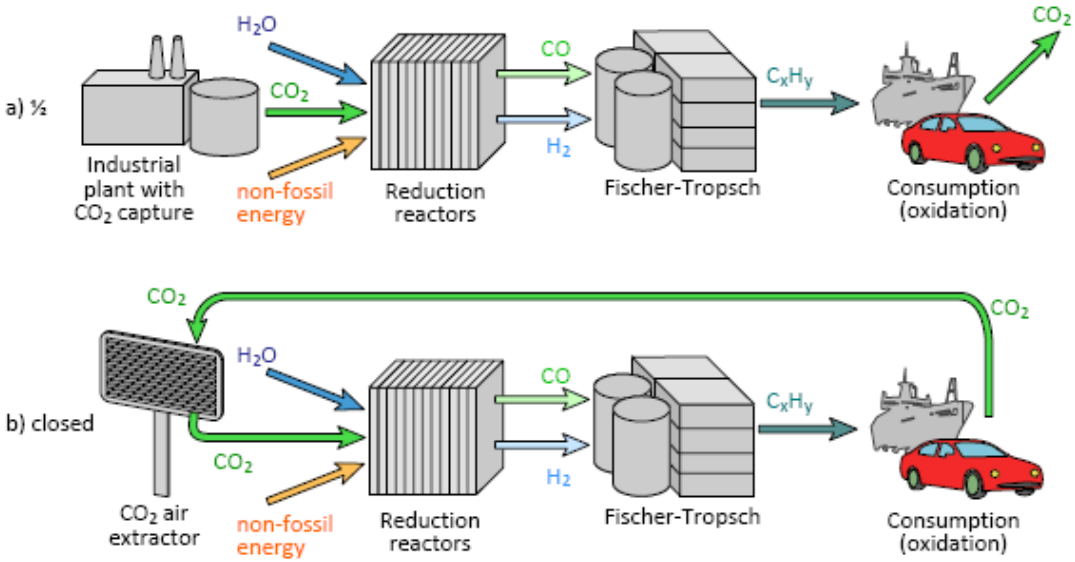

Figure 35: Proposed role of CO_2 in the production of synthetic fuels[5].

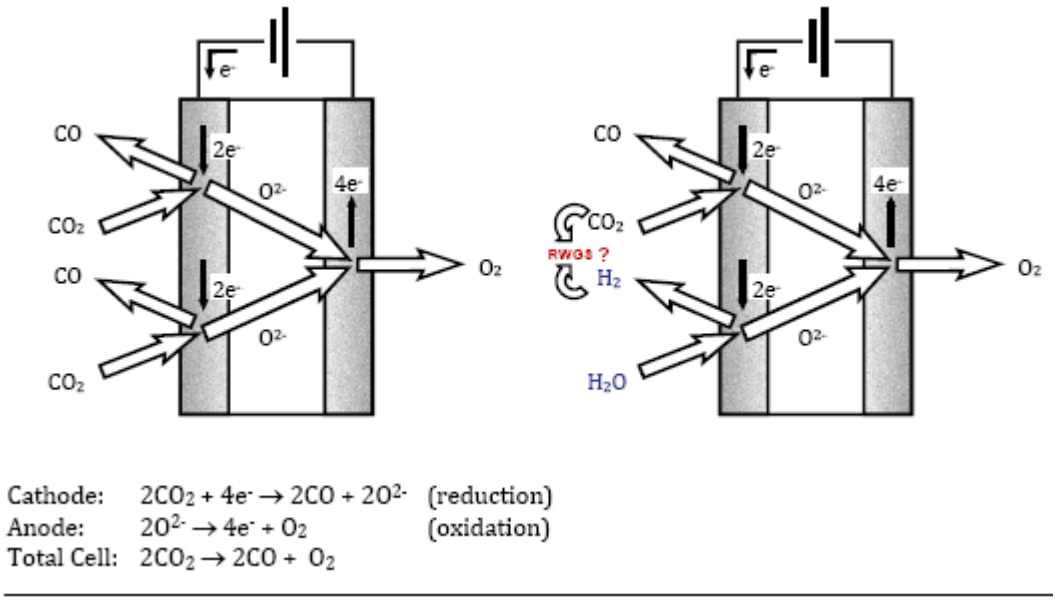

Cathode: $2CO_2 + 4e^- \rightarrow 2CO + 2O^{2-}$ (reduction)
Anode: $2O^{2-} \rightarrow 4e^- + O_2$ (oxidation)
Total Cell: $2CO_2 \rightarrow 2CO + O_2$

Figure 36: Principle Scheme of Solid Oxide Electrolyser, using CO_2 as a fuel (left) and both CO_2 and H_2O (right)[5].

By analogy to the dissociation of steam (Eq. 29), the reduction of CO_2 can also be carried out at the fuel-side electrode as described in equation 31:

$$CO_2 + 2e^- \rightarrow O^{2-} + CO \quad \textbf{(Equation 31)}$$

The Nernst potentials for electrolysis of H_2O and CO_2 are virtually identical. The operating principle of a SOE is illustrated on Figure 36.
SOE are capable of higher water electrolysis efficiencies compared to solution-based electrolysis cells because they operate higher temperature (<700°C). The higher

operating temperature results in a lower Nernst potential and in lower electrode overpotential[6].

There are a few reports in the literature for the electrochemical reduction of CO_2 to CO in SOE[7,8,9]. Most of these have focused on O_2 production for space missions and have employed expensive bulk Pt electrodes that would not be practical for large-scale CO_2 electrolysis as would be required for sustainable chemicals and fuels production. Furthermore, the overpotentials for the Pt electrodes used in these studies were very high, so that the efficiency for CO_2 reduction was low.

In conventional SOE used for steam electrolysis, the fuel-side electrode is a composite of Ni and YSZ[10,11,12], the same material that is used in SOFC for oxidation of H_2. In principle, Ni-YSZ electrodes can be used for CO_2 electrolysis[13] but they suffer from several important limitations. First, while Ni-YSZ electrodes are efficient for H_2 oxidation, electrode overpotentials for CO oxidation are much higher[14]. Indeed, a highly-optimized SOFC that was able to produce 1.8 W/cm^2 when H_2 was the fuel produced less than 0.3 W/cm^2 on a 44% CO-56% CO_2 mixture at 800°C[15]. When SOFC are operated on syngas, a mixture of CO and H_2, the oxidation of CO proceeds primarily through the water-gas-shift reaction, $CO + H_2O \rightarrow H_2 + CO_2$, with H_2 oxidation still being the primary electrochemical reaction [10,11]. Second, there are concerns about the stability of Ni-YSZ composites in a CO-CO_2 environment. Ni carbonyls are highly volatile[16], making it important to choose operating conditions for which carbonyl formation is less favourable. Ni is also a superb catalyst for the Boudouard reaction, $2CO \rightarrow C + CO_2$[17,18] so that operation would be limited to higher temperatures and CO_2:CO ratios to avoid equilibrium conditions favourable for this reaction. Finally, Ni-YSZ composites are severely damaged by re-oxidation[19]. Since Ni would be oxidized by pure CO_2, it would be necessary to ensure that the feed to any CO_2 electrolyser contained sufficient CO or H_2 to make the gas composition reducing over all parts of the electrode.

6.2. Results

Figure 37 compares the cell performance with the fuel-side electrode exposed to 90% H_2–10% H_2O and 90% CO–10% CO_2 mixtures at 700 ºC. Positive currents indicate the oxidation of H_2 and CO and negative currents indicate the reduction of H_2O and CO_2. The open circuit potentials were 1.05 V in H_2–H_2O and 1.07 V in CO–CO_2, which is close to the calculated Nernst potentials for these fuel compositions when the opposite electrode is exposed to ambient air. The overpotentials in the electrolysis mode are logically higher than in the fuel cell mode, since the feeds to the fuel side were dilute in both H_2O and CO_2. With the H_2–H_2O mixture, a current density of 1.14 A/cm^2 was obtained at a cell potential of 0.5 V, while the corresponding electrolysis current density at 1.5 V was only 0.64 A/cm^2. With CO–CO_2 mixtures, the corresponding current densities at 0.5 and 1.5 V were 0.75 and 0.34 A/cm^2, respectively. A fuel typically works better with H_2 than CO. In the same way, the electrolysis of H_2O is performed more efficiently than the electrolysis of CO_2.

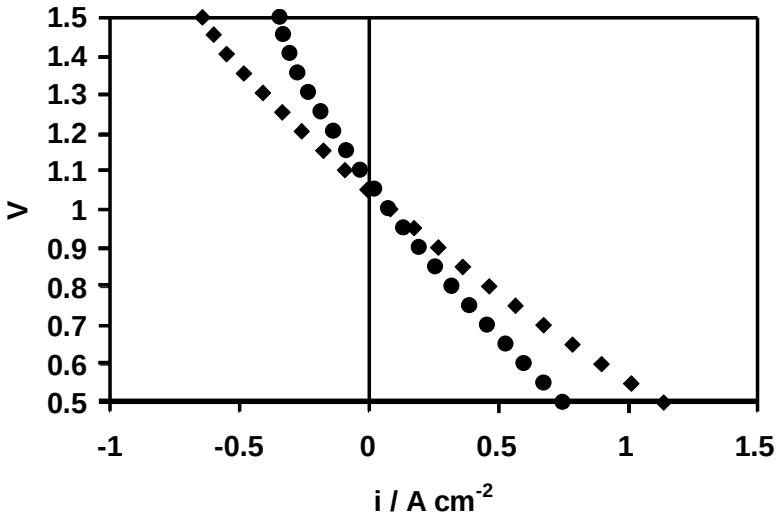

Figure 37: V-i polarization curves for 10% H_2O- 90% H_2 (♦) and 10% CO_2-90% CO (•) mixtures at 700°C. Negative currents correspond to electrolysis of H_2O or CO_2.

The corresponding open-circuit impedance spectra, shown on Figure 38, provide insight into the origin of the overpotential losses while operating in the electrolysis mode. As expected, a significant fraction of the cell losses was ohmic and attributable to the internal resistance drop in the 65 µm YSZ electrolyte. The measured ohmic losses were 0.37 $\Omega.cm^2$ for operation in H_2 and H_2O and 0.35 Ω,cm^2 for operation in CO and CO_2, in good agreement with the calculated resistance of 0.35 $\Omega.cm^2$ expected for the 65 µm electrolyte, using reported YSZ conductivities[20]. The nonohmic losses were 0.19 $\Omega.cm^2$ for operation in H_2–H_2O and 0.6 $\Omega.cm^2$ for operation in CO–CO_2. Losses for the LSF–YSZ air electrode are estimated to be between 0.1 and 0.15 $\Omega.cm^2$ at 700°C[21], suggesting that the fuel electrode losses in H_2–H_2O are approximately 0.1 Ω cm^2 and those in CO–CO_2 mixtures are 0.5 Ω cm^2. This difference in the non ohmic losses between the two fuel mixtures confirms that the electrochemistry is better performed for H_2O than CO_2.

Figure 39 and Figure 40 show the V-I relationships for the cell during electrochemical reduction of CO_2 and oxidation of CO as a function of the CO:CO_2 ratio in the fuel at 700 and 800 °C, respectively. When operating at a given current density, the overpotential decreases in the electrolysis mode as the CO_2/CO ratio increases, while the opposite trend is logically observed in the fuel cell mode. When pure CO_2 is fed to the fuel-side electrode, the open circuit potential is close to zero. While the LSCM anode can withstand such conditions, a Ni-YSZ electrode would obviously undergo oxidation in the same conditions. As one can expect, no fuel cell operation can be achieved when pure CO_2 is fed, while no electrolysis can be achieved when pure CO is fed. The cell potential rises to ~0.8 V as CO is produced by CO_2 reduction.

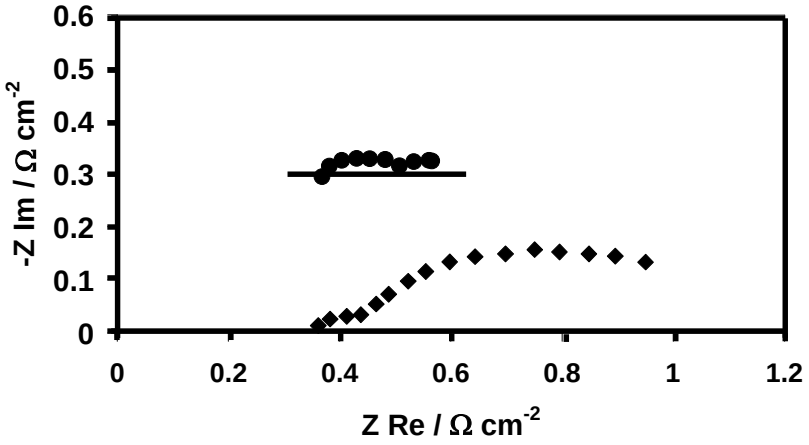

Figure 38:Cole-Cole plots, measured at the open-circuit potentials, for 10% H_2O- 90% H_2 (•) and 10% CO_2-90% CO (♦) mixtures at 700°C. Negative currents correspond to electrolysis of H_2O or CO_2.

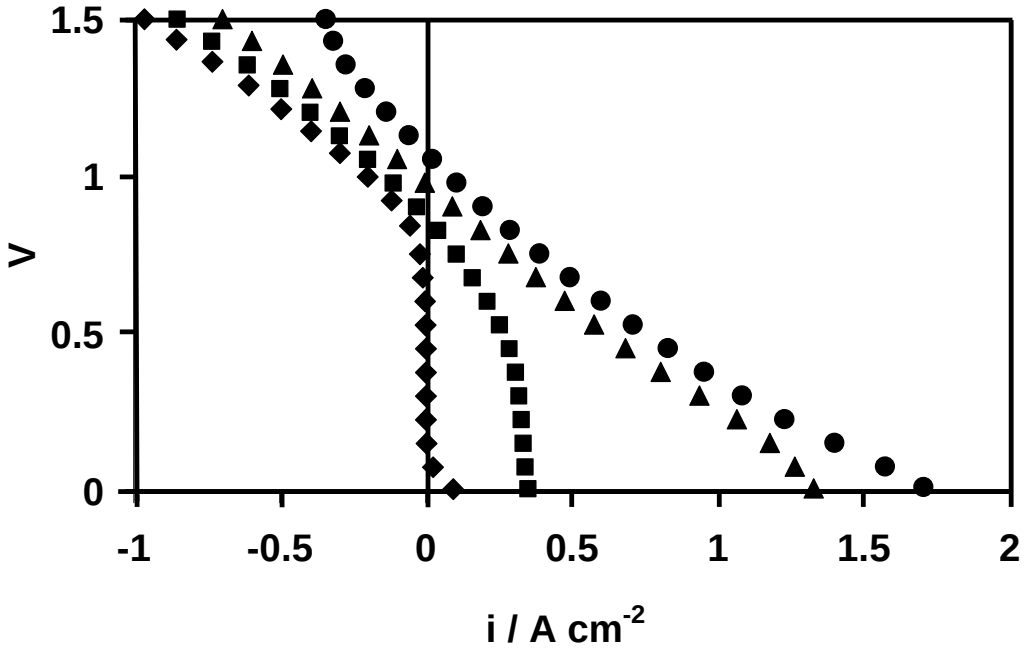

Figure 39: V-i polarization curves for mixtures of CO_2 and CO at 700°C. Negative currents correspond to electrolysis of CO_2. 100% CO_2-0% CO (♦); 90% CO_2-10% CO (■); 50% CO_2-50% CO (▲); 10% CO_2-90% CO (●).

At 1.5 V, the reduction current reaches 0.96 A/cm^2 at 700°C and 1.8 A/cm^2 at 800°C. At 800°C for a CO_2:CO ratio of 9:1, the open-circuit potential is 0.87 V and increases with decreasing CO_2:CO ratio. The slope of the V-i curve remains nearly the same as that for pure CO_2, however, as long as there is sufficient CO_2 to avoid diffusion limitations. Diffusion limitations are almost certainly the reason for the increase in the slope at higher current densities. The nearly constant slopes, approximately 0.63 Ω.cm^2 at 700°C and 0.36 Ω.cm^2 at 800°C, reflect the fact that the electrode

impedances are nearly current-independent so long as diffusion of CO_2 (for CO_2 reduction) or CO (for CO oxidation) are not limiting. Because 65-μm YSZ electrolyte contributes to the increased slope of these lines, 0.35 Ωcm^2 at 700°C and 0.15 Ωcm^2 at 800°C [20], significant improvements could be made by using a thinner electrolyte.

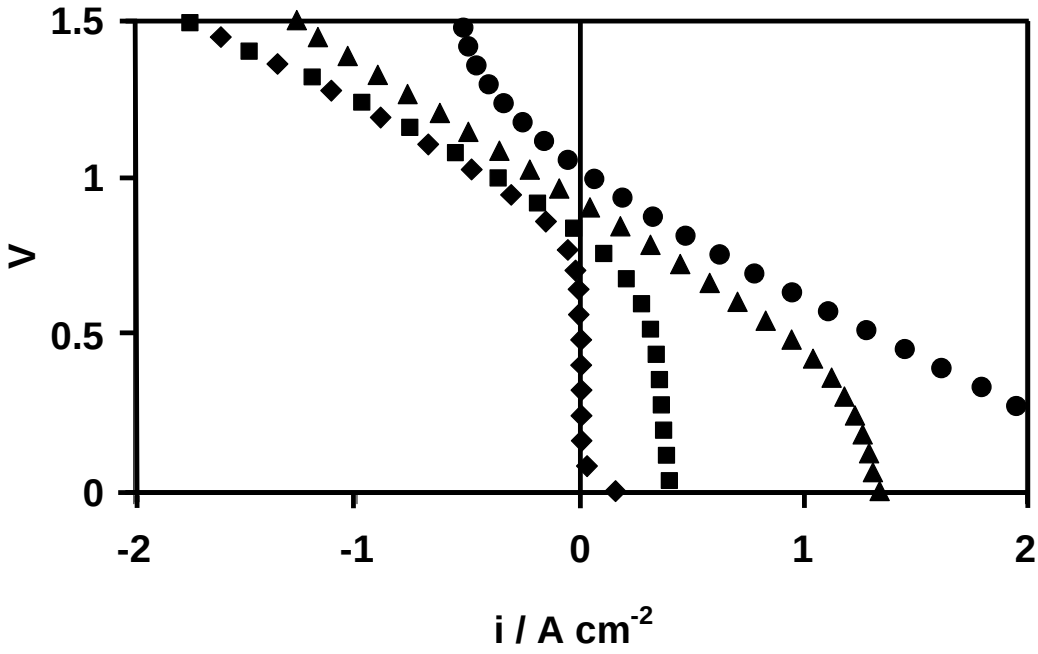

Figure 40: V-i polarization curves for mixtures of CO_2 and CO at 800°C. Negative currents correspond to electrolysis of CO_2. 100% CO_2-0% CO (♦); 90% CO_2-10% CO (■); 50% CO_2-50% CO (▲); 10% CO_2-90% CO (●).

It is interesting to consider how the LSCM-based electrode in the present study compares to the best Ni-YSZ electrodes. Since the only available CO_2 electrolysis data on cells with Ni-YSZ electrodes is for much higher temperatures, 950°C[22], the comparison is performed looking at the cells in the fuel cell mode. As mentioned in the introduction, a highly-optimized SOFC with a Ni-YSZ anode and a 10-μm thick electrolyte produced less than 0.3 W/cm^2 on a 44% CO-56% CO_2 mixture at 800°C, even though it was capable of producing 1.8 W/cm^2 on 100% H_2 at this temperature[15]. Figure 41, which shows the power density as a function of current density for our cell operating in the fuel-cell mode in various CO-CO_2 mixtures, demonstrates that our cell achieved 0.45 W/cm^2 in a 50% CO_2-50% CO mixture at this temperature, even with a 65-μm electrolyte. Clearly, the performance of these LSCM-based electrodes in CO-CO_2 mixtures is excellent.

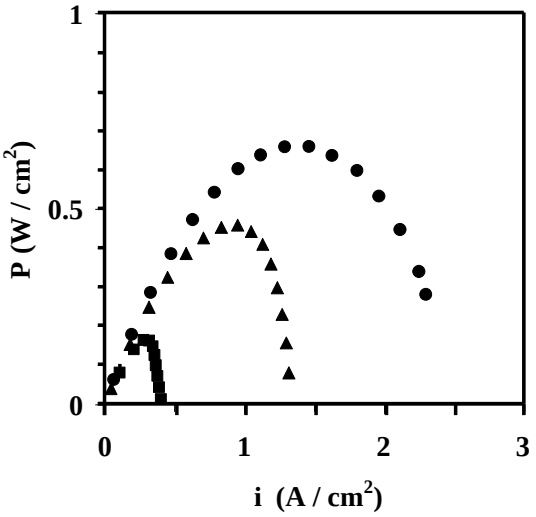

Figure 41:The power density as a function of current density for the cell operating in the fuel cell mode on CO-CO_2 mixtures at 800°C: 90% CO_2-10%CO (■)50% CO_2-50% CO (▲); 10% CO_2-90% CO (•). The cell composition was as follows: 40-wt% LSF in YSZ/YSZ (65µm)/ 0.5 wt% Pd, 5 wt. % CZY, and 45 wt. % LSCM in YSZ.

6.3. Conclusion

This work demonstrates that it is possible to reduced CO_2 electrochemically with an efficiency that is similar to that which can be achieved for H_2O electrolysis. LSCM electrodes have been shown to be able to operate on pure CO_2 and no carbon deposition was observed. An interesting feature of these electrodes is their ability to operate on pure CO_2. This results suggests that reduction of CO_2 by electrolysis could play a role in the development of sustainable and non greenhouse-gas-emitting energy and fuel cycles which use renewable energy sources such as wind and solar to produce chemicals and liquid fuels.

[1] A. Trovarelli, *Catal. Rev.-Sci. & Eng.*, 38, 439 (1996)
[2] G. Kim, M. D. Gross, W. Wang, J. M. Vohs, and R. J. Gorte, *Journal of the electrochemical society*, 155, B360 (2008).
[3] C. M. Sanchez-Sanchez, V. Montiel, D. A. Tryk, A. Aldaz, and A. Fujishima, *Pure Appl. Chem.* ,73 (2001) 1917.
[4] C. H. Bartholomew and R. J. Farrauto, "Fundamentals of Industrial Catalytic Processes", p. 398-461, 2nd edition, John Wiley, Hoboken, NJ (2006)
[5] http://www.energy.columbia.edu/solid-oxide-electrolysis, visited on the 15th of February 2009
[6] G. Parkinson, *Chem. Eng. Prog.*, 102, 7 (2006).
[7] T. Yamamoto, D. A. Tryk, A. Fujishima, H. Ohata, *Electrochemica Acata*, 47 (2002) 3327.
[8] K. R. Sridhar and B. T. Vaniman, *Solid State Ionics*, 93 (1997) 321.
[9] G. Tao, K. R. Sridhar, C. L. Chan, *Solid State Ionics*, 175 (2004) 621.
[10] O. A. Marina, L. R. Pederson, M. C. Williams, G. W. Coffey, K. D. Meinhardt, D. D. Nguyen, and E. C. Thomsen, *Journal of the Electrochemical Society*, 154 (2007) B452.
[11] A. Hauch, S. H. Jensen, J. B. Bilde-Sorensen, and M. Mogensen, *Journal of the Electrochemical Society*, 154 (2007) A619.
[12] S. Elangovan, J. J. Hartvigsen, and L. J. Frost, *Int. J. Appl. Ceram. Technol.*, 4 (2007) 109.
[13] S. H. Jensen, P. H. Larsen, and M. Mogensen, *Int. J. of Hydro Energy*, 32 (2007) 3253.

[14] O. Costa-Nunes, R.J. Gorte, J.M. Vohs, *Journal of Power Sources*, 141, 241 (2005).
[15] Y. Jiang and A. V. Virkar, *Journal of the Electrochemical Society*, 150, A942 (2003).
[16] K. Morikawa, T. Shirasaki, M. Okada, *Advances in Catalysis*, 20 (1969) 98.

[17] M. L. Toebes, J. H. Bitter, A. J. van Dillen, and K. P. de Jong, *Catalysis Today*, 76, 33 (2002).
[18] E. Perry Murray, T. Tsai, and S. A. Barnett, *Nature*, 400, (1999) 649.
[19] M. Cassidy, G. Lindsay, and K. Kendall, *Journal of Power Sources*, 61 (1996) 189.
[20] K. Sasaki and J. Maier, *Solid State Ionics*, 134 (2000) 303.
[21] W. S. Wang, M. D. Gross, J. M. Vohs, R. J. Gorte, *J. Electrochem. Soc.*, 154 (2007) B439.
[22] S. H. Jensen, P. H. Larsen, M. Mogensen, *Int. J. Hydrogen Energy*, 32 (2007) 3253.

Effect of the Catalyst on the performance

7.1. Introduction

To achieve high performances, it is critical that the anode exhibits a good electro-catalytic activity. The review on anode materials indicates that conductive oxides require high temperatures to show a sufficient activity. Fuel cells previously studied showed outstanding performances using Pd supported on ceria as a catalyst. The series of experiments presented hereafter investigates the role played by the catalyst in the high performance.

7.2. Results

Cells previously presented that use Ceria/Pd as a catalyst show outstanding performances. To demonstrate the performance enhancement obtained through the incorporation Ceria/Pd catalyst in the functional layer, cells have been prepared without any catalysts, i.e. the functional layer was impregnated only with 45 wt% LSCM. Figure 42 shows the IV curves obtained with and without the use of Ceria/Pd in the functional layer at 700ºC, while Figure 43 compares the corresponding impedance spectra.

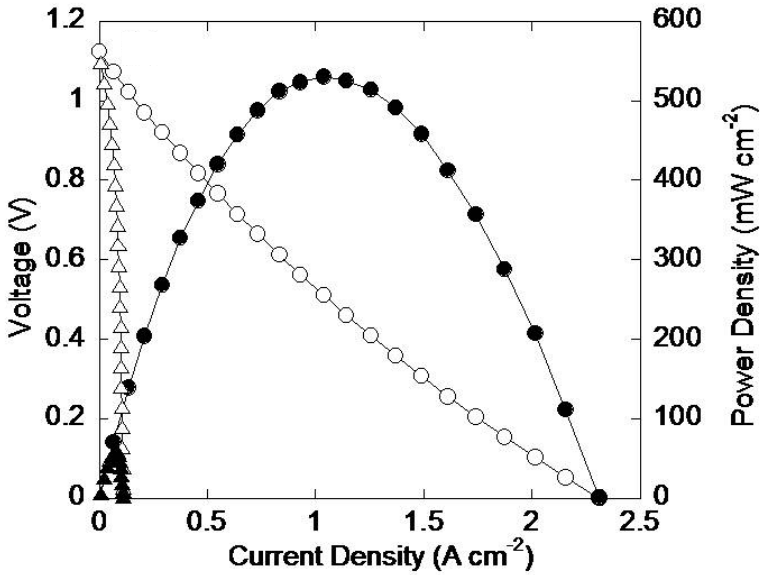

Figure 42: V-I polarization curves in humidified H_2 (3% H_2O) at 700 °C for cells having anodes with 45-wt% LSCM in YSZ and the following catalysts: (○) 5 wt% CeO_2 and 0.5wt% Pd, (Δ) no catalyst.

The performance drops dramatically without the use of the Ceria/Pd catalyst. A cell containing only LSCM offers poor performances at 700ºC (only 50mW/cm^2). The comparison of impedance spectra shows nearly identical ohmic losses for both cells, indicating that the electronic conductivity is due to the LSCM, while the non ohmic losses are considerably different (0.14 Ω.cm^2 with Ceria/Pd and about 2.2 Ω.cm^2

without) demonstrating the electrocatalytic activity enhancement obtained by introducing Ceria/Pd in the functional layer. At 800ºC, the maximum power density obtained without the use of any catalyst was 290 $mW.cm^{-2}$, to be compared with 1.1 $W.cm^{-2}$ when Ceria/Pd is used, thus increasing the performance by a factor 4. This result demonstrates that the high temperature requirement for LSCM efficient operation as an SOFC anode material can be overcome by the additional infiltration of a catalyst, thus allowing cell efficient operation at lower temperatures.

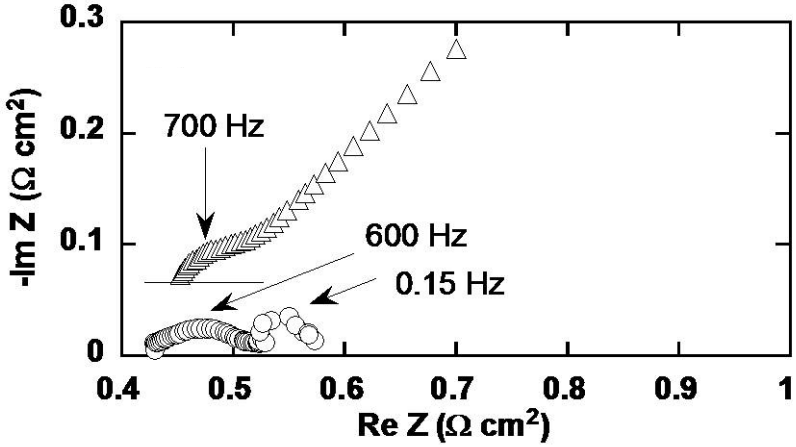

Figure 43: Impedance spectra measured at OCV on the cells in Figure 42: (○) 5 wt. % CeO_2 and 0.5 wt. % Pd, (∆) no catalyst. Only the high-frequency part of the impedance spectrum on the cell without catalysts is shown.

Since the addition of a catalyst is critical to achieve outstanding performance in LSCM impregnated functional layers, its effect on their performance has been further investigated in an attempt to understand how the catalyst perform its role and if other replacement materials could be used.

Pd and ceria were both added to the anode because ceria-supported Pd is one of the most active catalysts known for methane oxidation[1]. One question arises from the interaction between Ce and Pd. For the catalytic-reforming and water-gas-shift reactions, interactions between Pd and ceria lead to large enhancements in activity compared to either Pd or ceria individually[2,3,4]. Besides, Pd is known to react with some perovskites to form highly active oxidation catalysts[5,6], so that there is a question regarding whether other catalytically active, transition metals could be used in place of the Pd[7]. To address those important questions, cells have been prepared using different catalysts.

IV polarization curves at 700ºC in humidified H_2 for cells in which there was either no added catalyst, 5-wt% ceria, 0.5 wt. % Pd, or 5 wt. % ceria and 0.5 wt.% Pd are displayed on Figure 44. Although a being a little higher than in the first study on initial performance, the performance of the LSCM cell without any catalyst was only 105 mW/cm^2. Adding 5 wt. % ceria but no Pd increases the performance to 300 mW/cm^2. The power density is further increased by the addition of Pd. The performance of cells with only 0.5 wt. % Pd and with 0.5 wt. % Pd and 5 wt. % ceria was similar, (maximum power densities of 500 and 520 mW/cm^2) indicating that ceria is not essential to achieve high performance, while using only 0.5 wt. % of Pd is enough to obtain a dramatic performance enhancement. The high performance can

therefore be attributed to the Pd and those results indicate the high performance is not induced by interactions between Ceria and Pd.

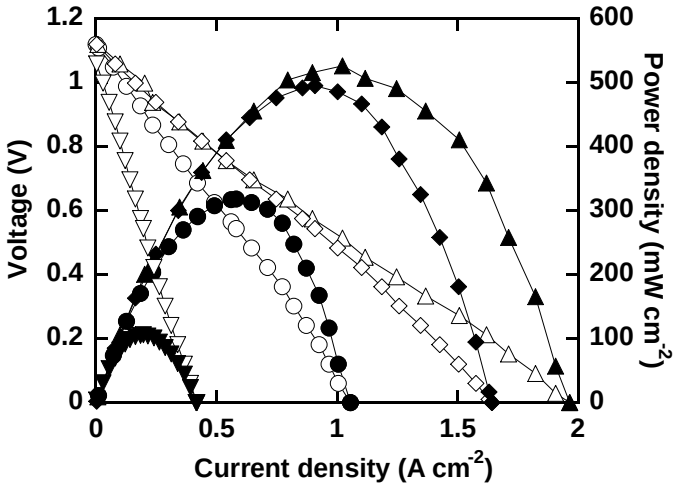

Figure 44: V-I polarization curves in humidified H_2 (3% H_2O) at 700°C for cells having anodes with 45-wt% LSCM in YSZ and the following catalysts: (○) 5 wt. % Ce, (Δ) 5 wt. % Ce + 0.5 wt. % Pd, and (◊) 0.5 wt. % Pd.

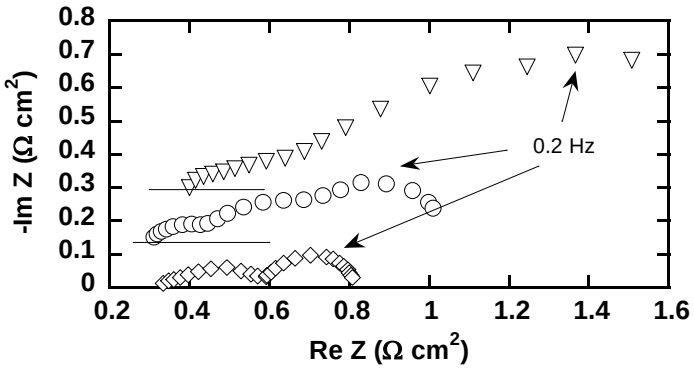

Figure 45: Impedance spectra measured at OCV on the cells in Figure 44: (Δ) no catalyst, (○) with 5. wt% ceria, (◊) with 0.5 wt. % Pd. Only the high-frequency part of the impedance spectrum on the cell without catalysts is shown.

Figure 45 shows the impedance plots corresponding to the IV curves shown in Figure 44 at open-circuit for the cells without catalyst, with 5-wt% ceria, and with 0.5 wt. % Pd. The ohmic losses varied slightly between cells but all were close to the expected ohmic losses for such a cell. The important data on this graph are the non ohmic losses associated with each cell, which vary according to the catalyst used. It is apparent that the electrode losses in the cell with Pd were much lower than that of the cell with ceria, which in turn were much lower than that of the cell without added catalyst.

To determine whether Pd is unique in being able to catalyze high anode performance, similar cells were prepared with either 0.5 wt. % Rh, 1 wt. % Ni, or 1 wt. % Fe. Each of these transition metals is a good oxidation catalyst but with different tendencies to undergo oxidation. For example, at 700ºC, Fe is expected to form FeO at $P(O_2)$ above 10^{-22} atm, while both Rh and Ni should remain metallic for all realistic H_2:H_2O ratios

at this temperature. The IV polarization curves in Figure 46 demonstrate that the cells with either Rh or Ni perform as well as the cell with Pd, with maximum power densities of approximately 530 mW/cm^2. The cell with the Fe catalyst had a slightly lower maximum power density, 400 mW/cm^2; but this is greater than the cell with only ceria as the catalyst. The impedance data for these three cells are not shown, but only the non-ohmic contributions were affected by the different catalysts.

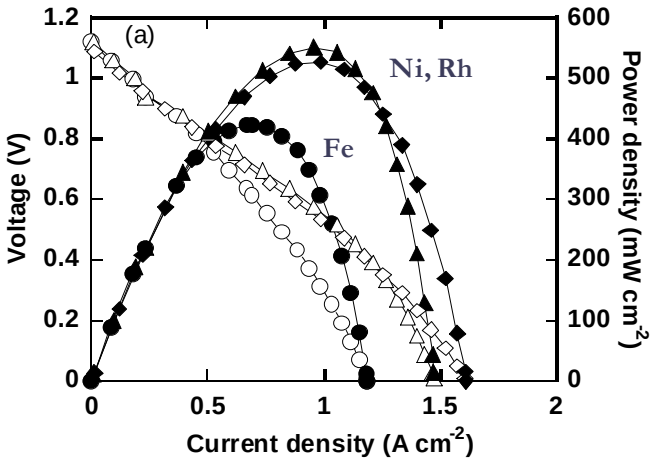

Figure 46: V-I polarization curves in humidified H_2 (3% H_2O) at 700°C for cells having anodes with 45 wt. % LSCM in YSZ and the following catalysts: (○) 1 wt. % Fe, (Δ) 1 wt. % Ni, and (◊) 0.5 wt.% Rh.

Every cell in this study involves Ag paste as a current collection layer, in a desire to minimize the addition of any catalytic activity to the functional layer studied. However, some studies in the literature employ Pt as a current collection material, which is obviously an active catalyst. In order to determine whether Pt paste at the anode surface might affect the anode performance, two cells were infiltrated with LSCM but no catalyst. One of them used Ag paste as a current collector, while Pt paste was used for the second one. Figure 47 reports the IV polarization curves for both cells at 800ºC in humidified H_2.

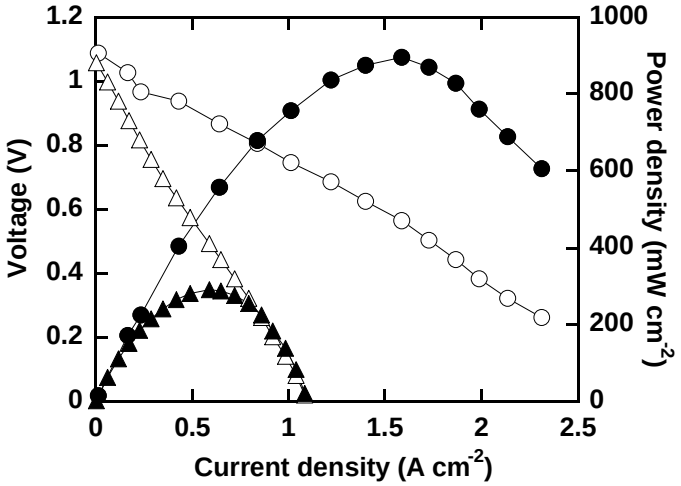

Figure 47: *V-I* polarization curves in humidified H_2 (3% H_2O) at 800°C for cells having anodes with 45 wt. % LSCM in YSZ and no added catalyst. Data are shown using Pt paste (•) and Ag paste (Δ) as the current collector.

The performance using Pt current collector was of 900 mW/cm^2, compared to a power density of only 290 mW/cm^2 when using the Ag current collector. This experiment clearly demonstrates that the use a Pt current collection layer dramatically increases the performance. At 700ºC, the maximum power density of the cell with Pt paste was approximately 500 mW/cm^2, similar to that found on cells using Ag paste when Pd, Rh, or Ni catalyst was added intentionally. The difference observed in the power densities between Pt and Ag paste indicate that some Pt must migrate into the anode layer at the triple phase boundary. While being slightly beyond the scope of this work, this experiment demonstrates that Pt paste current collectors should be avoided when testing anodes.

7.3. Conclusion

Fuel cell tests demonstrate that the infiltration of small amount of catalysts is essential to achieve high performance. While ceria was thought to be essential, results indicate that only a small amount of transition metal is required to obtain spectacular performance enhancements. Added amounts are so small that the effect on the performance can only be catalytic. Results indicate that the use Pt paste as a current collector for thin electrodes should be avoided.

[1] S. Colussi, A. Trovarelli, G. Groppi, and J. Llorca, *Catal. Commun.*, 8 (2007) 1263.
[2] T. Bunluesin, R.J. Gorte, and G.W. Graham, *Applied Catalysis B*, 15 (1998) 107.
[3] S. Sharma, S. Hilaire, J.M. Vohs, R.J. Gorte, and H.-W. Jen, *Journal of Catalysis*, 190, 199 (2000).
[4]X. Wang and R. J. Gorte, *Catalysis Letters*, 73, (2001).
[5] Y. Nishihata, J. Mizuki, T. Akao, H. Tanaka, M. Uenishi, M. Kimura, T. Okamoto, N. Hamada, N*ature*, 418 (2002) 164.
[6] J. Li, U. G. Singh, J. W. Bennett, K. Page, J. Weaver, J.-P. Zhang, T. Proffen, A. M. Rappe, S. L. Scott, R. Seshadri, *Chem. Mater.*, 19 (2007) 1418.
[7]X. Wang, R. J. Gorte, *Catalysis Letters*, 73(2001).

Study of the Microstructure

8.1. Introduction

The initial performance of thin cells using LSCM as the electronic conductor in the functional layer are outstanding and quite higher than those obtained for previous works done on the same type of cells. Previous works relied on other materials for the electronic conductivity but used the same catalyst. An intriguing fact is that materials used in previous works offer higher conductivities than LSCM does. Moreover, results obtained using various catalysts did not indicate interactions between the catalysts and the LSCM. As previously outlined, electrode performance is deeply related to the microstructure. Optimizing the electrode microstructure is necessary to ensure high performance. An ideal microstructure would offer the highest triple phase boundary (TPB) length for electrochemical reactions, an optimized contact between the electrolyte and the anode, and be stable during operation. Based on those observations, the microstructures of those functional layers have been intensively investigated. The study has then been extended to LSTM oxides to help understanding the interaction between the porous YSZ structure and the impregnated phase.

8.2. Results

8.2.1. LSCM-YSZ composites

Figure 48 shows high resolution SEM micrographs of a LSCM impregnated YSZ scaffold sintered in air at 1200ºC and the original YSZ structure after sintering at 1500ºC. The comparison of the SEM images of the structures with and without the LSCM indicates that the LSCM forms a uniform coating over the YSZ surface. Such a phenomenon has also been observed with $La_{0.8}Sr_{0.2}MnO_3$ (LSM) particles on YSZ single crystals [1,2], where the minimization of the surface free energy caused LSM particles to spread over the YSZ crystal to form a dense film upon calcination in air above approximately 1100 °C. However, in previous studies of impregnated YSZ porous structures, such a coating of the YSZ by the impregnated oxide was not observed. Instead, the impregnated phase formed particles easily distinguishable from the YSZ scaffold e.g. for impregnated ceria[3], for impregnated LSF[4] or for impregnated lanthanum strontium titanate, LST[5]. Therefore we may see two substantially different microstructures depending upon the nature of the impregnated phase. There is a strong analogy with the way a liquid would behave on a solid surface, by wetting this surface (LSCM, LSM) or forming a drop on this surface (LST, Ce, LSF).

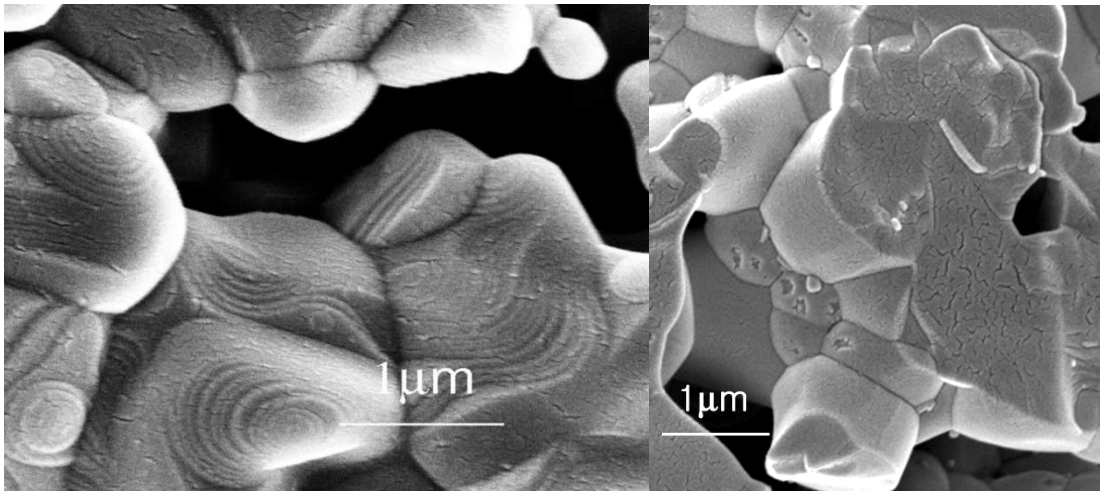

Figure 48: SEM images showing: (left) the original porous YSZ structure sintered at 1500°C in air and (right) the coating of $La_{0.75}Sr_{0.25}Cr_{0.5}Mn_{0.5}O_3$ (LSCM) over the pre sintered YSZ scaffold prepared by solution impregnation and then firing at 1200 °C in air. Note the crazed texture within the LSCM coating on the YSZ scaffold offering a rich three phase boundary structure.

The effect of the LSCM phase sintering temperature on the structure has been further investigated. Figure 49 displays SEM micrographs of LSCM-YSZ structures after high temperature sintering at 1100ºC (left) and 1300ºC (right). At 1300ºC, the structure seems identical to the one obtained after sintering at 1200ºC. At 1100ºC, a different structure can be observed. The coating is not as even as it is for higher temperature and lumps of LSCM can be observed, suggesting that the energy provided is not high enough for the LSCM to efficiently wet the YSZ.

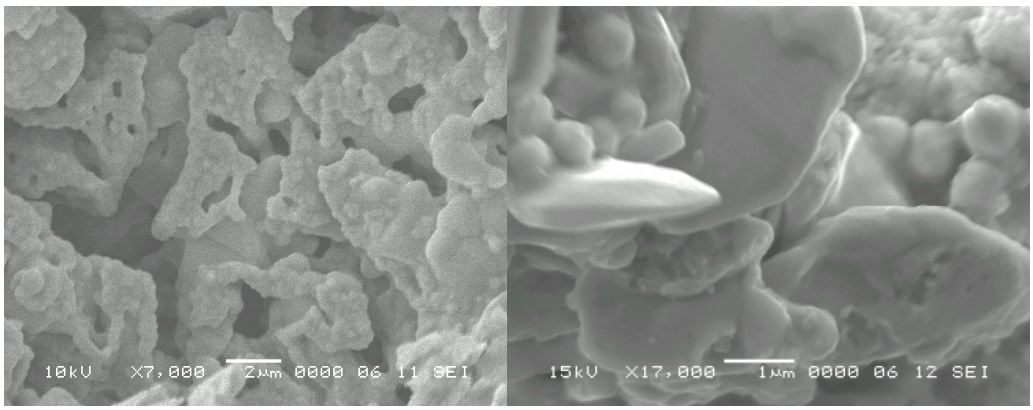

Figure 49: SEM images showing the structures of an impregnated LSCM-YSZ composite sintered at 1100°C (left) and 1300°C (right).

The wetting of the YSZ electrode scaffold by a conductive oxide is a structure of great interest. The wetting ensures a good connectivity for the electronic conductive phase and hence minimises ohmic losses in the composite electrode. However, whilst the YSZ coverage is optimum, such a uniform coating would restrict the three phase boundary length due to the LSCM insufficient ionic conductivity, and thus increase polarization resistances in such an anode. This structure cannot be expected to provide the excellent performance described above. However, it should be noted that the microcracking in the coating, visible in Figure 48, may provide the required three-phase boundary length for efficient operation as an SOFC anode

However, the assumption that the film microstructures produced at 1200^{o}C or above

in air is relevant to fuel cell anode conditions is incorrect as there is a complex and interesting evolution of the impregnated microstructure in a reducing environment. On annealing at 700ºC (Figure 50a), the structure remains close to that produced in air at 1200°C, but on annealing at 800ºC (Figure 50b) the dense film breaks up into interconnected nano-scale particles covering the YSZ surface. Under fuel conditions, a nano-porous conductive coating layer is therefore formed on the YSZ surface, which ensures a really high triple phase boundary length for electrochemical reactions within the anode. The increase in temperature from 700-800°C seems to allow this change of structure to happen. At 700ºC, such a porous structure cannot be observed in the timescales studied, and the anode offers therefore a smaller TPB. The quality of the structure produced in terms of surface area can be appreciated on Figure 53c, which shows a cross section of the structure after annealing for 5 hours at 800ºC. At 900ºC (Figure 50c), LSCM crystal growth can be observed, leading to a different structure with larger grains, that shows similarities to previously published LSCM anodes prepared by methods such as combustion synthesis[6]. The increase in temperature from 800-900ºC allows as well an important evolution of the structure. The comparison of SEM images for the three temperatures clearly shows that the evolution of the structure is strongly temperature dependent.

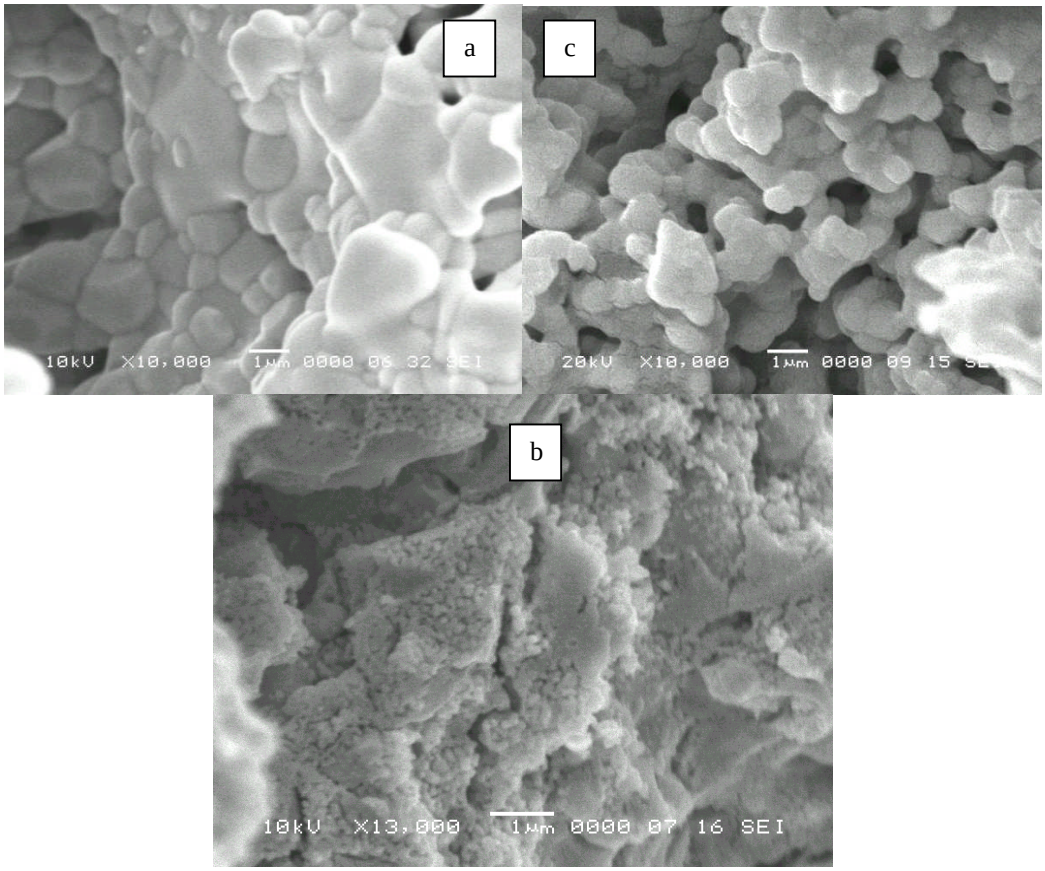

Figure 50: SEM images of LSCM-YSZ composites after reduction in humidified (3% H_2O) H_2 for 5 hours at (a) 700°C, (b) 800°C and (c) 900°C.

The remarkable change in LSCM film structure from 700ºC to 800ºC would suggest a change in LSCM stoichiometry. In order to characterize the redox properties of LSCM in this composite structure and determine oxygen stoichiometry under anode

conditions, the equilibrium oxygen content of the a 45-wt% LSCM-YSZ composite was measured as a function of $P(O_2)$ at 750ºC using coulometric titration. The data shown in Figure 51 were obtained after flowing a 90% N_2-10% H_2 mixture over the sample for 1.5 hours. The $P(O_2)$ were then determined after adding increasing amounts of oxygen; the oxygen stoichiometry was assumed to be that of $La_{0.75}Sr_{0.25}Cr_{0.5}Mn_{0.5}O_3$ at atmospheric conditions. For comparison purposes, data for $La_{0.8}Sr_{0.2}MnO_3$, reproduced from the literature[7], are also included in Figure 51. The data show that the equilibrium properties for LSM and LSCM are very similar in that reduction at 750ºC is negligible for $P(O_2)$ greater than 10^{-15} atm but becomes significant at lower $P(O_2)$. The big difference is that the oxygen stoichiometry decreases much more rapidly for LSM with decreasing $P(O_2)$. Indeed, it appears that Mn reduction occurs under similar conditions for LSM and LSCM, with the Cr in LSCM simply minimizing the extent of reduction and therefore stabilizing the structure to lower $P(O_2)$. Even so, given that a typical $P(O_2)$ under anode conditions at 1023 K might be 10^{-24} atm, the oxygen stoichiometry for LSCM would be reduced from 3 to 2.86, in accord with prior thermogravimetric studies on LSCM powders[8]. This large extent of reduction is therefore responsible to the structural changes observed in Figure 50.

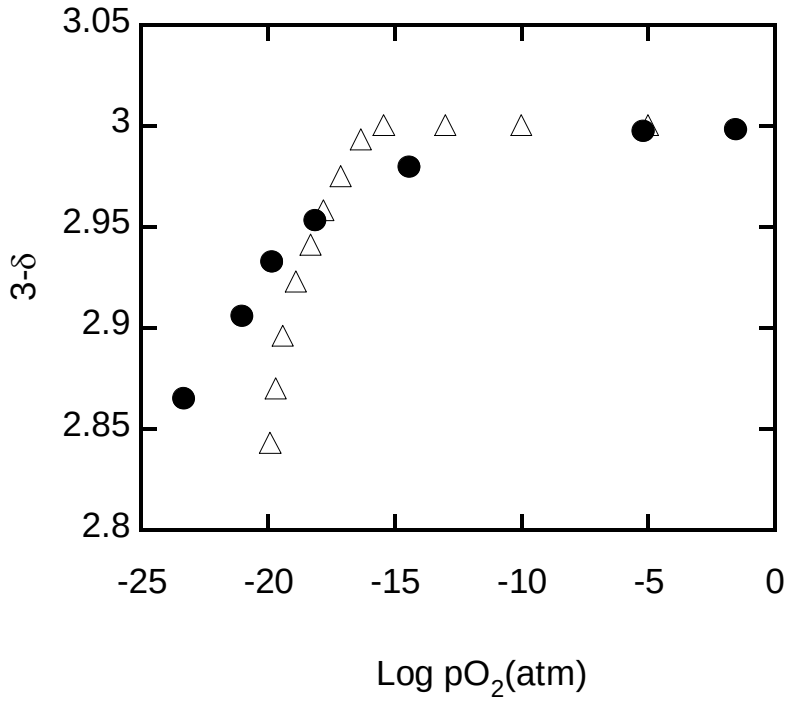

Figure 51: Equilibrium oxygen stoichiometries measured using coulometric titration at 750°C for a 45 wt % LSCM-YSZ (•) Data for bulk $La_{0.8}Sr_{0.2}MnO_3$−LSM (Δ), obtained from Ref. 7 are shown for comparison.

Initial conductivities of a LSCM impregnated YSZ structures have been discussed above and are high enough for a functional layer. However, it is of interest to monitor the evolution of conductivity with time, since the structure evolution can be expected to affect the conductivity of those composites. Figure 52 shows the evolution of this conductivity with time for a sample that had been equilibrated at 700^o C, then further heated and maintained at 800 ºC in humidified (3% H_2O) H_2, i.e. in fuel cell anodic conditions.

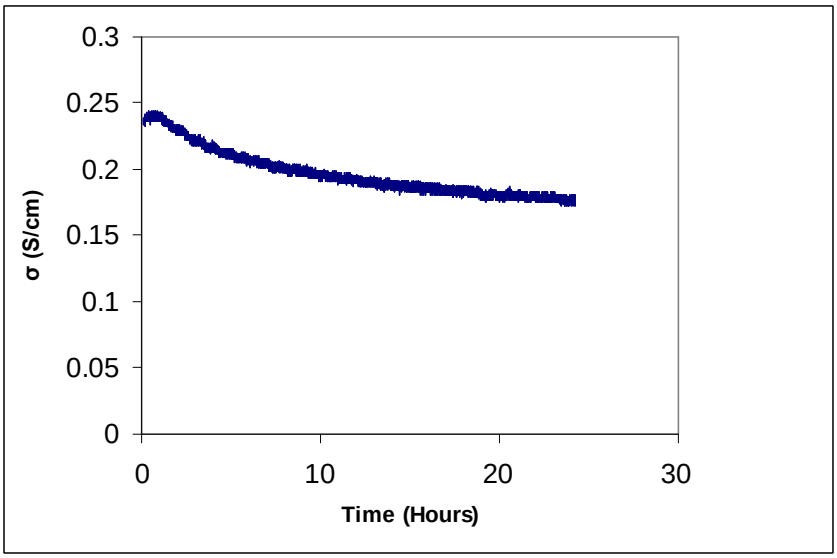

Figure 52: Evolution with time of the conductivity of a LSCM-YSZ composite at 800°C in humidified (3% H_2O) H_2.

The conductivity decreases continuously towards a stable value as the microstructure evolves. The greatest rate of this deterioration occurs within the first 24 hours and once completed, the conductivity has dropped by 28%. This microstructural induced conductivity decrease can be better understood by analyzing SEM images of the structure taken after different times of reduction, as displayed in Figure 53. The original structure is a dense LSCM film covering the YSZ (Figure 48) but after one hour at 800ºC (Figure 53a), the beginning of a new structure can be seen with individual grains becoming apparent on the nano-scale. After 3 hours (Figure 53b), the coating has a much more distinct granular type of morphology but it can be seen (upper right of the image) that there are still many necks between the particles and they are still very much interconnected and almost form a continuous layer. After 5 hours (Figure 53c), the grains appear to be more distinct than on the previous images, and although still interconnected, many gaps become visible between the grains. This loss of interconnectivity with the LSCM phase explains the loss of conductivity as a function of time. Meanwhile, it is responsible for an increase in the surface area of the LSCM phase and in turn of the TPB length within the anode, making initial performances outstanding.

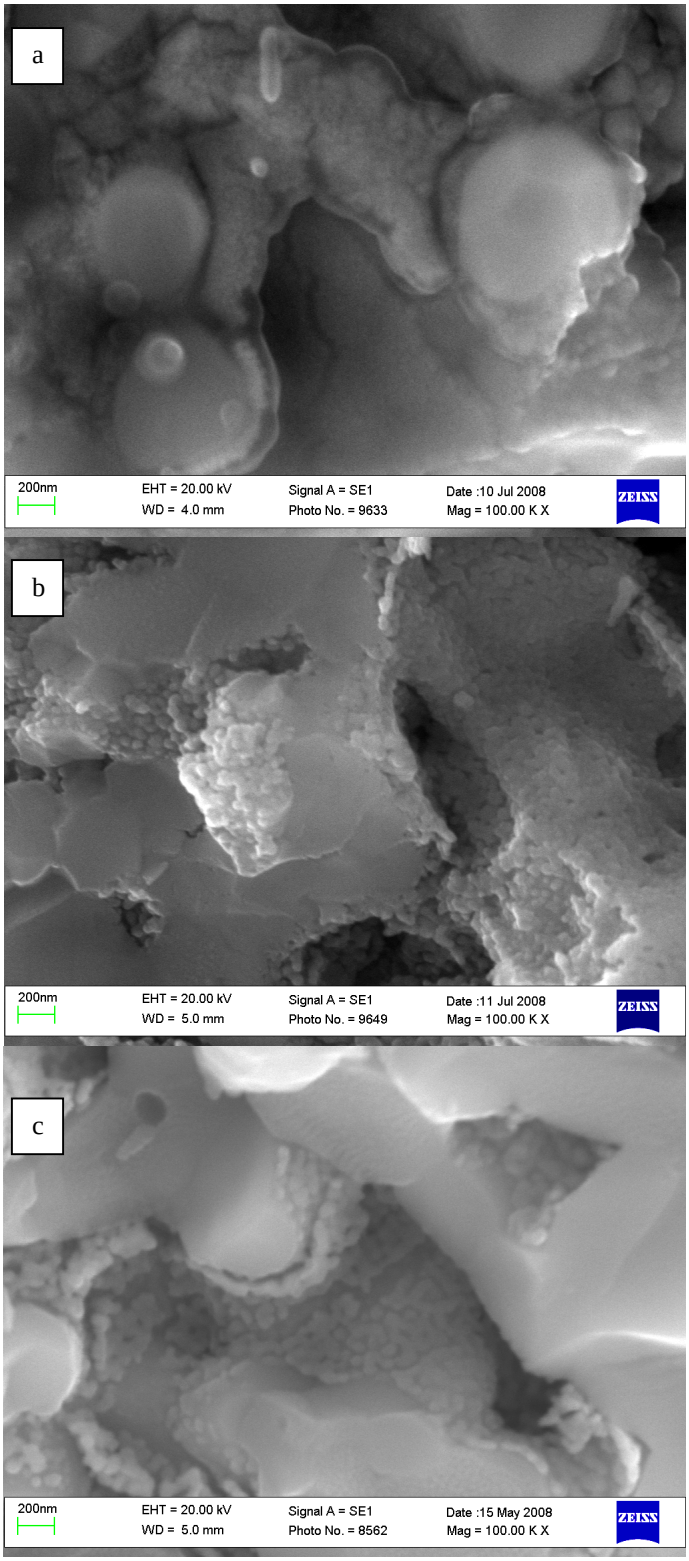

Figure 53: SEM images of LSCM-YSZ composites at different times of reduction in humidified (3% H_2O) H_2 : (a) 1 hours, (b) 3 hours and (c) 5 hours.

The reversibility of this structure evolution has been studied by reoxidizing at 800ºC in air samples that had been previously reduced at this temperature. Figure 54 displays

SEM images taken after 5, 10 and 20 hours of reoxidation. Those SEM micrographs indicate that the transition from an even coating of LSCM to the nano-scale particulate structure is reversed. After 5 hours oxidation (Figure 54a) the nano-particles are seen to have started to coalesce, after 10 and 20 hours (Figure 54b and Figure 54c) these particles are now fully merged, although the coating is not as smooth as initially observed after 1200°C sinter. The structural difference between the original coating and the one formed by re-oxidation can be expected to have an effect on the conductivity. Conductivity recorded a LSCM/YSZ composite in humidified hydrogen after a full redox cycle confirmed some irreversibility in the redox process. While the conductivity at 800ºC was initially measured to be 0.24 $S.cm^{-1}$, after reduction, structural re-organization and reoxidation at this temperature, the conductivity at 800ºC was only 0.15 Scm^{-1}. The conductivity is lower after a redox cycle as might be expected from the change in nature of coating.

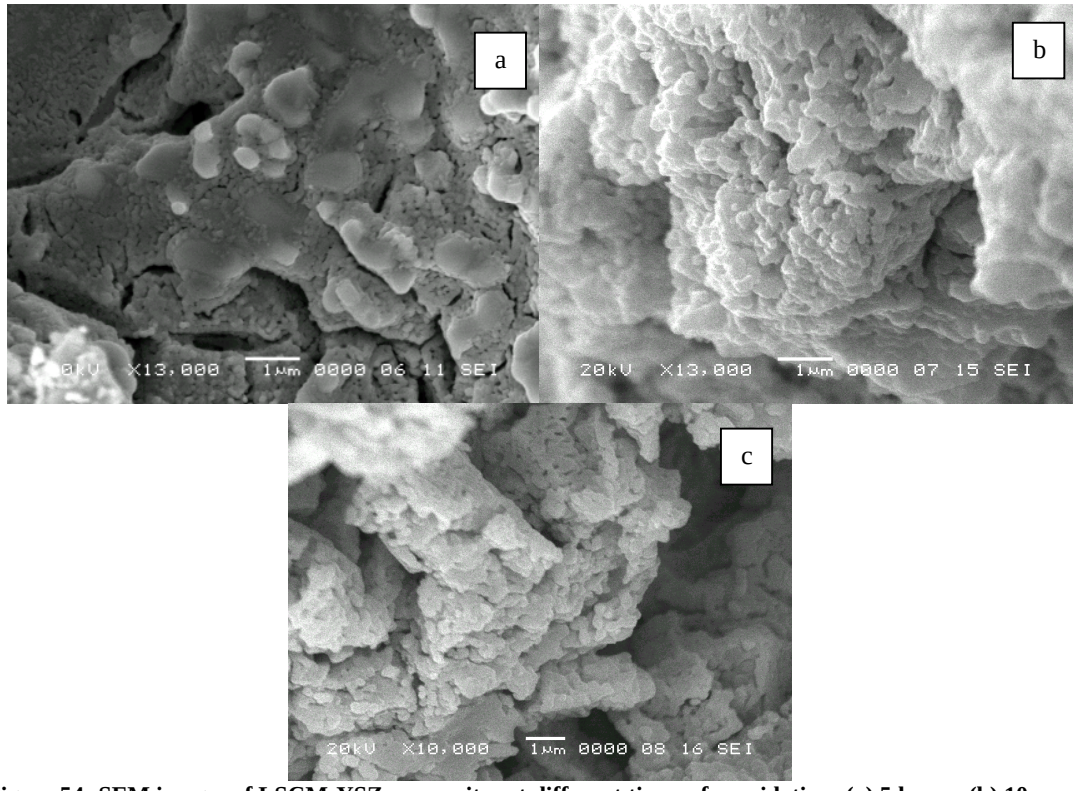

Figure 54: SEM images of LSCM-YSZ composites at different times of reoxidation: (a) 5 hours, (b) 10 hours, and (c) 20 hours.

8.2.2. $La_{0.33}Sr_{0.67}Ti_xMn_{1-x}O_{3+/-\delta}$ (LSTM)

In order to investigate the role played by Mn in the wetting of YSZ, structures of LSTM with different Mn/Ti ratios impregnated into a YSZ backbones have been analyzed after high temperature firing. Figure 55 reports the diffraction pattern obtained for a typical LSTM composition after firing at 1200ºC, showing that the desired perovskite structure has been obtained *in situ*.

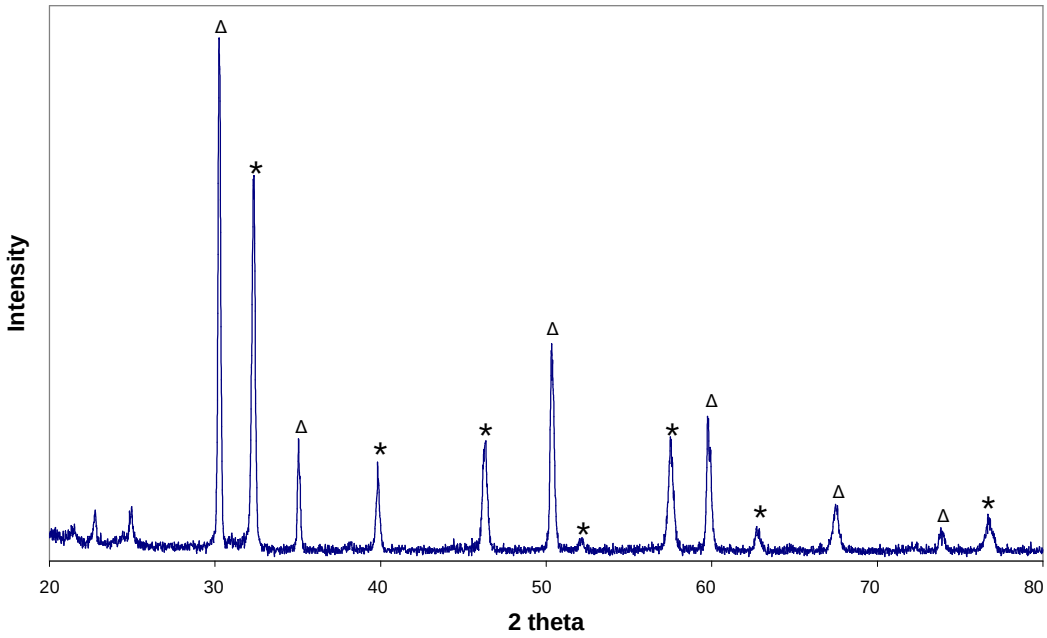

Figure 55: Typical XRD of a LSTM-YSZ composite with 30 wt % LSTM for $La_{0.33}Sr_{0.67}Ti_{0.67}Mn_{0.33}O_{3-\delta}$, formed by infiltration into porous YSZ: LSTM (*) and YSZ (Δ), peaks before 30° 2θ due to the XRD holder.

Figure 56a shows a SEM image of the structure after high temperature firing for $La_{0.33}Sr_{0.67}Ti_{0.67}Mn_{0.33}O_{3+/-\delta}$-YSZ, (Ti/Mn=2). This structure is similar to that observed for higher manganese content: $La_{0.33}Sr_{0.67}Ti_{0.5}Mn_{0.5}O_{3+/-\delta}$-YSZ (Ti/Mn=1) and $La_{0.33}Sr_{0.67}Ti_{0.33}Mn_{0.67}O_{3+/-\delta}$-YSZ (Ti/Mn = 0.5) composites.

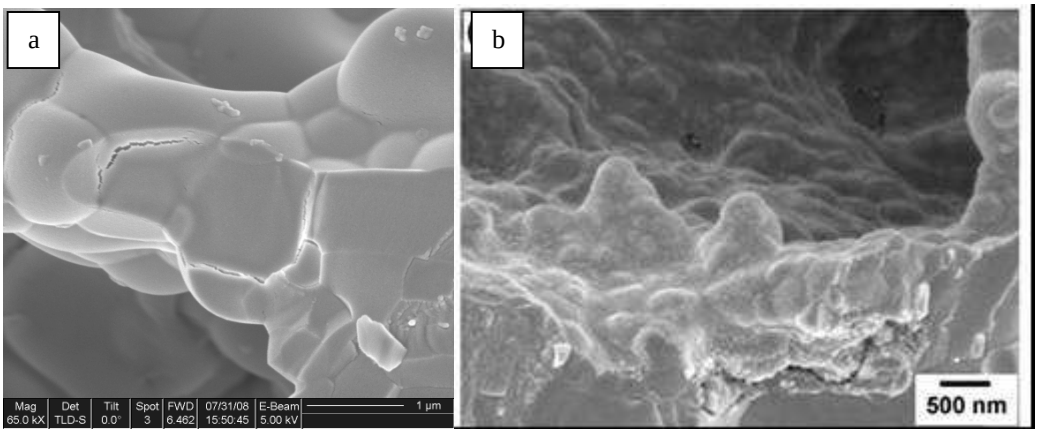

Figure 56: Scanning electron micrographs of (a) $La_{0.33}Sr_{0.67}Ti_{0.67}Mn_{0.33}O_{3-\delta}$-YSZ composite (Ti/Mn = 2) after sintering at 1200 °C and (b) $La_{0.8}Sr_{0.2}TiO_3$-YSZ composite after sintering at 1200 °C[5].

The LSTM oxides thus form a similar coating layer over the YSZ, as was previously described for LSCM. To demonstrate the presence of this coating layer, images have been purposely taken on a cracked surface. The fact that the YSZ grain boundaries remain apparent shows that a thin coating has been deposited. The YSZ wetting is particularly interesting for the composition featuring a high Ti content, since LST compounds do not form a coating over the YSZ surface[5], as shown on Figure 56 . Therefore, the wetting of the YSZ by the oxide can be attributed to the presence of Mn on the B-site of the ABO_3 structure.

Figure 57 shows the evolution of LSTM films in fuel conditions for the 3 Ti/Mn ratios

described above. SEM images were taken after the structures had been annealed for several hours in humidified H_2 at 800ºC. The LSTM dense film breaks up into interconnected nano-particles for each composition, but differences can be observed according to the Ti/Mn ratio. In Figure 57a (Ti/Mn = 2), two different morphologies can be seen on the LSTM film: a fine nano particulate layer visible in the bottom of the picture and a coarser LSTM structure visible in the upper part of the picture. Examination of the micrograph shows that the coarser structure is mainly located on the concave zones of the YSZ surface, while the finer structure is confined to more convex surfaces. This suggests that this phenomenon might be due to some unevenness in the deposition process, which is driven by capillary action, leading to thinner films on convex surfaces and thicker films in concave areas. To some extent, this phenomenon is apparent in all the micrographs shown in Figure 57 (Ti/Mn=1 in Figure 57b and Ti/Mn=0.5 in Figure 57c), but is certainly less apparent as the Mn content increases. This again shows/suggests that the Mn content has a significant effect on the characteristics of the evolved microstructure. The more Mn is present on the B site of the ABO_3 structure, the closer to a thin particulate coating the structure will get.

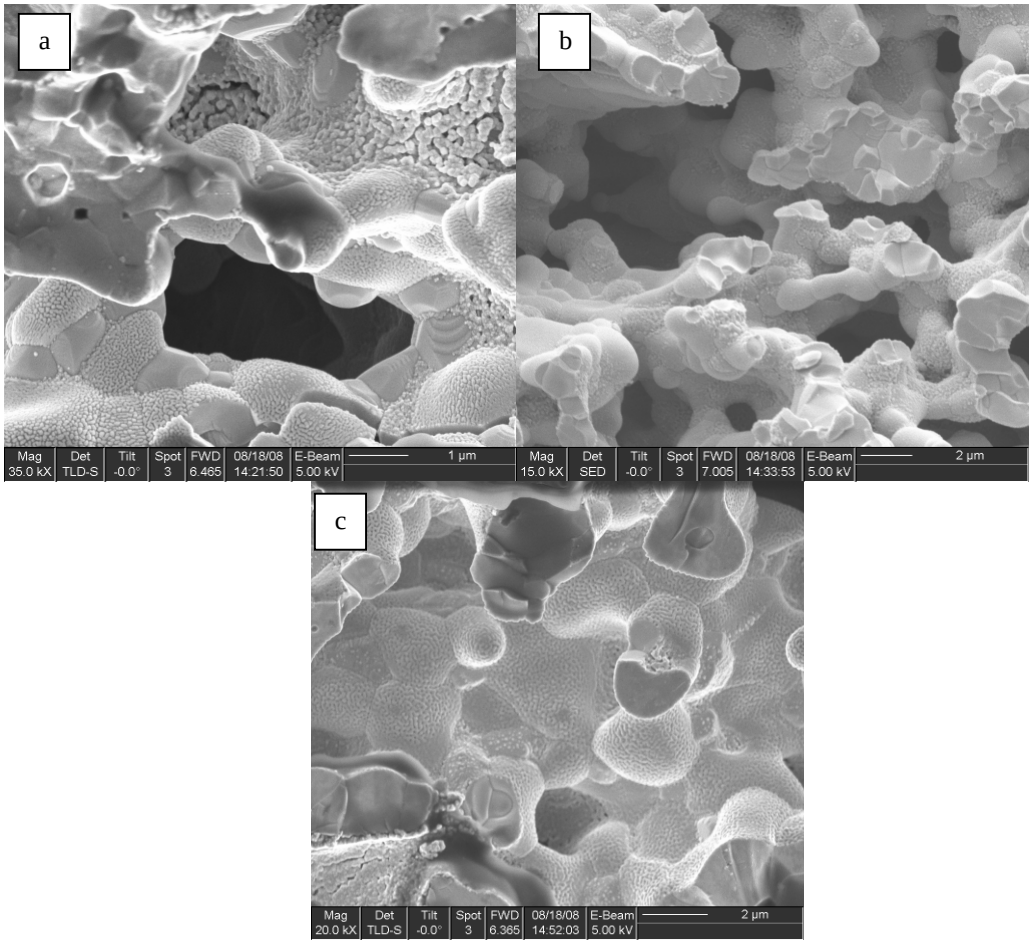

Figure 57: Scanning electron micrograph of LSTM-YSZ composites after reduction at 800 °C in humidified (3% H_2O) H_2 for several hours (a) Mn/Ti= 2 sintered at 1300 °C, (b) Mn/Ti= 1 sintered at 1200 °C, and (c) Mn/Ti= 0.5 sintered at 1300 °C.

The temperature at which the LSTM phase is formed has been studied in more detail for composites showing a high Ti content, Ti/Mn=11. Figure 58 shows images of the structures corresponding to different initial sintering temperature of the oxide phase,

after more than 100 hours reduction in humidified H_2 at 800ºC. For 1100ºC (Figure 58a), the structure morphology is close to a LST-YSZ composite one , with no wetting of the YSZ surface. At higher firing temperatures, wetting of the YSZ phase is obtained. Zones of coarsening are more apparent for 1200ºC (Figure 58b) than for 1300ºC (Figure 58c). This shows that a higher initial firing temperature can also facilitate a thin wetted coating layer on the YSZ surface, which in turn leads to a finer particulate structure on reduction. These results demonstrate that only a small amount of Mn (8%) on the B-site of the ABO_3 structure, along with a high enough sintering temperature, is sufficient to obtain wetting of the YSZ surface.

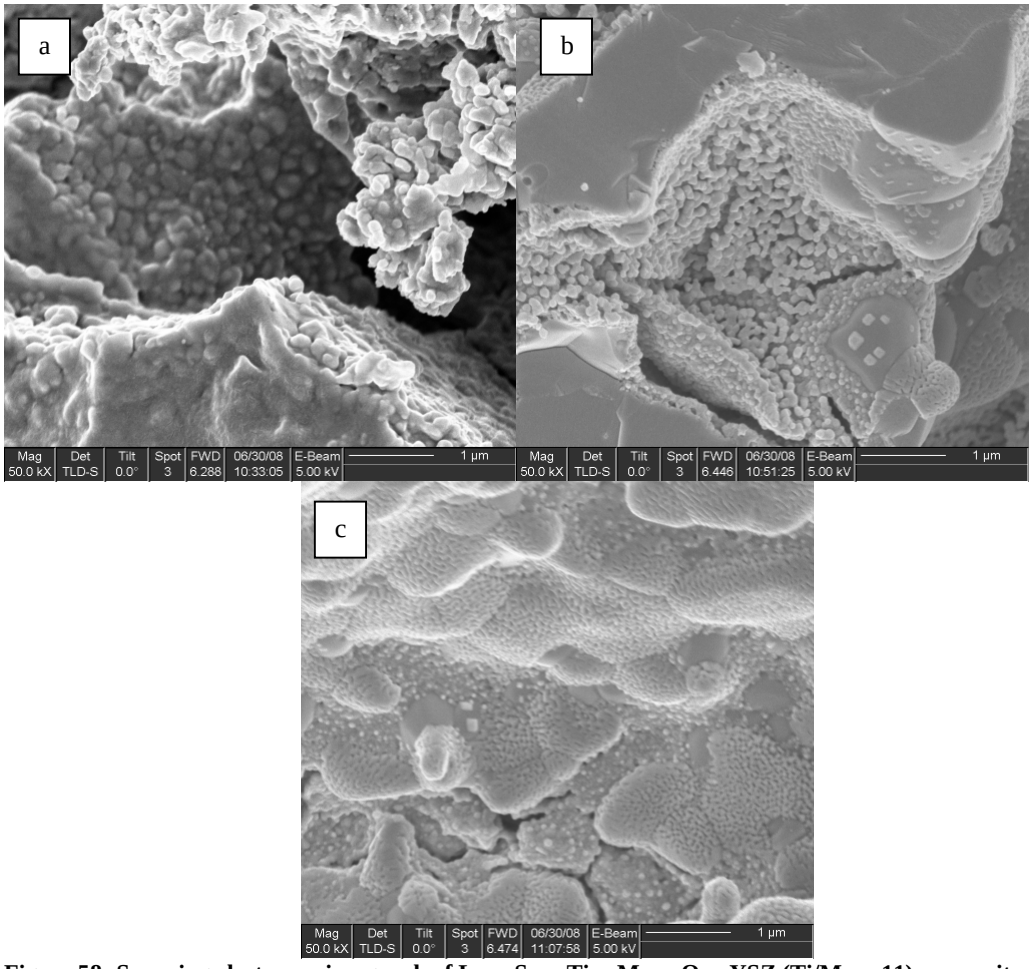

Figure 58: Scanning electron micrograph of $La_{0.33}Sr_{0.67}Ti_{0.92}Mn_{0.08}O_{3-\delta}$-YSZ (Ti/Mn = 11) composites after reduction in humidified (3% H_2O) H_2 at 800 °C for more than 100 h, with different initial sintering temperatures: (a) 1100 °C, (b) 1200 °C, and (c) 1300 °C.

Conductivity tests have also been carried out on LSTM composites. LSTM impregnated YSZ composites have undergone a thermal cycle in humidified H_2, from 700ºC to 900ºC. Figure 59 illustrates the conductivity evolution as a function of time during the thermal cycle for Ti/Mn = 2. A conductivity decrease, following a similar trend to the one observed for LSCM (Figure 52), can be seen at both 800ºC and 900ºC. As for LSCM, the diffraction patterns taken after the experiments show no discernable change in structure/ phase composition. This conductivity decrease can therefore be assigned to the microstructural reorganization. Once the film evolution process is completed at 900ºC, conductivities are stable when the temperature is decreased. The same behaviour was observed for Ti/Mn =1.

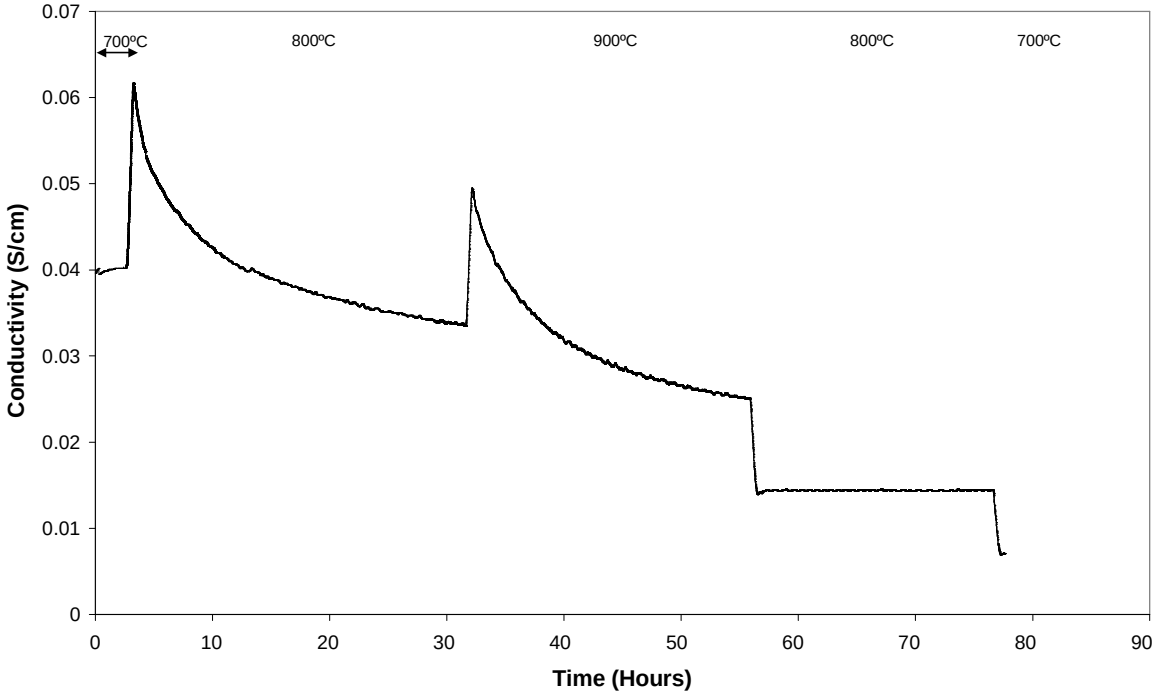

Figure 59: Evolution with time of the conductivity of a LSTM-YSZ (Ti/Mn = 0.5) composite during a thermal cycle in humidified (3% H_2O) H_2.

8.2.3. Conclusions

The microstructures obtained by the impregnation on Mn containing perovskites are of great interest. They certainly play a key role in the high performance previously presented. The presence of Mn on the B site of the ABO_3 structure is essential to obtain the wetting of the YSZ by the oxide. Very high surface area is available for electrochemical reaction once the structures have evolved in fuel cell conditions. Both the Mn content and the sintering temperature have been shown to influence the surface area created in reducing conditions. Conductivity measurements indicate that the evolution of the structures in reducing environment is temperature dependent.

[1] Y. Huang, J. M. Vohs, R. J. Gorte, *J. Electrochem. Soc*., 152 (2005) A1347.
[2] Y. Huang, J. M. Vohs, R. J. Gorte, *Electrochem. Solid-State Lett*., 9 (2006) A237
[3] M. D. Gross, J. M. Vohs, R. J. Gorte, *Electrochem. Solid-State Lett*., 10 (2007) B65
[4] J.M. Vohs, R.J. Gorte, Adv. Mater., 21 (2009) 943-956
[5] S. Lee, G. Kim, J. M. Vohs, R. J. Gorte, *J. Electrochem. Soc.*, 155 (2009) A1179.
[6] S.Tao, J.T.S. Irvine, *J. Electrochem. Soc*., 151 (2004) A252
[7] J. Mizusaki, N. Mori, H. Takai, Y. Yonemura, H. Minamiue, H. Tagawa, M. Dokiya, H. Inaba, K. Naraya, T. Sasamoto, T. Hashimoto, *Solid State Ionics*, 129 (2000) 163.
[8] S. M. Plint, P. A. Connor, S.W. Tao and J.T.S. Irvine, *Solid State Ionics*, 177 (2006) 2005.

Discussion

The results presented in the previous chapters demonstrate that outstanding performance can be achieved using thin functional layers impregnated with conductive oxides and catalytically active transition metals. The performance reported on LSCM based functional layers is excellent for an alternative anode, comparing well with the Ni-YSZ standards. The direct use of humidified methane has been demonstrated, achieving the highest power densities available in the literature. The same functional layers have proven to be capable of reducing efficiently CO_2 without any carbon deposition. The innovative concept used in those studies has proven to offer a suitable answer to the problems encountered in the search of alternative anode materials.

The key factor in producing those high power densities is the microstructure obtained when infiltrating conductive oxides that contain Mn on the B-site of the ABO_3 structure. The structures obtained in a reducing environment appear to offer a highly promising microstructure for a fuel cell electrode. The TPB area is maximized by interconnected nano-particles covering a percolated YSZ framework that has been co-sintered with the electrolyte. Following the infiltration process, we see interfacial interactions between impregnated and framework oxides reminiscent of wetting behaviour of liquids on solid surfaces. The strongest interactions with zirconia are for Mn-rich perovskites.

We suggest that this either relates to the interaction of Mn in perovskite with the surface or to volumetric changes of the perovskite on reduction. As the increase in unit cell volume of LSCM on reduction is at most 1%[1] and the structure remains cubic for both oxidised and reduced forms at these temperatures, we do not consider that structural changes are sufficient to drive these morphological changes. As wetting is much reduced under fuel conditions, with the perovskite dewetting and forming small grains, it seems that reduction of Mn from 3+ to 2+ dramatically changes the interaction between the LSCM film and YSZ. For LSCM it is well documented that the average oxidation state of Mn changes from ~3.5+ to ~2.5+ on changing from oxidising to fuel conditions at 800°C[2]. Investigations of Mn solubility in zirconia[3,4] clearly show that Mn II is more soluble in cubic YSZ than Mn III or Mn IV and its is suggested that this relates to the better suitability of the Mn II electronic configuration to the cubic 8-fold coordination associated with cubic fluorite structure. It therefore seems most likely that the solubility of lower oxidation state Mn in the cubic YSZ weakens the interfacial interaction, possibly by decrease the Mn concentration at the interface. allowing the Mn containing perovskites to reorganise into nanoscale particles.

The importance of the microstructure in the high performance is clearly demonstrated by the comparison with functional layers that have been impregnated with oxides that don't offer YSZ wetting. A recent study published by the professor Gorte's group at the University of Pennsylvania investigated the use of LST oxides in the functional layer to replace LSCM. The LST oxide used in this study offers a higher conductivity than LSCM but the microstructure obtained through the impregnation process is substantially different. LST does not coat the YSZ and forms instead particles easily

distinguishable from the YSZ. The surface area of the LST anode and therefore the TPB are lower than the ones of the LSCM anodes, which translates into lower performance despite higher conductivities. Figure 60 compares the microstructures for both cells and their performance. Since the only difference between the cells was the conductive oxide employed, the higher performance is clearly due to the microstructure.

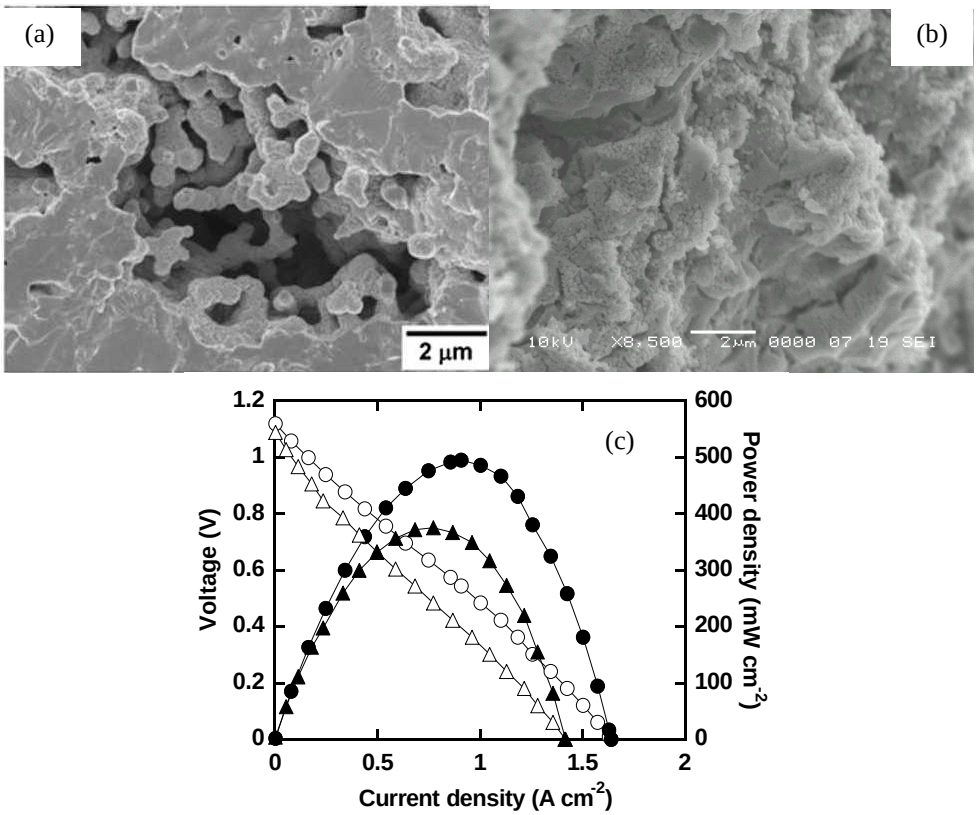

Figure 60: Comparison of impregnated LST-YSZ and LSCM-YSZ composites. (a) SEM micrograph of an impregnated LST-YSZ composite; (b) SEM micrograph of an impregnated LSCM-YSZ; (c) comparison of the IV curves obtained at 700C in himdified (3% H_2O) H_2 for the two composites in similar cells: LSCM (cirles) and LST (triangles).

The role of the added metals is also remarkable. First, the amounts of metal required to provide good electrode performance were so small that the effect must be catalytic. Electrode performance was enhanced by the addition 1 wt% or less of Pd, Rh, Ni, and Fe and this amount of metal is incapable of providing significant conductivity within the electrode. More likely, the catalytic metals must reside near TPB sites, where they can promote the oxidation reactions. Indeed, the location of the metal atoms is likely critical, since other studies presented in the review of anode materials found that addition of Pd to an LSCM-YSZ composite had little effect on electrode performance, other than what might be expected for reforming activity on the Pd itself[5]. That study used a more conventional approach to prepare the LSCM-YSZ composite, simply sintering the mixed oxides. We suggest that the difference between our two studies is due to differences in the structures of the LSCM-YSZ composites. Apparently, the metal atoms were unable to migrate to the required locations in the conventional composite. In our system, the thin coverage of the YSZ by the LSCM allows the metal atoms to migrate at the TPB when the film evolves to nano-particles.

Clearly, both the structural and catalytic properties observed in this study have a strong influence on the electrode performance. Developing a better understanding of how these properties influence performance should allow the development of improved materials with more optimal properties. If further knowledge is gained in the interactions between the YSZ and the oxides, and in the evolution of the structure with time, the functional layer could be engineered to display ideal and stable microstructures. Fuel cell test have only been carried out for LSCM impregnated layers but many other oxides could be used. The presence of Mn is however critical to obtain the desired wetting of the YSZ.

The power densities achieved with this innovative concept are definitely within the range of commercialization. The concept will probably be better suited to planar designs and appropriate manufacturing processes would have to be designed to go beyond the laboratory scale. We believe that the performance presented here can be further improved. Using a thinner electrolyte would obviously reduce the ohmic losses and further improve the power output. Further studies need to address the microstructure of the impregnated composites. While being of great interest for fuel cell electrodes, the microstructures obtained in this work have the potential to find interest beyond the fuel cell community.

[1] S.W. Tao, J.T.S. Irvine, *J. Electrochem. Soc.* 151 (2004) A252.
[2] S.M. Plint, P.A. Connor, S.Tao, J.T.S. Irvine, *Solid State Ionics*,**,** 177, (2006) 2005.
[3] M. Chen, B. Hallstedtb, L.J. Gauckler, *Solid State Ionics*,**,** 176 (2005) 1457.
[4] M. Occhiuzzi, D. Cordischi and R. Dragone, *Phys. Chem. Chem. Phys*.,5 (2003) 4938
[5] Y.M. Ye, T. M. He, Y. Li, E. H. Tang, T. L. Reitz, and S. P. Jiang, *J. Electrochem.Soc.*, 155 (2008) B811.

PART III

DIRECT ETHANOL SOFCS

Ethanol for SOFCs

10.1. Introduction

This chapter reviews the different aspects of the use of ethanol as a fuel for SOFCs. Fuels for SOFCs are first discussed. Hydrogen, the preferred fuel for fuel cells is presented and the technological advances required for implementing any hydrogen economy are exposed. Bio-ethanol can be an interesting alternative to hydrogen among the potential practical fuels. Characteristics and advantages of bioethanol are presented and discussed.

However, the use of ethanol in a high temperature process such as a SOFC has many implications. The high temperature chemistry that occur when ethanol is used as a fuel and the literature available on SOFCs fuelled with ethanol are both reviewed.

10.2. Fuels for SOFCs

10.2.1. The hydrogen economy

Although commonly associated with hydrogen, a major advantage of SOFCs is their potential ability to use any fuel capable of oxidation. This feature could considerably broaden the energy sources for SOFCs as compared to other types of fuel cells, making them attractive versatile electricity producing devices.

Hydrogen remains however the preferred fuel for SOFCs for many reasons. In terms of power output, hydrogen is the most attractive fuel since it shows the highest energy density per unit of mass and its oxidation requires only the breakage of the H-H bond, allowing for fast oxidation kinetics. As shown in the review of anodes materials presented in this thesis, fuel cells typically produce higher power output when fueled with H_2 than with any other fuels. In terms of the environmental impact, the oxidation of hydrogen produces only water, allowing for pollution-free electricity generation. Finally hydrogen does not contain any carbon, as opposed to hydrocarbons. Therefore, any concern related to solid carbon deposition on the anode, presented hereafter, does not apply to hydrogen.

Because they can convert efficiently hydrogen to electricity, fuel cells are considered as a keystone of a potential future economy based on hydrogen. In the hydrogen economy, H_2 would be used as a widespread energy carrier providing the energy source for motive power, stationary power and portable electronic devices. Due to their high efficiency and the range of application covered, fuel cells would then play a major role in converting the hydrogen to CO_2 free electricity and possibly valuable heat in the case of high temperature fuel cells. Nonetheless, many technological

hurdles need to be overcome before the transition to any hydrogen based economy can be considered. Important advances are required mainly in the transport, storage and production of hydrogen.

Since molecular hydrogen is not available on earth in convenient natural reservoirs (most of the hydrogen on earth is bonded to oxygen in water), it needs to be produced. The vast majority of hydrogen is currently being generated by the reforming of hydrocarbons, which has two important consequences. The feedstock used is non renewable and the production process emits CO_2. The hydrogen economy makes little sense unless we develop the ability to produce renewable and CO_2 free hydrogen on a wide scale at cheap energy costs. Different production methods are under development to achieve this essential prerequisite.

Hydrogen can be produced through the electrolysis of water. In this process, electricity is used to split water molecules into hydrogen and oxygen. Pollution free electricity generated using renewable sources such as solar and wind energy can be used, meaning such a process is well suited for decentralized hydrogen production. In this respect, an interesting example is the one Shetland Islands in Scotland, where wind power is used to produce hydrogen in the aim of fulfilling the community energy needs. This project is the first off-grid renewable hydrogen system in Europe and the first community owned hydrogen production plant in the world[1]. On a larger scale, the use of nuclear energy could be considered to provide the electricity required for water electrolysis but uranium is non renewable and the development of this energy is opposed in many countries. High Temperature Electrolysis (HTE) is another process being considered. In this process, both electricity and heat are used to convert water to hydrogen.

Another interesting alternative would the reforming of biofuels. Whilst the current reforming of fossil fuels uses non renewable feedstock, replacing fossil fuels in this process with renewable biofuels could provide a sustainable mean of hydrogen production. The first hydrogen production plants reforming bio-ethanol have recently been built in the USA. However, if the same biofuels could be efficiently oxidized in SOFCs, both efficiency and system simplicity could be gained. Other means of hydrogen production include fermentative production and biological production

Besides its production, many issues associated with hydrogen storage and transport need to be addressed. As for the production, considering a transition to a hydrogen economy requires the ability to safely and efficiently transport and store molecular hydrogen. The difficulties associated with storage and transport stem from hydrogen low energy density per unit of volume at gas ambient conditions. Despite showing a really high energy per unit of mass, hydrogen has a low molecular weight. To be stored for practical applications such as on board a vehicle for motive power, hydrogen must be pressurized or liquefied to provide sufficient driving range. Achieving high pressures required to obtain reasonable storage volumes necessitates high use of energy to power the compression. Alternatively, the use of liquid hydrogen is being considered. Liquid hydrogen possesses a higher volumetric energy density but is cryogenic and boils at -250°C. While being attractive in terms of weight, cryogenic storage is energy consuming. Moreover, liquefied hydrogen has lower energy density by volume than gasoline by approximately a factor 4, due to the low density of liquid hydrogen (there is actually more hydrogen in a liter of gasoline

(116 grams) than there is in a liter of pure liquid hydrogen (71 grams)).

The inherent difficulties related to both compressed and liquefied hydrogen storage have led to the investigation of alternative storage methods. Hydrogen can be stored as a chemical hydride. In this storage method, hydrogen gas is reacted with a solid material to produce the hydrogen hydride, which is much easier to transport. The hydride is then made to decompose at the point of use, yielding hydrogen gas. Current barriers to practical storage systems stem from the high pressure and temperature conditions needed for hydride formation and hydrogen release. For many potential systems, hydriding and dehydriding kinetics and heat management are also problems that need to be overcome. Another method is to absorb molecular hydrogen into a solid storage material such as carbon nanotubes. Unlike hydrides, the hydrogen does not dissociate/recombine upon charging/discharging the storage system and hence does not suffer from kinetics limitations. Illustrations of different proposed storage methods are shown on Figure 61.

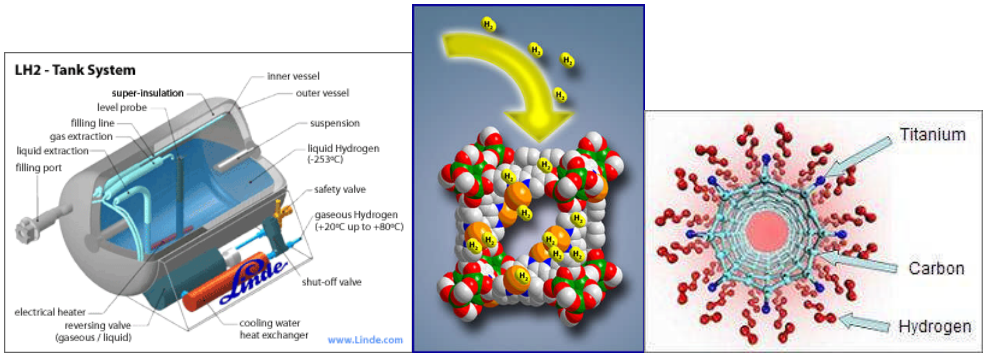

Figure 61: Illustration of different methods for hydrogen storage. From left to right: liquid hydrogen tank, hydrogen hydride, and carbon nanotubes.

The problems related to hydrogen transport basically stem from the same causes as for the storage. Although the infrastructure used for the transport of natural gas could be used, the hydrogen embrittlement of steel requires the pipes to be coated on the inside or new pipelines to be installed. Although expensive to install, once in place, pipelines are the cheapest way to transport hydrogen. Transport can be achieved using compressed hydrogen tanks or liquid hydrogen tanks, but involving the energy costs previously mentioned.

To summarize, the hydrogen economy could offer an interesting alternative to the current fossil fuel based economy. The implementation of a hydrogen economy will undoubtedly accelerate the research and development fuel cells. But before the technological hurdles mentioned above are overcome, the use of hydrogen as an energy carrier will be limited to small scale projects and community such as the Shetlands community, the hydrogen highway in California or public transports in big cities[234]

.

10.2.2. Ethanol

Among potential fuels being considered and investigated for fuelling SOFCs, ethanol offers several advantages and definitely is a serious candidate. When evaluating advantages and drawbacks of any potential fuels, it appears relevant to assess how

they compare with hydrogen. A review of ethanol properties interestingly shows how the use of ethanol as a fuel for SOFCs could provide an answer to the problems posed by the use of hydrogen.

Ethanol is a liquid fuel at ambient temperature making it easy to store, transport and handle. Liquid fuels seem to be the easiest way to store and transport energy. Indeed, our present economy being based on oil, the infrastructure required to use liquid fuels as an energy source and carrier is already into place. Moreover, liquid fuels typically offer a higher volumetric energy density than gases, making them more attractive in terms of storage capacities. With respect to its production, ethanol offers the outstanding advantage of being renewable. Ethanol can indeed easily be produced from biomass though fermentation processes. Ethanol produced from biomass is a renewable fuel and is therefore referred to as bioethanol. Concerning the environmental impact, the oxidation of ethanol will inevitably release CO_2. However, biomass consumes CO_2 from the atmosphere through the photosynthesis growing process. Hence, even if the energy production process releases CO_2, an equivalent amount of CO_2 would have been consumed from the atmosphere to produce the fuel. In such a case, a zero carbon or carbon neutral cycle is achieved, which limits the environmental impact of bioethanol use. The bioethanol carbon neutral cycle is depicted on Figure 62.

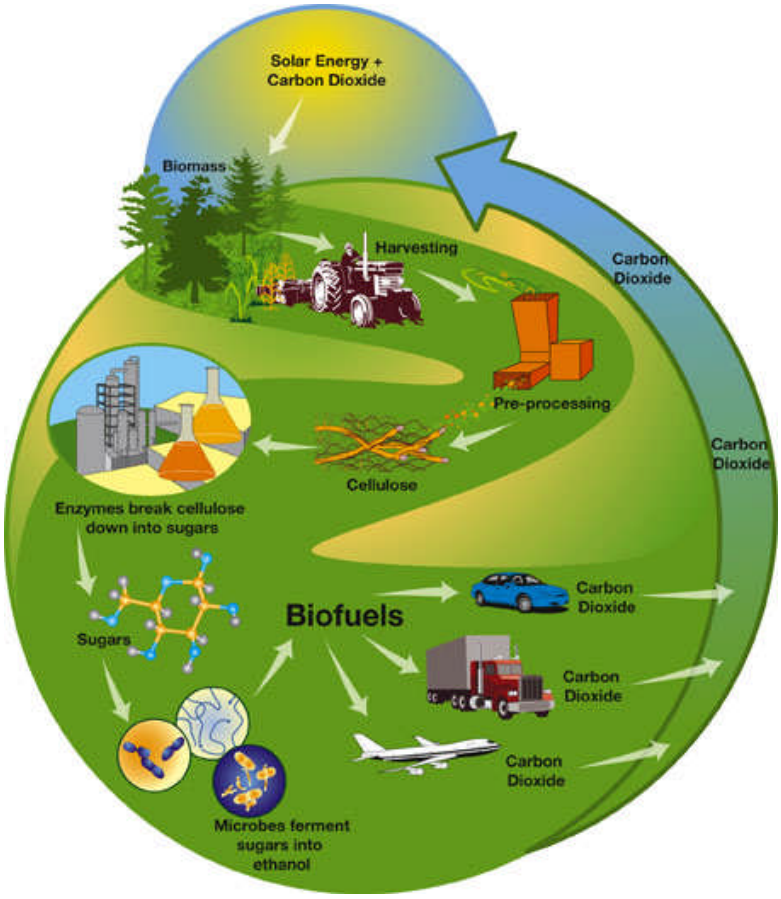

Figure 62: The bioethanol carbon neutral cycle represented here for cellulosic ethanol[5].

Ethanol thus offers an interesting alternative to hydrogen, since production, storage and transport do not pose any problems when it is used as an energy carrier. Due to

those intrinsic properties, bio-ethanol has recently received considerable amount of attention as a replacement of gasoline to fuel conventional internal combustion engines for transport applications or as an oxygenate additive.

As indicated in the introduction of this thesis, the oil based economy is a growing concern for our society. Oil resources are limited, and even if new reservoirs continue to be discovered, a transition to an economy based on renewables will be required. The emergence of third world developing economies such as India or China considerably accelerates the consumption of oil resources. As a consequence, the price of oil has steadily increased in recent years. When this research project was started in 2005, the world was becoming concerned about the oil barrel reaching 70$. In 2008, the price did reach the threshold of 150$, clearly meaning the cheap oil era was over. Although, the price has fallen down considerably with the 2008/2009 credit crunch, a serious warning has been received by governments, leading to the intensification of the research for gasoline replacements among which bioethanol has received the most attention.
Moreover, a major inconvenience for many countries with an oil based economy is the energy dependence. Countries that do not possess oil reserves are dependent on other countries for their energy needs. This dependence can be a problem in terms of geopolitics and many countries are looking to use energy sources that can be found or grown locally to gain their energy independence. This has been an important factor in USA's decision to massively invest in biofuels over the past few years. Since a considerable amount of different feedstock can be used in the ethanol fermentation process, each country can produce bioethanol using its local resources. Corn is the main feedstock used in the USA, while Brazil uses sugar cane. Alongside the energy independence, growing biomass to produce fuel contributes to boost local agricultural activities. Another driver for the development of biofuels has been environmental concerns. The oil based economy implies important CO_2 emissions that we must cut off in order to limit global warming. The use of renewable biofuels can limit the environmental impact of our energy needs by the achievement of carbon neutral cycles.

The combination of those factors has thus contributed to the important development of bioethanol. Ethanol can be used as an additive to conventional gasoline without any engines modifications. If large quantities of ethanol have to be used, engine modifications are required due to different compression rates.

The two leading countries for bioethanol development and use are Brazil and USA. 70% of the world bioethanol supply comes from those two countries. Brazil produces its bioethanol from sugar cane, and biofuels already play an important role in the Brazilian economy. Bioethanol is already largely distributed in gas station for use in conventional cars. It accounts for half of the fuel used by particulars. Cars have been released that can use either ethanol, conventional fuel or a mix of both. In the USA, bioethanol development has been recent, and the main resource use is corn. The development of corn based ethanol has been spectacular. In 2007, the USA had 114 operating bioethanol refineries and 80 were being constructed. The US government has fixed the objective of replacing 75% of oil importations with home grown ethanol by 2025. A small but growing amount of vehicles are designed to run on E85, a fuel containing 85% of ethanol and 15% of conventional fuel. Europe definitely stands behind the two leading countries in terms of biofuels production. However, the

biofuels industry is steadily growing and energy ministers of the European Union have agreed to enforce the use of 10% biofuels in vehicles fuels for 2020.

Bioethanol can be divided in two categories: conventional ethanol, which is the first generation, and cellulosic ethanol, the second generation. While the final product is of course the same, those two types of bioethanol are rather different because they use different feedstock and conversion processes.

Conventional ethanol is produced via simple sugars fermentation and therefore uses plant seeds. The process works best when derived from plants that concentrate starches in their seed, meaning than sugar cane is more efficient than corn, which is more efficient than wheat. Seeds are converted to ethanol either by dry or wet milling processes. In dry milling operations, liquefied starch is produced by heating grains with water and enzymes. A second enzyme converts the liquefied starch to sugars, which are fermented by yeast into ethanol and carbon dioxide. Wet milling operation separate the fiber, germ (oil), and protein from the starch before it is fermented to ethanol. Grain based ethanol utilizes fossil fuels to produce heat during the conversion process, generating substantial greenhouse gas emissions and lowering the overall net energy gain.

The recent development of bioethanol has been almost exclusively based on this first generation. The pace of this development has been hectic with important investments especially in the USA. This rapid development has neglected the potential problems that would rise from a widespread use of the first generation. Although presented as an efficient and clean alternative, first generation bioethanol suffers from poor global net energy efficiency. If corn is used in the production process, the net energy efficiency is believed to be 26%, i.e. the combustion of ethanol in a conventional engine will produce only 26% more energy than required for the production. As mentioned above, although a carbon neutral process is achieved through ethanol combustion, the production requires the use of fossil fuels.
Besides energy efficiency and environmental concerns, the development of first generation bioethanol has received considerable criticism for its political consequences. The main cause of this has been the conflict caused by bioethanol with food resources. Most of the plants used in the fermentation process are edible and if bioethanol has to be produced on a large scale, it must compete with existing agricultural land already dedicated to other productions. An important consequence has been the contribution to the rise of food prices. As an example, the price of corn had quickly gone up by 50% in the USA following the intensification of bioethanol production, and had considerable impact on the Mexican economy where corn is an important part of the average diet. Another related negative point is that the seeds used to produce fuels can be used to feed populations. 250 kg of corn are required to produce the ethanol needed to fill a 4 wheel drive tank. This amount of corn is believed to be enough to feed one person for one year. In the current geopolitical context, that has seen many demonstrations against hunger taking place in different countries in 2008, the first generation of biofuels can struggle to find acceptance.

While the first generation of biofuels seems to create more problems than it solves, the second generation is much more attractive and appears as a credible alternative to both oil and hydrogen.

Second generation cellulosic ethanol is bioethanol produced from lignocellulose, a structural material that comprises much of the mass of plants. Cellulosic biomass is composed of cellulose, hemicellulose and lignin, with smaller amounts of proteins, lipids (fats, waxes and oils) and ash. Cellulosic ethanol can be produced from a variety of cellulosic biomass feedstock including agricultural plant wastes (corn stover, cereal straws, sugarcane bagasse), plant wastes from industrial processes (sawdust, paper pulp), solid municipal waste and energy crops grown specifically for fuel production, such as switchgrass. Examples of feedstock for cellulosic ethanol production are displayed on Figure 63. Lignocellulose is diverse and abundant, and can be tapped from waste or the non edible part of plants. Hence, feedstock involved does not interfere with food production and economy. With respect to the feedstock that can be used, cellulosic is much more attractive than conventional ethanol that relies on simple sugars. The production process can thus use only a relatively small proportion of each plant, meaning a lot of biomass goes unused in the process. Instead, waste can be turned into valuable fuel with this second generation, which can potentially create new economies. As a result, an acre of grasses or other crops grown specifically to make ethanol could produce more than two times the number of gallons of ethanol as an acre of corn, in part because the whole plant can be used instead of just the grain

Figure 63: Examples of potential feedstock for cellulosic ethanol. From left to right: (1) switchgrass, a non-edible native American plant perfectly suited for biofuel production, (2) waste from relansdcaping.

As with grain, processing cellulosic biomass aims to extract fermentable sugars from the feedstock. But the sugars in cellulose and hemicellulose are locked in complex carbohydrates called polysaccharides. The production process hence requires an extra production step called cellulosys that breaks down complex polymeric structures into fermentable sugars. Two processing options are employed to produce fermentable biomass. One approach utilizes acid hydrolysis to break down the complex carbohydrates into simple sugars. An alternative method, enzymatic hydrolysis, utilizes pre-treatment processes to first reduce the size of the material to make it more accessible to hydrolysis. Once pre-treated, enzymes are employed to convert the cellulosic biomass to fermentable sugars. The final step involves microbial fermentation.

Reducing the cost and improving the efficiency of separating and converting cellulosic materials into fermentable sugars is one of the keys to a viable industry. Lignin and protein, two important co-products, have the potential to significantly improve the economics of biorefinneries. Lignin is a non fermentable residue from the hydrolysis process. It has an energy content similar to coal, and is employed to power

the operation, therefore reducing costs and avoiding the use of fossil fuels. There is enough residues left over to meet the energy needs of the process, plus make additional ethanol or electricity. This energy source in the production process is another advantage over conventional ethanol, since fossil fuels are not required to power the conversion. This improves both the environmental impact and the overall net energy gain. The well to wheel model, established by Michael Wang from Argone National laboratories, showed greenhouse gas emission reduction of about 80% for cellulosic ethanol compared to fossil fuels, when corn based ethanol show a reduction of only 20 to 30% for corn ethanol.

Research and development on the extra cellulosis step in the production process is still required to cut down the production costs of cellulosic ethanol. When costs will be competitive, cellulosic ethanol will certainly play an important role in our economy. Both because replacements to oil are required and it can be produced from waste, which is still a largely untapped source of energy in our economies. Progresses are being made in this sense, and the first commercial plants are now being built.

10.2.3. Fuel processing for SOFC

The mismatch between the desired fuel, hydrogen, and available ones, has definitely contributed to the limited commercial implementation of fuel cells so far. The important drawbacks that hinder the widespread use of hydrogen as an energy carrier have led to the development of fuel cell systems that rely on practical fuels. Figure 64 illustrates the general concepts and requirements of processing gaseous, liquid and solid fuels for fuel cell applications[6]. Different strategies must be applied according to the type of fuel cell involved. Higher temperatures release the requirements on fuel purities, and typically, less processing is required with higher temperatures.

Low temperature fuel cells, such as PEMFC and PAFC require many fuel processing steps. The fuel has to be converted to a fairly pure hydrogen rich gas. The conversion of hydrocarbon-related fuels to hydrogen can be done mainly by steam reforming, partial or complete oxidation, and is performed in a set of reactors external to the fuel cell stack. Catalysts are poisoned by CO at low temperatures. The CO content of the fuel entering the fuel cell stack needs to be reduced to the purity levels required by the type of cell involved. Requirements can be as tight as tens of ppms for PEMFC.
The on site pre-processing of the fuel provides a suitable solution for supplying hydrogen to fuel cells. The transport and storage are no longer subjects of concern, since hydrogen is stored chemically in liquid fuels or gases that can be more easily transported. However, the addition of external reactors leads to significant complications in the system, by increasing system complexity and costs and decreasing efficiency.

As opposed to low temperature cells, CO is not a poison for SOFCs but can be oxidized and therefore acts as a fuel. SOFCs are the most flexible fuel cells with respect to their multifuel capability so that not only hydrogen and carbon monoxide but also various kind of hydrocarbon related species could be used in the feed However, anodes will typically produce higher performance when fuelled with H_2 than with any other fuel as was highlighted by the numerous works presented the

review of anode materials. Therefore, purity requirements are less stringent for SOFCs. The desulfurization step is still required but as can be seen on Figure 64, the route form chemicals to electricity could be greatly simplified if SOFCs were to be fed directly on hydrocarbons. Hence, research has been intensive in developing SOFCs that can operate directly on hydrocarbons. Since hydrogen is currently produced from hydrocarbons, producing directly electricity from the same hydrocarbons would be more efficient.

The main problem when feeding a SOFC with hydrocarbon is the carbon deposition, which is a serious problem with any processes that involve hydrocarbons at high temperature. Catalysts active for the formation of carbon need to be avoided

Another route involves performing the fuel conversion within the SOFC. The conversion process occurs then within the anode chamber taking advantage of the high operating temperature. Hydrogen fuel gas is produced in situ the anode, which serves both as a catalyst and electro catalyst, eliminating the need for external converters. This approach requires the fuel to be diluted with steam, carbon dioxide or oxygen to provide reactants for steam reforming and/or partial oxidation reactions. This approach will as well lessen the overall efficiency by diluting the fuel.

The most attractive concept is certainly to feed directly dry hydrocarbon-related fuels on the anode.

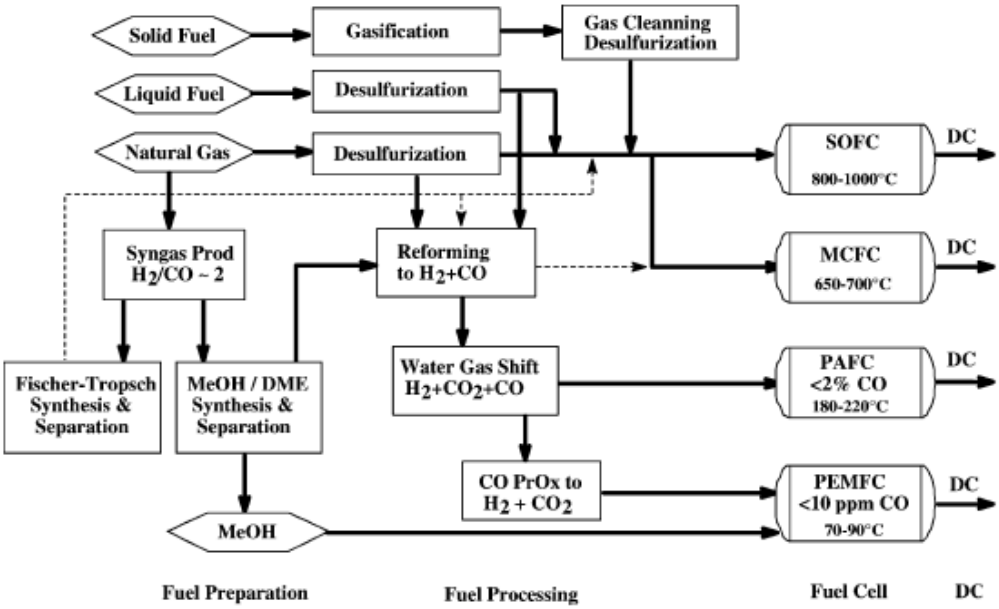

Figure 64: The concepts and steps for fuel processing of gaseous, liquid and solid fuels for high temperature and low temperature fuel cells[6].

Potential fuel range from methane to diesel to coal. Specific energies of different fuels are shown on Table 2. Based on the availability of natural gas (methane with small amounts of other hydrocarbons) most stationary fuel cells have been designed for this fuel. Methane is therefore the hydrocarbon fuel that has been the most studied so far.

Fuels	Energy densities (kWh / kg)
H_2	32.8
H_2 in tank (1.5 wt % storage)	0.42
CH_3OH	6.1
CH_3CH_2OH	8.6
$(CH_2OH)_2$	5.2
NH_3	5.7
NH_2-NH_2	2.6

Table 2: Theoretical mass energy density of different fuels.

10.3. High temperature chemistry of ethanol

Despite displaying significant advantages as an energy carrier, bioethanol has received only little attention as a fuel for SOFCs. Studies addressing the use of ethanol as a fuel for PEMFCs can be found in the literature[7]. Only the Cu-ceria based anode developed at the University of Pennsylvania has been claimed of being capable to achieve the direct oxidation of ethanol[8]. However, questions remain about the long term stability of those anodes. A few studies have addressed the use of diluted ethanol as a feed for nickel based anodes. Yet, most of the studies that can be found in the literature address the steam reforming of ethanol, which is a very attractive process for hydrogen production[9]. While being a distinct process from the electrochemical oxidation generating the direct current in a SOFC, steam reforming will occur within the anode SOFC chamber.

The direct oxidation ethanol can be described by the following overall reaction:

$$C_2H_5OH + 3O_2 \rightarrow 2CO_2 + 3H_2O \quad \textbf{(Equation 32)}$$

which corresponds to the complete combustion of ethanol in pure oxygen. The Gibbs energy change of this reaction is calculated, in standard conditions, as follows:

$$-\Delta G_r^\circ = 2\Delta G_{CO_2}^f + 3\Delta G_{H_2O}^f - \Delta G_{C_2H_5OH}^f - 3\Delta G_{O_2}^f = -1325 kJ/mol \quad \textbf{(Equation 33)}$$

This allows calculating the standard electrochemical force:

$$E^\circ = \frac{-\Delta G^\circ}{nF} = \frac{1325\times10^3}{12\times96485} = 1.145V \quad \textbf{(Equation 34)}$$

The specific energy of ethanol can then be calculated as follows:

$$W_e = \frac{-\Delta G^\circ}{3600\text{x}M} = \frac{1325\text{x}10^3}{3600\text{x}0.046} \approx 8.00 \text{ kWh/kg} \quad \textbf{(Equation 35)}$$

However, the high temperature chemistry in the SOFC anode chamber is quite

complex when fuelled with hydrocarbons. Many reactions of different types can occur, and although direct utilization of hydrocarbons has been demonstrated, the parent hydrocarbon may not be the species responsible for the charge transfer chemistry[4]. Before direct current is created at the TPB by charge transfer reactions, both homogeneous and heterogeneous chemistry play an important role in (1) converting initial hydrocarbons into more reactive species, and (2) depositing carbon into the anode. The different processes occurring in the anode chamber are depicted in Figure 65. Homogeneous chemistry happens in the gas phase, and is unrelated to the nature of the materials present in the anode chamber, while the heterogeneous chemistry is promoted by solid surfaces. Therefore, the heterogeneous chemistry can be controlled via appropriate choice of materials, while the homogeneous chemistry will depend only on pressure, temperature, residence time and gas inlet composition. The extent of the homogeneous chemistry will hence strongly depends on the design of the SOFC stack and the time the fuel is exposed to high temperature in the flow distribution networks. Substantial gas phase reactions can be expected before the gaseous mixture reaches the active surfaces of the porous anode, where catalytic reactions on those surfaces will further modify the gas composition. Hence, the gaseous mixture available for electrochemical reactions will strongly differ from the original feed.

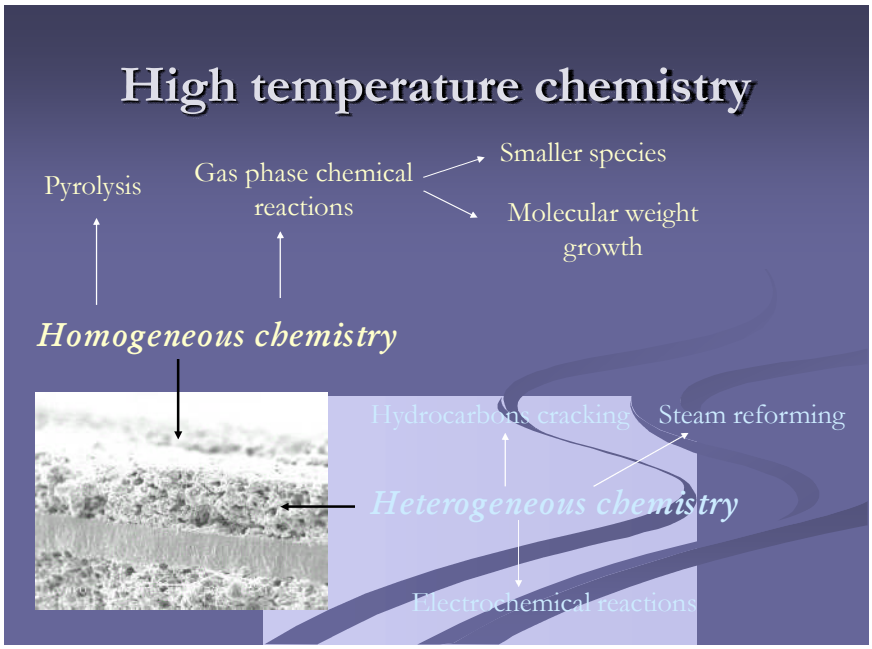

Figure 65: High temperature chemistry in the chamber of a SOFC.

10.3.1. Pyrolysis

The parent hydrocarbon will first undergo pyrolysis. Under the effect of the high temperature, hydrocarbons decompose, without any interaction either with catalytic surfaces or with additional species in the inlet stream. The importance of homogeneous pyrolysis in the operation of hydrocarbon fuelled SOFCs has been demonstrated by Dean et al. [10,11], in studies of a variety of fuels under typical SOFCs conditions. Experiments carried out with residence times of a few seconds confirmed

kinetic models prediction that hydrocarbon are readily converted to smaller stable compounds. As an example, at 800 °C, butane undergoes full conversion for a residence time of 5 seconds.

In a subsequent study, the reactivity of ethanol has been investigated[12] and compared to the one of butane, which is considered as a representative hydrocarbon, while ethanol is an oxygenate. The presence of the OH group in ethanol leads to a weakening of the C-H bonds, meaning that ethanol might be more reactive than a hydrocarbon. The decomposition of ethanol has been studied as well by Li et al[13], both numerically and experimentally. The detailed chemical mechanism used in that analysis includes detailed oxidation and pyrolysis kinetics for hydrocarbons up to C6 and involves about 350 species and over 3450 reactions.

The two channels for ethanol dissociation are:

$$C_2H_5OH \Leftrightarrow C_2H_4 + H_2O \quad \textbf{(Equation 36)}$$

$$C_2H_5OH \Leftrightarrow CH_3 + CH_2OH \quad \textbf{(Equation 37)}$$

The dehydration reaction (Eq. 36) is the dominant reaction. All those studies have shown a very good agreement between kinetics predictions and experimental observations. Figure 66 displays the conversion rate of ethanol obtained by Gupta et al [12] for 700, 750 and 800°C, where residence time varied from 2 to 4 seconds

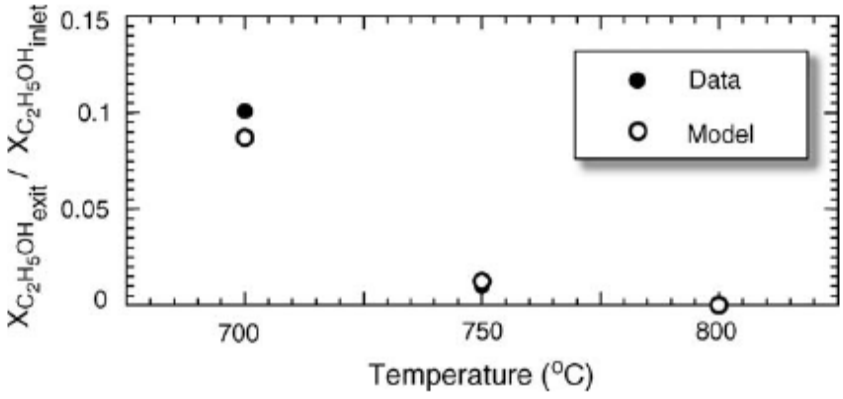

Figure 66: Comparison of the ratio of exit to inlet mole fraction of ethanol observed experimentally with the model predictions as a function of temperature[12].

At 700°C, for a residence time of 3.0s, 87% of the ethanol is converted, while complete conversion is achieved at 800°C. As expected, the extent of the fuel conversion has been shown to be higher for ethanol than butane. Regarding the product distribution, as compared with butane pyrolysis, the amount hydrocarbons are lower in ethanol pyrolysis. Figure 67 displays the major species predicted for ethanol pyrolysis as a function of the temperature. Ethanol pyrolysis produces relatively large amounts of CO and H_2. Substantial amounts of H_2O and ethylene are produced from the primary ethanol dissociation reaction. As compared to butane, the amounts of CH_4 and C_2H_6 are significantly lower in ethanol pyrolysis.

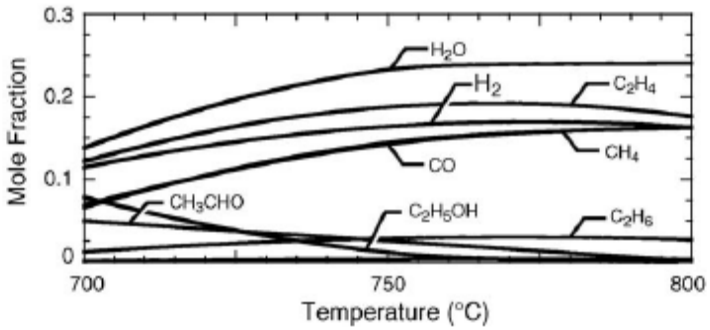

Figure 67: Predicted major species at the end of the hot zone as a function of temperature for ethanol pyrolysis in helium[12].

The study has indicated that the addition of H_2O in the feed has little effect on the pyrolysis reaction. Figure 68 displays the predicted extent of the conversion for ethanol and butane as a function of the steam content. It can be seen that even in the presence of large amounts of steam the level of conversion is only slightly less than the system without any added steam for both fuels. The results are similar when H_2O is replaced by N_2, suggesting that the primary effect of steam addition on the gas-phase reaction is dilution.

Those studies demonstrate that important gas phase reactions can be expected, even in the presence of large amounts of steam. Even at 700°C, within a few seconds of residence time in the high temperature channels, most of the ethanol will be converted. Hence, even if the feed is dry ethanol, only a small fraction of ethanol, if at all, will reach the TPB and be available for direct electrochemical oxidation.

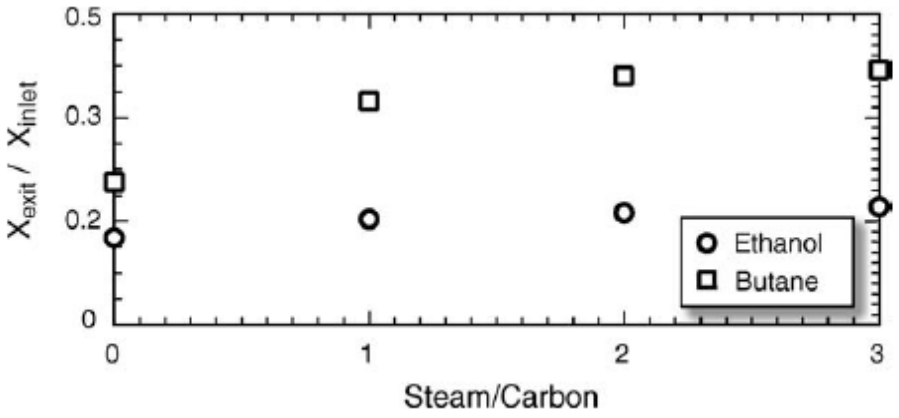

Figure 68: Predicted ratio of exit to inlet mole fraction of butane and ethanol at 700C as a function of steam to carbon ratio[12].

Another important result advanced by Gupta et al. is that the comparison to equilibrium predictions shows that a kinetic model is essential to predict levels of conversion, product distribution and deposits formation.

10.3.2. Carbon deposition

The formation of carbon is a serious problem with many processes that involve hydrocarbons at high temperature, among which SOFCs. To understand when and how carbon will deposit, it is necessary to understand the reactions that will deposit and remove carbons. Two substantially different mechanisms are known to exist at high temperature for carbon deposition.

10.3.2.1. **Catalytic carbon formation**

The first mechanism already mentioned in the review of anode materials, results from reactions over a catalyst and thus belongs to the heterogeneous chemistry. This process is well know from 'dry corrosion', which is the problem of pitting when steels are exposed to hydrocarbons at high temperature [14,15] and has been well studied over Ni, Fe and Co catalysts[16,17,18,19,20,21]. The mechanism occurring over Ni, depicted in Figure 69, involves deposition of a carbon source onto the metal surface, dissolution of the carbon into the bulk of the metal, and finally precipitation of carbon as a graphite fiber at some surface of the metal particle[22]. It is important to recognize that the metal is not merely covered by carbon in this reaction, but becomes part of the carbon fiber, explaining the pitting that is observed in dry corrosion. The mechanism also explains the requirement for high steam to carbon ratio for the steam reforming of hydrocarbons higher than methane on Ni catalysts[23,24].

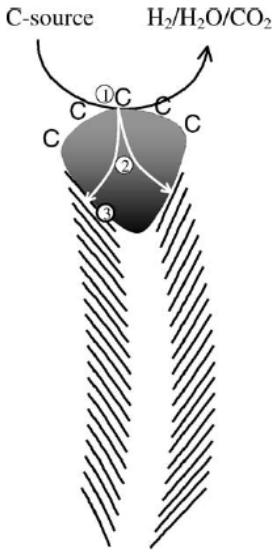

Figure 69: The mechanism of carbon deposition through catalytic reaction[22].

The following three reactions are the most probable catalytic reactions that lead to carbon formation in high temperature systems[2526]:

$$2CO \Leftrightarrow CO_2 + C \quad \textbf{(Equation 38)}$$

$$CH_4 \Leftrightarrow 2H_2 + C \quad \textbf{(Equation 39)}$$

$$CO + H_2 \Leftrightarrow H_2O + C \quad \textbf{(Equation 40)}$$

The thermodynamic possibility of carbon deposition has been studied by different authors. Those calculations provide information on the system composition at thermodynamic equilibrium, and hence do not take into account any kinetic effects.

Because the Boudouard reaction (Eq. 38) shows the largest Gibbs energy change, it is often employed to examine the thermodynamic possibility of carbon formation. A carbon activity can be defined to determine the possibility of carbon formation (based on the Boudouard equation) [25,26]:

$$\alpha_c = K_1 \frac{p_{co}^2}{p_{co_2}} \quad \textbf{(Equation 41)}$$

where K_1 represents the equilibrium constant of the boudouard equation and p_i the partial pressure of the component i. When $\alpha>1$ the system is not in equilibrium and carbon formation is observed. The system is at equilibrium when $\alpha=1$. When $\alpha<1$, carbon formation is thermodynamically impossible.

All those studies have been used to determine the condition that will lead, thermodynamically, to carbon formation in the system. Sasaki et al.[27] have performed the carbon-hydrogen-oxygen (C-H-O) ternary diagram, exhibiting the position of alcohols based fuels used in the study, pure alcohols and related species, along with carbon deposition limits line calculated for different temperatures, as shown on Figure 70. It can be seen from such diagrams that the position of pure alcohols lie within the carbon deposition region in the whole temperature range, while addition of H_2O can shift the position of such fuels outside the deposition region. This study already indicates that a small amount of H_2O, for example, is essential to be added in order to prevent carbon deposition, in the case that thermodynamic equilibrium is achieved. Addition of O_2 or CO_2 in to hydrocarbon-related fuel gases enables the prevention of carbon deposition as well. However, too high concentration of those added species will increase the oxygen partial pressure and thus decrease the cell voltage.

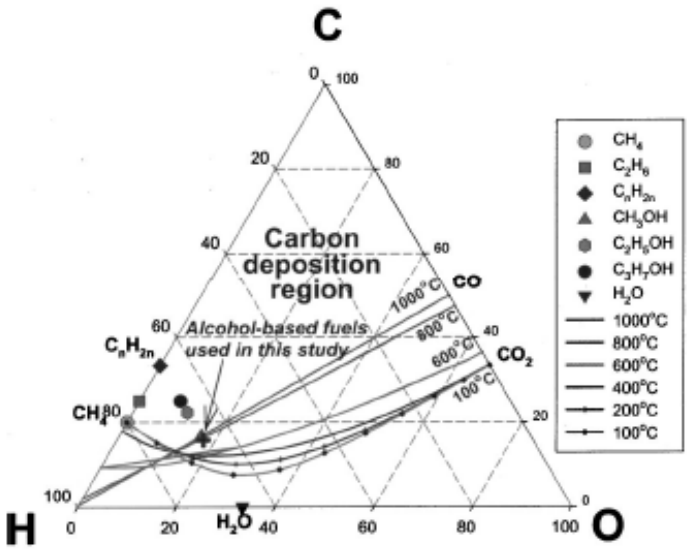

Figure 70: Positions of alcohol based fuels in the C-H-O ternary diagram denoted by a crosshair symbol, and positions of pure alcohol and related species. The carbon deposition region at various temperatures shown as the region on the carbon-rich side of the deposition limit lines thermochemically calculated[27].

Figure 71 shows the minimum amount of H_2O to be supplied per carbon atom in the feed to prevent carbon formation in the equilibrium as calculated by Sasakiet al[27].

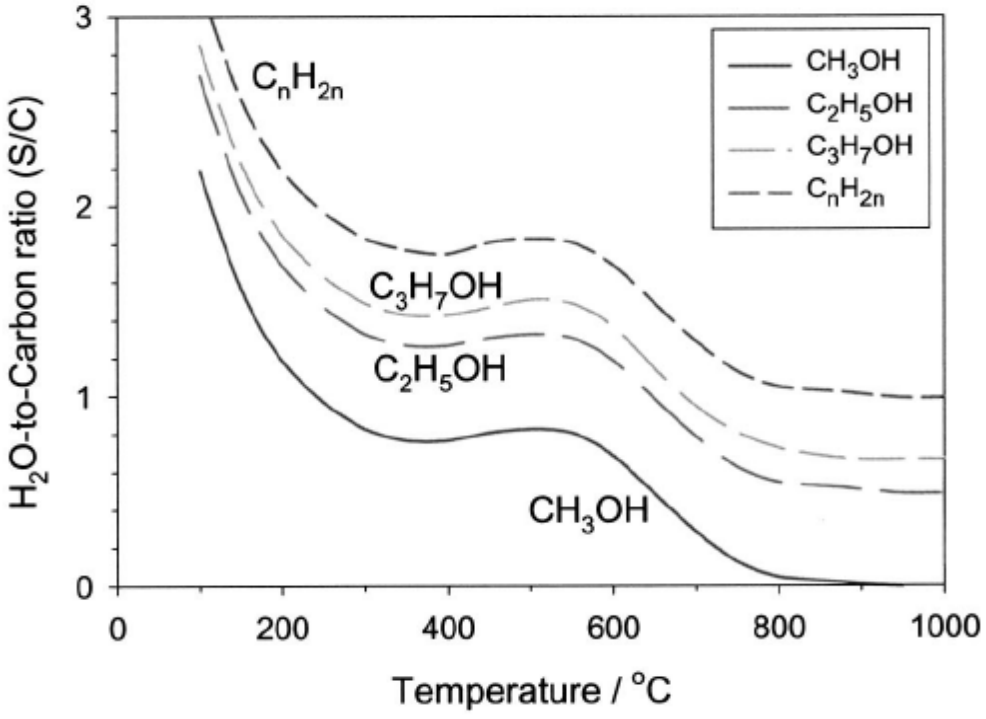

Figure 71: minimum amounts of H_2O supplied per carbon in the fuels needed to prevent carbon formation in the thermodynamic equilibrium[27].

Same type of results has been observed by various workers, i.e. addition of water in

the feed and an elevated temperature will prevent carbon formation. A ratio of 3:1 is usually required at intermediate temperatures, and this decreases for highest temperatures. It is interesting to note that for an initial ratio 1:1, thermodynamic equilibriums always predict carbon formation for temperatures up to 1000°C.

However, Filament formation on Ni can occurs when carbon deposition onto the Ni surface occurs more rapidly than carbon removal by steam, even if thermodynamic calculations show that carbon should not be stable at equilibrium.

10.3.2.2. **Gas phase carbon formation**

The second mechanism of carbon deposition occurs in the absence of a catalyst via free radical gas phase reactions[28]. Those reactions, usually initiated by the C-C bond scission, are more important for hydrocarbon larger than methane. While the primary products of pyrolysis are molecules that are smaller than the parent hydrocarbons, the olefins that are formed by pyrolysis can react with radicals to form larger molecules. The carbonaceous products that are ultimately formed by pyrolysis are high-molecular weight, polyaromatic compounds, perhaps best referred to as tars and quite different in form from the graphitic fibers on Ni, Co, or Fe catalysts. Those polyaromatic compounds have very low vapour pressure and hence easily deposits on surfaces[29]. The mechanism is therefore quite different than catalytic carbon deposition. While the catalytic deposition damages irreversibly the active surface, the carbon deposits from gas phase reactions do not chemically interact with the anode surface. Hence, effects on the anode performance are quite different. Carbon deposition from gas-phase reactions has been well documented by Gorte and co-workers in a series studies addressing the use of hydrocarbons on copper-ceria anodes[30,31,32,33,]. Carbon deposition by free-radical, gas-phase reaction is probably unavoidable for most hydrocarbon fuels other than methane above 700°C.

SEM images showing the morphology of those carbon deposits are given on Figure 72, while Figure 73 provides the chemical composition of deposits formed on a copper plate after 24H exposure to n-butane at 800°C[30].

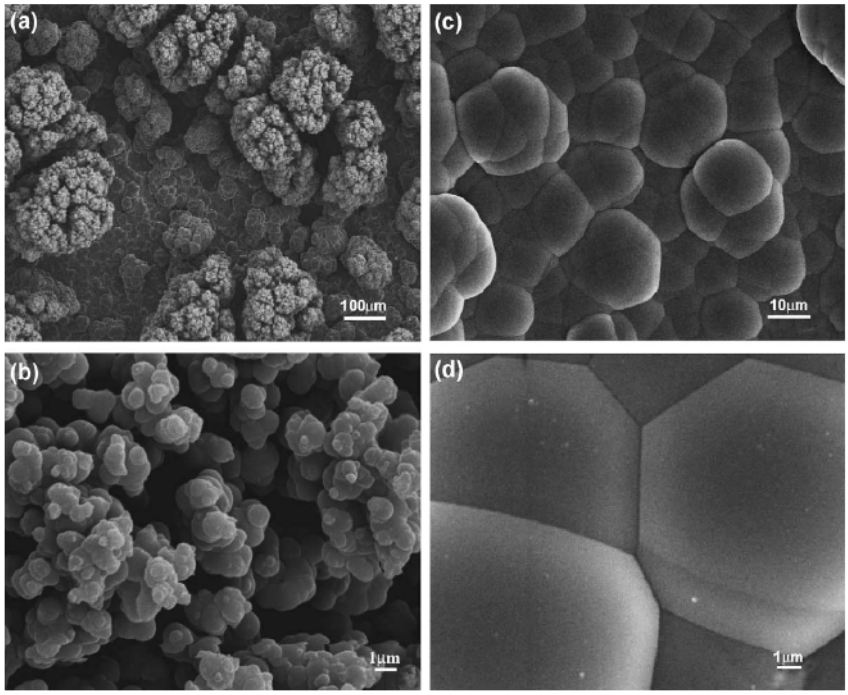

Figure 72: The morphology of carbonaceous deposits from gas-phase reactions after long term testing on n-butane at 800 °C[33].

Table I. Chemical composition of the carbon deposit formed on a Cu plate after 24 h exposure to n-butane at 973 K.

Name	*m/e*	No. of aromatic rings
Styrene, bicyclo [4,2,0]octa-1.3.5-triene	104	1
Ethyl methyl benzene, Propenyl benzene, etc.	118	1
1,4-Dihydronaphthalene	130	1
Naphthalene: $C_{10}H_8$	128	2
Acenaphthene: $C_{12}H_{10}$	154	2
Acenaphthylene: $C_{12}H_8$	152	2
Phenanthrene, Anthracene: $C_{14}H_{10}$	178	3
2-Methy-phenanthrene, 1-methyl-anthracene: $C_{15}H_{12}$	192	3
2Phenylnaphthalene: $C_{16}H_{12}$	204	3
Pyrene: $C_{16}H_{10}$	202	4
Benzo[a]fluorine, benzo[b]fluorine: $C_{17}H_{12}$	216	3
Benzo[a]anthracene, chrysene, triphenylene: $C_{18}H_{12}$	228	4
Benzo-pyrene, perylene: $C_{20}H_{12}$	252	5
Benzo[ghi]perylene, anthanthrene: $C_{22}H_{12}$	276	6

Figure 73: Chemical composition of the carbon deposit formed on a Cu plate after 24H exposure to n-butane at 700°C[30].

Sheng and Dean[28] have suggested that the mass of deposits formed could be correlated with the total mole fraction of species with molecular weight larger than butane, denoted as C_5+. Although this approach is clearly an approximation, those species are typically cyclic unsaturated compounds which are considered as likely precursors of polynuclear aromatic hydrocarbons. Using a factor of F=0.02 in the proportional relation:

Predicted deposit (mass fraction) = F . C_5+ (mass fraction)

Gupta et al.[12] have obtained a reasonable agreement between predicted and deposited amounts. An example of the predicted mass of C_5+ compounds for butane conversion is shown on Figure 74.

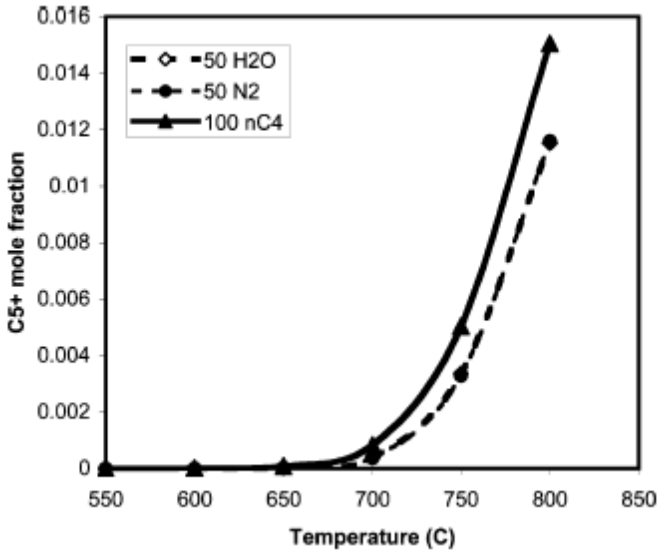

Figure 74: Modeling results showing increase in mole fractions of C_5+ species with temperature[28].

The kinetic model used in this study captured well experimental observations. C_5+ compounds, and thus carbon deposits, start to form above 650°C and become exponentially important with temperature.

A small amount of deposited tars has been shown to be beneficial for the anode performance. Indeed, those carbonaceous deposits are electronically conductive. Figure 75 shows the electronic conductivity of a porous YSZ slab as a function of gas exposure at 700°C. The slab, which is initially non conductive as can be expected from YSZ, becomes conductive with exposition to butane due to the deposition of tars on the YSZ surface.

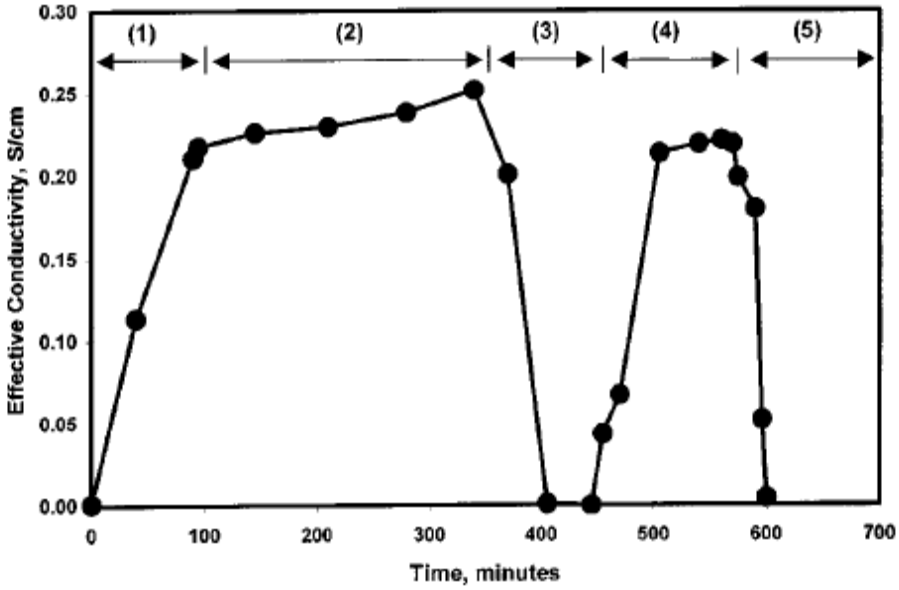

Figure 75: Electrical conductivity of porous YSZ slab as a function of gas exposure at 700°C. The slab was exposed to (1) n-butane, (2) H_2, (3) 50% He/O_2, (4) n-butane and (5) 50% He/O_2[33].

It can be seen as well that the deposits are readily removed when exposed to oxygen. Figure 76 displays the power output as a function of time of a cell containing 20 wt. % Cu at 700°C while changing the fuel from H_2 to n-butane and back to H_2. During the cell operation on n-butane, tars deposit onto the anode. When the cell is switched back to hydrogen, the performance has clearly improved.

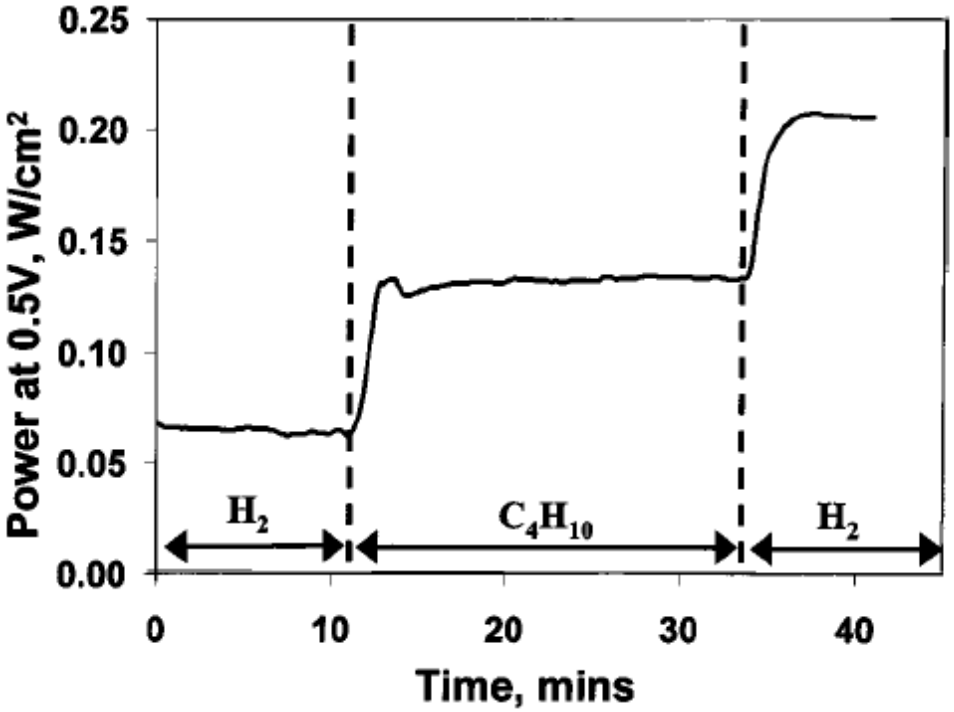

Figure 76: Evolution of the power density as a function of time when the fuelled is changed from H_2 to butane and back to H_2 on an anode containing 20 wt.% Cu operated at 700°C[30].

Impedance spectra shown on Figure 77 provide more insight into this performance enhancement. Measurements indicate that the ohmic resistance has decreased after the operation on n-butane. This enhancement has been shown to decrease with Cu content, implying that the deposits improve the connectivity within the metallic phase in the anode. The mechanism that improves the anode performance is shown on Figure 78.

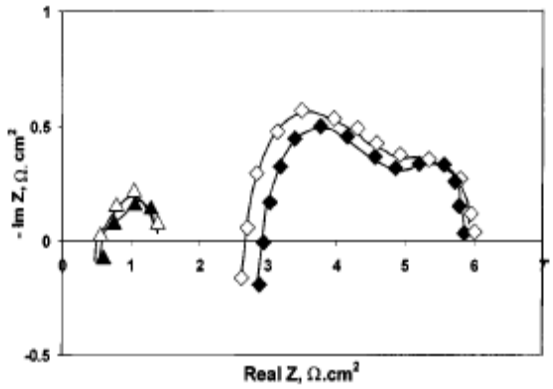

Figure 77: Influence of carbon deposits on the performance of a SOF operated at 700°C[30]. OCV impedance spectra in H_2 from a cell with an anode consisting of 10% CeO_2 and 15% Cu at 700°C. Results are shown following the initial heating in H_2 , followed by 1 h in n-butane fuel, subsequent exposure to 10% O_2 in He, and after exposure to n-butane[30].

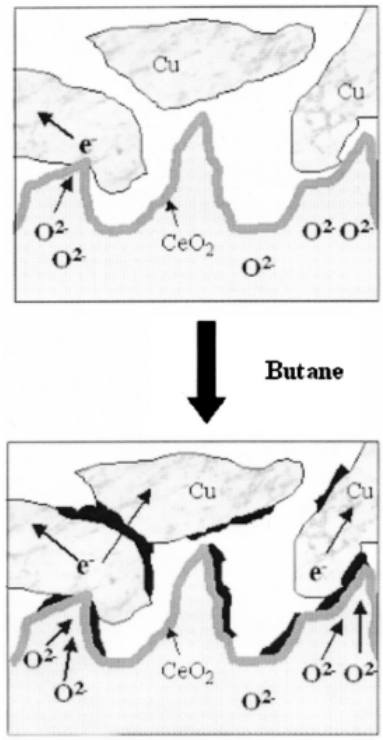

Figure 78: Role of carbon deposits in the performance enhancement of SOFC anodes. The deposits improve the connectivity in the conductive phase, Cu in this example[30].

Temperature-programmed oxidation and weight changes measurements have demonstrated that the deposits that enhance performance correspond to ~1 wt % of the anode. Test carried out using other fuels including propane, n-decane and toluene have led to similar performance enhancements.

An interesting feature of those deposits is that the enhancement of the cell performance after exposure to n-butane has been shown to be fully reversible upon oxidation and subsequent reduction in H_2. This result is of great interest. It demonstrates that the anode is not damaged by this type of deposits, as opposed to deposits. This reversibility can be seen both on Figure 75 and Figure 77. The conductivity returns to zero on the YSZ porous slab upon oxidation, while the cell performance is back to the original one. When butane is flown again, conductivity is once again introduced into the system, and the cell performance reaches the level it displayed before oxidation. The small irreversibility seen in the fuel cell test is actually due to oxidation of the anode.

As shown on Figure 74, deposits become increasingly important above 800° C. Experiments have shown that the performance starts to decay when deposits are becoming too important. Indeed, while a small amount improves connectivity, an overwhelming deposition leads to the blockage of the pores[31]. Comparatively, at 700°C, even at open circuit, the carbonaceous layer appears to reach a steady state coverage and does not lead to deactivation of the cell.

Experiments have shown that the deposits can be removed by steam, but the required temperature for this reaction is considerably higher than with oxygen. While deposits are removed at 500°C with oxygen, it was found that a temperature of 900°C is required for steam to remove deposits[33]. However, it is important to note that deposits can also be removed by steam at 800°C, but the amount of deposits will be controlled by the speed of removal and formation from the gas-phase reaction.

The presence of ceria in the anode has been shown to decrease the temperature required to oxidize the deposits[31]. Figure 79 shows the TPO of carbon deposits on a YSZ slab and a YSZ –Ceria slab. While deposits formed on YSZ are unreactive to about 800°C, the deposits formed on ceria-YSZ have been shown to be removable at temperatures a slow at 500°C. This indicates that ceria catalyses the deposits reaction removal. When ceria is added, only the carbon removal rate is affected, since in the absence of steam, no difference is observed in the deposition rates onto YSZ and YSZ-Ceria.

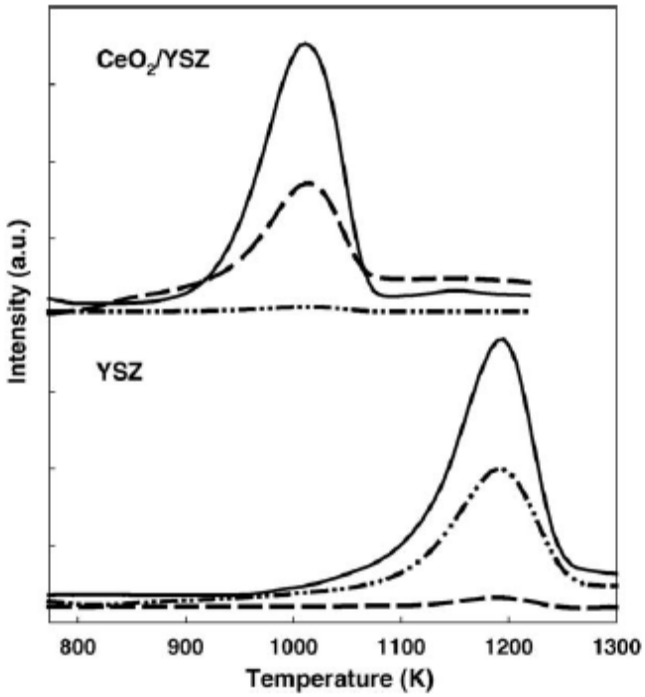

Figure 79: TPO results, using 20 vol.% H2O in He as an oxidant, for ceria-YSZ and YSZ slabs exposed to n-butane at 700C for 2 hours. The monitored products were H_2, CO_2 and CO[30].

The study carried out by Gupta et al[12], comparing butane and ethanol, demonstrated that carbonaceous deposits are less important for ethanol than for butane. This stems from the lower concentration of C_3H_6 in the ethanol system. This in turn results in much lower mole fractions of C_3H_5 and C_3H_3, which are radicals responsible for formation of the cyclic C5 species. Therefore, the propensity for carbon deposition is much lower for ethanol.

10.3.3. Steam reforming

When the gaseous mixture reaches the surface of porous anodes, catalytic reactions will occur and play a definite role in further converting the fuel mixture before it participates in electrochemical reactions. The heterogeneous processes likely to occur are the steam reforming, CO_2 reforming, partial oxidation and autothermal reforming. These are basically the processes commonly used in the upstream processing of the fuel presented on Figure 64. The nature of the ones occurring in the anode chamber along their extent will be dictated by the nature of the catalysts present in the anode chamber, and the reactants. Since hydrocarbons are often diluted in stream rather than O_2 or CO_2, the steam reforming will be the dominant conversion catalytic process within the anode.

Steam reforming is the catalytic reaction of steam with hydrocarbon fuels to produce H_2 and CO, usually with high H_2/CO ratios. Steam reforming is an endothermic reaction. Steam reforming of hydrocarbons has been extensively studied for hydrogen production. The extent of steam reforming with the anode SOFC chamber will depend on the catalytic activity of the materials used and the amount of steam. Even if the feed is a dry hydrocarbon, gas phase reactions have been shown to produce steam,

while electrochemical reactions at the TPB will as well produce steam during operation.

The steam reforming of ethanol has received some attention for hydrogen production. Both thermodynamic and experimental studies can be found in the literature. All the numerical studies available address the thermodynamic study of the steam reforming process. The reason is that in the case reforming and /or decomposition kinetics are sufficiently fast, the composition of fuel gases are identical to those in thermodynamical equilibrium. To establish optimal operational conditions, relevant conditions such as fuel gas composition and operational temperature should be adjusted. Thermochemical calculations will give such information. Thermodynamic studies have shown that ethanol steam reforming could be an efficient process for hydrogen production [34 35 36 37 38]. An issue of major importance is then to develop highly active, selective and durable catalysts for the reaction. Aiming to produce hydrogen, the working catalyst is required to be both very efficient for abstracting hydrogen atoms from the carbon containing reactant and oxidize the carbon atoms to CO_2 as much as possible. For SOFCs internal conversion purposes, the H_2 to CO ratio is important, since it will affect the power generation characteristics.

Thermodynamic studies of ethanol steam reforming consist in calculating the products distribution in the thermodynamical equilibrium considering an initial gaseous mixture. Two different approaches can be followed to perform such a calculation, namely the stoichiometric and non-stoichiometric methods. In the non stoichiometric approach, the equilibrium composition of the system is found by the direct minimization of the Gibbs free energy for a given set of species without any specification of the possible reactions which might take place in the system. On the other hand, in the stoichiometric approach, the system is described by a set of stoichiometric independent reactions. It is very important to note here that thermodynamic studies do not account for kinetic effects. Due to the complexity of the reaction system, the effect of operational parameters on the equilibrium composition can be investigated only using numerical methods.

One of the first works has been carried out by Garcia and Laborde[39], who investigated ethanol steam reforming by estimating the thermodynamic equilibrium composition at low temperatures (400-800K) and at three H_2O/EtOH ratios of 0.1, 1 and 0. Later on, a modified approach was used by Vasudeva et al.[40] to re-examine those results, in which carbon is considered as equilibrium species. The difference in the equilibrium compositions obtained from those two approaches outlines the importance of the way carbon is treated, but the same general trends were observed. In a more recent study on the alcohol based fuel cells, Sasaki et al.[27] have carried out a study to examine power generation characteristics of SOFCs for alcohol based fuels. Extensive calculations on alcohol/water systems have been performed to find out equilibrium compositions [4142] and conditions leading to carbon formation. Calculations were based as well on the Gibbs minimization procedure, using an extensive database of compounds that could possibly formed, using the program HSC chemistry (version 4.1, Outokumpu Research Oy, Finland).

All those studies provide results in good agreement. In the thermodynamic equilibrium, a mixture containing initially water and ethanol will consist of only five gaseous species in the thermodynamic equilibrium: H_2, H_2O, CO, CO_2, CH_4. Their

distribution will depend on both the initial H_2O/EtOH ratio and the temperature. Figure 80 shows products distribution for an initial ratio of 1.5 as a function of temperature, while Figure 81 shows the predicted ratio of the moles of hydrogen produced to the moles of ethanol in the feed. 6 hydrogen molecules can be extracted from an ethanol molecule.

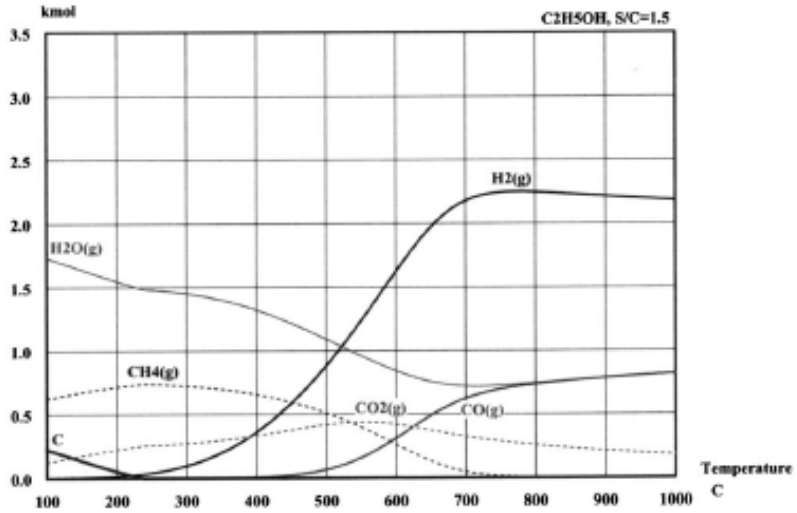

Figure 80: Products distribution in the thermodynamic equilibrium as a function of temperature for an initial H_2O/EtOH ratio of 1.5 [41].

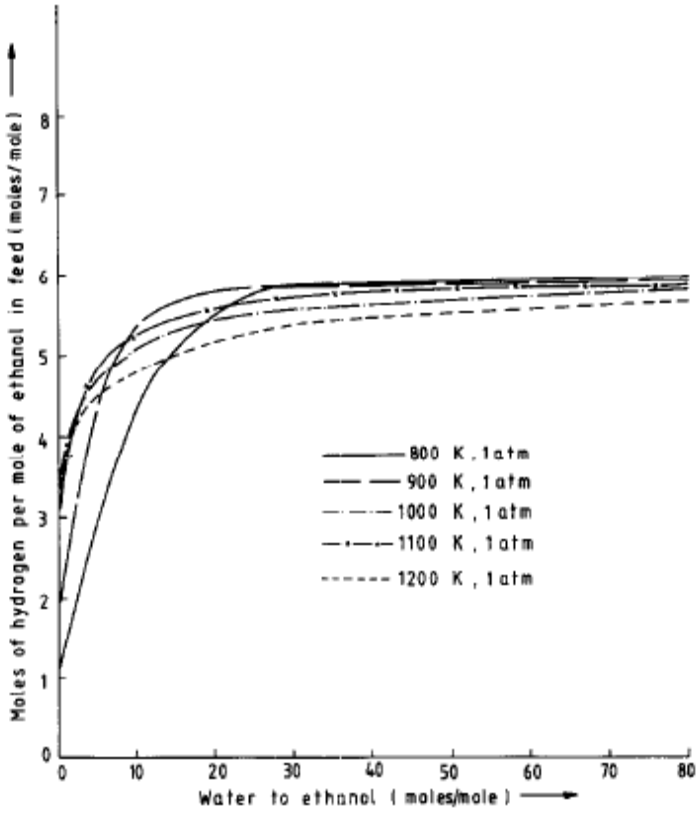

Figure 81: Moles of hydrogen per mole of ethanol in the fed against water-to ethanol ratio in the feed (mole/mole) at different temperatures[36].

According to those thermodynamic calculations, no ethanol is present at equilibrium and neither are any C_2 compounds. Thermodynamic studies show that both the temperature (Figure 80) and the initial steam content (Figure 81) have a positive effect on the hydrogen final concentration. In the same way, an increase in the initial water content would decrease methane and carbon dioxide production. While high concentrations of those products might be a concern in the hydrogen production process production or in upstream fuel processing for low temperature fuel cells, their presence is less problematic in the SOFC case.

The stoichiometry of the reaction for maximum hydrogen production is described by the following reaction:

$$CH_3CH_2OH + 3H_2O \rightarrow 6H_2 + 2CO_2 \quad \textbf{(Equation 42)}$$

Despite the apparent simplicity of the stoichiometry of the reaction, no exact knowledge of the reactions involved in the oxidative steam reforming of ethanol exists. The steam reforming of ethanol for hydrogen production involves a complex multiple reaction system. The final hydrogen production will be affected by many undesirable side reactions. Many reaction pathways are possible. The type of catalyst used for the reaction can dictate which reaction path will be favored. The yield of hydrogen is depends in a complex manner on the process variables such as pressure, temperature or reactant ratio.

Usually, three main partial reactions are recognized to account for the steam reforming process, namely the steam reforming reaction, the water gas shift (WGS) reaction and the carbon monoxide hydrogenation (or methanation) [43,44] :

$$C_2H_5OH + H_2O \Leftrightarrow 4H_2 + 2CO \quad \textbf{(Equation 43)}$$

$$\Delta H = +57 \text{ kcal/mol}$$

$$CO + H_2O \Leftrightarrow H_2 + CO_2 \quad \textbf{(Equation 44)}$$

$$\Delta H = -10 \text{ kcal/mol}$$

$$CO + 3H_2 \Leftrightarrow CH_4 + H_2O \quad \textbf{(Equation 45)}$$

$$\Delta H = -49 \text{ kcal/mol}$$

When hydrogen production is wanted, the WGS reaction has to be favored. Species can be classified in two groups: CH_4 and H_2 which compete for the hydrogen atoms and the oxygenated products CO and CO_2.

To obtain more information on the predominant reactions occurring in the steam reforming process, calculations following a different approach have been performed by Fishtik et al.[45]. Their work has focused on the steam reforming process using the

response reactions (RER) approach. Such an approach provides a straightforward manner to predict the behavior of the system by selecting a particular limited set of reactions whose contribution to the system's response is the most significant. Results obtained by Fishtik et al. are in excellent agreement with results previously published and provide different information from other works. Figure 82 provides the complete set of reactions used to characterize the system.

1. $R(C_2H_5OH, H_2O, CO_2, H_2)$	$C_2H_5OH + 3H_2O = 2CO_2 + 6H_2$
2. $R(C_2H_5OH, H_2O, CO_2, CO)$	$C_2H_5OH + 4CO_2 = 6CO + 3H_2O$
3. $R(C_2H_5OH, H_2O, CO_2, CH_4$	$2C_2H_5OH = CO_2 + 3CH_4 + 0H_2O$
4. $R(C_2H_5OH, H_2O, CO_2, CH_3CHO)$	$5C_2H_5OH + 2CO_2 = 6CH_3CHO + 3H_2O$
5. $R(C_2H_5OH, H_2O, H_2, CO)$	$C_2H_5OH + H_2O = 4H_2 + 2CO$
6. $R(C_2H_5OH, H_2O, H_2, CH_4)$	$C_2H_5OH + 2H_2 = 2CH_4 + H_2O$
7. $R(C_2H_5OH, H_2O, H_2, CH_3CHO)$	$C_2H_5OH = CH_3CHO + H_2 + 0H_2O$
8. $R(C_2H_5OH, H_2O, CO, CH_4)$	$3C_2H_5OH = 4CH_4 + 2CO + H_2O$
9. $R(C_2H_5OH, H_2O, CO, CH_3CHO)$	$3C_2H_5OH + 2CO = 4CH_3CHO + H_2O$
10. $R(C_2H_5OH, H_2O, CH_4, CH_3CHO)$	$3C_2H_5OH = 2CH_3CHO + 2CH_4 + H_2O$
11. $R(C_2H_5OH, CO_2, H_2, CO)$	$C_2H_5OH + CO_2 = 3CO + 3H_2$
12. $R(C_2H_5OH, CO_2, H_2, CH_4)$	$2C_2H_5OH = CO_2 + 3CH_4 + 0H_2$
13. $R(C_2H_5OH, CO_2, H_2, CH_3CHO)$	$C_2H_5OH = CH_3CHO + H_2 + 0CO_2$
14. $R(C_2H_5OH, CO_2, CO, CH_4)$	$2C_2H_5OH = CO_2 + 3CH_4 + 0CO$
15. $R(C_2H_5OH, CO_2, CO, CH_3CHO)$	$2C_2H_5OH + 3CO = CO_2 + 3CH_3CHO$
16. $R(C_2H_5OH, CO_2, CH_4, CH_3CHO)$	$2C_2H_5OH = CO_2 + 3CH_4 + 0CH_3CHO$
17. $R(C_2H_5OH, H_2, CO, CH_4)$	$C_2H_5OH = CO + CH_4 + H_2$
18. $R(C_2H_5OH, H_2, CO, CH_3CHO)$	$C_2H_5OH = CH_3CHO + H_2 + 0CO$
19. $R(C_2H_5OH, H_2, CH_4, CH_3CHO)$	$C_2H_5OH = CH_3CHO + H_2 + 0CH_4$
20. $R(C_2H_5OH, CO, CH_4, CH_3CHO)$	$CH_3CHO = CH_4 + CO + 0C_2H_5OH$
21. $R(H_2O, CO_2, H_2, CO)$	$CO + H_2O = CO_2 + H_2$
22. $R(H_2O, CO_2, H_2, CH_4)$	$CH_4 + 2H_2O = CO_2 + 4H_2$
23. $R(H_2O, CO_2, H_2, CH_3CHO)$	$CH_3CHO + 3H_2O = 2CO_2 + 5H_2$
24. $R(H_2O, CO_2, CO, CH_4)$	$CH_4 + 3CO_2 = 4CO + 2H_2O$
25. $R(H_2O, CO_2, CO, CH_3CHO)$	$CH_3CHO + 3CO_2 = 5CO + 2H_2O$
26. $R(H_2O, CO_2, CH_4, CH_3CHO)$	$4CH_3CHO + 2H_2O = 5CH_4 + 3CO_2$
27. $R(H_2O, H_2, CO, CH_4)$	$CH_4 + H_2O = CO + 3H_2$
28. $R(H_2O, H_2, CO, CH_3CHO)$	$CH_3CHO + H_2O = 2CO + 3H_2$
29. $R(H_2O, H_2 CH_4, CH_3CHO)$	$CH_3CHO + 3H_2 = 2CH_4 + H_2O$
30. $R(H_2O, CO, CH_4, CH_3CHO)$	$CH_3CHO = CO + CH_4 + 0H_2O$
31. $R(CO_2, H_2, CO, CH_4)$	$CH_4 + CO_2 = 2CO + 2H_2$
32. $R(CO_2, H_2, CO, CH_3CHO)$	$CH_3CHO + CO_2 = 3CO + 2H_2$
33. $R(CO_2, H_2, CH_4, CH_3CHO)$	$2CH_3CHO + 2H_2 = CO_2 + 3CH_4$
34. $R(CO_2, CO, CH_4, CH_3CHO)$	$CH_3CHO = CO + CH_4 + 0CO_2$
35. $R(H_2, CO, CH_4, CH_3CHO)$	$CH_3CHO = CO + CH_4 + 0H_2$

Figure 82: A complete set of RERs for steam reforming of ethanol[45] .

A complete set of RERs contain all the necessary information to interpret the system's thermodynamic behavior. Although there are 20 reactions in which ethanol is involved, the system can be adequately described using 8 of them. The relative importance of the reactions involving ethanol are plotted as a function of temperature on Figure 83 and amount of feed water are plotted in Figure 84. It may be seen that ethanol decomposition reactions are predominant at low amount of added steam. Those reactions are important as well for both lowest and highest temperature. The steam reforming of ethanol is becoming increasingly important with the amount of added steam.

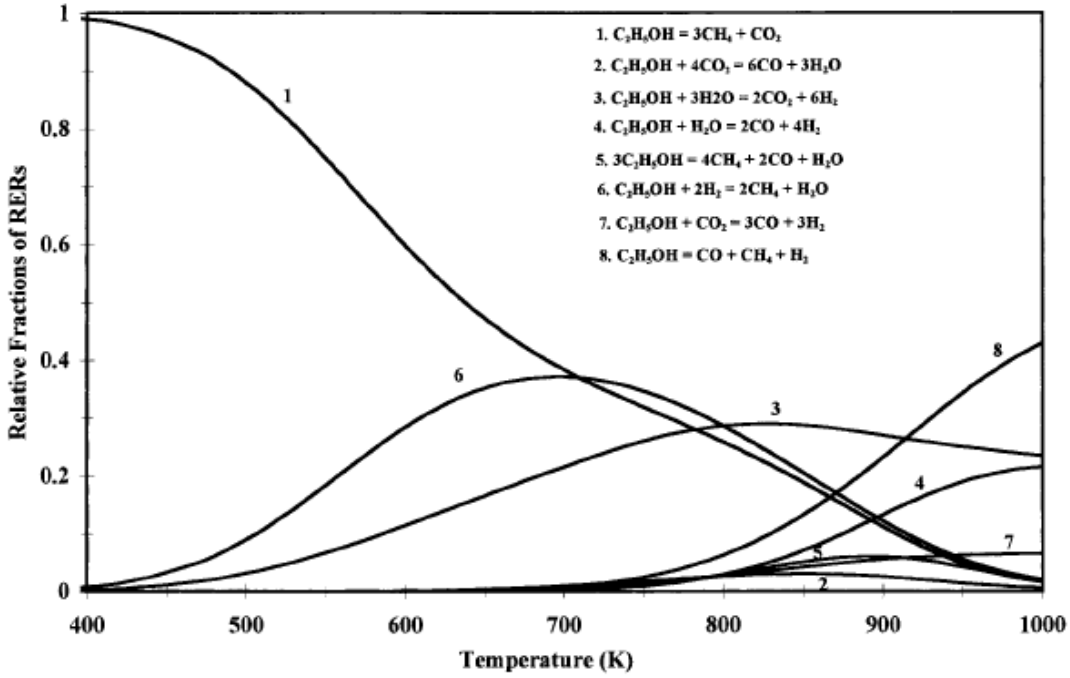

Figure 83: Relative fractions of RERs in which ethanol is involved as a function of temperature at P=1 atm, n(EtOH)=1, n(H_2O)=3mol [45].

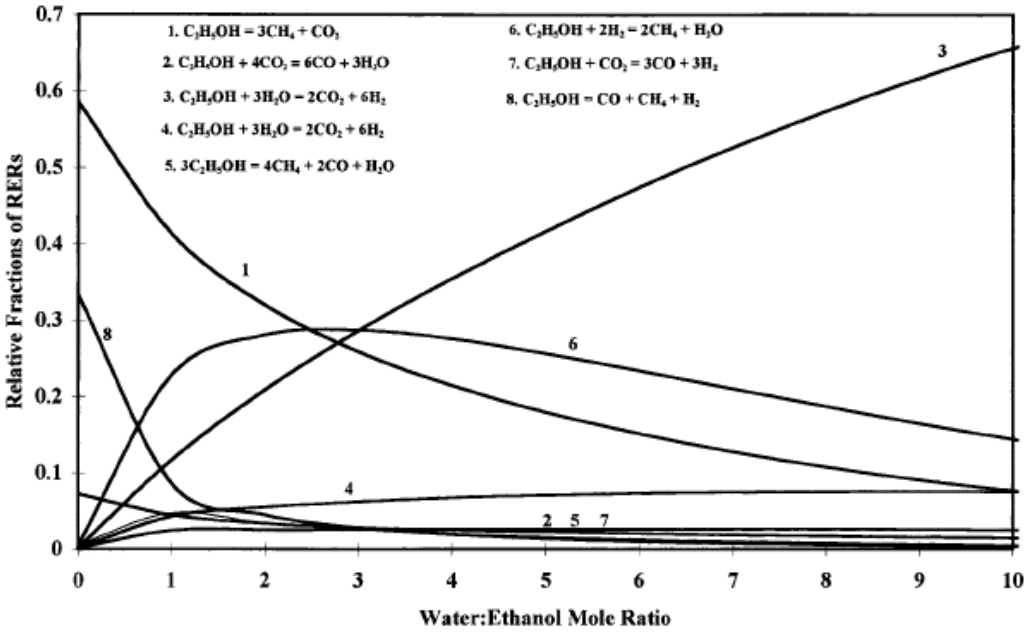

Figure 84: Relative fractions of ReRs in which ethanol is involved as a function of the initial amount of water at T= 800K, P= 1 atm, n(EtOH)=1 mol[45].

Based on the RERs, one may conclude that an increase in the amount of water can only increase the H_2 production and, as a function of temperature, the amount of H_2

can have an extremum (maximum). The thermodynamic conclusions obtained in this work are also in reasonable agreement with the experimental results from steam reforming of ethanol in packed-bed reactors.

The desired steam reforming reaction can be made predominant in the temperature range of 700-800 K and above as well at higher water/ethanol ratios. An increase in the amount of water has also the effect of increasing the extents of the water gas shift and methane steam reforming reactions, and consequently, a reduction in the amounts of the undesired products, CO and CH_4. This analysis is however limited to equilibriums, which it describes the changes in the system equilibrium when modifying operating parameters. For a kinetic analysis, one may have to consider an additional set of reactions involving intermediate species.

10.3.4. Experimental studies

The development effective catalysts for ethanol steam reforming has been investigated by many authors. Experimental catalytic studies reported in the literature investigate the effect of the reaction temperature on the conversion rates and selectivity toward the hydrogen and by-products obtained. Behavior of catalysts with time has been studied as well. Different reaction paths are favored according to the catalyst used. Supported group VIII metals are good catalysts for ethanol steam reforming.

Nickel and cobalt are known to be efficient catalysts for the steam reforming of reaction. For both of those catalysts, it is important to understand the mechanism of the reactions to avoid carbon deposition since both Ni and Co are active catalysts for carbon deposition.

Fatsikostas et al. [46] have studied the reaction of steam reforming over nickel catalyst supported on γ-Al_2O_3, La_2O_3 and La_2O_3/γ-Al_2O_3, employing transient and steady-state techniques. Techniques employed in this study have highlighted that the interaction of ethanol with the catalytic material leads to a highly complicated reaction network. Indeed, reactions can occur as well in the gas phase, especially at elevated temperatures, and on the carriers surfaces. The possibility of interaction between these three domains, in the sense that reaction intermediates produced in one domain react further on other domain, cannot be excluded. The presence of Ni shifts the activity towards lower temperatures. Ni promotes reforming of ethanol and acetaldehyde as well as the water-gas shift and methanation reactions. The interaction with the oxide supporting the nickel was demonstrated. Catalyst carriers such as Al_2O_3 and La_2O_3 interact strongly with ethanol at relatively low temperatures. Al_2O_3 promotes dehydration and cracking while La_2O_3 promotes dehydrogenation and cracking. In the presence of alumina, carbon deposition occurs at very high rate, a result of ethylene polymerization. Impregnation of Al_2O_3 with La_2O_3 results in a significantly reduced rate of carbon deposition. Fierro et al.[47] have studied the steam reforming of ethanol on different type of catalysts. The active materials selected were two commercial Ni-based catalysts (11 and 20%) and five bimetallic catalysts all of them supported on Al_2O_3. These bimetallic were also Ni-based (20%) and doped with Cr, Fe, Zn and Cu. In a similar, study same workers have focused on Ni-Cu/SiO_2 catalysts[48].

The role of the support has been highlighted by other authors. Breen at al.[49] have tested a range of oxide metal supported catalysts. The supports included alumina and ceria-zirconia, and the catalyst tested were Rh, Pd, Ni, Pt. Llorca et al. [50] have studied hydrogen production over supported cobalt catalysts. The reaction between ethanol and water was studied in the temperature range 573-723K over different supports, which included: MgO, γ-Al_2O_3, SiO_2, TiO_2, V_2O_5, ZnO, La_2O_3, CeO_2, and Sm_2O_3. Ethanol steam reforming occurred to a large degree over ZnO-, La_2O_3-, Sm_2O_3, and CeO_2 supported catalysts. ZnO supported catalysts showed the best catalytic performances. With 100 % ethanol conversion, selectivity up to 73.8% to H_2 and 24.2% to CO_2 was obtained. Catalysts containing cobalt particles showed a significant enhancement of the catalytic performance in the steam reforming of ethanol. Batista et al.[51] have reported results of studies of the catalytic activity and stability of supported cobalt catalysts

Benito et al.[52] have extensively studied three different catalysts using different active phases (Ni, Cu, and Co) which have been patented. The two catalysts based on Ni and Co showed 100% of ethanol conversion and a high selectivity to hydrogen (70%) at 700 °C. In particular, the one based on Co, working in the temperature range 650-700 °C, shows excellent stability after 60h in operation conditions, CO and CH_4 being the only by-products and hydrogen production being close to that predicted by thermodynamic equilibrium. The catalyst based on Cu did not show good performances.

Influence of temperature has been tested on the Cobalt catalyst. It is observed that ethanol conversion increases when reaction temperature is increased to reach 100% at 600°C, the value predicted by thermodynamic equilibrium for the temperature range tested. In the temperature range studied (500 to 700 °C), the selectivity to H_2, CO_2 and CO are very close to equilibrium predictions, as shown on Figure 85:

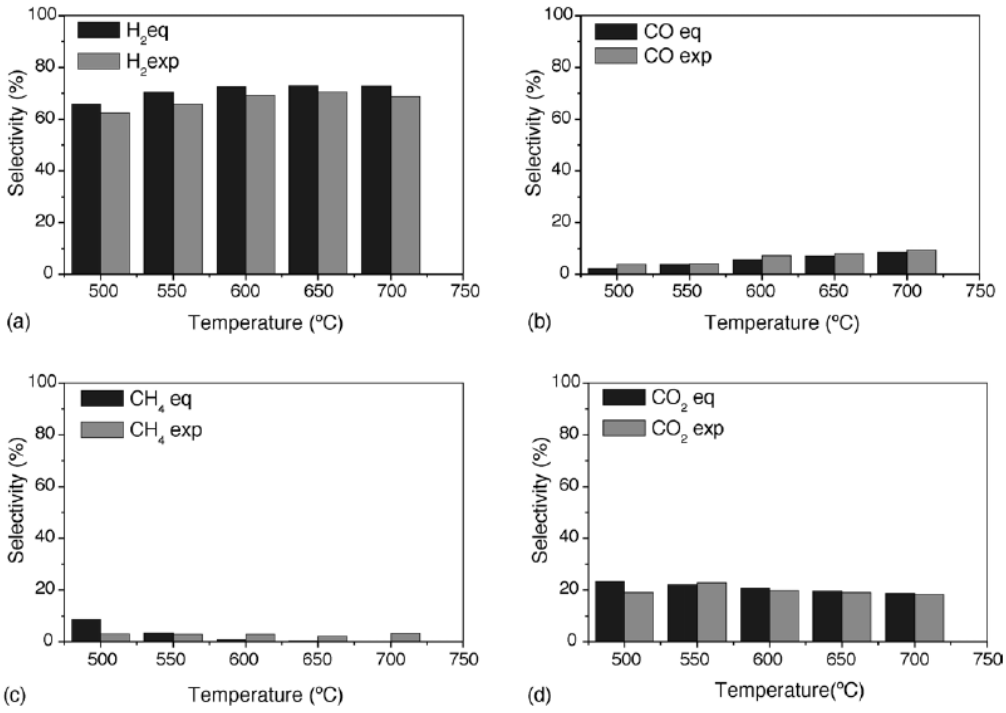

Figure 85: Effect of reaction temperature on the product selectivity for the cobalt catalyst vs.

thermodynamic equilibrium[52].

Cavallaro and Freni [53] have investigated supported oxide catalysts. CuO/ZnO/Al_2O3 exhibit a good activity, with CO, CO_2 and H_2 being the main products obtained at temperatures above 630K. Marino et al. [54] have studied the effect of different copper loading on catalytic behavior of Cu/Ni/K/Al_2O_3 catalysts. Acceptable performances for hydrogen production have been found at low temperatures. Diagne et al.[55] have investigated the reforming in excess of water on Rh/CeO2, Rh/ZrO2 and Rh/CeO2-ZrO_2. At 400-500°C, all catalysts showed high activity and selectivity towards hydrogen production (between 5 and 5.7 mol of H_2 per mol of ethanol inlet). Liguras et al.[56] have found that supported Rh catalysts are acceptably stable under severe conditions (800°C) and could be used for the production of hydrogen for fuel cell applications. Vargas et al. [57] have studied a fluorite type Ce-Zr-Co oxide, $Ce_2Zr_{1.5}Co_{0.5}O_{8-\delta}$. This catalyst was reported as efficient to convert ethanol to hydrogen.

10.3.5. Internal steam reforming

Beyond the steam reforming as an external intrinsic process, some studies available in the literature have focused on the internal steam reforming of ethanol on SOFC anodes. When occurring on the anode, the steam reforming, as compared to an external process, is disturbed by the electrochemical reactions that will affect the equilibrium. Mainly, H_2 and CO are consumed while H_2O and CO_2 are produced. Available studies generally account for the electrochemical reactions by adding source/sink terms for H_2 and H_2O.

Assabumrungat et al.[25] have performed the thermodynamic analysis for SOFC with direct internal reforming of ethanol, aiming at finding suitable ranges of operating conditions where carbon formation is thermodynamically prohibited. Freni et al.[58] have studied the effect of the electrochemical activity on the equilibrium composition.

The production of water, through consumption of hydrogen, affects the equilibrium of both the steam reforming and water gas shift reactions. In the steam reforming process, the excess inlet steam reacts with carbon monoxide and generates carbon dioxide via the water gas shift reaction. The increased carbon dioxide concentration prevents the possible carbon formation by the Boudouard reaction. Therefore, both the carbon dioxide and the extra steam generated from the electrochemical reactions can help in preventing carbon formation. CO_2 and H_2O concentrations increase monotonically with the current density. Evolution of products distribution in the thermodynamic equilibrium as a function of the electrochemical reaction rate is shown on Figure 86.

Calculations have been performed to provide the minimum H_2O/EtOH ratio in the initial system at which carbon formation in the equilibrium system is thermodynamically impossible, using the carbon factor mentioned above. Figure 87 displays the influence of operating temperature on the inlet H_2O/EtOH ratio required

for different values of the extent of the electrochemical reaction. The required inlet H_2O/EtOH ratio for avoiding carbon formation is seen to decrease both with increasing operating temperature and the extent of the electrochemical reaction. The temperature effect is due to the decrease in the carbon formation factor at high operating temperatures, as the Boudouard reaction is exothermic. Therefore, increasing the SOFC operating temperature is one possibility that will prevent carbon formation at the anode.

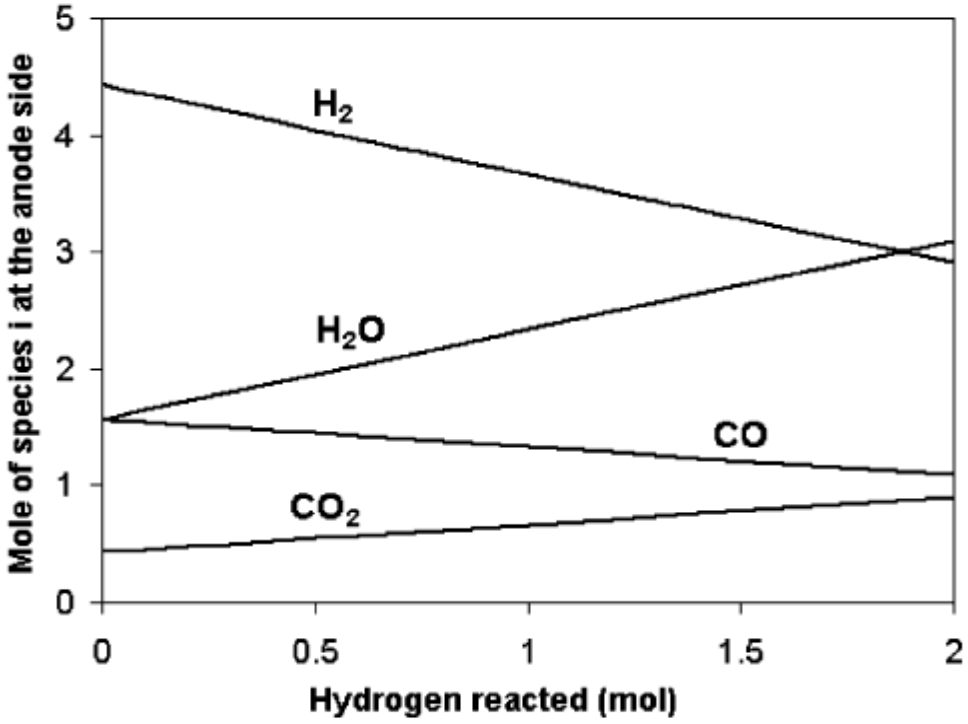

Figure 86: Effect of the electrochemical reaction extent on the gas composition at the anode[58].

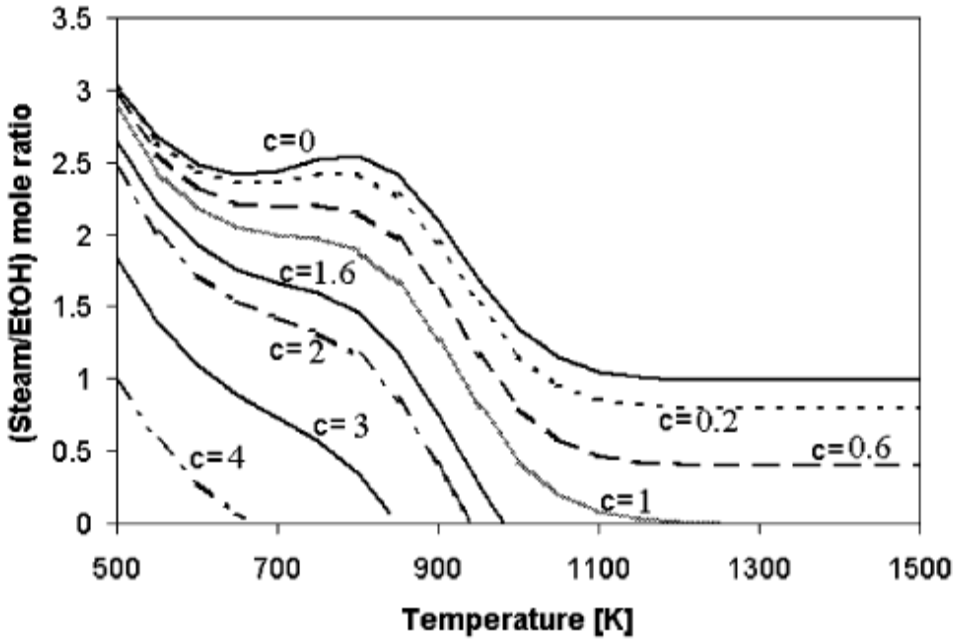

Figure 87: Required steam to ethanol ratio to avoid carbon deposition as a function of temperature; c accounts for the extent of the electrochemical reaction[25].

Assabumrungat et al.[25] have stressed out that the data available for verifying all calculated results are very limited. Nevertheless, the calculation for the case with c=0 (no electrochemical reactions) agrees well with the results from the literature.

It should be here pointed out that all the studies presented herein are based on thermodynamics equilibrium. For the carbon formation, it is recognized that other factors such as mass transfer or rate of reactions may also affect the prediction of the carbon formation boundary. Local composition which would allow carbon formation may exist, although carbon formation is not favored according to the calculation based on equilibrium bulk compositions. More importantly, carbon species may form via other chemical reactions such as the thermal cracking of hydrocarbons.

This applies as well for the ethanol conversion. Thermodynamic studies suggest that ethanol is not present in the system at those temperatures but that does not account for kinetics. In this respect, the study carried out by Sasaki et al.[59] provides useful information.

In this study, many diluted alcohols have been tested for powering SOFCs. The experiments involved as well a mixture of gases that simulated a reformed alcohol mixture in the thermodynamic equilibrium. Figure 88 shows current voltage (I-V) characteristics for various alcohol based fuels at 1000 °C. As the C-H-O number was common, the same gas composition and the same cell voltage were expected assuming complete equilibrium. However, I-V characteristics for these fuels depended on the carbon number of alcohols, clearly indicating non negligible kinetics effects for alcohols. OCV depended as well on the type of fuel and decreased with increasing carbon number of alcohols. The I-V characteristics for the methanol based fuel were almost identical to those for the simulated reformed gas. This indicates that thermal decomposition of methanol is fast enough to achieve complete equilibrium at

the elevated temperatures. For higher alcohols, the concentrations of H_2 and CO were lower and the concentrations of by-products, including CH_4 and C_2H_4, were higher compare to those for the methanol based fuel. Results for methanol have been confirmed analyzing exhaust gas composition under different operating conditions. This result indicates that decomposition and reforming reaction became more difficult with increasing carbon number of alcohols. It is one of the main reasons explaining lower OCV and lower electrochemical performance.

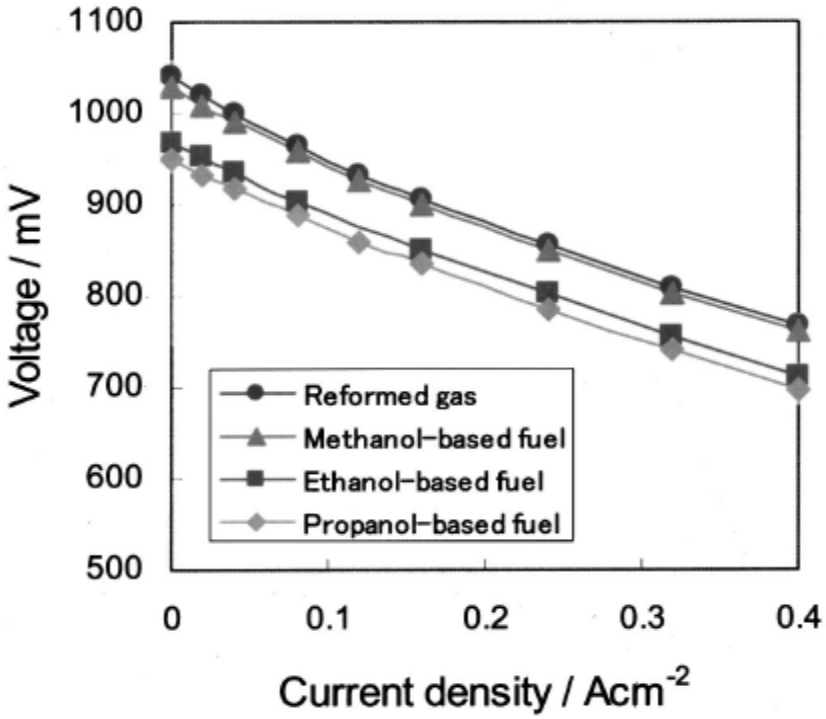

Figure 88: I-V characteristics for alcohol based fuels at 1000□C. Alcohols were premixed with water and the C-H-O ratio were of all fuel was 9-38-10[59].

The temperature study suggests that direct-alcohol SOFCs may be possible even at intermediate operational temperature around 800 °C. Indeed the decrease in cell voltage was a hundreds of millivolts. At 700°C, cell voltage was too low to obtain sufficiently high power output.

R.Mucillo et al.[60] have studied ethanol direct oxidation on Ni cermets with either YSZ or GDC as a ceramic phase. The ethanol fuel stream was obtained by flowing N_2 into liquid ethanol (92.8% GL, commercially available in Brazil for domestic use) at room temperature. High polarization resistances were reported and cells were found to deactivate due to carbon deposits on both type of cermets. The deactivation was found to be more pronounced at high temperatures (>800ºC) and for high Ni content.

Et al.[61] have studied ethanol on anodes made of a Ni/YSZ featuring a screen printed Cu-CeO_2 catalyst layer on top. However, it has to be stressed out that this study has been carried out using Pt paste as a current collector. Although the anode layer is 600μm thick, results produced using Pt paste have to be analyzed with care. Pt might not influence the electrochemical of the cell due to the anode thickness but surely

interferes with the catalytic behavior of the Cu-CeO2 layer, thus rendering the effectiveness of the catalyst layer difficult to interpret.

10.4. Conclusions

Although fuel cells are commonly associated with hydrogen, the use of hydrogen as an energy carrier is impossible with the current technologies available for its storage, production, and transport. Important technological improvements are required before any hydrogen economy could be considered.

Liquid fuels bring some answers to the problems inherent to the hydrogen economy. Our current economy being based on oil, any renewable, liquid fuel that shows a high enough energy content would constitute a credible alternative. In this respect, second generation bioethanol appears to be a serious candidate if we manage to bring down its production costs within the competitive range. Important investments have been done in this sense, and the first commercial plants using waste as feedstock have already been built (Spain, USA).

As with any fuel, the conversion of bioethanol to electricity would be more efficient if it was done in a SOFC as compared to conventional combustion methods. Ethanol has experienced a recent important development based on the first generation where the main targeted application was the combustion engine for motive applications. However, interest seems to be growing for the direct use of ethanol in SOFCs.

This review shows the numerous reactions are involved when ethanol is used at high temperature. Reactions occur both in the gas phase and on the surface of the catalysts used for the anode. Even with a dry feed, it is likely that only a very small fraction, if any at all, of the ethanol will be present at the triple phase boundary. This will depend on the flow distribution configuration and the residence time of the fuel mixture at high temperature. Depending on the extent of the steam reforming and gas-phase conversion, the fuel mixture available for electrochemical reactions can be made to be dominated by H_2 and CO.

Both catalytic and gas-phase reactions can play another important role by promoting carbon deposition onto the anode. Catalytic carbon deposition that occurs on Ni in the absence of significant steam has irreversible effects on the anode due to the deposition mechanism involved and thus must be avoided. The carbon deposition from the gas-phase reaction has been shown to have positive effects if kept in small amounts. In such a case, the connectivity is improved in the conductive phase, which in turns enhances the performance. If the deposits become too important, as was observed from 800°C by Gorte and coworkers, pores can be clogged and the access to electrochemically active sites hindered.
However, those deposits can be removed by steam through heterogeneous reactions. In this respect Ceria has been shown to be an active catalyst for the removal of carbon deposits.

A few studies have addressed the use of diluted ethanol on Ni-YSZ. While operation seems to be possible when enough steam is added, questions remain regarding the long term stability of those systems.

Developments in this area of direct ethanol will likely stem from alternative anode materials that do not show catalytic activity for carbon deposition. Although carbon deposition from gas phase reactions will occur, anode chambers could be designed to sustain high performance, by using appropriate temperature and catalysts. Appropriate design could limit the carbon deposition to a steady thin layer which can be beneficial to the performance. Due to their reversibility, carbon deposits along with other impurities can be cleared periodically without affecting the performance. Such a possibility is a great advantage for long term operation on hydrocarbons.

However, no studies are available for the long term operation of SOFCs on ethanol. This review shows that steady long term operation is definitely achievable, and works addressing this issue will certainly be soon carried out.

[1] www.pure.shetland.co.uk
[2] M. Ormerod, *Chem. Soc. Rev.*, 32 (2003) 17-28
[3] A. Atkinson, S. Barnett, R.J. Gorte, J.T.S. Irvine, A.J. McEvoy, M. Mogensen, S.C. Singhal and J.Vohs., *Nature materials*, 3 (2004) 17-27
[4] R.J. Kee, H. Zhu, D.G. Goodwin, *Proceeding of the combustion institute*, 30 (2005) 2379-2404
[5] http://www.jgi.doe.gov/education/bioenergy/bioenergy_1.html, visited on 20th of January 2009
[6] C.Song, *Catalysis today*, 77 (2002) 17-49
[7] C. Lamy, A. Lima, V. LeRhun, F. Delime, C. Coutaneau and J-M. Leger, *Journ. Pow. Sour.*, 105 (2002) 283-296
[8] R.J. Gorte, S.Park, J.M. Vohs, C. Wang, *Advanced materials*, 12 (19) (2000) 1465-1469.
[9] K. Sasaki, K. Watanabe, and Y. Teraoka, *Jour. Elect. Soc.*, 151 (7) (2004) A965-A970
[10] K.M. Walters, A.M. Dean, H. Zhu, R.J. Kee, J.Power Sources 123 (2003) 182–189.
[11] C.Y. Sheng, A.M. Dean, J. Phys. Chem. 108 (2004) 3772–3783.
[12]G.K.Gupta, A.M.Dean, K. Ahn, R.J.Gorte, *Journal of power sources*, 158 (2006) 497-503
[13]J. Li, A. Kazakov, F.L. Dryer, J. Phys. Chem. A 108 (2004) 7671–7680.
[14]C.M. Chun, J.D. Mumford, T.A. Ramanarayanan, SOFC VI, in: S.C.Singhal, M. Dokiya (Eds.), Proceedings of the Electrochemical Society Series PV 1999-19, The Electrochemical Society, Pennington, NJ, 1999, p. 621.
[15] C.H. Toh, P.R. Munroe, D.J. Young, K. Foger, *Mater. High Temp*, 20 (2003) 129.
[16] R.T.K. Baker, M.A. Barber, P.S. Harris, F.D. Feates, R.J. Waite, *J.Catal.*, 26 (1972) 51.
[17] R.T.K. Baker, P.S. Harris, J. Henderson, R.B. Thomas, *Carbon*, 13 (1975) 17.
[18] R.T.K. Baker, P.S. Harris, S. Terry, *Nature*, 253 (1975) 37
[19] C.W. Keep, R.T.K. Baker, J.A. France, *J. Catal.* 47 (1977) 232.
[20] C.H. Bartholomew, *Catal. Rev. Sci. Eng.*, 24 (1982) 67
[21] R.T.K. Baker, *Carbon*, 27 (1989) 315.
[22] M.L. Toebes, J.H. Bitter, A.J. van Dillen, K.P. de Jong, *Catalysis today*, 76 (2002) 33-42
[23] T. Sperle, D. Chen, R. Lødeng, A. Holmen, *Appl. Catal.*, A 282 (2005) 195.
[24] X. Wang, R.J. Gorte, *Catal. Lett.*, 73 (2001) 15
[25] S.Assabumrungat, V.Pavarajarn, S.Charojrochkul, N.Laosiripojana, *Chem. Eng. Sci.*, 59 (2004) 6015-6020
[26] T.Tsiakaras, A.demin, *journal of power sources.*, 102 (2001) 210-217
[27] K. Sasaki, K. Watanabe, and Y. Teraoka, *Jour. Elect. Soc.*, 151 (7) (2004) A965-A970
[28] C.Y. Sheng, A.M. Dean, *J. Phys. Chem. A*, 108 (2004) 3772.
[29] C.H. Toh, P.R. Munroe, D.J. Young, K. Foger, *Mater. High Temp*,.20 (2003) 129.
[30] S. McIntosh, H. He, S.-I. Lee, O. Costa-Nunes, V.V. Krishnan, J.M.Vohs, R.J. Gorte, *J. Electrochem. Soc.*, 151 (2004) A604–A608.
[31] T.Kim, G.Liu, M.Boaro, S-I.Lee, J.M.Vohs, R.J. Gorte, O.H. Al-Madhi, B.O.Dabboussi, *Journal of power Sources*, 155 (2006) 231-238
[32] S. McIntosh, J.M. vohs, R.J. Gorte, *Journal of the electrochemical society*, 150 (4) A470-A476 (2003)
[33] H.He, J.M Vohs, R.J. Gorte, *Journal of power sources*, 144 (2005) 135-140
[34] A.N. Fatsikostas, D.I. Kondaries, X.E. Verykios, *catalysis today*, 75 (2002) 145-155
[35] E.Y. Garcia, M.A. Laborde, *Int. J. Hydrogen Energy*, 16 (1991) 307-312
[36] K. Vasudeva, N. Mitra, P. Umasankar and S.C. Dhinggra, *Int J. Hydrogen Energy*, 21 (1996) 13-18

[37] A. Fishtik, R. Alexander, D. Datta, D. Geena, *Int. J. Hydrogen energy*, 25 (2000) 31
[38] S. Cavallaro, S. Freni, *Int J. hydrogen energy*, 21 (1996) 465
[39] E.Y. Garcia, M.A. Laborde, *Int. J. Hydrogen Energy*, 16 (1991) 307-312
[40] K. Vasudeva, N. Mitra, P. Umasankar and S.C. Dhinggra, *Int J. Hydrogen Energy*, 21 (1996) 13-18
[41] K. Sasaki, Y. Teraoka, *Journal elect. Soc.*, 150 (7) (2003) A878-A884
[42] K. Sasaki, Y. Teraoka, *Journal elect. Soc.*, 150 (7) (2003) A885-A888
[43] S. Freni, G. Maggio, S. Cavallero, *Journal of power sources*, 62 (1996) 67-73
[44] S.Assabumrungat, V.Pavarajarn, S.Charojrochkul, N.Laosiripojana, *Chem. Eng. Sci.*, 59 (2004) 6015-6020
[45] A. Fishtik, R. Alexander, D. Datta, D. Geena, *Int. J. Hydrogen energy*, 25 (2000)
[46] A.N. Fatsikostas, X.E. Verykios, *Journal of catalysis*, 225 (2004) 439-452
[47] V.Fierro, O. Akdim, H. Provendier, C.Mirodatos, *Journal of power sources*, 5 (2003) 20-24
[48] .Fierro, O. Akdim, C.Mirodatos, *green chemistry*, 5 (2003) 20-24
[49] J.P. Breen, R. Burch, H.M. Coleman, *Applied catalysis B: environmental*, 39 (2002) 65-74
[50] J.Llorca, N. Homs, J.sales, P. Ramirez, *Journal of catalysis*, 209 (2002) 306-317
[51] M.S. Batista, R.K.S.Santos, E.M. Assaf, J.M. Assaf, E.A. Ticianelli, Journal of power sources, 124 (2003) 99-103
[52] M. Benito, J.L. Sanz, R. Isabel, R. Padilla, R. Arjona, L. Daza, *Journal of power sources*, 151 (2005) 11-17
[53] S. Cavallaro, S. Freni, *Int J. hydrogen energy*, 21 (1996) 465
[54] F.J. Marino, E.G. Cerrela, S. Duhalde, M. Jobbagy, M.A. Laborde, *Int. j. hydrogen energy*, 23 (12) 1998 1095-1101
[55] C. Diagne, H.Idriss and A.Kiennemann, *catalysis communications*, 3 (2002) 565-571
[56] D.Liguras, D. Kondarides, X.E. Verykios, *App. Catal. B: environ.*, 43 (4) (2003) 345
[57] J.C. Vargas, S. Libs, A. Roger, A. Kiennenmann, *catalysis today*, 107-108 (2005) 417-425
[58] S. Freni, G. Maggio, S. Cavallero, *Journal of power sources*, 62 (1996) 67-73
[59] K. Sasaki, K. Watanabe, and Y. Teraoka, *Jour. Elect. Soc.*, 151 (7) (2004) A965-A970
[60] R.Mucillo, E.N.S. Mucillo, F.C. Fonseca, D.Z. de Florio, *Journal of the electrochemical society*, 155 (3) (2008) B232-B235
[61] X.Ye, S.R.Wang, Z.R. Wang, L.Xiong, X.F. Sun, T.L.Wen, *Journal of power sources*, 177 (2008) 419-425

Experimental methods

Half cell electrochemical measurements have been performed in this study of ethanol/steam mixtures. In half cell measurements, only the electrochemistry of one electrode is under investigation. Half cell measurements require an additional electrode, the reference electrode, and therefore three-electrode configurations are employed. The commonly used terminology of electrodes is working, counter and reference electrode. The working electrode is the electrode whose performance or characteristics are under study. The counter electrode is the other current carrying electrode positioned on the opposite site of the electrolyte. The reference electrode is used for controlling and measuring the potential of the working electrode and does not carry any appreciable current.

All the fuel cell samples used in the study of ethanol fuelled SOFCs have been prepared following the standard procedure used in our laboratory for half-cell measurements. The arrangement of the working, counter and reference electrode used in this work is schematized in Figure 89. This geometry minimizes uncertainties in potential lines by using a thick electrolyte, placing the reference in the centre of the counter electrode and, and having parallel working and counter electrodes.

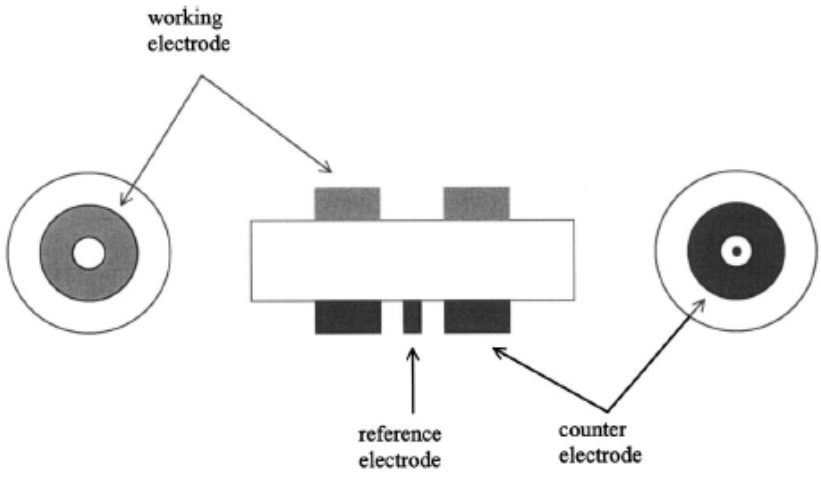

Figure 89: Schematic drawing of the three-electrode arrangement of the electrochemical cells. The YSZ electrolyte pellets are 20 mm diameter and 2 mm thick.

The samples are supported by a 2mm thick electrolyte. Such a thickness is used for mechanical strength purposes so as weight can be applied on cells without any risks for their mechanical integrity. Electrolyte pellets feature a 20mm diameter. The active area of both the working and counter electrode are 1 cm^2. Due to the thickness of the electrolyte and the associated ohmic losses, such samples can not produce high power outputs.

The first step in preparing those samples is to produce a dense YSZ pellet. YSZ pellets are produced by uni-axially pressing 3.7g of powder. Commercially available (pi-kem) 8% YSZ was used. After pressing, pellets were fired at 1500°C for 12H.

The anode is first deposited onto the dense YSZ pellet by screen printing inks containing the desired materials. The preparation of inks for screen printing is performed in two stages. First raw powders are ball milled in acetone using a planetary mill. 2 wt.% of dispersant (KD1) was added to the mixture to ensure deagglomeration of the particles. Once the ball mill step is completed, a binder is added to the solution which is then slowly stirred until complete evaporation of the acetone. The amount of binder used was typically 66% of the solid weights. The binder used in this work was provided by Rolls Royce Fuel Cells Systems.

For Ni-YSZ anodes, commercially available NiO raw powder has been used in the preparation process: NiO available from Novamet, grade F. Particle size distribution of this powder is shown on Figure 90.

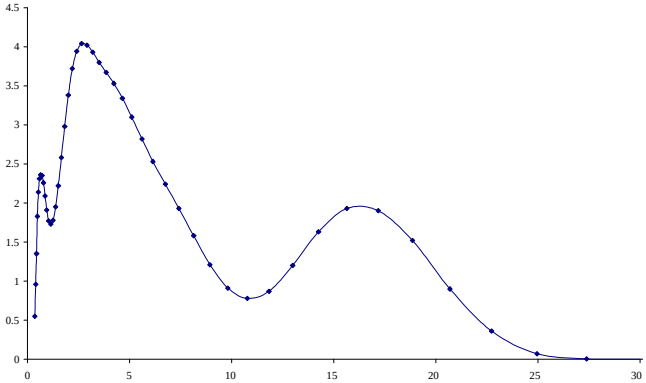

Figure 90: powder particle size distribution, as received from Novamet Grade F.

For LSCM based anodes, two different types of LSCM powders have been used. The first one was commercially available from EMPA and the composition was $(La_{0.75}Sr_{0.25})_{0.97}Sr_{0.5}Mn_{0.5}O_3$. The second powder was prepared by combustion synthesis of a stoichiometric mixture of La_2O_3, $Sr(NO_3)_2$, $Cr(NO_3)_3.9H_2O$, $Mn(Ac)_2.4H_2O$ in ethylene glycol and 69% HNO_3. Ashes from the combustion synthesis were then grinded and fired at high temperature to obtain the LSCM phase. The composition used in this work was $(La_{0.75}Sr_{0.25})_{0.95}Sr_{0.5}Mn_{0.5}O_3$. The composition of the CGO powder was $Ce_{0.8}G_{d0.2}O_2$.

Just after the anode has been printed, the sample is placed in an 80ºC oven to allow the binder to evaporate. Several printed layers are often desirable to obtain the required anode thickness. Indeed, a printed anode layer is about 5 µm thick and the active layer in Ni-YSZ cermets is known to extend to about 10-20 µm from the electrolyte. Two or three layers are therefore required to maximize performances.

After the anode has been sintered at high temperature, the counter and reference electrodes were deposited on the opposite side of the YSZ pellet. Pt paste was used and the deposition was performed by hand painting. The sample was first dried at 80°C and then sintered at 900°C for two hours. Figure 91 shows SEM images at various magnification of a typically Pt paste counter electrode that was used in this work. The microstructure is quite discontinuous. Important agglomerations of Pt can

be seen implying that the TPB of such electrode is clearly not optimized. However, it is important to note here that since half cell measurements are performed, the optimization of the counter electrode is not required. The counter electrode is not under electrochemical investigation. Hence, the use of Pt paste is acceptable for the purposes of those studies.

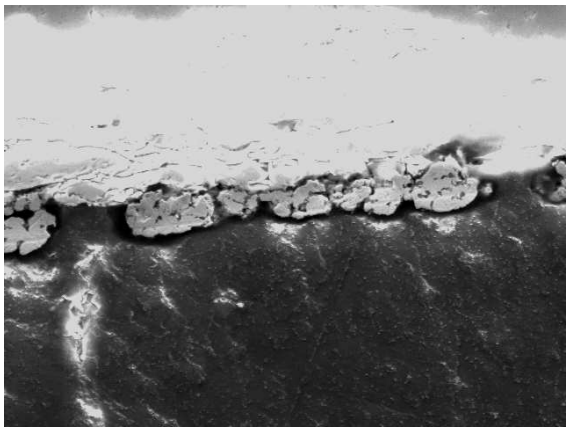

Figure 91: SEM image of a Pt counter electrode made of one hand painted layer, sintered at 900°C for 2 hours. The image was taken after electrochemical tests have been performed.

The ceramic sample holder used for electrochemical measurements is shown in Figure 92. The sample holder has an open structure to allow gas flow from and to the electrodes. Oxygen is flown on the counter electrode and the fuel under study is flown to the working electrode. A Pt/Pt-13%Cr (R-type) thermocouple is placed near the electrode for temperature measurements. The current collection for the working electrode is done by the mean of a gold mesh, which is attached to the electrode by applying gold paste. The paste is sintered at 900ºC for 2 hours. Sealing of the cells was performed by the use of a gold ring and a weight applied on top of the cell.

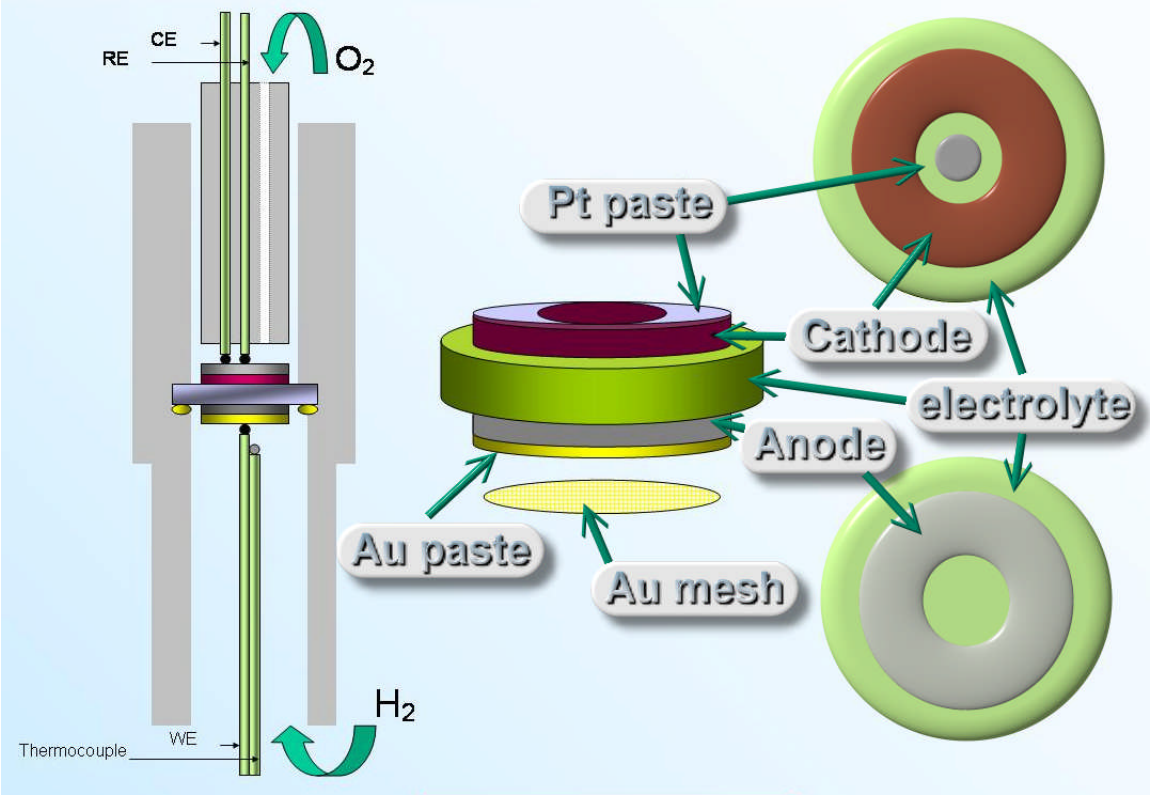

Figure 92: Set-up used for electrochemical tests of SOFC samples featuring a thick electrolyte. The sampler holder is an alumina tube. The sealing is achieved through the use of a gold ring. Pt paste is used as a current collector for the cathode, while a gold mesh is used for the anode. Gold paste is used to attach the gold mesh onto the anode.

Ethanol is a liquid fuel at room temperature and its boiling point is 78.5°C. The technique employed to flow ethanol onto the anodes was a heated bubbler. An ethanol/water liquid solution is heated inside a bubbler, through which Ar is flown. The typically Ar flow used in this work was 30 ml/min. Figure 93 shows the liquid-vapour diagram for ethanol mixtures. The gaseous phase above the liquid at a given temperature features the composition provided by the equilibrium diagram. Hence, the liquid composition has to be chosen according the composition of the vapour that will produced. For each experiment, the temperature of the liquid was set to be just at the boiling point and care was taken to avoid ebullition.

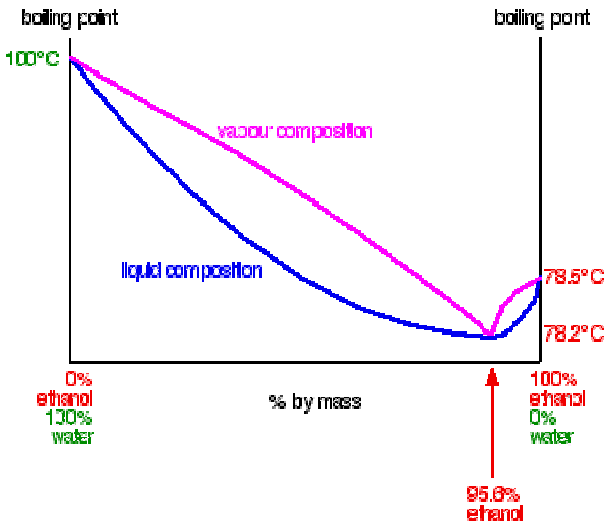

Figure 93: Liquid vapour diagram for ethanol-water mixtures.

Fuel cell studies

12.1. Introduction

This chapter presents the study of the performance of ethanol as a direct fuel for SOFCs. Three different types of anodes have been tested: Ni/YSZ, LSCM/YSZ, and LSCM-CGO/YSZ.

Before studying alternative anode materials, it appeared essential to establish performance that can be obtained on Ni-YSZ standard anodes. This will provide the tool to assess performance on alternative materials. Moreover, only poor and/or non durable performance on Ni-YSZ will justify the research and development on alternative anodes design. After an initial work on the optimization of the microstructure of those anodes, fuel cell tests have been performed at high steam to carbon ratios at which carbon deposition is thermodynamically unfavoured. The standard diluted ethanol content that was used was 15 mol. % ethanol in steam. This composition corresponds to a steam-to-carbon molar ratio (S/C) of 2.8. Carbon deposition has been reported to be non favoured at such a steam to carbon ratio[1,2].

Following the characterization of performance on standard Ni/YSZ anodes, alternative anode materials have been investigated. LSCM was first studied as one of the most promising oxides. Then Gadolinium Doped Ceria (CGO) was added to the LSCM in an attempt to improve the catalytic activity and reduce the carbon deposition. The standard ethanol content of the vapour used was 15% mol as well, but higher ethanol contents have been used.

For each anode under investigation, fuel cell tests are carried out in humidified hydrogen and diluted ethanol so as performance obtained for both fuels can be compared.

12.2. Ni-YSZ anodes

Anodes will show different microstructures depending on the Ni:YSZ ratio used. To study the influence of the Ni:YSZ ratio on the microstructure, three different anode compositions were tested, having NiO/YSZ weight ratios of: 40/60, 60/40 and 80/20. The sintering conditions used to compare these anodes were 1350ºC for 3 hours. Figure 94 shows SEM images of the three electrode microstructures obtained. 2 SEM micrographs are shown for each electrode.

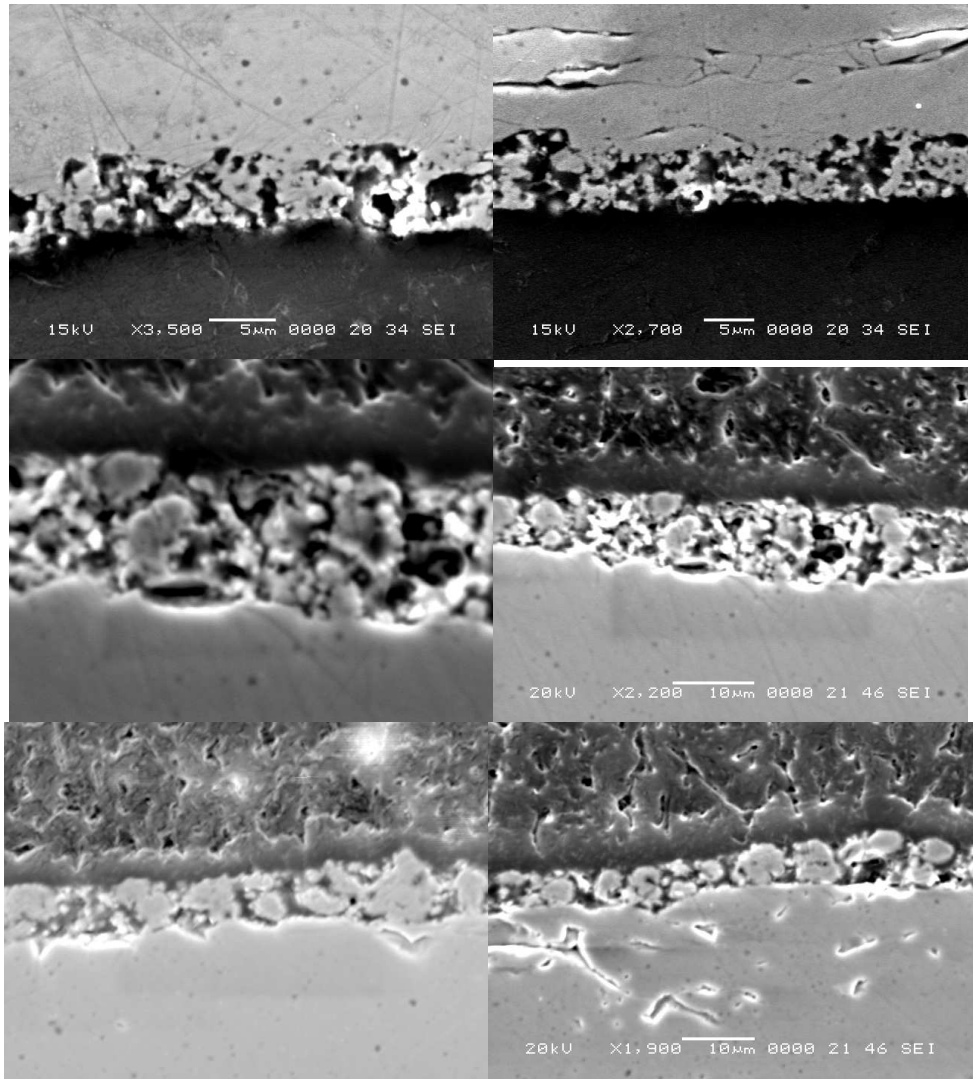

Figure 94: Ni-YSZ anodes sintered at 1350°C for 3 hours with different Ni/YSZ ratios: 40/60 (top), 60/40 (middle), 80/20 (bottom).

The microstructure is clearly influenced by the nickel content. A 60/40 weight ratio seems to yield the most homogeneous microstructure among those compositions. The EDX analysis shown on Figure 95 confirms that the 80/20 and 40/60 weight ratios yield non homogeneous structures. Important Ni grains can be seen in the 80/20 composition suggesting a small TPB whilst no suitable connections within the Ni phase can be seen at the ratio 40/60.

The sintering time was then decreased in an attempt to decrease the size of the Ni grains. Figure 96 shows the SEM image of an anode having a 60/40 weight ratio sintered at 1350 °C for one hour. The grain size is seen to be considerably smaller and the EDX analysis shown on Figure 97 indicates that the connectivity in the Ni phase has been improved by the reduction of the sintering time. Theses analyses indicate that the reduction of the sintering time to one hour has increased the TPB area. Based on those observations, electrochemical tests have been carried out using anodes sintered at 1350°C for one hour and having a NiO/YSZ weight ratio of 60/40.

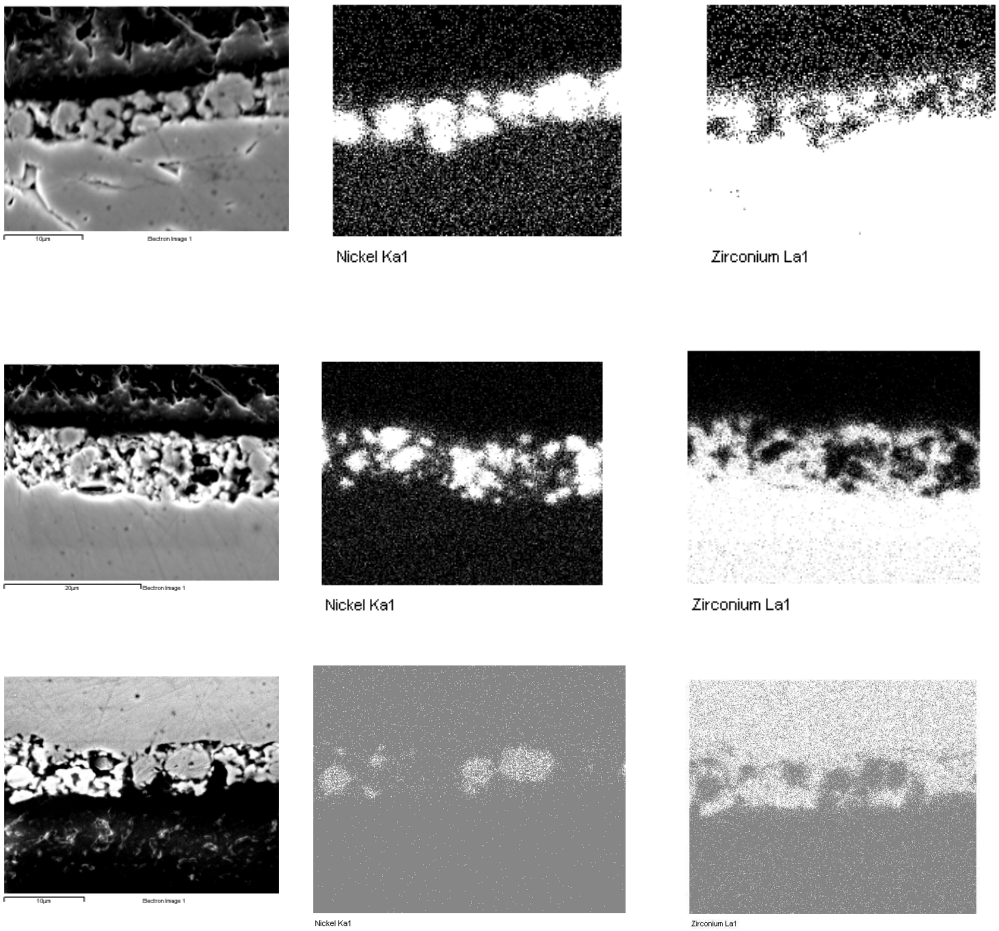

Figure 95: EDX analysis for the three NiO/YSZ weight ratios sintered at 1350°C for 3 hours: 80/20 (top), 60/40 (middle) and 40/60 (bottom).

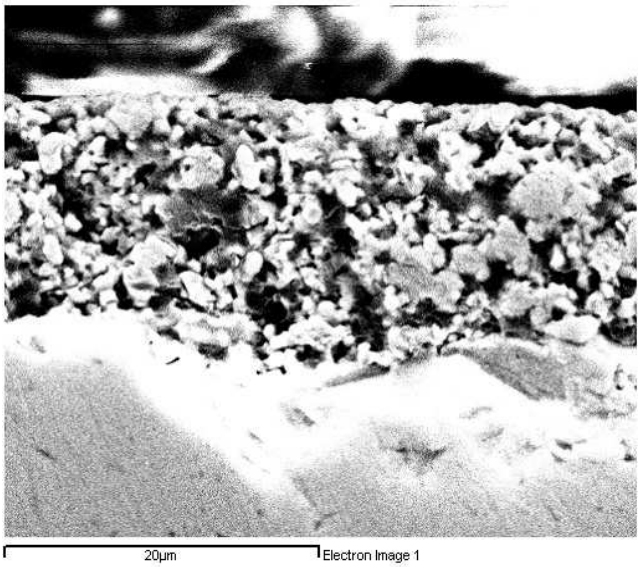

Figure 96: SEM image of an anode containing a NiO/YSZ weight ratio of 60/40 sintered at 1350°C for 1 hour.

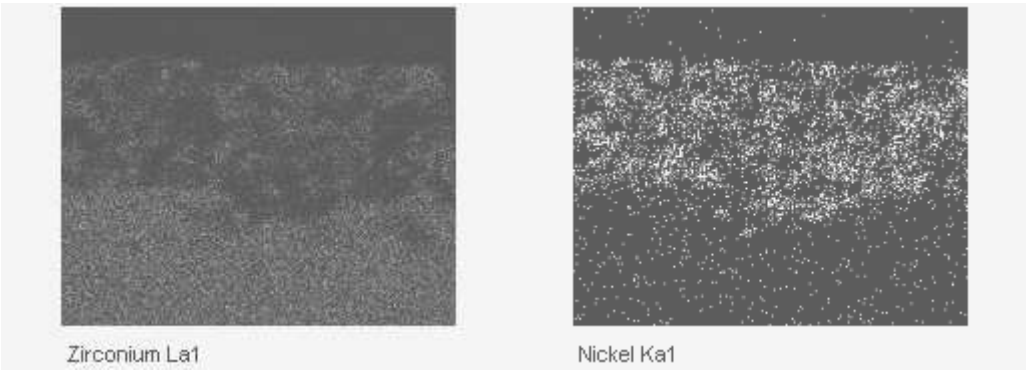

Figure 97: EDX analysis of an anode containing a NiO/YSZ weight ratio of 60/40 sintered at 1350°C for 1 hour.

Figure 98 shows the impedance spectra recorded on a Ni-YSZ anode in humidified hydrogen when various biases are applied. Each spectrum is composed of 3 arcs. At OCV, the anode polarization resistance is about 0.87 $\Omega.cm^2$. However, the anode impedance decreases when the cell is under load. The anode polarization resistance is close to 0.3 $\Omega.cm^2$ at 900°C, when the cell is operated below 0.7V. Those area specific resistances (ASR) are quite above the standards that can be expected for Ni-YSZ anodes[3]. However, the performance of these anodes was considered suitable for the purposes of our studies.

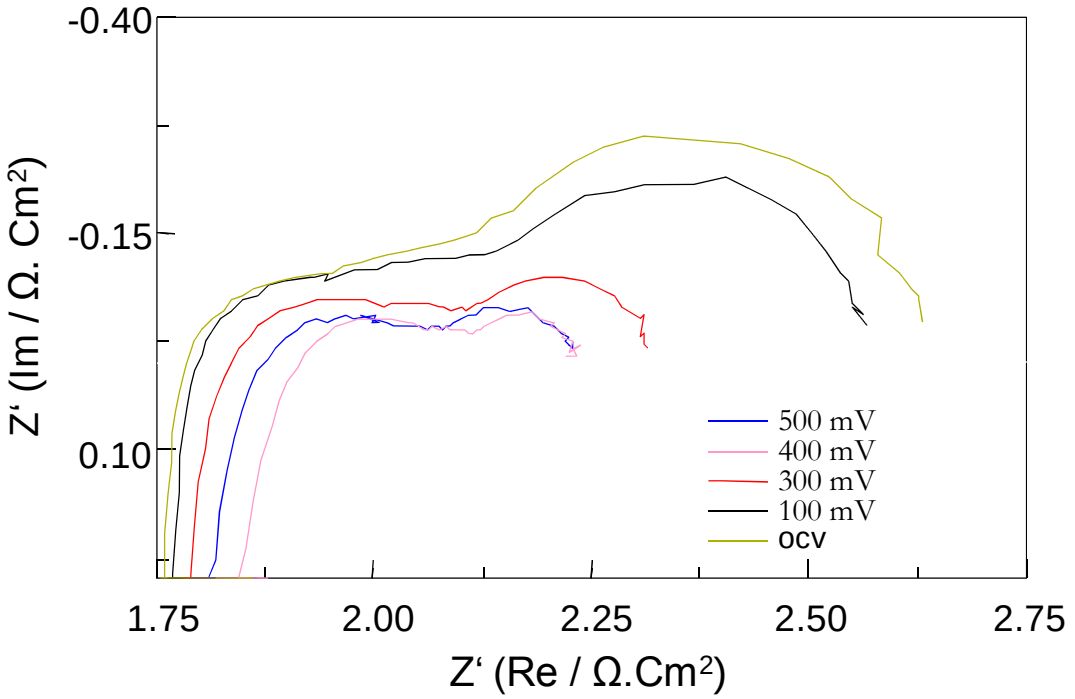

Figure 98: Impedance spectra recorded at various biases on Ni-YSZ anodes in humidified (3% H_2O) hydrogen at 900°C.

Ni-YSZ anodes have been first tested on the azeotropic ethanol/water mixture. This composition is the one obtained by distillation and contains about 4.4 vol.% of water. Figure 99 shows a photograph of a sample after testing on the azeotropic ethanol/steam mixture at 900°C.

Figure 99: Evidence of catalytic carbon deposition on a Ni-YSZ anodes: (left) cell after operation on a ethanol/water azeotropic mixture (4.4 vol. % H_2O) at 900°C; (right) cell before reduction and test.

The pellet on the right of the picture is the original sample shown before reduction and operation, while the sample after operation on azeotropic ethanol/steam mixture can be seen on the left. The gold mesh used for current collection can be seen on top the sample. This simple test illustrates the impossibility of running a Ni-YSZ anode on ethanol with low steam content. As can be observed on the picture, the carbon production is considerable and damages irreversibly the anode. As expected from the

Ni catalytic activity, Ni-YSZ anodes cannot be operated on ethanol without excess steam.

Anodes have then been tested with high steam content in conditions where carbon deposition is not thermodynamically favoured[1,2]. Figure 100 displays I-V polarization curves recorded on Ni-YSZ anode both in humidified hydrogen and diluted ethanol (15 mol. %) in steam at 900 °C. A higher performance is obtained when the cell is operated on hydrogen. The three different curves that are displayed for ethanol correspond to different operation times, with higher overpotentials corresponding to longer operation time. When the cell is run on diluted ethanol, the performance is seen to decrease with time and overpotentials are becoming important. When the cell is switched back to hydrogen, the cell performance has clearly deteriorated. Figure 101 shows SEM micrographs of the Ni-YSZ anode after the operation on diluted ethanol. Important carbon deposits can be observed even at such high steam contents, and are responsible for the anode performance degradation. These experiments have been repeated and the same trend of results was obtained.

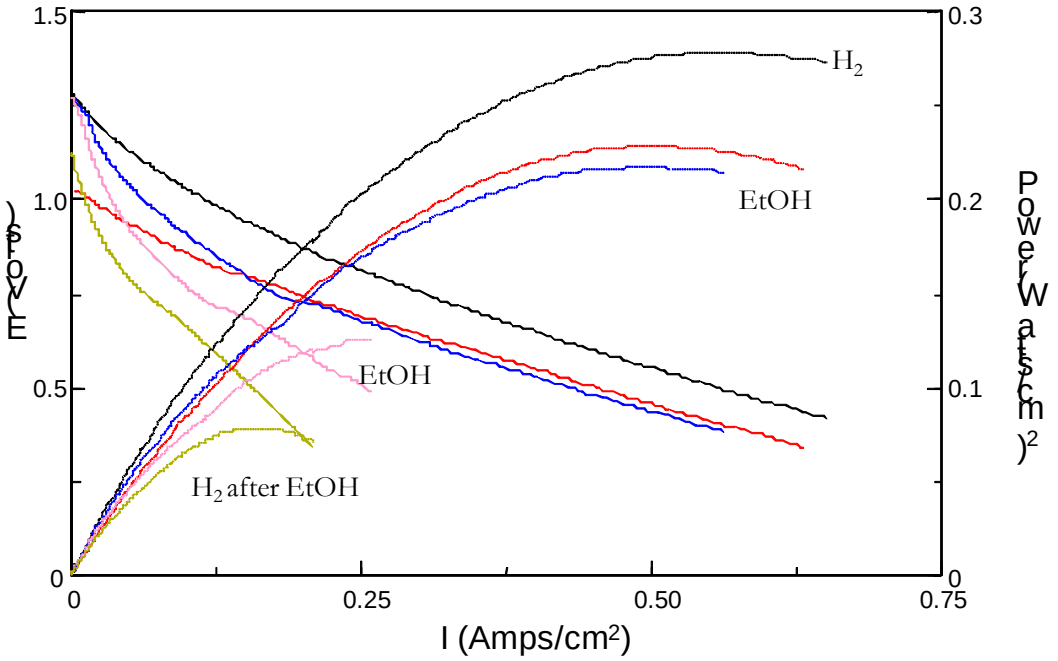

Figure 100: IV curves for a Ni-YSZ anode operated at 900°C in: (top curve) H_2, (middle curves) on diluted ethanol at various operation times; longer operation times correspond to higher overpotentials and (bottom curve) in H_2 after operation on diluted ethanol.

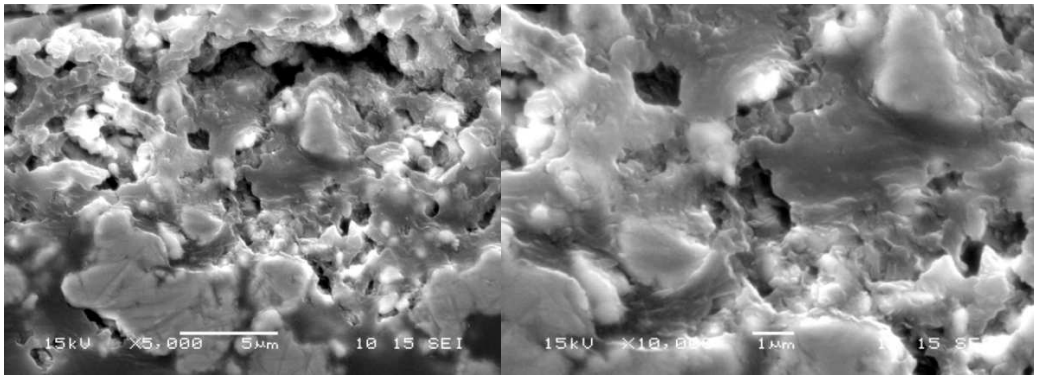

Figure 101: SEM images of the Ni-YSZ anode after operation on 15 mol% ethanol at 900°C. Important catalytic carbon deposition can be observed.

12.3. LSCM

A typical microstructure of a LSCM anode used in this work is displayed on Figure 102. LSCM readily forms good microstructures with high surface area.

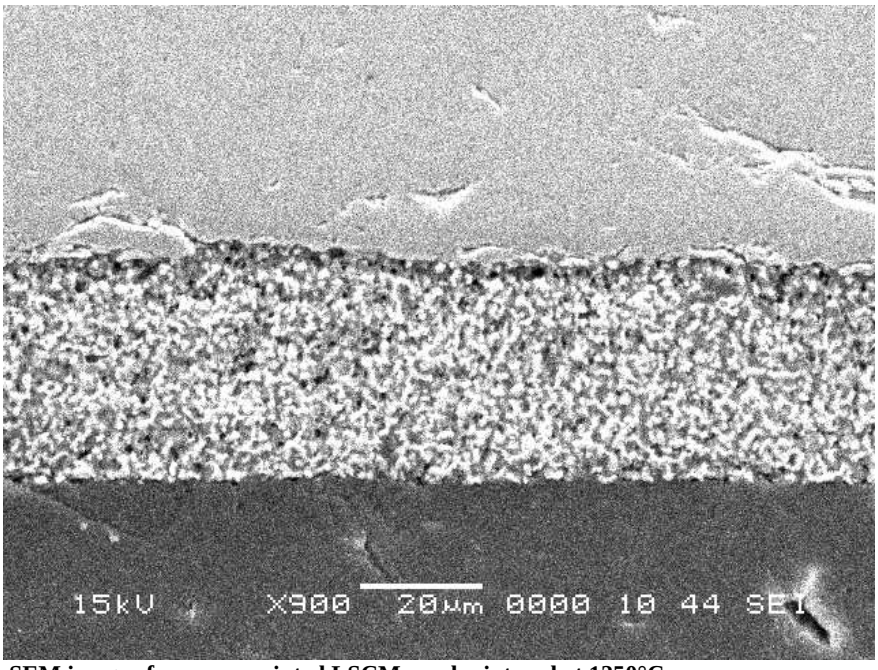

Figure 102: SEM image of a screen printed LSCM anode sintered at 1250°C.

Fuel cell tests have been performed on LSCM-YSZ anodes using ethanol/steam mixtures having an ethanol content of 15 mol. %. Figure 103 displays the IV curves obtained on a LSCM-YSZ anode at 920°C. The OCVs were close to 1.1V for hydrogen and 0.89V for the ethanol/water mixture. Figure 104 displays the impedance spectra recorded at OCV on both fuels. The many data shown for ethanol on this graph have been recorded chronologically (from right to left on the graph) over 60 minutes. The red curve is the half cell impedance at the beginning of the measurement

while the grey curve (far left) is the half cell impedance after one hour. When the LSCM anode is operated on ethanol, the ohmic resistance decreases with time, while the non ohmic resistance is increasing with time. Both the ohmic resistance and non-ohmic resistance stabilize with time to reach steady values. Both sets of data indicate that the anode performs better with hydrogen than ethanol.

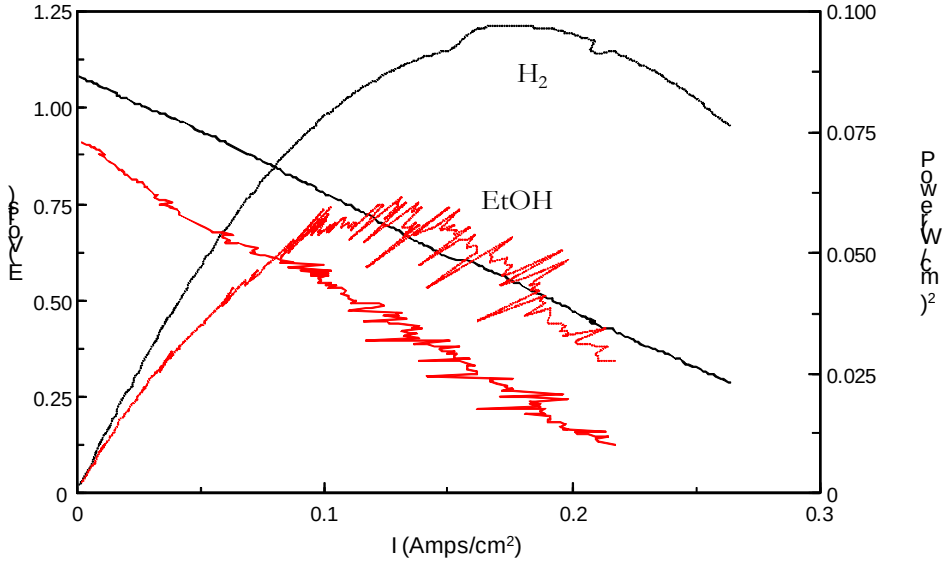

Figure 103: IV curves obtained on a LSCM-YSZ anode operated on hydrogen and 15mol.% ethanol at 920°C.

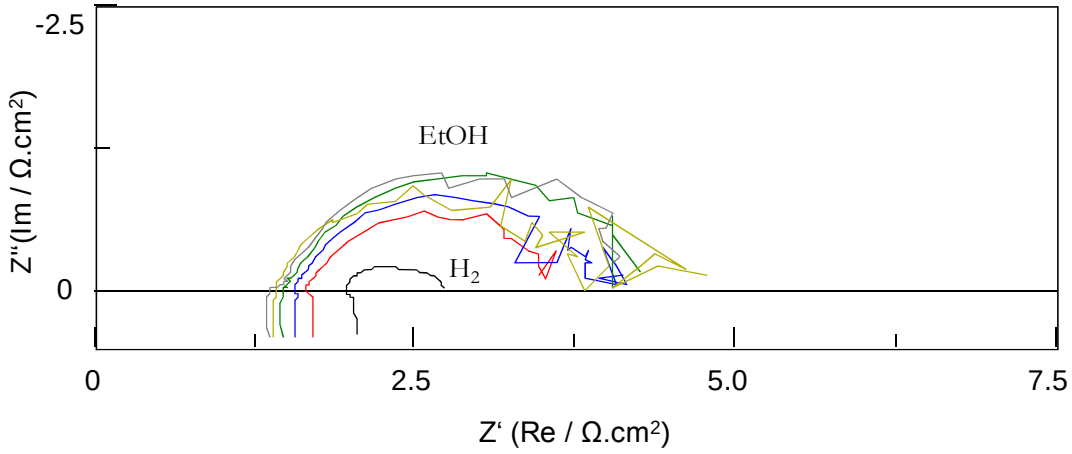

Figure 104: Impedance spectra obtained on a LSCM-YSZ anode operated on hydrogen and 15mol.% ethanol at 920°C. Spectra corresponding to ethanol have been recorded chronologically over 60 minutes from right (red curve) to left (grey curve).

The operation on diluted ethanol is achievable at this temperature, i.e. just above 900°C since a steady performance is reached with time. However, the performance displayed by the anode when operated on diluted ethanol is lower than the performance when operated on hydrogen. . Although, the anode ohmic resistance is smaller than for hydrogen, non ohmic losses are considerably higher for ethanol, indicating higher losses in the electrochemical processes. The total resistance is increase by about 1.25 $\Omega.cm^2$ for the operation on diluted ethanol as compared to hydrogen. This value is approximated since data recorded at low frequencies on ethanol tend to be scattered as can be seen from the impedance spectra, which is

probably due to some instability in the ethanol supply. The decrease in the ohmic losses when the cell is operated on ethanol can be attributed to carbon deposition from gas phase reactions and a higher electronic conductivity for the LSCM phase. Indeed, LSCM is a p-type conductor and the OCV is lower for the diluted ethanol.

The effect of the temperature has been further investigated. Figure 105 shows impedance data recorded on a LSCM-YSZ cell at 780°C. The cell was first operated on humidified (3% H_2O) hydrogen, then on 15 mol. % ethanol, before being switched back to humidified (3% H_2O) hydrogen. The operation on 15 mol.% ethanol at this temperature produces extremely low performance with really high polarization resistance. Clearly, the operation of LSCM-YSZ anodes on diluted ethanol below 800°C seems impossible. When the cell is switched back to hydrogen, impedance data indicate that the performance has been dramatically affected by the operation on diluted ethanol. This drop in the performance can only be attributed to carbon deposition. Operation on diluted ethanol of LSCM-YSZ anodes at 770°C seems to produce substantial carbon deposits that hinder the anode operation.

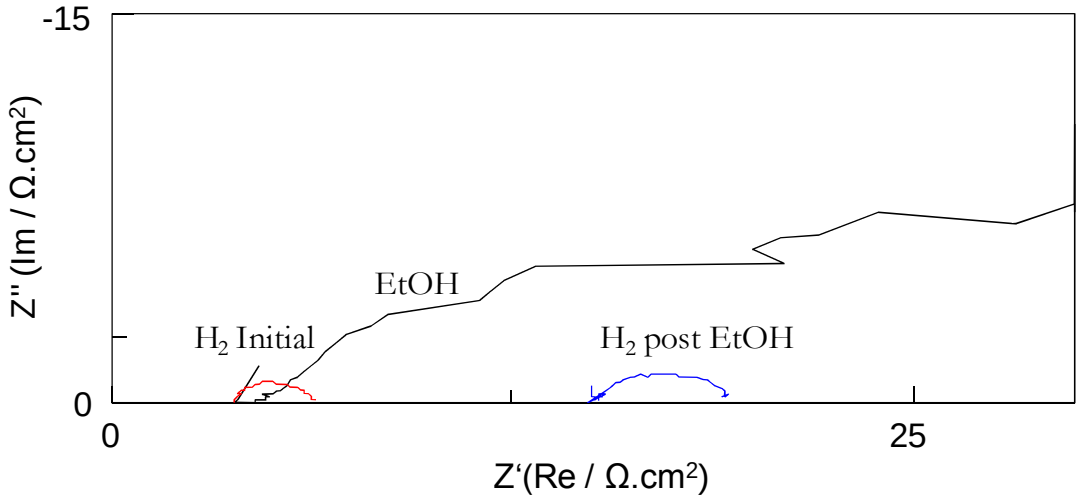

Figure 105: Impedance data recorded on a LSCM-YSZ anode at 780°C obtained successively on humidified (3% H_2O) hydrogen (red), 15 mol.% ethanol (black) and back to humidified (3% H_2O) hydrogen (blue).

To demonstrate that the performance drop was due to carbon deposition, the anode has been oxidized with oxygen at the same temperature, 780°C. Figure 106 shows impedance data recorded on the same LSCM-YSZ anode for a full redox cycle involving operation on ethanol at 700°C. The data show the original performance obtained on humidified hydrogen and after operation diluted ethanol from Figure 105. After operation on diluted ethanol, the cell has been oxidized in oxygen to remove the deposits before switching back the fuel to humidified hydrogen. Data indicate that the deposition process is fully reversible. The carbon deposition had considerably deteriorated the performance. After oxidation, the impedance spectrum recorded on humidified hydrogen is identical to the one recorded originally. The ohmic resistance is back to the original value, while the non ohmic resistance is seen to have slightly decreased. This slight improvement could be due to an incomplete removal of the tars. However, the anode performance is clearly not affected after a full cycle hydrogen-diluted ethanol- oxygen-hydrogen. Screen-printed LSCM anodes are thus redox

stable, and gas-phase carbon deposits can be fully removed with any performance deterioration.

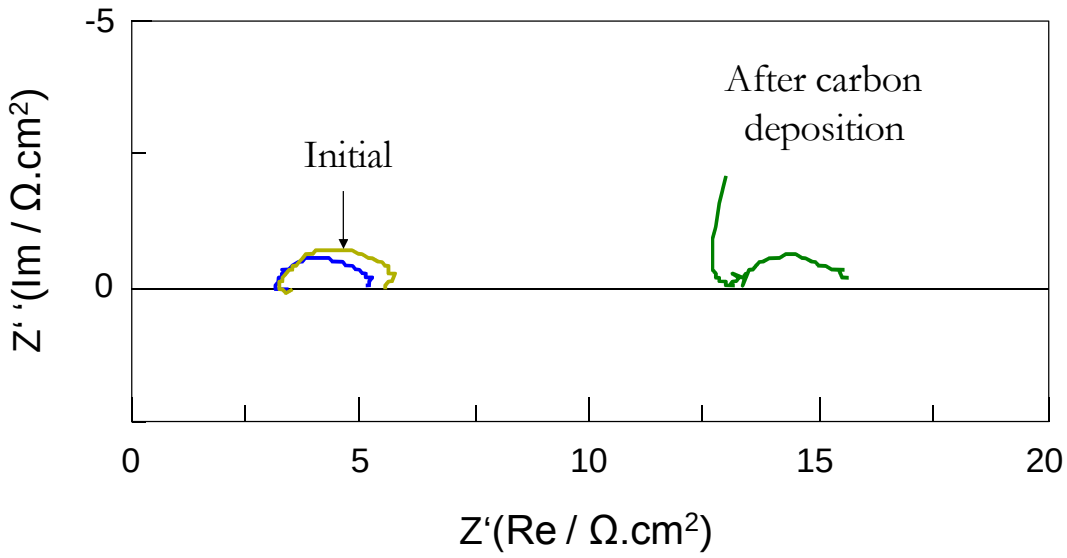

Figure 106: Impedance spectra recorded at 780°C on a LSCM-YSZ anode in humidified hydrogen, original peformance (yellow), after operation on ethanol (green) and after subsequent oxidation in oxygen (blue).

12.4. LSCM-Ceria

Figure 107 shows the impedance spectra recorded at various temperatures on an anode containing LSCM with 10% CGO using humidified (3% H_2O) hydrogen. The total half cell resistance was about 11 Ω.cm^2 at 860°C, 10 Ω.cm^2 at 890°C and 6.5 Ω.cm^2 at 941°C. The resistance displayed by this anode is clearly higher than performance that has been reported for LSCM anodes[4], indicating a non optimized microstructure. However, the performance was considered suitable for the purposes of this study. These impedance spectra are composed of three arcs. The arc at low frequency, that can be assigned to concentration polarization is temperature independent. This indicates a small conversion of the fuel[5].

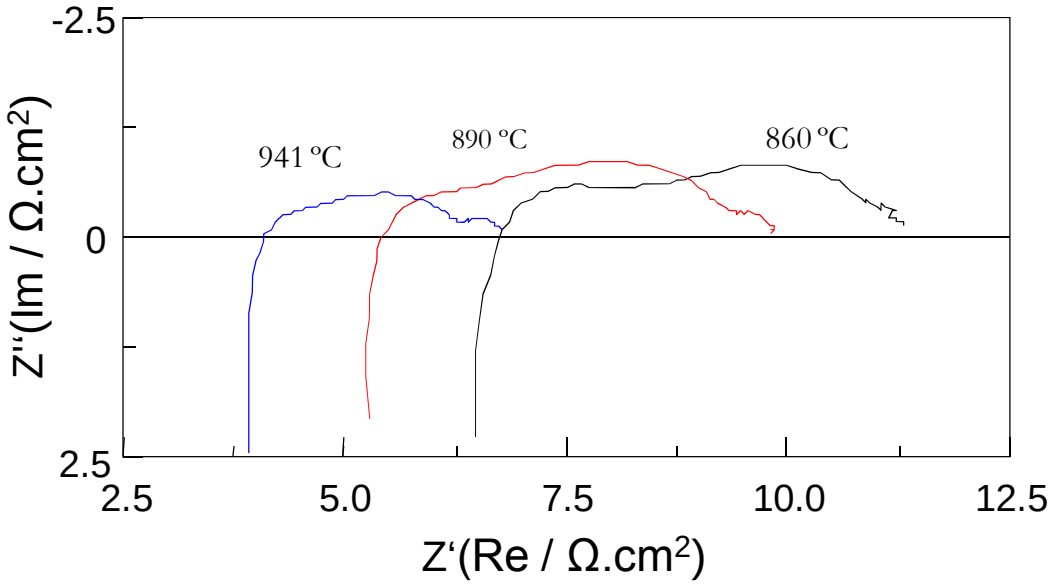

Figure 107: Impedance spectra recorded on a LSCM-CGO in humidified (3% H_2O) H_2 at various temperatures.

Figure 108 displays IV curves recorded on the same anode operated on humidified (3% H_2O) H_2 and 15 mol.% ethanol at various temperatures. The OCV on 15 mol.% ethanol was identical to the OCVs obtained on hydrogen, about 1.08V. The comparison of the IV curves obtained for 15 mol. % ethanol and hydrogen at 860°C indicates that the performance is higher on ethanol. While the OCVs are similar, overpotentials are clearly smaller when 15% ethanol is used. Both curves approach straight lines, and the slope of the curve is higher in the hydrogen case. Such a phenomenon was not observed on LSCM-YSZ anodes, indicating the introduction of CGO in the anode is beneficial for the operation on diluted ethanol. Figure 108 indicates that the overpotentials are identical when the cell is operated on humidified hydrogen at 941°C and 15mol. % ethanol at 860°C.

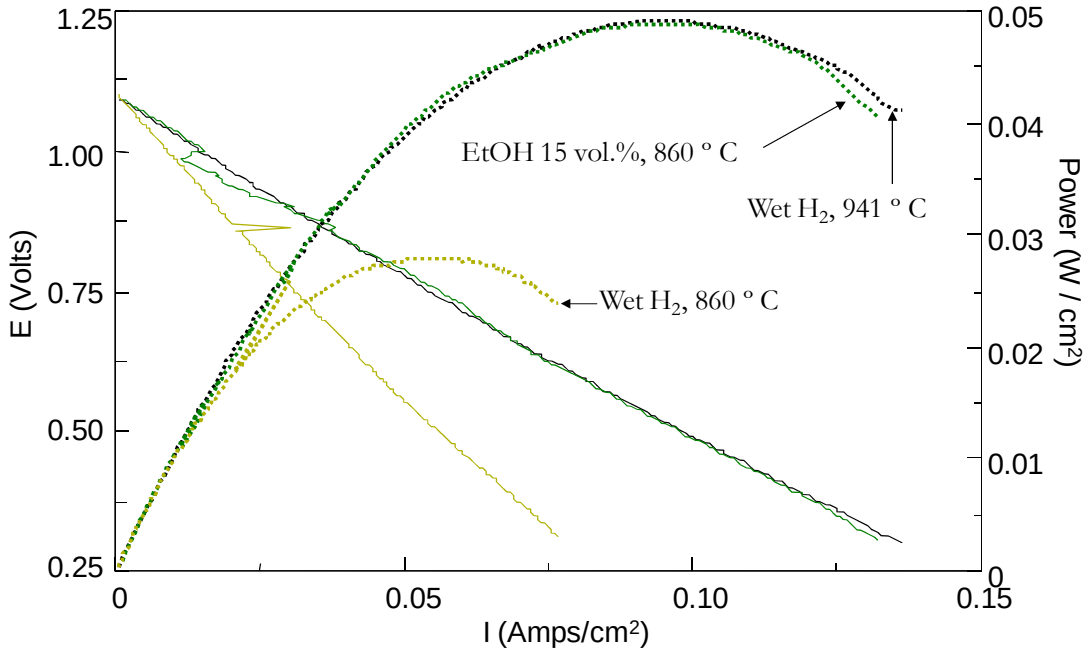

Figure 108: IV curves recorded on a LSCM-CGO anode in humidified H_2 at 860°C (yellow) and 941°C (black), and on 15 mol. % ethanol at 860°C (green).

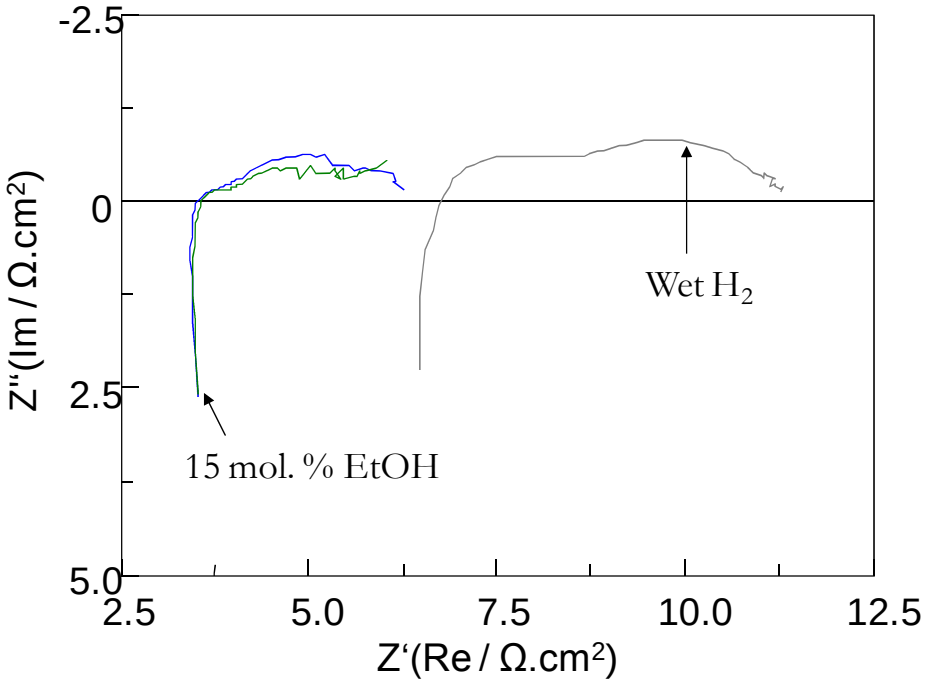

Figure 109: Impedance spectra recorded at 860°C on a LSCM-CGO anode in humidified (3% H_2O) H_2 and 15 mol.% ethanol.

Figure 109 shows the corresponding impedance spectra recorded at 860°C on humidified (3% H_2O) H_2 and 15 mol.% ethanol. The ohmic resistance is considerably decreased when the cell is operated on ethanol as compared to humidified hydrogen. Accordingly the non ohmic resistance of the anode is decreased as well.

The improved performance when the cell is operated on diluted ethanol can be better understood when the cell is switched back to hydrogen. The effect of the operation of the cell on diluted ethanol can be appreciated on Figure 110. Impedance spectra shown have been recorded using wet (3% H_2O) as a fuel before and after the cell had been operated on 15 mol.% ethanol for about 30 minutes at 860°C. These data clearly indicate that the performance of the anode has improved following operation on ethanol. Both spectra display similar shapes and contain three different arcs, indicating that the same processes occur in both cases. After operation on ethanol, the ohmic resistance of the cell has decreased indicating that the conductivity of the anode has improved. The non ohmic resistance has been reduced as well. This performance improvement can therefore be surely attributed to carbon deposition on the anode. SEM image of an anode taken after such an experiment is shown on Figure 111. This anode was cooled down under wet hydrogen to prevent any oxidation of the carbon deposits. The initial microstructure has been retained and no evident carbon deposition was observed. This agrees well with results reported by Gorte et al.[6] Tars deposited in amounts as small as 1 wt% of the anode were found to dramatically improve the performance. TPO measurements performed on such an anode have shown no significant weight loss.

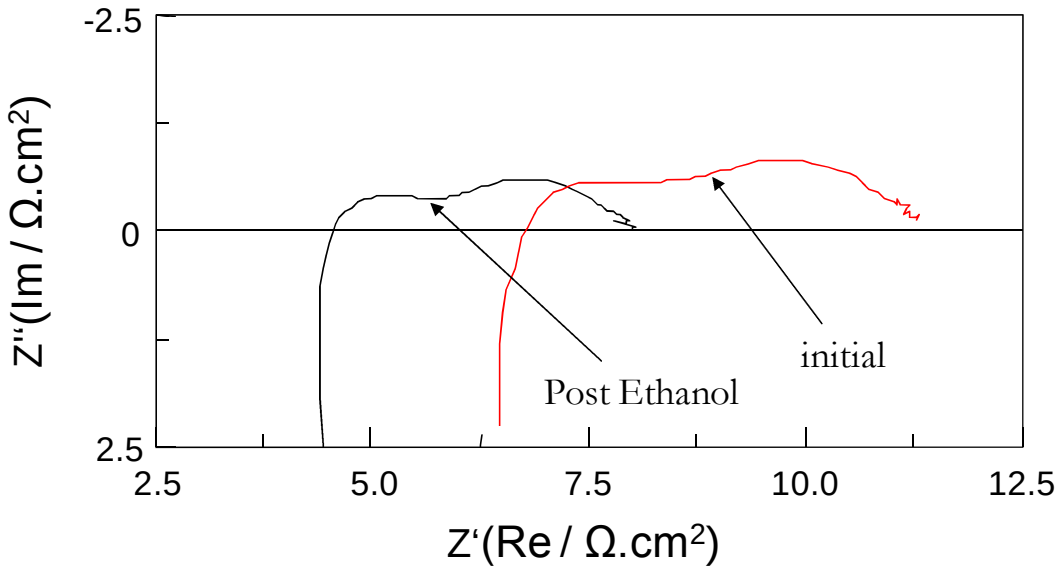

Figure 110: Impedance spectra recorded at 860°C on a LSCM-CGO anode in humidified (3% H_2O) H_2: initial performance (red) and after operation on 15% ethanol (black).

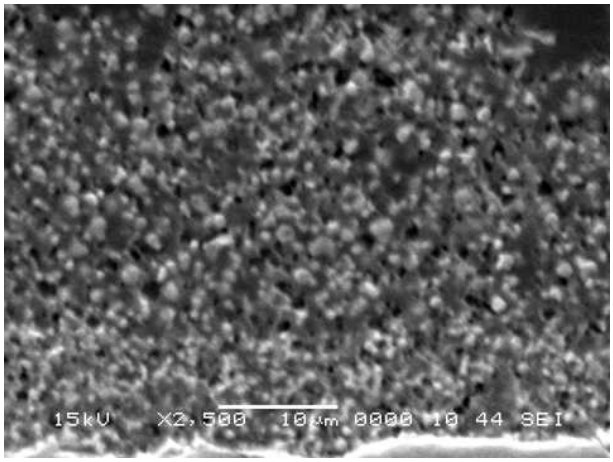

Figure 111: SEM image of a LSCM-CGO anode after operation on 15 mol. % ethanol at 860°C.

Figure 112 shows IV curves recorded on humidified (3% H_2O) hydrogen on a LSCM-CGO anode for two temperatures, 860°C and 940°C both before and after the cell has been operated on ethanol. Two measurements are shown for 860°C: the initial performance (green curve) and the performance after operation on diluted ethanol (red curve). Three measurements are shown for 940°C: the initial performance (blue curve), after operation on diluted ethanol (black curve) and about one hour after operation on diluted ethanol (yellow curve). Data indicate that the OCVs were identical for each test and that each curve approaches a straight line, all having different slopes. As was already shown by the impedance spectra on Figure 110, the operation on diluted ethanol improves the anode performance and overpotentials are reduced. The comparison between the data obtained at 860°C and 940°C indicates that the performance enhancement following operation on 15 mol.% ethanol is less pronounced at higher temperatures. The two different measurements recorded after the operation on diluted ethanol at 940°C indicate the performance enhancement obtained from the carbon deposits decreases with time. After one hour of operation on humidified hydrogen, data indicate that overpotentials have slightly increased after meaning that carbon deposits are slowly removed at such high temperatures. This result is in agreement with observations made by Gorte et al[7]. It was shown that the presence of ceria and a high temperature can lead to deposits removal by steam.

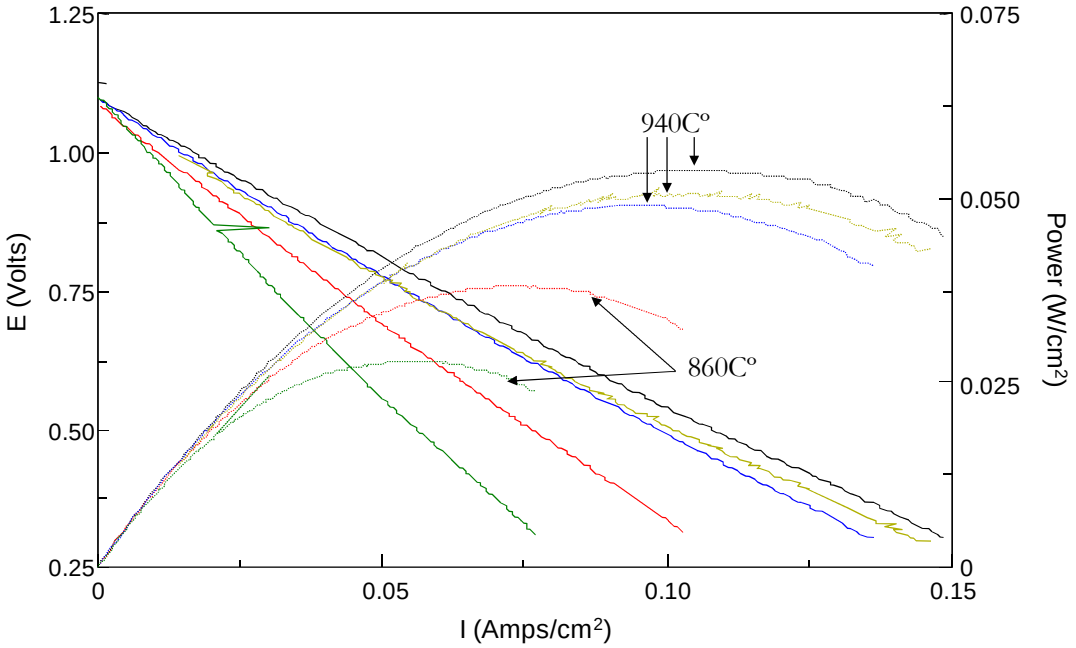

Figure 112: IV curves recorded on a LSCM-CGO anode in humidified H_2 at 860°C: initial performance (green) and after operation on diluted ethanol (red) and 941°C: Initial performance (blue), after operation on diluted ethanol (black) and about one hour after operation on ethanol (yellow).

The effect of ethanol concentration has been investigated. Figure 113 shows the IV curves recorded at 800°C on a LSCM-CGO anode with different ethanol concentrations in the feed. Three different feed compositions have been tested: 15, 30 and 40 mol. %. The OCV was quite similar for the 3 compositions and was around 0.90V. No clear trend was therefore observed for the OCV as a function of the ethanol content. The three IV curves exhibit similar shapes, but overpotentials seem to be decreased when the ethanol content is increased. The overpotential decrease as a function of the ethanol content becomes more pronounced at higher current densities. This can be attributed to the fact that concentrations of species available for electrochemical oxidation will be higher at higher ethanol content. Hence diffusion limitations will be smaller for higher ethanol contents meaning that overpotentials are smaller at high current densities.

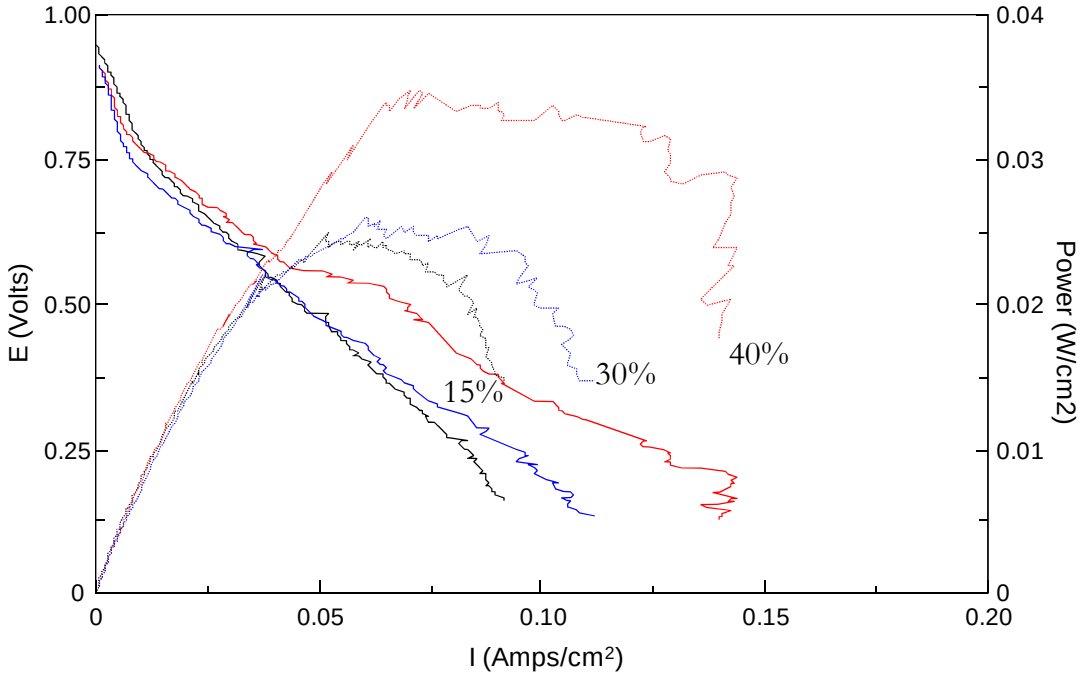

Figure 113: IV curves recorded on a LSCM-CGO anode at 800°C for various ethanol content.

When carbon deposition occurs, the long term stability of the anode will be questioned. To provide information about the long term behaviour, cells have been operated on diluted ethanol at a constant applied potential of 0.5V and the current density was monitored as a function of time. Figure 114 displays such data for two different LSCM-CGO anodes operating on a 30 mol.% ethanol mixture at 850°C. Carbon deposition has previously been shown to occur in such conditions. The anode performance is seen to be steady during the time of measurement which was here about one hour. No decrease of the performance was observed and the current density drawn from the cell can be seen to slightly increase with time. While this test should still be considered as a short time, it provides encouraging information about the stability of the system LSCM-CGO-Ethanol. A Ni–YSZ anode would considerably deteriorate within the same time frame. LSCM-CGO anodes have undergone multiple measurements in diluted ethanol for times up to 6 hours without displaying any noticeable performance degradation.

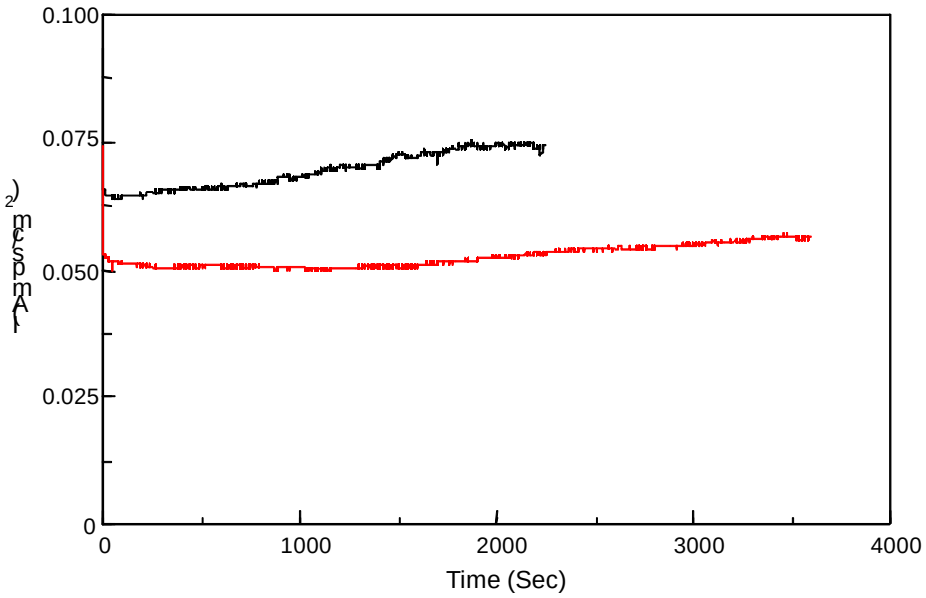

Figure 114: Current density monitored as a function of time for two different LSCM-CGO anodes operated on 30.mol % ethanol at 850°C. The voltage applied was 0.5V.

This series of tests have been performed on anodes that did not feature an optimized microstructure as indicated by the initial impedance spectra recorded on humidified hydrogen, displayed on Figure 104.Whilst useful information on the operation of LSCM-CGO anodes in diluted ethanol was obtained, the optimization of LSCM-CGO anodes was further investigated.

The best results were obtained by introducing YSZ in the anode and by applying graded layers. Several layers were screen printed and the both the YSZ content and the firing temperature were decreased for each new screen printed layer. The best results were obtained by using 75 wt% YSZ in the layer adjacent to the electrolyte and a firing temperature of 1350°C. The next layer contained 25 wt% YSZ and was fired at 1300°C. The outer layer contained only LSCM and CGO and was fired at 1200°C.

Figure 115 shows the impedance spectra recorded on an optimized anode at 950°C. With wet hydrogen, the ohmic resistance was about 1.50 $\Omega.cm^2$ and the non ohmic resistance was 0.7 $\Omega.cm^2$. Those values show how the grading of the anode can improve the performance. Without being outstanding, those resistances are acceptable for a Ni free anode. When the cell is switched to 15mol.% ethanol, the performance is further improved. The open circuit voltage with the diluted ethanol was 0.85V. The ohmic resistance is reduced to 1.13 $\Omega.cm^2$, and the non ohmic resistance is divided by a factor 2 and is around 0.3 $\Omega.cm^2$. Hence, good performance can be obtained by using diluted ethanol on graded LSCM-CGO-YSZ.

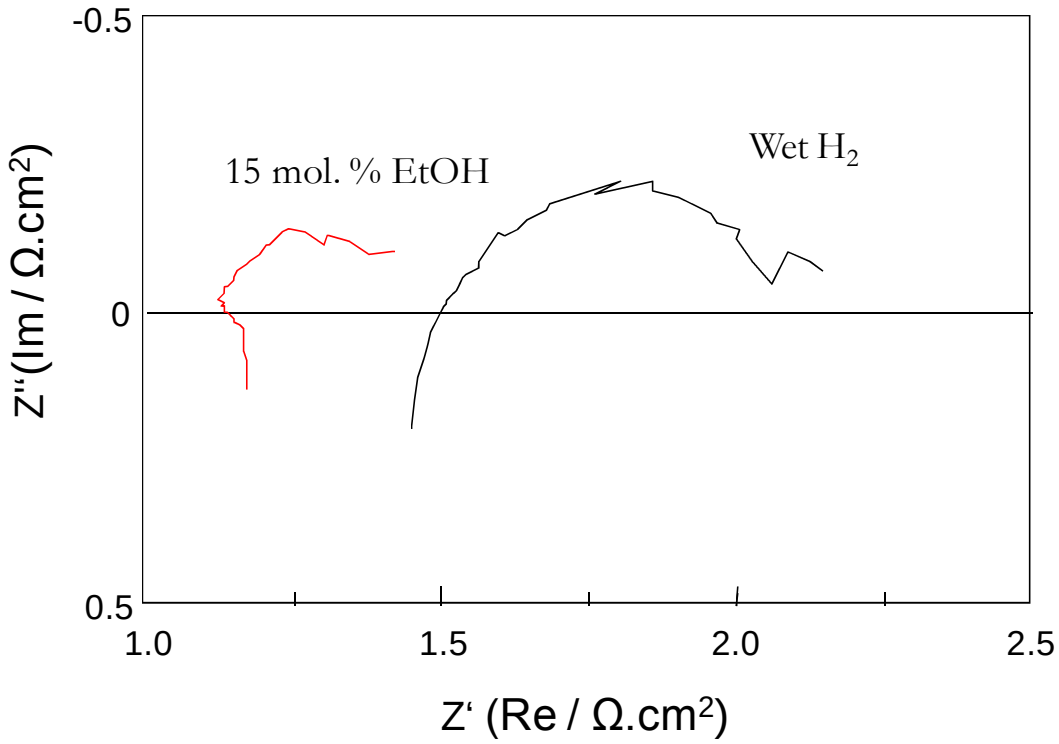

Figure 115: Impedance spectra recorded on a graded LSCM-YSZ-CGO anode at 950°C in humidified hydrogen and 15 mol.% ethanol.

12.5. Conclusions

No sustainable operation of Ni-YSZ anodes on ethanol/steam mixtures was achieved in the set up used for those experiments. Even at steam to carbon ratio excepted to prevent carbon deposition, anodes were found to quickly deteriorate with the growth of carbon filaments, as indicated by both electrochemical and post test SEM analysis. As suggested by others[7], deposition reactions must occur quicker than the removal reactions, allowing for carbon filaments to build up. Due to the mechanism of the catalytic deposition, Ni-YSZ anodes are damaged during the deposition process.

LSCM anodes can be operated on diluted ethanol. While the performance is lower than when hydrogen is used, steady operation can be achieved but only if the temperature is high enough. Steady operation is achievable above 900°C but the performance deteriorates quickly and dramatically at lower temperatures. Carbon deposition has been shown to be responsible for the performance deterioration. Access to the active sites is prevented by the presence of tars that considerably reduce the anode porosity. Those results are in agreement with the ones reported by Gorte and co-workers[8]. Their series of work indicated that steam could help in deposit removal but only at higher temperatures. Deposits have been shown to be non reactive towards steam below 800 °C. Hence when the cell is operated at 900 °C, the presence of steam will limit the carbon deposits by participating in removal reactions, allowing

the carbon deposits to reach a steady coverage of the anode. At lower temperatures, those reactions do not occur or with very slow kinetics, allowing for deposits to build up with and obstruct the anode porosity.

In the case of catalytic deposition on Ni-YSZ, the anode is irreversibly damaged by the deposition mechanism. Experiments conducted on LSCM anodes have indicated that the initial performance was fully recoverable after oxidation of the deposits. This result confirmed observations reported during the study of gas-phase carbon deposits[7,8]. This possibility to recover the initial performance by oxidation is of great importance. In practical systems, should carbon deposition become too important during the long term operation, an oxidation cycle could be performed to clean the anode from impurities without endangering the anode performance.

The addition of CGO to the LSCM anodes has a clear positive effect. Operating LSCM-CGO anodes on diluted ethanol yields higher performance than with hydrogen. Overpotentials are reduced in diluted ethanol and carbon deposits have been shown to be responsible for this enhancement. Deposits have been shown to be beneficial to the operation on humidified hydrogen in the temperature range investigated (850-950°C). Those results are again in good agreement with observations reported in the literature[6,7,8]. The presence of ceria catalyses the carbon removal reactions with steam. Hence, deposits are less important on a LSCM-CGO anode than on a LSCM anode. A steady state deposition seems to be achieved, and the improved performance has been shown to be stable over time. Moreover, the presence of CGO will certainly improve the electrocatalytic activity of the anode.

Using LSCM-CGO-YSZ anodes with graded microstructures, a polarization resistance of 0.3 $\Omega.cm^2$ was achieved on diluted (15mol. % in steam) ethanol. The total anode resistance, both ohmic and non ohmic, was higher for hydrogen than for the ethanol/steam mixture.

---

[1] S.Assabumrungat, V.Pavarajarn, S.Charojrochkul, N.Laosiripojana, *Chem. Eng. Sci.*, 59 (2004) 6015-6020

[2] S. Sasaki, K. Watanabe, and Y. Teraoka, *Jour. Elect. Soc.*, 151 (7) (2004) A965-A970

[3] N.Q. Minh, *J. Am. Ceram. Soc*., 76 (1993) 563-588

[4] S.Tao, J.T.S. Irvine, *Journal of the electroch. Soc.*, 151(2) (2004) A252-A259

[5] B. Barfold, A. Hagen, S. Ramousse, P.V. Hendriksen, M. Mogensen, *Fuel Cells*, 6 (2) (2006) 141-145

[6] S. McIntosh, J.M. Vohs, R.J. Gorte, Journal of the electrochemical society, 150 (4) (2003) A470-A476

[7] T.Kim, G.Liu, M.Boaro, S-I.Lee, J.M.Vohs, R.J. Gorte, O.H. Al-Madhi, B.O.Dabboussi, *Journal of power Sources*, 155 (2006) 231-238

[8] S. McIntosh, H. He, S.-I. Lee, O. Costa-Nunes, V.V. Krishnan, J.M.Vohs, R.J. Gorte, *J. Electrochem. Soc*., 151 (2004) A604–A608.

DISCUSSION AND CONCLUSIONS

The studies presented on the development of anodes for SOFCs and direct ethanol SOFCs have provided some interesting and encouraging results that could help in the design of practical SOFC systems. Alternative efficient anode materials are required to accelerate the development of SOFCs and second generation bioethanol will certainly play an important role in the near future energy landscape.

Results have demonstrated that efficient anodes could be designed to replace the Ni-YSZ cermets. Power densities obtained on cells involving impregnated LSCM composite anodes were comparable to the Ni-YSZ standards. Direct operation of SOFCs on ethanol has been demonstrated to be achievable when using LSCM-ceria composite anodes. The performance of these anodes was better on ethanol/steam mixtures than on hydrogen. Hence, the use of diluted ethanol on engineered composite LSCM based anodes can lead to the development of powerful and versatile energy conversion devices that will be part of the answer to the energetic and environmental challenges our economies are facing today.

The development of efficient anodes for SOFCs requires the microstructures to be engineered on the micro-scale to produce high and durable performance. The possibility to control the microstructure in situ, which has been demonstrated for impregnated Mn containing perovskites, is of great interest. The in situ formation of a nano-porous coverage of the electrolyte by the electronic conductive phase provides a powerful tool for the development of novel microstructures. More work is required in this area but results presented in this thesis should help in the development of optimized microstructures that are required for efficient and durable operation. Application of this technique could find interest beyond the SOFC community.